

# **XENOBIOTIC COMPOUNDS DEGRADATION AND THEIR EFFECTS ON IMPORTANT ENZYMES**

**Ph.D. THESIS**

*by*

**NEHA SINGH**



**DEPARTMENT OF BIOTECHNOLOGY  
INDIAN INSTITUTE OF TECHNOLOGY ROORKEE  
ROORKEE – 247 667 (INDIA)  
APRIL, 2018**



# **XENOBIOTIC COMPOUNDS DEGRADATION AND THEIR EFFECTS ON IMPORTANT ENZYMES**

**A THESIS**

*Submitted in partial fulfilment of the  
requirements for the award of the degree*

*of*

**DOCTOR OF PHILOSOPHY**

*in*

**BIOTECHNOLOGY**

*by*

**NEHA SINGH**



**DEPARTMENT OF BIOTECHNOLOGY  
INDIAN INSTITUTE OF TECHNOLOGY ROORKEE  
ROORKEE – 247 667 (INDIA)  
APRIL, 2018**



**©INDIAN INSTITUTE OF TECHNOLOGY ROORKEE, ROORKEE-2018  
ALL RIGHTS RESERVED**





# INDIAN INSTITUTE OF TECHNOLOGY ROORKEE ROORKEE

## CANDIDATE'S DECLARATION

I hereby certify that the work which is being presented in the thesis entitled "**XENOBIOTIC COMPOUNDS DEGRADATION AND THEIR EFFECTS ON IMPORTANT ENZYMES**" in partial fulfilment of the requirements for the award of the Degree of Doctor of Philosophy and submitted in the Department of Biotechnology of the Indian Institute of Technology Roorkee, Roorkee is an authentic record of my own work carried out during a period from January, 2013 to April, 2018 under the supervision of Dr. Pravindra Kumar, Associate Professor, Department of Biotechnology, Indian Institute of Technology Roorkee, Roorkee.

The matter presented in this thesis has not been submitted by me for the award of any other degree of this or any other Institution.

(NEHA SINGH)

This is to certify that the above statement made by the candidate is correct to the best of my knowledge.

(PRAVINDRA KUMAR)  
Supervisor

**Date:** April-2018



## ABSTRACT

Xenobiotic compounds are man-made chemicals that are present in the environment at unnaturally very high concentrations. One such xenobiotic compound phthalates or phthalic acid esters (PAEs), are the dialkyl or alkyl aryl esters of o-phthalic acid, which are ubiquitous environmental pollutants. They are frequently used as plasticizers to provide stability to the plastic products. They have different properties which certainly depend on the composition and the type of alcohol that usually makes up the alkyl chain of phthalates. Several experimental and in silico molecular docking studies have highlighted the toxic effects related to phthalate exposure. This may eventually lead to the inhibition of normal activities of various receptors such as peroxisome proliferator-activated receptors, glucocorticoid receptors, estrogen receptors and progesterone receptors and etc. Six PAEs namely Dimethyl phthalate (DMP), Diethyl phthalate (DEP), Di-n-butyl phthalate (DnBP), Butyl benzyl phthalate (BBzP), Bis-(2-ethylhexyl) phthalate (DEHP) and Di-n-octyl phthalate (DnOP) are in the priority pollutants list of United States Environmental Protection Agency (USEPA) and European Union (EU) due to their explored toxicological, teratogenic and mutagenic properties.

Likewise, polychlorinated biphenyls (PCBs) are groups of man-made organic chemicals consisting of carbon, hydrogen and chlorine atoms. The number of chlorine atoms and their location in a PCB congener determines many of its physical and chemical properties. Due to their non-flammability, chemical stability, high boiling point and electrical insulating properties, PCBs were extensively used in hundreds of industrial and commercial applications. Polychlorinated biphenyls (PCBs) are among the most persistent chlorinated environmental pollutants despite long-term regulation of their manufacture and use. The discovery of many bacterial strains that are able to partially degrade PCBs has fueled research directed towards improving the bioremediation strategies for the clean-up of PCB contaminated site.

Keeping in mind the toxic effects of such harmful xenobiotic compounds and understanding the emergence of underlying concern; related to their toxicological aspect, to combat them with newer the bioremediation strategies, integrated structure based approaches have been used in the thesis objectives.

**Chapter 1** gives the brief introduction about the xenobiotic compounds. It further illustrates the use of microbial activity based bioremediation strategy to combat the continuing problem of xenobiotic pollution.

**Chapter 2** deals with the overview of computational approaches used for assessing the binding of commonly used high molecular weight phthalates such as dicyclohexyl phthalate (DCHP) and its monophthalate metabolite monocyclohexyl phthalate (MCHP), to the important human glucocorticoid receptor (hGR). The rise in rates of metabolic disorder is ultimately related to increase in exposure, usage, and production of these xenobiotic compounds. A large variety of environmental endocrine disrupting substances influence adipogenesis and obesity. “Obesogens” are chemical agents that improperly regulate the genes involved in glucose metabolism and adipocyte differentiation and promote lipid accumulation and adipogenesis. The human glucocorticoid receptor (hGR) is a steroid hormone triggered transcriptional factor and regulates target genes important in basal glucose homeostasis. Molecular docking analysis was performed in order to assess the in-silico structure based toxic effects of high molecular weight phthalate dicyclohexyl phthalate (DCHP) and its monophthalate metabolite mono-cyclohexyl phthalate (MCHP). DCHP and MCHP were docked within the active site cavity of the human glucocorticoid receptor (hGR). Molecular docking results show that the binding affinities of DCHP and MCHP lie within the comparable range with Dexamethasone (DEX), a potent agonist for hGR. Molecular Docking and simulation results emphasize that DCHP and MCHP can efficiently bind to hGR, which further leads to glucocorticoid-mediated adipogenesis in a synergistic manner.

**Chapter 3** explains the binding of phthalates with human  $\alpha$ -amino- $\beta$ -carboxymuconate- $\epsilon$ -semialdehyde decarboxylase (hACMSD), a zinc-containing amidohydrolase which is a vital enzyme of the kynurenine pathway of tryptophan metabolism. It prevents the accumulation of quinolinic acid (QA) and helps in the maintenance of basal Trp-niacin ratio. To assess the structure based inhibitory action of PAEs such as DMP, DEP, DBP, DIBP, DEHP and their metabolites, these were docked into the active site cavity of hACMSD. Docking results show that the binding affinities of PAEs lie in the comparable range with Dipicolinic acid, a substrate analog of hACMSD. PAEs interact with the key residues such as Arg47 and Trp191 and lie within the 4 Å vicinity of zinc metal at the

active site of hACMSD. Dynamics and stability of the PAEs-hACMSD complexes were determined by performing molecular dynamics simulations using GROMACS 5.14. Binding free energy calculations of the PAEs-hACMSD complexes were estimated by using MMPBSA method. The results emphasize that PAEs can structurally mimic the binding pattern of tryptophan metabolites to hACMSD, which further leads to inhibition of its activity and accumulation of quinolate in the kynurenine pathway of tryptophan metabolism.

**Chapter 4** describes the isolation and characterization of three bacterial strains capable of degrading phthalates namely *Pseudomonas* sp. PKDM2, *Pseudomonas* sp. PKDE1 and *Pseudomonas* sp. PKDE2 for their degradative potential. These strains efficiently degraded 77.4% - 84.4% of DMP, 75.0% - 75.7% of DEP and 71.7% - 74.7% of DEHP, provided the initial amount of each phthalate is 500 mg L<sup>-1</sup>, after 44 hours of incubation. GC-MS results reveal the tentative DEHP degradation pathway, where hydrolases mediate the breakdown of DEHP to phthalic acid (PA) via an intermediate MEHP. MEHP hydrolase is a serine hydrolase which is involved in the reduction of the MEHP to PA (phthalic acid). The predicted 3D model of MEHP hydrolase from *Pseudomonas mosselii* was docked with phthalate monoesters (PMEs) such as mono-ethylhexyl phthalate (MEHP), mono-n-hexyl phthalate (MHP), mono-n-butyl phthalate (MBP) and mono-n-ethyl phthalate (MEP), respectively. Docking results show that the distance between the carbonyl carbon of respective phthalate monoester and the hydroxyl group of catalytic serine lies in the range of 2.9 to 3.3 Å, which is similar to the enzyme-substrate (ES) complex of other serine hydrolases. This structural study highlights the interaction and the role of catalytic residues of MEHP hydrolase involved in the biodegradation of phthalate monoester metabolites to phthalate.

**Chapter 5** describes the characterization of phthalate dioxygenase reductase (RePDR), an important enzyme of the PDO-PDR system from *Ralstonia eutropha* strain CH34, a gram-negative bacteria important from remediation viewpoint. PDR from *Ralstonia eutropha* strain CH34 was cloned, expressed and purified and characterized. The crystal structure of phthalate dioxygenase reductase is available from *Burkholderia cepacia*, a gram-negative bacterium (PDB ID: 2PIA). PDR has been reported to have three domains, the N-terminal FMN binding domain, central NAD (H) binding domains, and C-

terminal [2Fe-2S] domain. The overall stability of the model of *RcPDR* was assessed by simulation studies and compared with 2PIA. In silico analysis of the complex formation of (phthalate dioxygenase), *RePDO-RePDR* is also studied and important interactions involved in complex formation were analyzed. Important interface residues from both the individual counterparts, i.e. *RePDO* and *RePDR* have been elucidated. The evolutionary relationship between important interface residues has also been established.

**Chapter 6** describes the screening of polychlorinated biphenyl (PCB) library with native Biphenyl dioxygenase (BPDO) structure from *Pandoraea pnomenusa* B-356, in order to evaluate the influence of the pattern and degree of chlorination on the catalytic activity of BPDO. Therefore, for that purpose, PCB congener library of 209 congeners was made and screened to elucidate the enhanced degradation abilities of BPDO. The important features related to congener specificity were highlighted. Through docking studies the binding ability of BPDO from *Pandoraea pnomenusa* B-356 w.r.t. PCB congeners was measured and important active site residues involved in the interaction were acknowledged. Moreover, the geometrical properties of the congeners such as aromatic benzene dimer ring offset, and the angle of rotation in between the two aromatic biphenyls influencing the rate of catalysis is also highlighted. The results related to the geometry and electrostatic properties of chlorinated biphenyls can be useful to rationalize their selective toxicities. Furthermore, structure determination of biphenyl dioxygenase from *Pandoraea pnomenusa* B-356 in complex with 2,3',5'trichlorobiphenyl was also done.

## ACKNOWLEDGEMENTS

Well to start with, I feel myself extremely fortunate to reach up to this phase of the journey of five years of hard work, commitment, and continuous efforts. First and foremost, I would like to thank almighty for being my spiritual guiding light, in shaping my journey so far and so wonderful. Then I would like to thank my supervisor Dr. Pravindra Kumar for giving me this opportunity to pursue the carrier of my dreams. Right from the masters, I was determined to enter into the field of research and I reared all my ambitions at this place in IIT Roorkee. I would also like to thank Dr. Shailly Tomar, for her encouragement and initial training under her expertise.

I feel fortunate enough to live up to the expectations of my parents, Smt. Madhu Singh and Shri Tirath Singh. They both have always supported me, stood by me as a pillar of my strength in my hard times. I am thankful and feel blessed to have such parents. I would also like to thank my in-laws, Smt. Shakuntla Devi and Shri Balesh Singh; they have always shown faith in me and boosted up my confidence level.

I would also like to thank my wonderful lab mates Madhusudan Rao Kaitiaki, Vijay Sharma, Anchal Sharma. All of them were extremely helpful and cooperative throughout the course. I would like to thank Vikram Dalal, my co-labmate, without whose efforts this journey would not have been possible. He has a crucial role in this journey as his scientific inputs have helped me in shaping my thesis as well as my manuscripts. His suggestions were always fruitful. I endow my special thanks to Neetu, Poonam Dhankar, Jai Krishna Mahto, Pooja Kesari, and Monika, for their full support through my thick and thins. I would like to thank Department of Biotechnology and Institute Instrumentation Centre for providing me facility for conduction of experiments.

Now its turn for the last but definitely not the least, my husband, my source of energy, my everything, Mr. B.K. Chaudhary. His patience and perseverance have taught me how to deal with the situations which were way beyond my control. He has endlessly helped me and encouraged me every day and pushed me up to the limits to bring out the best out of me. I love and thank my daughter Devpriya, although she is just 2 years old... but she is a source of my positivity and brings optimism in my life.

NEHA SINGH



## TABLE OF CONTENTS

ABSTRACT	i
ACKNOWLEDGEMENTS	v
LIST OF FIGURES	xiii
LIST OF TABLES	xvii
LIST OF ABBREVIATIONS	xix
LIST OF PUBLICATIONS	xxiii
<b>Chapter 1. Introduction and review of literature</b>	
1.1 Xenobiotic compounds in the environment	3
1.2 Classification of xenobiotic compounds	4
1.3 Bioremediation: a strategy for combating xenobiotic compounds	6
1.3.1 Bioavailability of organic compound: portion available for microorganism	6
1.3.2 Bioaugmentation strategy for remediation of a contaminated site	8
1.3.3 Innovative approaches and their application	8
1.3.3.1 Use of compost for the treatment of the polluted site	9
1.3.3.2 Electrobioremediation	9
1.3.3.3 Microbial remediation utilizes the potential of plants	10
1.3.3.4 Use of probes required for monitoring and testing effectiveness of bioremediation of contaminated sites	10
1.4 Toxicity of phthalates	13
1.5 Biodegradation pathway of phthalic acid esters (PAEs)	19
1.5.1 Aerobic degradation of phthalic acid esters (PAEs)	19
1.5.2 Anaerobic biodegradation pathway of phthalic acid esters (PAEs)	21
1.6 Enzymes involved in phthalate degradation	21
1.6.1 Esterase/hydrolase role degradation of phthalates	21
1.6.2 Permeases activity	22



1.6.3 Phthalate dioxygenase (PDO) system	22
1.6.4 Protocatechuate dioxygenase	22
1.7 Toxicity of polychlorinated biphenyls (PCBs)	23
1.8 Biodegradation of PCBs	24
1.8.1 Anaerobic transformation of PCBs	25
1.8.2 Aerobic transformation of PCBs	27

## **Chapter 2. In-silico approach for elucidating toxic effects of high molecular weight phthalate dicyclohexyl phthalate (DCHP) in glucocorticoid receptor-mediated adipogenesis**

2.1 Introduction	35
2.2 Material and methods	37
2.2.1 System preparation and Molecular docking of ligands	37
2.2.2 Molecular dynamics simulation	38
2.2.3 MMPBSA binding free energy calculations	39
2.3 Results	40
2.3.1 Molecular docking of the ligands	40
2.3.2 Molecular simulation results	43
2.3.2.1 Root-mean-square deviation (RMSD)	43
2.3.2.2 Root-mean-square fluctuation (RMSF)	45
2.3.2.3 Radius of gyration (Rg)	46
2.3.2.4 Hydrogen bond analysis	47
2.3.3 MMPBSA Binding free energy calculation	49
2.4 Discussion	49
2.5 Conclusion	52

## **Chapter 3. Structure-based mimicking of phthalic acid esters (PAEs) and inhibition of hACMSD, an important enzyme of the tryptophan-kynurenine metabolism pathway**

3.1	Introduction	57
3.2	Material and methods	59
3.2.1	Protein and ligand preparation	59
3.2.2	Molecular docking of ligands	60
3.2.3	Molecular dynamics simulation	62
3.2.4	MMPBSA binding free energy calculation	63
3.3	Results and discussion	63
3.3.1	Molecular docking of ligands	63
3.3.2	Molecular simulation results	73
3.3.2.1	Root-mean-square deviation (RMSD)	74
3.3.2.2	Root-mean-square fluctuation (RMSF)	77
3.3.2.3	Radius of gyration (Rg)	79
3.3.2.4	Solvent accessible surface area (SASA)	82
3.3.2.5	Hydrogen bond analysis	84
3.3.3	MMPBSA binding free energy calculation	88
3.4	Conclusion	90
<b>Chapter 4. Biodegradation of phthalic acid esters (PAES) and in silico structural characterization of mono-2-ethylhexyl phthalate (MEHP) hydrolase on the basis of close structural homolog</b>		
4.1	Introduction	93
4.2	Materials and Methods	94
4.2.1	Chemicals and Media	94
4.2.2	Isolation and characterization of bacterial strains	94
4.2.3	16S rRNA gene amplification and phylogenetic analysis	95
4.2.4	Antibiotic susceptibility test	95
4.2.5	Biodegradation of DMP, DEP, and DEHP	95
4.2.6	Identification of DEHP degradation pathway intermediates	96

4.2.7 Comparative molecular modeling and structure validation	97
4.2.8 Molecular docking	98
4.3 Results and discussion	98
4.3.1 Isolation and characterization of bacterial strains	98
4.3.2 16S rRNA gene amplification and phylogenetic analysis	100
4.3.3 Antibiotic susceptibility test	102
4.3.4 Biodegradation of DMP, DEP, and DEHP	103
4.3.5 Identification of DEHP degradation pathway intermediates	106
4.3.6 Comparative molecular modeling and structure validation	109
4.3.7 Molecular docking	113
4.4 Conclusion	119
<b>Chapter 5. Characterization of phthalate reductase from <i>Ralstonia eutropha</i> CH34 and in silico study of phthalate dioxygenase and phthalate reductase interaction</b>	
5.1 Introduction	123
5.2 Material and Methods	125
5.2.1 Chemicals	125
5.2.2 Molecular biology kits and enzymes	125
5.2.3 Cloning, expression of <i>RePDR</i>	126
5.2.4 Purification of <i>RePDR</i> protein	127
5.2.5 Insilico prediction of <i>RePDR</i> and <i>RePDO</i> interaction	127
5.2.5.1 Comparative molecular modeling and validation of <i>RePDR</i> and <i>RePDO</i>	128
5.2.5.2 Determination of <i>RePDR</i> and <i>RePDO</i> interface residues	128
5.2.5.3 <i>RePDR</i> - <i>RePDO</i> docking using HADDOCK	129
5.2.5.4 Evolutionary relationship between conserved <i>RePDR</i> and <i>RePDO</i> Residues	130

5.3 Results and discussion	131
5.3.1 Cloning and expression of <i>RePDR</i>	131
5.3.2 Purification of <i>RePDR</i>	133
5.3.3 In silico prediction of <i>RePDR</i> and <i>RePDO</i> interaction	134
5.3.3.1 Comparative molecular modeling and validation of <i>RePDR</i> and <i>RePDO</i>	134
5.3.3.2 Determination of <i>RePDR</i> and <i>RePDO</i> interface residues	139
5.3.3.3 <i>RePDR</i> - <i>RePDO</i> docking using HADDOCK	141
5.3.4.4 Evolutionary relationship between conserved <i>RePDR</i> and <i>RePDO</i> residues	144
5.4 Conclusion	147
<b>Chapter 6. Structure determination of biphenyl dioxygenase from <i>Pandoraea pnomenusa</i> B-356 in complex with 2,3',5' trichlorobiphenyl</b>	
6.1 Introduction	151
6.2 Material and methods	155
6.2.1 System preparation	155
6.2.2 PCB Library preparation	155
6.2.3 Screening of library using PyRx	155
6.2.4 Determination of pi-stacking interactions	156
6.2.5 Chemicals	158
6.2.6 Structure determination of BPDO <sub>B356</sub> -2,3',5' trichlorobiphenyl complex	158

6.3 Results and Discussion	159
6.3.1 Screening of library using PyRx	159
6.3.2 Importance of pi-stacking interactions	168
6.3.3 Structure determination of 2,3',5'trichlorobiphenyl-BPD0 <sub>B356</sub> complex	171
6.4 Conclusion	175
7. Summary	177
8. Bibliography	179



## LIST OF FIGURES

1.1. Global distribution of phthalic acid esters metabolites.	15
1.2. Steps involved in the aerobic degradation of phthalic acid esters (PAEs).	20
1.3. Numbering and nomenclature of PCBs.	23
1.4. The common steps involved in anaerobic degradation of commercial Aroclor 1260, a heptachlorobiphenyl in <i>Dehalococcoides</i> .	26
1.5. The metabolic pathway involved in PCB degradation.	28
1.6. The specific nature of PCB degradation in different microorganisms.	30
2.1. The ribbon diagram of human glucocorticoid receptor (hGR)-ligand binding domain, active site cavity with DEX, DCHP and its metabolite MCHP.	41
2.2. Pictographic representation of hydrophobic interaction involved in DEX-hGR, DCHP-hGR and its metabolite MCHP-hGR complex formation using Maestro 11.2.	42
2.3. RMSD graphs of hGR with DEX, DCHP, and MCHP.	44
2.4. RMSF plots of molecular dynamics simulation study of hGR-DEX, hGR-DCHP and hGR-MCHP complexes for 20 ns.	45
2.5. Radius of gyration (Rg) graphs of DEX-hGR, DCHP-hGR, and MCHP-hGR complexes.	46
2.6. Hydrogen bond number results of DEX-hGR, DCHP-hGR, and MCHP-hGR complexes.	47
2.7. Bar representation of the hydrogen bond numbers distribution of hGR with DEX and PAEs.	48
3.1. Kynurenine pathway of tryptophan metabolism.	58
3.2. The ribbon diagram of hACMSD binding active site cavity with PDC, DEHP and its metabolites.	68
3.3. The cartoon representation of hACMSD binding with low molecular weight dipthalates.	71

3.4. The binding interaction of low molecular weight Monophthalates with hACMSD.	73
3.5. RMSD graph of hACMSD with PDC and PAEs.	77
3.6. RMSF molecular dynamics simulation results of hACMSD for 20ns.	79
3.7. Radius of gyration (Rg) plots of PDC-hACMSD and PAEs-hACMSD.	81
3.8. Solvent accessible surface area profile of hACMSD with PDC and PAEs.	84
3.9. Hydrogen bond number results of PDC-hACMSD and PAEs-hACMSD complexes during the 20ns of simulation.	86
3.10. Bar representation of the hydrogen bond number distribution of hACMSD with PDC and PAEs.	88
4.1. SEM micrographs of the isolates at 5000X magnification.	99
4.2. Phylogenetic tree analysis of 16S rRNA gene sequences.	101
4.3. Degradation of PAEs by the isolated strains.	104
4.4. GC-MS chromatograms of DEHP and its biodegradation intermediates.	107
4.5. GC-MS spectra of DEHP degradation pathway.	108
4.6. Modeled structure of mono-2-ethylhexyl phthalate (MEHP) hydrolase.	110
4.7. ProSA energy profile of MEHP hydrolase model structure.	110
4.8. Multiple sequence alignment of MEHP hydrolase from <i>P. mosselii</i> with homologs from the C-C hydrolases from different bacteria.	112
4.9. Surface view of the MEHP hydrolase binding pocket.	114
4.10. Proposed mechanism of catalysis mediated by MEHP hydrolase.	115
4.11. Ribbon diagram of MEHP hydrolase binding cavity.	117
4.12. Superposition of catalytic triad residues (His-Asp-Ser) of MEHP hydrolase and crystal structures of various serine hydrolases.	118
5.1. Sequential steps for initial phthalate degradation.	124
5.2: Steps used for <i>RePDR-RePDO</i> docking in HADDOCK.	129

5.3. Steps utilized for determining evolutionary relationships using CONSURF.	131
5.4. Amplification and cloning of <i>RcPDR</i> gene.	132
5.5. Optimized purification of recombinant <i>RcPDR</i> .	133
5.6. Pairwise sequence alignment.	135
5.7. Homology models of <i>RePDR</i> and <i>RePDO</i> .	136
5.8. The Ramachandran plot of the finalized <i>RePDR</i> and <i>RePDO</i> models.	137
5.9. RMSD graph of <i>RePDO</i> and <i>RePDR</i> models.	138
5.10. The important interactions at the interface of <i>RePDR</i> and <i>RePDO</i> complex are shown.	143
5.11. A) Consurf results for <i>RcPDO</i> B) Consurf results for <i>RcPDR</i> .	146
6.1. The basic chemical structure of Biphenyl and IUPAC based nomenclature.	151
6.2. Microbial degradation of biphenyl.	153
6.3. Screening of PCB congeners and analysis.	160
6.4. Pictorial representation of binding of top 15 congeners along with biphenyl in the active site.	166
6.5. Structural superposition of the complex structure of 2,3',5'-trichlorobiphenyl-BPD0 complex with biphenyl- BPD0 <sub>B356</sub> complex	172
6.6. Display of 2,3'5'-trichlorobiphenyl-BPDO <sub>B356</sub> complex formation (in ball and stick models).	173





## LIST OF TABLES

1.1. The description of physiochemical properties of common environmental xenobiotic compounds.	5
1.2. Important abiotic and biotic factors influencing the process of bioremediation.	11
1.3. Commonly used phthalates and their basic properties.	14
1.4. Different aspects of health effects related to phthalates exposure.	16
2.1. General properties and uses of DCHP and MCHP.	37
2.2. Molecular docking results showing binding affinities of DEX, DCHP, and MCHP.	41
2.3. Average RMSD and RMSF of hGR-DEX, hGR-DCHP, and hGR-MCHP complexes.	44
2.4. Binding energies of hGR-DCHP and hGR-MCHP complexes calculated by MMPBSA.	50
3.1. Commonly used Phthalates and their usage.	61
3.2. Details of molecular docking results of PAEs-hACMSD complexes.	64
3.3. Average values of RMSD and RMSF of hACMSD-PAEs complexes.	75
3.4. Binding energies of hACMSD-PAEs complexes by MMPBSA.	89
4.1. General characteristics of the isolated strains.	99
4.2. Antibiotic susceptibility tests.	102
4.3. Residual amount (%) of PAEs after 44 hours of bacterial incubation at 30°C and 180 rpm.	104
4.4. Overview of metabolization of different PAEs by <i>Pseudomonas</i> species isolated from different environments.	105
4.5. Identification of DEHP and its intermediate metabolites by gas chromatography-mass spectrometry.	107
4.6. Docking results showing details of ligands used for the molecular docking.	116
5.1. Ramachandran plot statistics for <i>RePDO</i> and <i>RePDR</i> models.	137
5.2. The average RMSD values of the <i>RePDR</i> and <i>RePDO</i> models as well as of the template structures.	139
5.3. Predicted active and passive residues of <i>RePDR</i> and <i>RePDO</i> derived from the WHISCY	140

and CPORT program.	
5.4. Final statistical analysis of <i>RePDR-RePDO</i> complex docking result acquired by HADDOCK.	142
5.5. <i>RePDR-RePDO</i> docking results showing details of important interactions occurring at the interface of the complex.	142
5.6. Conservation scores of important interface interacting residues of <i>RePDR-RePDO</i> docked complex.	144
6.1. General properties of best scoring PCBs.	157
6.2. Binding affinities (kcal/mol) of PCBs.	162
6.3. Distance of mononuclear iron and active site water from proximate ligand ring carbon.	167
6.4. Aromatic interaction of top 15 PCBs, including biphenyl with $\text{BPDO}_{\text{B356}}$ .	169
6.5. Differences in the binding of 2,3',5'- trichlorobiphenyl congener and biphenyl to $\text{BPDO}_{\text{B356}}$	172
6.6. Crystallographic details of 2,3',5'- trichlorobiphenyl- $\text{BPDO}_{\text{B356}}$ complex.	174

## LIST OF ABBREVIATIONS

The following section enlists the various abbreviations and acronyms used throughout the thesis.

AMS	$\alpha$ -amino- $\beta$ -muconate- $\epsilon$ -semialdehyde
AIR	Ambiguous interaction restraints
ATB	Automated Topology Builder
ATCC	American type culture collection
BBzP	Benzyl butyl phthalate
BPA	Bisphenol A
BPDO	Biphenyl dioxygenase
CaCl <sub>2</sub>	Calcium chloride
CoA	Coenzyme A
CMC	Critical micelle concentration
CNS	Central nervous system
CPORT	Consensus Prediction Of interface Residues in Transient complexes
CSI	Carbon specific isotope
Da	Dalton
DCHP	Dicyclohexyl phthalate
DiDP	Diisodecyl phthalate
DMP	Dimethyl phthalate
DEP	Diethyl phthalate
DEHP	Bis(2-ethylhexyl) phthalate
DBP	Dibutyl phthalate
DIBP	Diisobutyl phthalate
DiNP	Diisononyl phthalate
DPHP	Di-2-propylheptyl phthalate
DDT	Dichlorodiphenyltrichloroethane
DEX	Dexamethasone
DTT	Dithiothreitol
DITP	Diisotridecyl phthalate



DOP	Diethyl phthalate
DOPE	Discrete optimized potential energy
DS suite	Discovery studio suite
EDCs	Endocrine disrupting chemicals
EU	European Union
FMN	Flavin mononucleotide
GC-MS	Gas chromatography-mass spectrometry
GR	Glucocorticoid receptor
hACMSD	Human $\alpha$ -amino- $\beta$ -carboxymuconate- $\epsilon$ -semialdehyde decarboxylase
HEPES	4-(2-hydroxyethyl)-1-piperazineethanesulfonic acid
HMW	High molecular weight
IA	Isophthalic acid
IPTG	Isopropyl $\beta$ -D-1-thiogalactopyranoside
KCl	Potassium chloride
$K_{ow}$	Octanol/water partition coefficient
LBD	Ligand binding domain
LMW	Low molecular weight
LOD	Limit of detection
MBP	Monobutyl phthalate
MBzP	Mono-benzylbutyl phthalate
MCNP	Mono-cyclononyl phthalate
MCPA	4-chloro-2-methylphenoxyacetic acid
MCPP	Mono-cyclopropyl phthalate
MEHHP	mono-(2-ethyl-5-hydroxyhexyl) phthalate
MEHP	Mono-(2-ethylhexyl) phthalate
MEOHP	Mono-(2-ethyl-5-oxyhexyl) phthalate (MEOHP)
MEP	Monoethyl phthalate
MiBP	Mono-isobutyl phthalate
MMP	Monomethyl phthalate
MMPBSA	Molecular Mechanic/Poisson-Boltzmann Surface

	Area
MnBP	Mono-n-butyl phthalate
MD	Molecular dynamics
MgCl <sub>2</sub>	Magnesium chloride
MSM	Minimal salt medium
M.wt	Molecular weight
NaCl	Sodium chloride
NAD <sup>+</sup>	Nicotinamide adenine dinucleotide, oxidized form
NADH	Nicotinamide adenine dinucleotide, reduced form
Na <sub>2</sub> SO <sub>4</sub>	Sodium sulphate
NH <sub>4</sub> Cl	Ammonium chloride
NIST	National Institute of Standards and Technology
NPT	Number of particles, pressure, and temperature
NRs	Nuclear receptors
ns	Nanosecond
NVT	Number of particles, volume, and temperature
O.D. 600	Optical density at 600 nm
Pa	Pascals
PA	Phthalic acid
PDC	Dipicolinic acid
PVC	Polyvinyl chloride
PMs	Phthalate metabolite
PAEs	Phthalic acid esters
PAHs	Polycyclic aromatic hydrocarbons
PCBs	Polychlorinated biphenyls
PCDD	Polychlorinated dibenzo- <i>p</i> - dioxin
PCDF	Polychlorinated dibenzofuran
PDB	Protein Data Bank
PCR	Polymerase chain reaction
PDR	Phthalate dioxygenase reductase
PDO	Phthalate dioxygenase oxygenase

PEG	Poly(ethylene glycol)
PME	Particle Mesh Ewald
PMSF	Phenylmethylsulfonyl fluoride
POP	Persistent organic pollutants
PPAR $\gamma$	Peroxisome proliferator-activated receptor gamma
ps	Picosecond
QA	Quinolinic acid
RDO	Rieske dioxygenases
Rg	Radius of gyration
RMSD	Root mean square deviation
RMSF	Root-mean-square fluctuation
SASA	Solvent accessible surface area
SDS-PAGE	Sodium dodecyl sulfate polyacrylamide gel electrophoresis
SPC	Simple point charge
TA	Terephthalic acid
TBT	Tributyltin
TPT	Triphenyltin
TCA	tricarboxylic acid cycle
TF	Tolylfluanid
Tris	Tris (hydroxymethyl) aminomethane
UGT	Uridine-5-diphosphate-glucuronyltransferase
USEPA	US Environmental Protection Agency
WHISCY	What information does surface conservation yield
2,3,7,8 TCDD	2,3,7,8-Tetrachlorodibenzodioxin

## LIST OF PUBLICATIONS

### A) Research papers in Journals

1. **Neha Singh**, Vikram Dalal, Jai Krishna Mahto and Pravindra Kumar. Biodegradation of Phthalic acid esters (PAEs) and in silico structural characterization of mono-2-ethylhexyl phthalate (MEHP) hydrolase on the basis of close structural homolog. *Journal of Hazardous Materials* 338 (2017) 11–22.
2. **Neha Singh**, Vikram Dalal and Pravindra Kumar. Structure-based mimicking of Phthalic acid esters (PAEs) and inhibition of hACMSD, an important enzyme of the tryptophan kynurenine metabolism pathway. *International Journal of Biological Macromolecules* 108 (2018) 214-224.
3. **Neha Singh**, Vikram Dalal and Pravindra Kumar In-silico approach for elucidating toxic effects of high molecular weight phthalate dicyclohexyl phthalate (DCHP) in glucocorticoid receptor mediated adipogenesis (manuscript communicated).

### B) Abstract published in journals

1. An in silico toxicity assessment of DEHP and its metabolites on metabolism of essential amino acid. **Neha Singh**, Vikram Dalal and Pravindra Kumar. **Journal of proteins and proteomics** 8(3), 2017, 49.
2. Binding of Polychlorinated biphenyl to Hormone receptor: an in silico study. Vikram Dalal, **Neha Singh** and Pravindra Kumar. **Journal of proteins and proteomics** (3), 2017 45.

### C) Article in Books

1. Biodegradation of Explosives. Vikram Dalal, Ravi Yadav, **Neha Singh** and Pravindra Kumar. *Environmental Pollution Biodegradation and Bioremediation of the series Envi. Sci. & Engg.* Studium Press, 2017, pp 331-357.

### D) Worksops/Conference/attended and/or poster presentation

1. **Neha Singh** and Pravindra Kumar. In-silico studies on phthalate dioxygenase from *Mycobacterium vanbaalenii* PYR-1. INDO-US International Conference on Recent



advances in structural biology and drug discovery. Indian Institute of Technology-Roorkee, India from October 9-11, 2014.

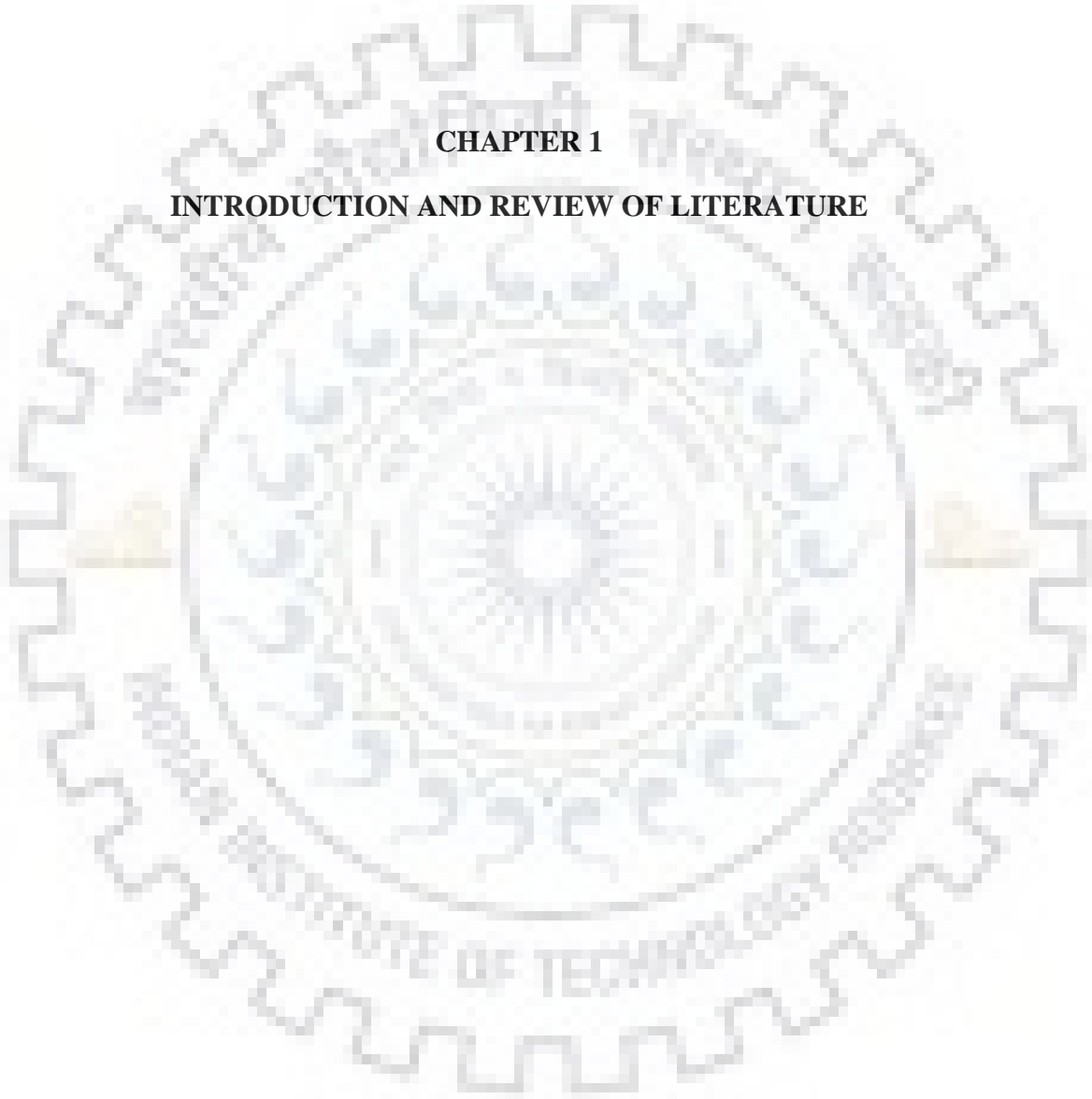
2. International conference on molecular signalling: recent trends in biomedical and translational research. 17-19, 2014 December at Indian Institute of Technology-Roorkee, India.
3. **Neha Singh**, Jai Krishna Mahto and Pravindra Kumar. Identification and Characterization of Phthalates degrading bacterial strains from plastic landfill site. 57th International Annual Conference of the Association of Microbiologists of India & International Symposium on "Microbes and Biosphere: What's New What's Next, p. 154-155, Gauhati University, Guwahati, Assam, India, November 24-27, 2016.
4. **Neha Singh**, Jai Krishna Mahto, Vikram Dalal and Pravindra Kumar. Identification and In Silico Structural Characterization of Mono-2-Ethylhexyl Phthalate Hydrolase on the Basis of Close Structural Homologue. Indian Biophysics Symposium (IBS) 2017, p.148, Indian Institute of Science and Educational Research (IISER), Mohali, Chandigarh, India, March 23-25, 2017.
5. **Neha Singh**, Vikram Dalal and Pravindra Kumar. An in silico toxicity assessment of DEHP and its metabolites on metabolism of essential amino acid. Breaking barriers through bioinformatics & Computational biology 2017, Indian Institute of Technology, Delhi, India, July 31 and August 01, 2017, p.76.
6. Vikram Dalal, **Neha Singh** and Pravindra Kumar. Binding of Polychlorinated biphenyl to Hormone receptor: an in silico study. Breaking barriers through bioinformatics & Computational biology 2017, Indian Institute of Technology, Delhi, India, July 31 and August 01, 2017, p.89.





**CHAPTER 1**

**INTRODUCTION AND REVIEW OF LITERATURE**





## 1.1 Xenobiotic compounds in the environment

Over the last few decades, dependence upon synthetic chemicals has eventually led to their increased production, enhanced application and hence larger amount of their discharge into the environment [1]. Such xenobiotic compounds are synthetic or man-made recalcitrant compounds which are difficult to degrade and are persistent in the environment for a longer period of time. Appropriate determination of chemical persistence is vital for strategic risk assessment and management interrelated to their usage and disposal. These compounds are hazardous in nature and on exposure exhibit the feature associated with acute or chronic toxicity, for example, phenolic compounds, cyanides, several long chain aliphatic compounds, polycyclic aromatic compounds and many more [2].

Biochemically, microorganisms do not synthesize these compounds, so these compounds or their basic structural frame either do not or very rarely found in natural biological products. Therefore, it is to be noted that, during the course of evolution, microorganisms have not encountered these structural compounds, and consequently they have not developed the ability to completely degrade or mineralize these synthetic compounds in the environment [3]. However, few smaller xenobiotic compounds such as low molecular weight halogenated compounds are relatively water soluble and can be anaerobically/aerobically degraded via incorporating different metabolic pathways. There are many recalcitrant environmental chemicals such as Polyhalogenated biphenyls, phthalic acid esters (PAEs), aromatic nitro-compounds, etc. that can be partially mineralized by microorganisms as a sole source of carbon and energy [4]. The description of physiochemical properties of common environmental xenobiotic compounds is shown in **Table 1.1**. Several attempts have been made for microbial enrichments and development of pure cultures and mixed population, that can completely degrade these unsafe chemicals. Several synthetic organic compounds can be removed with the help of microbes after providing appropriate process conditions under normal environmental condition [5]. Therefore, a foremost objective of environmental biotechnology is the eradication and detoxification of these harmful chemicals via the establishment and optimization of highly proficient biological methods that can efficiently utilize the naturally accessible catabolic potential for the same purpose.

## 1.2 Classification of xenobiotic compounds

Large-scale pollution arising as a result of excessive usage of synthetic chemical substances and to some degree by means of natural entities, is raising the alarm on a global scale [1]. As compared to pre-industrial times, there are several factors which contribute to environmental degradation and pollution, such as industrialization with increased use of chemical materials such as, petroleum oil-based products, hydrocarbons (for e.g. aliphatic, aromatic and polycyclic aromatic hydrocarbons (PAHs), halogenated hydrocarbons such as polychlorinated biphenyls (PCBs), perchloroethylene, organophosphorus compounds, nitroaromatic compounds), pesticides, several solvents and heavy metals. Many organic chemicals, due to seepage and continuous run-offs, have entered into a hydrological cycle of volatilization and condensation related to processes of rain, fog or snow formation [6]. It has been reported that about 1.7 to 8.8 million metric tons of oil is discharged into the water bodies globally, and a maximum of this pollution is due to human activities, manual failures, and deliberate waste disposal [7]. Many of the PAHs are mutagenic and toxic in nature and are specifically included in the priority pollutant list of US Environmental Protection Agency (USEPA) (<https://www.epa.gov/eg/toxic-and-priority-pollutants-under-clean-water-act>). These chemicals include PCBs used in hydraulic fluids, adhesives, plasticizers, dielectric fluids used in transformers, flame retardants are reported to be carcinogenic and degrade at a slower pace in the environment [8].

**Table 1.1. The description of physiochemical properties of common environmental xenobiotic compounds.**

S.no	Compound	M.wt	Vapour pressure (Pa)	Half life $T_{1/2}$ (days)	Solubility (g/m <sup>3</sup> )	Log $K_{ow}$	Sources/uses	Ref
1.	Benzene	78	12700	5-16	1800	2.13	Used as an intermediate for the production of other chemicals such as ethylbenzene, cumene, cyclohexane	[9]
2.	Toluene	92.15	2933	4-22	515	2.73	Solvent for paints, used for dinitrotoluene production	[10]
3.	Xylene	106.18	880	7-28	178	3.13	Precursor to terephthalic acid, dimethyl terephthalate	[11]
4.	Naphthalene	128	11.3	1-20	32	3.36	For the production of phthalic anhydride, azo dyes, surfactants	[12]
5.	Anthracene	178.24	0.002266	50-460	0.044	4.45	Organic semiconductor, doping agent in plastic products	[13]
7.	Pyrene	202	0.00033	210-1900	0.132	5.2	Used as yes and dyes precursors	[14]
8.	Benzo(a)pyrene	252.32	0.000000746	530	0.0038	6.06	Tar production and storage, landfills	[15]
9.	Dibutyl phthalate	278.38	0.00133	1-23	13	5.6	Used as a plasticizer	[16]
10.	Bis(2-ethyl hexyl) phthalate	391	0.00086	23	0.34	7.30	Plasticizer in PVCs, cosmetic and medical devices	[17]
11.	2,3,7,8 TCDD	321.96	0.00000000149	590	0.0000079	6.72	Formed as a side product of chlorophenol	[18]
12.	DDT	354.48	0.00002533	730-5708	0.0055	6.19	Developed as an insecticide	[19]



### **1.3 Bioremediation: a strategy for combating xenobiotic compounds**

Bioremediation is defined as a process that makes use of biological entities such as microorganisms, plants, or their relevant enzymes for efficient management of contaminated sites, for recovering or upgrading their original condition [20]. It is to be noted that, remediation in any form, whether biological, chemical or incorporating combination of both strategies, is an improved and cost-effective alternative for controlling and solving the problem of pollution and reducing the load of contamination.

Microorganisms are ubiquitous in nature, have broad diversity and capabilities in their catalytic mechanisms for degradation of different compounds. The basis of microbial transformation is driven by the energy requirements of the organism or may be the need for detoxification of that pollutant or for cometabolism aspect [21]. In general, the progression of bioremediation relies on the metabolic potential of microbial community to transform or detoxify the contaminant, which also depends on the abiotic factors associated with accessibility and bioavailability of the concerned compound [22, 23]. Here within in the following section, the fundamental factors related to bioremediation have been discussed w.r.t. 1.) Bioavailability of organic compound; 2.) Role of bioaugmentation in the treatment of polluted sites; 3.) Innovative approaches in bioremediation and their application; 4.) Utility of probes for supervising and evaluating the effectiveness of bioremediation strategies for contaminated sites.

#### **1.3.1 Bioavailability of organic compound: portion available for microorganism**

The considerable point in the efficacy of the bioremediation process revolves around the constitution of the bioavailable fraction of the pollutant [24]. As the pollutant enters into the soil environment, it tends to rapidly associate itself with a solid phase (organic matter), by means of chemical and physical combination processes. The process of interaction between soil and pollutant includes, sorption of pollutant followed by complex formation and precipitation of the contaminant. Eventually, the capability of soil particles to release (desorb) the pollutant helps in the determination of the propensity of its microbial degradation and hence, this factor influence the effectiveness of bioremediation process [5]. The bioavailability of the pollutant is often restricted by efficient transport of contaminant molecules into a microbial cell. The degradation of a sorbed pollutant occurs via microorganism-mediated desorption process presumably facilitated by biosurfactant

production followed by the development of vertical gradient amid soil solid phase in addition to interfacial pollutant [25-27]. Many reports have also shown that bioavailability of a particular pollutant is species specific and depends upon the capability of particular species to desorb the contaminant to degrade it [28]. The theory of equilibrium partitioning is used for the estimation of the dissolved portion of a contaminant in pore water and several different factors such as aqueous solubility, reactivity, or volatility of contaminants influence their availability in the water and contaminated soils [29, 30].

In case of cultured bacteria, the process of sorption depends upon isolation and enrichment the procedures. The conventional technique is providing the pollutant as a solitary source of carbon in the aqueous bacterial culture medium [31]. It has been observed in case of phenanthrene degradation the use of a polyacrylic porous resin having phenanthrene attached to it led to faster degradation of the organic pollutant. Variation in contaminant bioavailability fraction is observed due to many factors such as chemical nature of the contaminant, various soil types, temperature and water content in the surroundings [30]. The sequestration of contaminants w.r.t. the time depends on various factors such as organic content matter, micropore volume, capacity for cation exchange, surface area and soil consistency [32]. Measurement of bioavailability of pollutant is important for optimization of bioremediation process, however, it becomes difficult, since the lower concentrations of contaminants are present in the soil, the overall absence of baseline values associated with variations in compositional, geological and allocation prototypes of pollutants [33].

Use of surfactants for the treatment of polluted soils is an important strategy as it increases the mass transfer of often highly hydrophobic organic pollutants [34, 35]. These surfactants are amphiphilic molecules that have hydrophilic moieties such as anionic (sulfate or carboxylic groups), cationic groups (quaternary ammonium group) or non-ionic (sucrose) group attached to hydrophobic core content made up of olefins, paraffin, alkylphenols or alcohol. For example, Triton X-100 and Tween 80 are produced from petroleum products. Surfactants having zwitterionic (together anionic and cationic moieties) components have lower values of critical micelle concentration (CMC) values, enhanced activity at the surface and higher solubilization ability. It has been observed that

with the application of surfactants there is an increase in rate of desorption of sorbed pollutants from soils, which makes the pollutants available for remediation [36].

### **1.3.2 Bioaugmentation strategy for remediation of a contaminated site**

Delay in biological response is observed when the remediation site has come across the newer class of pollutant, the one which has not yet been encountered by the local microbiota. Then, the concept of “soil activation” comes into play, which is usually the cultivation of the original biomass from a portion of another polluted site, and its successive application as an inoculum for bioaugmentation for the soil [37]. In such procedure, the soils having modified microbiota via previous exposure to organic pollutants such as hydrocarbons can be utilized as a source of microorganisms for the remediation of freshly contaminated soils. For example, it has been observed that priming of 2% bioremediated soil has increased PAH degradation, in fuel oil treated soil [38]. It is to be noted that, prior to inoculation, pre-adaptation of catabolic bacteria to the target environmental conditions helps in improving the survival rates, and enhance the degradative potential of the microorganisms and leads to improve the remediation of contaminated soil [39]. For example, in case of *Sphingomonas* sp. RW1 having a Tn-5 lacZ transposon was pre-adapted by growing in the soil extract culture medium. This treatment has led bacterium to exhibit better survival rate and increase the efficiency of degradation of soil contaminated with dibenzo-p-dioxin and dibenzofuran, as compared to the bacterium grown in a simple nutrient enriched medium. The continuous exposure to stress in soil condition helps in determination of survival rate and efficiency of microbiota.

It has been observed in the case of PCB contaminated soil that repeated application of carvone-induced bacteria led to enhanced degradation rates [40, 41]. For improvement of bioaugmentation process, researchers have suggested the utilization of microbial mats having stratified communities of microorganisms from different physiological groups can work in a coordinated manner [42, 43].

### **1.3.3 Innovative approaches and their application**

The ultimate fate of the contaminants is often determined by the course of degradation and sorption, which includes together the adsorption taking place on the surface and absorption pertaining to a portion defined by the surface. Availability and accessibility of pollutants to

the microorganisms is an important aspect for the successful treatment of the contaminated site [44]. Several constraints have driven the constant need for the development of innovative remediation methods.

#### **1.3.3.1 Use of compost for the treatment of the polluted site**

The intended use of traditional compost concept for the treatment of contaminated site is important and accomplished either by composting the contaminated soils or direct addition of composted materials for efficient degradation. This technology has been extensively used, for example, the addition of compost materials to herbicides [benthiocarb and 4-chloro-2-methyl phenoxyacetic acid (MCPA)] contaminated soil improved the degradation [45]. The use of spent mushroom waste obtained from *Pleurotus ostreatus* helped in mineralization of DDT contaminated soil [46]. It is to be noted that important parameters regarding use of compost material depends on the type of pollutants and waste material composition utilized for treatment processes. Other factors influencing the efficacy of the treatment depend on the temperature and the appropriate ratio of mixture constituting soil and waste composts [47]. Introduction of compost material to the soil is a sustainable technology as organic material in the waste is utilized for enhanced microbial activity, and thus improving the soil nutrient quality. During the process of composting, processes such as mineralization, volatilization along with the formation of non-extricable bound residues lead to degradation of contaminant. Understanding of various factors related to the nature and activity of specific microorganism in diverse phases of composting, the stability of compost and humus matter, will help in the evaluation of compost material as a successful tool for bioremediation of contaminated site [5].

#### **1.3.3.2 Electrobioremediation**

It is a hybrid methodology which combines the aspects of the bioremediation with electrokinetics for the treatment of hydrophobic organic compounds. It utilizes the application of microbial degradation along with direct current between suitably positioned electrodes for acceleration of pollutant and transport of contaminants [48, 49]. It utilizes weak electric fields of range  $0.2-2.0 \text{ Vcm}^{-1}$  for incorporating basic phenomenon of electrolysis, electromigration, and electroosmosis for efficient remediation [50]. For example, the process of electroosmosis was utilized for transport of *Sphingomonas* sp.

L138 and *Mycobacterium frederiksbergense* to the subsurface for the treatment process [51, 52]. Few factors which are influencing the outcome of electrobioremediation technology are solubility of the contaminant, ratio amid target and non-target ion concentration, toxic electrode effects on microbial metabolism [53, 54].

#### **1.3.3.3 Microbial remediation utilizes the potential of plants**

In general, plants help in the dissipation of organic pollutants by the process of immobilization and promotes microbial degradation. There are limitations associated with microbial remediation such as insufficient subsurface microbial activity, heterogeneity, and bioavailability of the pollutant, toxic effect of contaminant etc., therefore, an association of microbial remediation with phytoremediation enhances the processes of bioremediation [55]. It has been reported that the activity of PAH-degrading microorganisms had increased by root activities [56]. The phyto-production of complex aromatic compounds such as flavonoids, and coumarins help in microbial colonization in roots and as they are structurally similar to PCBs, PAH, this provides a chance for analog-enrichment based stimulation of the degradation pathway in microorganisms [57]. Several secondary plant metabolites such as limonene, carvone, cymene etc., are also pollutant analog and helps in enhanced degradation of PCBs [41, 58]. For example, in case of *Pseudomonas putida* PCL1444, which was isolated from *Lolium multiflorum*, utilizes root exudates for growth and transcription of catabolic genes for naphthalene degradation [59]. The rhizosphere metabolomics-driven approach is an important means for application of enhanced phytoremediation based degradation approaches.

#### **1.3.3.4 Utility of probes for supervising and evaluating the effectiveness of bioremediation strategy of contaminated sites**

Supervision and evaluation of the efficiency of the bioremediation approach is an upcoming and important feature to be considered. Nowadays, there is an advancement in this aspect of remediation technology. For this purpose, 'Conservative markers' are used for the evaluation studies, for example, a compound called dimethyl chrysene can be used for monitoring purposes [60]. As this compound is non-biodegradable, the concentration of specific individual contaminant (which is under case study) can be standardized w.r.t. conservative internal marker. This can be illustrated as a decrease in the relative ratio of



specific contaminant under investigation to the internal marker used during the process of bioremediation. The proper monitoring and efficiency testing require a specific information regarding various factors playing a crucial role in remediation approach. Some of these factors are mentioned in **Table 1.2**.

**Table 1.2. Important abiotic and biotic factors influencing the process of bioremediation.** Some of the important factors involved in determining the fate of organic pollutant bioremediation process in soil and aquatic ecosystems (Adapted from [61])

S.no	Influencing factor	Related effect for the process of bioremediation
1.	Water content of vicinity	Associated with the transport of pollutants and the degraded products;
2.	Temperature of environment	It affects the distribution and composition of microbial communities and influences the rate of degradation; in general, pollutants tend to persist for a longer duration at a lower temperature
3.	pH	Microorganisms and enzymes have been shown to exhibit pH-dependent activity maxima
4.	Redox potential	Concentrations and ratios of electron donors/acceptors in the environment, determine the efficacy of degradative pathways
5.	Solubility factor, volatility rate, particle shape and size, sorption rate, occlusion	All these factors help in the determination of bioavailability of the contaminant for the degradation purpose.
6.	Organic matter composition	This factor influences the process of degradation and sorption/entrapment mechanism
7.	Nutrients availability	This is related to growth and reproduction of degradative microorganisms
8.	Presence of Auxiliary (co-) substrates	These co-substrates enable the process of co-metabolic transformation of contaminants
9.	Co-contaminants	Generally influence the bioavailability of contaminant and enhance/inhibit the process of biodegradation
10.	Microbial communities	Pollutant-tolerant members within microbial communities helps to evaluate and determine the rate of pollutant degradation

Several cultures based and molecular biology techniques like real-time PCR of genes are involved in the degradation of organic pollutants such as naphthalene dioxygenase, toluene mono/dioxygenases, fingerprinting analysis for participating microbial populations. These techniques help in the right evaluation of effectiveness and the state of the site remediation source [62]. Recently, compounds with carbon specific isotope (CSI) has emerged as an important tool for evaluation of bioremediation. In this approach, the lighter isotope is utilized by microbes for its own metabolism and heavier isotopes into the surroundings, thereby resulting in a distinct fractionation profile for  $^{12}\text{C}$  and  $^{13}\text{C}$  [11, 63-65].

Another important parameter which is an essential division of the bioremediation deals with the toxicity feature of the concerned pollutant. One of the aims of bioremediation revolves around the reduction in toxicity aspect of pollutants with the application of remediation approach [30]. Several studies have illustrated that chemical analysis of the pollutant with experimental bioassay is crucial for toxicological assessments [66]. In one such study, related to remediation of atrazine polluted soil, by *Pseudomonas* sp., the efficiency of the approach was assessed by incorporating ecotoxicological endpoints for an overall stability of the ecological system in the study, concerning total plant biomass production, microalgae growth, earthworm reproduction [67]. All the technology used for the remediation of the contaminated site needs the precise utilization of experimental controls and performance indicators for optimization and implementation of regulatory decisions and guidelines.

Substantial research on different chemical pollutants, provides a better understanding of their persistence, recalcitrance and toxicity feature. Keeping in mind the above aspects of bioremediation approach based elimination of pollutants, studies on the structure and function of microbial communities on different spatial and temporal scales have been conducted. The application of the principle of function based remediation to minimize the risk of pollutants. From the above section, it is clear that the strategy of bioremediation is by far the most successful way of remediation of contaminated sites. In the following subsections, two most important pollutant i.e. phthalates (phthalic acid esters, PAEs) and polychlorinated biphenyls (PCBs) will be discussed in brief details.

#### 1.4 Toxicity of phthalates

Phthalates are the esters of 1,2-benzene dicarboxylic acid (o-phthalic acid), having a chemical structure with at least one benzene ring and two specific ester functional group. Phthalic acid esters (PAEs) are formed by the reaction of an alcohol with the phthalic anhydride. The choice of types of alcohol varies from methanol to tridecanol, for the production of various types of phthalates [68]. These alcohols contribute to either straight or branched hydrocarbon chains components of the ester groups in phthalates and generally owe to different properties of phthalates. On the basis of varying carbon chain length, PAEs are classified into two discrete groups; in the first group, an ester chain with 7-13 number of carbon atoms are termed as high molecular weight (HMW) phthalates; and second group comprises of chain of 3-6 carbon atoms in phthalate backbone, are termed as low molecular weight (LMW) phthalates. The most common HMW phthalates are diisodecyl phthalate (DiDP), diisononyl phthalate (DiNP), di-2-propylheptyl phthalate (DPHP), and diisotridecyl phthalate (DTDP) and they are widely used in industry as plasticizers to increase softness, flexibility, elongation, and durability. [69, 70]. Properties of some of the phthalates are shown in **Table 1.3**.



**Table 1.3. Commonly used phthalates and their basic properties.** The details of phthalic acid esters (PAEs) such as DMP, DEP, DBP, DIBP, DEHP and their general basic properties are mentioned.

S.no.	Phthalate group	Phthalates	Molecular weight (g/mol)	Alkyl chain length	Melting point (°C)	Specific gravity (20°C)
1	Low Molecular weight	DMP	194.18	1	5.50	1.19
		DEP	222.4	2	-40	1.12
		DBP	278.34	4	-35	1.04
		DIBP	278.34	4	-58	1.05
2	High molecular weight	DEHP	390.56	8	-40	0.99
		BBzP	312.37	4 and 6	-35	1.11
		DOP	390.57	8	-25	0.98
		DINP	418.6	9	-48	0.97
		DIDP	446.7	10	-46	0.96

These are commonly utilized as plasticizers for the manufacturing and processing of plastic based products. In recent times, these chemicals have acquired a remarkable amount of attention because of their ubiquitous nature and exposure related adverse health effects on ecosystem functioning and human health issues [71-75]. Global assessment of total phthalate metabolite (PMs) levels detected in adult urine samples, from the data published in several studies conducted between 2000 and 2015, are shown in **Figure 1.1**.

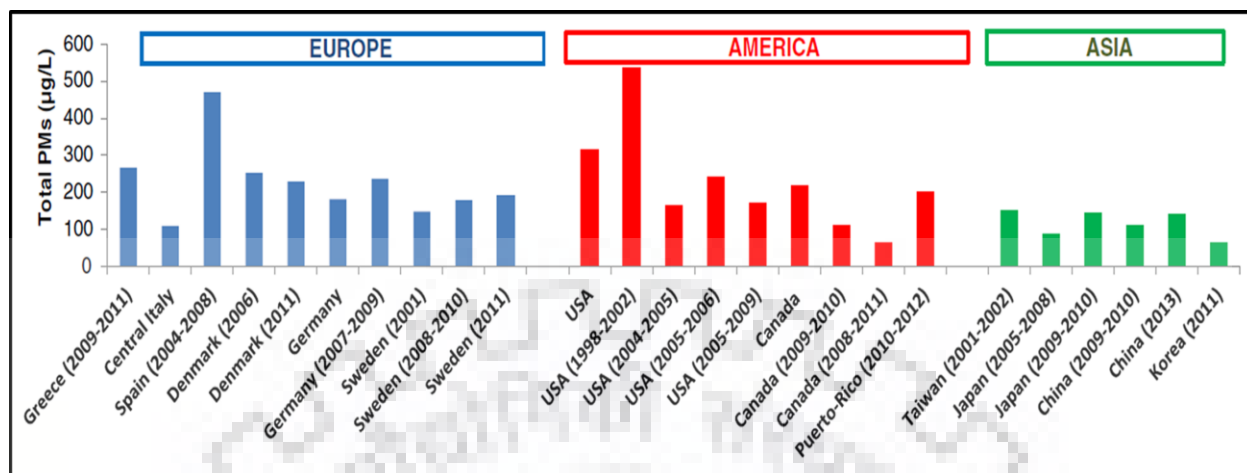


**Figure 1.1. Global distribution of phthalic acid esters metabolites.** The graphical depiction of global comparison of total phthalic acid ester metabolites levels detected in adult urine samples from the studies published between 2000 and 2015 (adapted from [69]).

It has been reported that the interaction between plasticizer and polymer resin is not permanent and these are not chemically bound to the polymer. Under the influence of temperature and pH variation, they tend to leach, migrate or evaporate into the surroundings, including food products and many more [76, 77]. PAEs have been detected in various environments, including atmospheric aerosols and air, solid waste sludge, river and marine sediments [78-80]. This observation suggests that humans are continuously exposed to ingestion, inhalation and dermal exposure to these harmful chemicals [81, 82]. Several fields and laboratory-based studies have illustrated the correlation between the pace of PAEs exposure with that of increased harmful effects, such as in case of reproduction based problems, such as fertility problems, proper development of newborns, etc. [69]. Children toys are made up of a variety of plastics that often use these endocrine-disrupting chemicals such as bisphenol-A (BPA) and phthalates as their building blocks [83]. Phthalates have endocrine disrupting properties and are established reproductive and developmental toxicants. It has also been reported that inhibition of an important enzyme for tryptophan metabolism, human  $\alpha$ -amino- $\beta$ -carboxymuconate- $\epsilon$ -semialdehyde decarboxylase (hACMSD), by phthalates eventually leads to the accumulation of quinolate

[84]. Developmental toxicities effects of several phthalates have already been established. Continuous usage and exposure to these harmful chemicals lead to their bioaccumulation in ecological food chains [85]. Different aspects of health effects related to phthalate exposure are shown in **Table 1.4**. Details of health effects occurring in the different population are reported. Due to their rising health associated risk assessment, six PAEs such as DMP, DEP, DnBP, BBzP, DEHP, and DnOP have been included as priority pollutants in the lists of several bodies such as USEPA, European Union (EU) and Chinese waters list [86-89].

**Table 1.4. Different aspects of health effects related to phthalate exposure.** Details of health effects in the different population are reported. Serious outcomes of phthalate exposure are studied in three different categories of the population; 1. Mother and infant pairs 2. Children and 3. Adults.

S.no	Health effects/Category	Study population	Mean/median range of compounds ( $\mu\text{g/L}$ )	Outcome/consequences	Ref.
<b>1.</b>	<b>Mother/infant pairs</b>				
	<b>Developmental toxicity</b>	201 mother-infant pairs, China	DEP, DBP, DEHP, MEHP, MnBP; median range: 500–2700 (cord blood); 600–2900 (maternal blood); 1.7–5.5 (meconium sample)	Dose-response associations with short birth length (DEHP) and low birth weight associated with (DBP, MnBP, DEHP, MEHP)	[90]
		287 pregnant women, France	MEP, MnBP, MiBP, MBzP, MCPP, MEHP, MEOHP, MECPP, MCNP; median range: 3.1–105.53	Possible involvement of MCNP and birth length	[91]
		391 pregnant women-infant pairs, Spain	MEHP, MEHHP, MEOHP, MECPP, MBzP, MEP, MiBP, MnBP; Median range: 11.0–405 $\mu\text{g/g}$ creatinine	Associations with a lower rate of weight gain (MEHP, MEHHP, MEOHP, MECPP, MBzP)	[92]
	<b>Anti-androgen effects</b>	134 pregnant women-male newborns, USA	MBP, MBzP, MCPP, MEP, MiBP, MMP; median range: 0.7–128.4	Inverse associations with anogenital index (AGD/weight) (MEOHP, MEHHP, MEP, MBzP, MiBP, MnBP)	[93]
		65 pregnant women, Taiwan	MnBP, MEHP, MEP, MBzP, MMP; median range: <LOD-85.2 (amniotic fluid); <LOD-78.4 (urine)	Significant positive correlation between MnBP in the two matrices, a significantly negative correlation between MnBP in amniotic fluid.	[94]
<b>2.</b>	<b>Children</b>				
	<b>Behavioral disorders</b>	1044 children (aged 6–11), Canada	MBzP, MnBP, MCHP, MEP, MEHP, MEHHP, MEOHP, MnOP,	Significant positive associations with emotional symptoms in girls (MBzP) and hyperactivity (MCHP)	[95]

			MMP, MCP, MiNP; mean range: <LOD-33.11		
		122 pregnant women-children pairs (8), Taiwan	MMP, MEP, MnBP, MiBP, MBzP, MEOHP, MEHHP, MEHP; mean range: 20.20–124.5	Positive associations with externalizing problems and aggressive behavior (MEP, MnBP, MiBP, MEOHP, MEHHP, MEHP), significant positive associations with social problems (MEOHP)	[96]
		328 pregnant women-children pairs (7), USA	MnBP, MBzP, MEHHP, MEHP, MEP, MiBP; mean range: 4.95–160.5	Significant inverse associations with IQ scores (MnBP, MiBP), perpetual reasoning (MnBP, MiBP, MBzP), processing speed (MnBP, MiBP), verbal comprehension (MiBP) and working memory (MnBP, MiBP)	[97]
		153 pregnant women-children pairs, USA	MEHP, MEHHP, MEOHP, MiBP, MnBP, MBzP, MEP; mean range: 2.34–81.01	Positive associations with somatic complaints and inverse associations with anxiety problems in girls (MEHHP, MEHP, MEOHP, MBzP) In boys, there were positive associations with attention problems, oppositional/defiant problems, conduct problems, rule-breaking and externalizing behavior (MiBP, MnBP, MBzP).	[98]
	<b>Risk of hypertension</b>	1619 children (6–19), USA	MEP, MnBP, MiBP, MCP, MBzP, MCP, MEHP, MEOHP, MCP, MEHHP, MCP, MiNP	Significant positive association with systolic blood pressure MCP, MiNP) No associations with triglyceride or high-density lipoprotein	[99]
		391 pregnant Women-children (1–7), Spain	MEHP, MEHHP, MEOHP, MCP, MBzP, MEP, MiBP, MnBP; median range: 11.0–405 µg/g creatinine	Significant negative associations with BMI in boys and positive in girls (MEHP, MEHHP, MEOHP, MCP, MBzP)	[92]
		2838 children (6–19), USA	MEP, MnBP, MiBP, MBzP, MCP, MEHP, MEOHP, MCP, MEHHP	Positive associations with systolic blood pressure (MEHP, MEHHP, MEOHP, MCP)	[100]
<b>3.</b>	<b>Adults</b>				
	<b>Impaired semen quality</b>	687 men (32 ± 5.4), China	MMP, MEP, MnBP, MBzP, MEHP, MEHHP, MEHHP, MEOHP, MnOP;	Significant positive associations with decreased sperm volume (MnBP, MEHP, MEHHP, MEOHP), abnormal heads and tails (MBzP), VCL and VSL (MBzP, MEHP, %MEHP) and	[101]

			median range: <LOD-0.85	negative associations with abnormal mid sections (MBzP)	
		1040 men (32 ± 5.36), China	MMP, MEP, MnBP, MBzP, MEHP, MEHHP, MEOHP, MnOP; median range: 0.03–69.89	Significant associations with low sperm concentration and total sperm counts (MnBP), significant positive associations with abnormal sperm heads (MEHP)	[102]
		269 men (22–57), Poland	MEHHP, MEHP, MBzP, MnBP, MEP, MiNP; median range: 1.1–83.4	Significant associations with a decrease in sperm motility (MEHP, MEHHP, MiNP), VSL, VCL (MnBP) and testosterone level (MEHP)	[103]
	<b>Altered reproductive hormone levels</b>	314 men (17–20), Sweden	MEP, MnBP, MBzP, MEHP, MECPP, MEOHP, MEHHP, median range: 0.028–1.1 (serum); 2.8–47 (urine)	Positive associations with semen volume (%MEHP), inverse associations with testosterone and free testosterone (%MEHP), inverse associations with sperm motility (MEHP, MEOHP, MEHHP, MECPP)	[104]
		180 pregnant women (20–42), USA	MnBP, MBzP, MEP, MiBP, MEHP, MEHHP, MEOHP; median range: 2.70–126.40	Associations with testosterone levels (MEHP, MEHHP, MEOHP, MnBP have a positive correlation but MEP has an inverse association)	[105]
	<b>endometriosis</b>	287 women (25–34), USA	MEHP, MEHHP, MEOHP, MECPP, MBzP, MEP, MiBP, MnBP; median range: 1.3–61.9	Significant inverse association with endometriosis risk (MEHP, MEHHP, MEOHP) Non-significant association between MBzP and MEP and increased endometriosis risk	[106]
		1227 women (20–54), USA	MnBP, MEP, MEHP, MBzP, MEHHP, MEOHP; mean range: 3.3–216.2 ng/mg creatinine	Positive (MnBP) and inverse (MEHP) associations with endometriosis and leiomyomata MEHHP and MEOHP were positive associated with endometriosis.	[107]

## 1.5 Biodegradation pathway of phthalic acid esters (PAEs)

The microbial degradation is an important route for the breakdown of DEHP and other harmful PAEs, as their photodegradation and hydrolysis rates are very slow under natural conditions [108]. Nowadays, different methods were adopted for evaluation of substrate removal and product formation during the course of the phthalate degrading reaction. Phthalates degrading microorganisms from the different genera including *Bacillus* sp., *Arthrobacter* sp., *Rhodococcus* sp., *Enterobacter* sp., *Acinetobacter* sp., *Gordonia* sp., *Pseudomonas* sp., and *Sphingomonas* sp. have been isolated from the various environmental samples such as natural contaminated soil and water, sediments, landfills and wastewaters [87, 109-115].

### 1.5.1 Aerobic degradation of phthalic acid esters (PAEs)

Exploration of the PAEs degradation pathways provides the useful link for an enhanced understanding of the complete mineralization progression and unravel the toxicology behavior of phthalate metabolites. Steps involved in the aerobic degradation of phthalic acid esters involve a particular series of reactions which are common to most of the Gram-negative phthalate degrading microbes, as shown in **Figure 1.2**. As it can be seen that during the initial step of phthalate hydrolysis cleavage of ester linkages between alkyl chains and the aromatic ring occurs. Subsequently, the dioxygenase catalyzed reaction differs in Gram-positive and Gram-negative bacteria. It can be seen that phthalic acid ester is converted to protocatechuate via *cis*-3,4-dihydro-3,4-dihydroxyphthalate and 3,4-dihydroxyphthalate in Gram-positive bacteria, whereas in gram-negative bacteria such conversion is mediated by *cis*-4,5-dihydro-4,5-dihydroxyphthalate and 4,5-dihydroxyphthalate. Then protocatechuate is transformed via *ortho* or *meta*-cleavage pathways to organic acids leading to TCA tricarboxylic acid cycle. Most of the aerobic degrading bacteria are from *Arthrobacter* sp., *Pseudomonas* sp., *Sphingomonas* sp., *Burkholderia* sp., *Ochrobactrum* sp., and *Acinetobacter* sp. some of these are also facultative anaerobes, such as *Bacillus* sp., *Serratia* sp. and *Enterobacter* sp [85, 116].

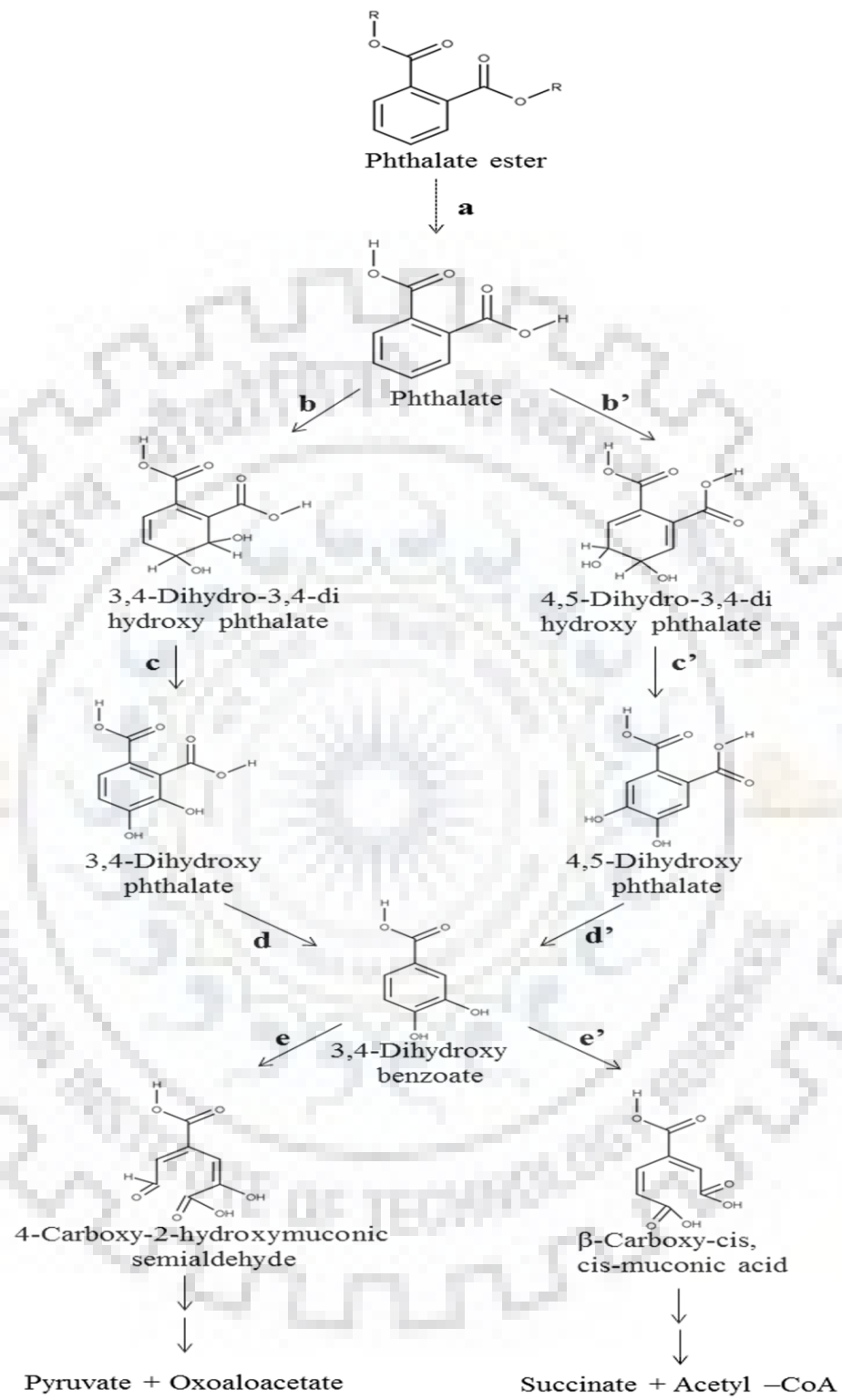




## **Figure 1.2. Steps involved in the aerobic degradation of phthalic acid esters (PAEs).**

Phthalate esterases (a) mediate the first step in which PAEs are degraded to their corresponding phthalic acid. The second step is mediated by 3,4-phthalate dioxygenase (b) in Gram-positive bacteria and 4,5-phthalate dioxygenase (b') in Gram-negative bacteria to protocatechuate(3,4-Dihydroxybenzoate). Degradation of protocatechuate can be mediated by either protocatechuate 3,4-dioxygenase to 4-carboxy-2-hydroxymuconic acid; or to  $\beta$ -carboxy-cis-muconic acid by the action of protocatechuate 4,5-dioxygenase. Final degradation steps lead to the formation of pyruvate and succinate.

### **1.5.2 Anaerobic biodegradation pathway of phthalic acid esters (PAEs)**

Several reports have reported, anaerobic degradation of PAEs is mediated by several classes of bacteria, including *Clostridium* sp., *Bacillus* sp., *Pelotomaculum* sp., *Pseudomonas* sp., and others. Primarily, methanogenic consortia are reported to be involved in anaerobic degradation of PAEs [117]. It has been reported that rate of degradation of short-chain phthalates is higher than that of long-chain phthalate counterparts. De-esterification of PAEs is the primary step in the anaerobic degradation pathway and anoxic metabolic processing of phthalic acid is the rate-limiting step in the anaerobic degradation of phthalic acid esters. Phthalic acid is subsequently biodegraded into benzoate through the process of decarboxylation. Then the ring cleavage of benzoate occurs leading to the formation of CO<sub>2</sub>, H<sub>2</sub>, and acetate [118-120]. In the final step, acetate is converted to methane in the process of anaerobic degradation of PAEs [85].

### **1.6 Important enzymes involved in phthalate degradation**

Different steps of phthalate degradation are mediated by the plethora of enzymes. Details of the important enzymes involved in degradation of PAEs are mentioned.

#### **1.6.1 Role of Esterases in primary degradation of phthalates**

The early step in the degradation of phthalates is phthalate hydrolysis, which is mediated by esterases or hydrolases [121]. This step involves hydrolysis reaction in which phthalate diesters are transformed into phthalate monoesters [122, 123]. These esterases are very specific and inducible in nature and can exist in monomeric as well as dimeric form. For example, a serine hydrolase from *Gordonia* sp. has the conserved signature conserved motif of GX SXG [124].



### 1.6.2 Permeases activity

These enzymes are accountable for the specific transport of PAEs cross the cell membrane in bacteria. These permeases belong to the family of transport proteins. Permease from *Burkholderia cepacia* ATCC17616 and *Pseudomonas putida* NMH102-2 have shown similar with anion-cation symporter family [125, 126]. Multiple genes corresponding to catabolic operon are involved in the functioning of permeases.

### 1.6.3 Phthalate dioxygenase (PDO) system

The key step involved in degradation of PAEs is hydroxylation of phthalate isomers. This crucial step is mediated by ring-hydroxylating dioxygenases. Phthalate 4,5-dioxygenase is a well-characterized enzyme from Gram-negative bacteria, *Burkholderia cepacia* DB01 [127]. It has been reported to have two important components: First is flavin-iron-sulfur containing monomeric phthalate dioxygenase reductase (PDR) protein. It has FMN binding domain and plant type ferredoxin type [2Fe-2S] center and it requires NADH as a cofactor for its activity [128]. The crystal structure of PDR from *Burkholderia cepacia* is resolved at 2.0 Å (PDB ID: 2PIA). This important protein is involved in the transfer of electrons from [2Fe-2S] center of PDR C-terminal to the Rieske type [2Fe-2S] center of phthalate dioxygenase reductase (PDO), a second important component of PDO system [129]. In *Burkholderia cepacia* DB01 PDO is a non-heme homotetrameric protein having one Rieske-type [2Fe-2S] center and one mononuclear iron center, present at the actual site of double hydroxylation of the phthalate aromatic ring.

### 1.6.4 Protocatechuate dioxygenase

This enzyme is a very important ring cleavage enzyme, which is involved in the breakdown of ring aromaticity and produces aliphatic intermediates which eventually enters the central carbon metabolic cycle. On the basis of a specific position of ring cleavage, the enzyme can be classified as protocatechuate 3,4-dioxygenase (*ortho*, EC. No. 1.13.11.3) or protocatechuate 4,5-dioxygenase. Both of these are well-characterized iron-dependent heterodimers with  $\alpha$  and  $\beta$  subunits. In both types of protocatechuate dioxygenase, different architecture of active site residues is involved in specificity associated with substrate metabolism [130-132].

### 1.7 Toxicity of polychlorinated biphenyls (PCBs)

Polychlorinated biphenyls (PCBs) are persistent environmental organic pollutants which have biphenyl aromatic backbone structure with one to ten substitutions of chlorine atoms, yielding theoretically total 209 PCB configurations (congeners). PCBs have flame resistant properties and have chemical and thermal stability. Due to their stability and slow degradation rate, they eventually tend to accumulate in the ecosystem and pose a great threat to human health [133]. PCBs are lipophilic and highly persistent environmental polluting chemicals and are of great concern due to their adverse toxic effects on organisms. Due to their widespread industrial utilization as heat transfer fluids, solvent extenders, hydraulic fluids, etc., they have been detected in various environmental samples such as soils, sediments, indoor air, blood and human adipose tissues. Several non-coplanar PCB congeners affect biological actions that contribute to toxicity from environmental exposures to PCBs. They can easily accumulate in the food chain and present a high risk of environmental contamination and toxic effects for human and animal health [134, 135]. Most of the accumulating PCB congeners in environmental matrices are having penta, hexa or hepta chlorinated substitutions used in the commercial formulations, 'aroclers'. The numbering and nomenclature (ortho-, meta-, para-) convention of PCBs w.r.t. biphenyl nucleus, are shown in **Figure 1.3**.

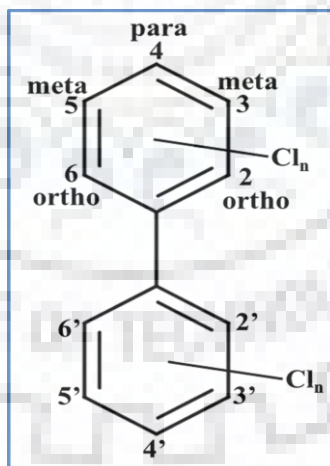


**Figure 1.3. Numbering and nomenclature of PCBs.** The numbering pattern and nomenclature (ortho-, meta-, para-) convention of PCBs w.r.t. biphenyl nucleus is shown.

It has been reported that PCBs can cross the placental barrier and enter into the fetus inside the mother during the gestation period. These chemicals are associated with a broad spectrum of biological consequences which includes, interaction with the endocrine system and also involved in developmental toxicity [136]. Several studies have established a correlation between prenatal and postnatal PCB exposure related to neurodevelopmental disorders [137]. They have been reported to have interaction with estrogen/androgenic receptors, thyroid receptors. There have been many reports illustrating the interaction of hydroxyl-PCBs and thyroid hormone-binding proteins such as transthyretin (TTR), which eventually leads to displacement of  $T_4$  from its TTR receptor and is often associated with increased TSH level [138-140]. Moreover, PCBs have been involved in the induction of activity of liver enzymes such as e.g. uridine-5-diphosphate glucuronyltransferase (UGTs) [141].

Toxicokinetics studies provide a systemic relationship between exposure of a compound in humans and experimental animals to its toxicity aspect and related environmental risk assessment. Several toxicokinetics studies have shown that the rate of metabolism and excretion of PCBs in humans is slow, as owing to longer half-lives and lipophilic properties of certain PCB congeners [142]. Intestinal absorption of PCBs was also accounted in the breast-fed infants population [143]. This study reflected the great extent of accumulation of PCBs in mammary adipose tissues which gets mobilized during the course of lactation. PCBs can easily cross the placental barrier and their presence has been detected in human cord serum, placental, and fetal tissues [144]. Other plethora of toxicological effects include dermal effects, chronic bronchitis, liver effects and many more [145-147].

### **1.8 Biodegradation of PCBs**

Microorganisms play an important role in biodegradation of PCBs by producing metabolic enzymes, which eventually modify these persistent organic halogenated pollutants to smaller and simpler counterparts. In nature, there are two complementary distinct biodegradation processes involved in the biotransformation of the polychlorinated biphenyls (PCBs) [148]. These processes include an anaerobic reductive phase and aerobic oxidative phase. In the process of anaerobic PCB dechlorination phase, conversion of highly chlorinated PCBs to less chlorinated ortho-enriched congeners [149]. In the

subsequent aerobic degradation process, products from the anaerobic process are readily degraded [150].

For complete degradation of PCBs in natural soil and water environment, there is a combination of degradation process involving anaerobic microorganisms responsible for reductive dehalogenation and aerobic microorganisms involved in further complete biodegradation of halogenated congeners [151]. The rate of PCBs biodegradation is influenced by various environmental abiotic factors such as pH, temperature, accessibility to suitable electron acceptors, presence of toxic compounds, important interactions among microorganisms [152].

### **1.8.1 Anaerobic transformation of PCBs**

In this process, reductive dehalogenation of organic polychlorinated biphenyls (PCBs) compound takes place. In this transformation, organic halogenated compound serves as a source of an electron acceptor and the respective halogen substituent is exchanged with hydrogen [149, 153]. Thus, microorganisms that could efficiently utilize PCB congener as a terminal electron acceptor, generally participate in this phase of biotransformation [154]. This process of dechlorination can attack a large variety of chlorinated aromatic as well as aliphatic hydrocarbons. Some of the isolated anaerobic dechlorinated bacteria involve, *Desulfomonile tiedjei*, *Desulfitobacterium*, *Dehalobacter restrictus*, *Dehalospirillum multivorans*, [155, 156]. The steps involved in anaerobic degradation of PCBs in *Dehalococcoides*, are shown in **Figure 1.4**.

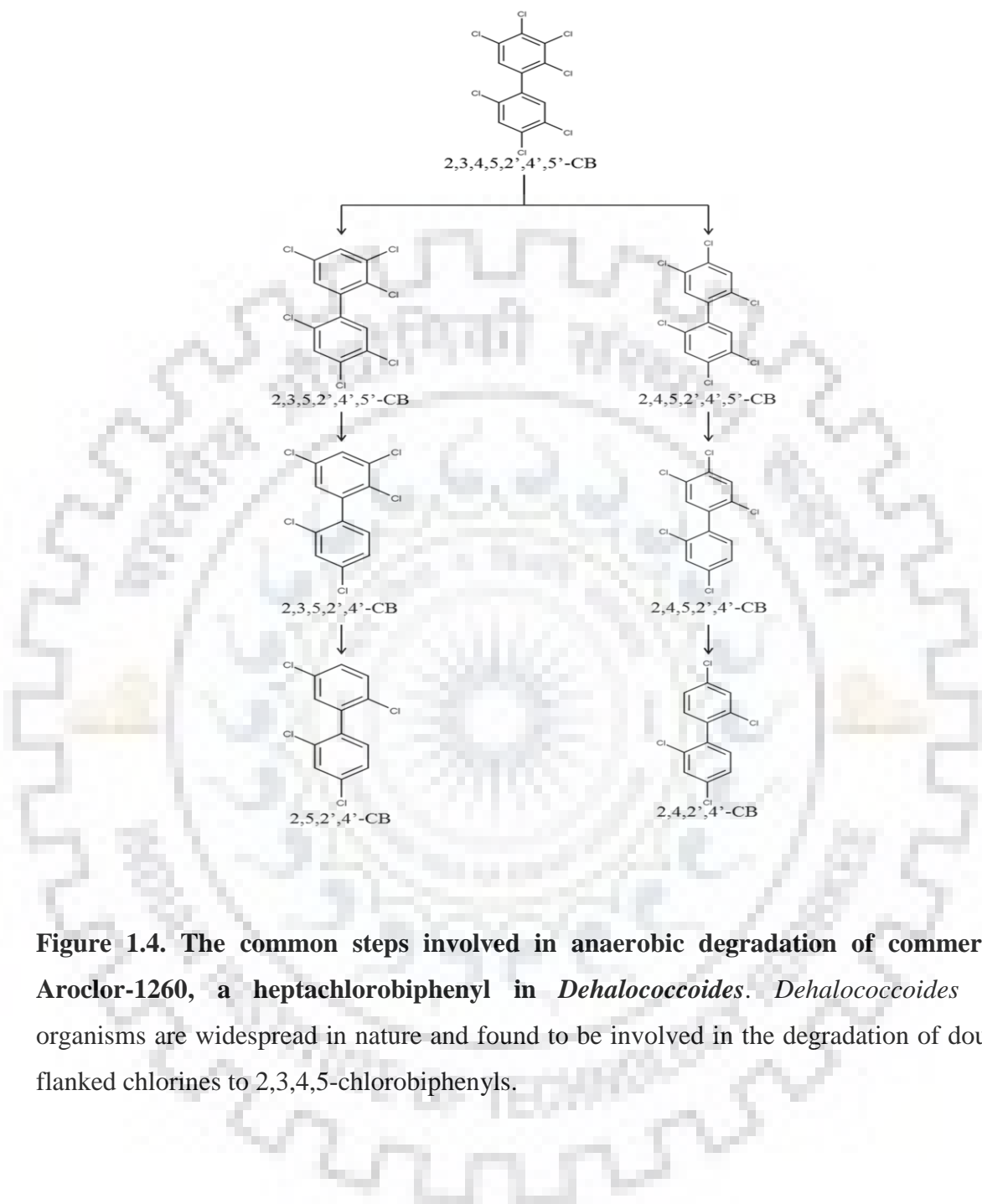


**Figure 1.4. The common steps involved in anaerobic degradation of commercial Aroclor-1260, a heptachlorobiphenyl in *Dehalococcoides*.** *Dehalococcoides* like organisms are widespread in nature and found to be involved in the degradation of doubly flanked chlorines to 2,3,4,5-chlorobiphenyls.

The basis for congener selectivity and residual activity for the dehalogenation depends on the type of microorganism harboring distinctive dehalogenating enzymes. In laboratory scale experiments, it has been observed that the rate of dechlorination of available commercial PCBs tends to decrease with the increase in the chlorination pattern [154]. It has also been seen the presence of organic substrate as electron donors such as electron-rich alkenes, pyruvate, and acetate have increased the rate of dechlorination [157]. On a similar scale, the presence of electron acceptors in the reaction medium tends to decrease the rate of dechlorination [149]. This is because electron acceptors such as sulfate, bromomethane sulfonate, generally compete with PCBs and pose selective pressure on microorganisms. Temperature and pH also play an important role in the pattern of dechlorination and have significant role in the growth and subsequent metabolism of PCBs in microorganisms. The process of reductive dehalogenation is very important as it lowers the risk associated with polychlorinated biphenyls (PCBs) [158]. Firstly, it led to the production of PCBs with less halogen substitution, which can be readily used by the indigenous bacterial population for further degradation. Secondly, this process leads to the reduction of the ecological bioconcentration potential of PCB mixture which implies that, this anaerobic process reduces the risk associated with bioaccumulation of highly substituted PCBs in the food chain [159].

### **1.8.2 Aerobic transformation of PCBs**

For aerobic bacterial degradation, less chlorinated PCB congener, resulting from anaerobic reductive dechlorination of highly chlorinated congener, acts as substrates. Two genes clusters are actively involved in complete aerobic oxidative degradation of PCBs. The first cluster involved the genes responsible for the biotransformation of PCBs cluster to chlorobenzoic acid and the second clusters harbor the genes for further biodegradation of chlorobenzoic acid [160, 161]. The metabolic pathway involved in PCB degradation and *bph* gene cluster organization in *Pseudomonas pseudoalcaligenes* KF707, is shown in **Figure 1.5**.

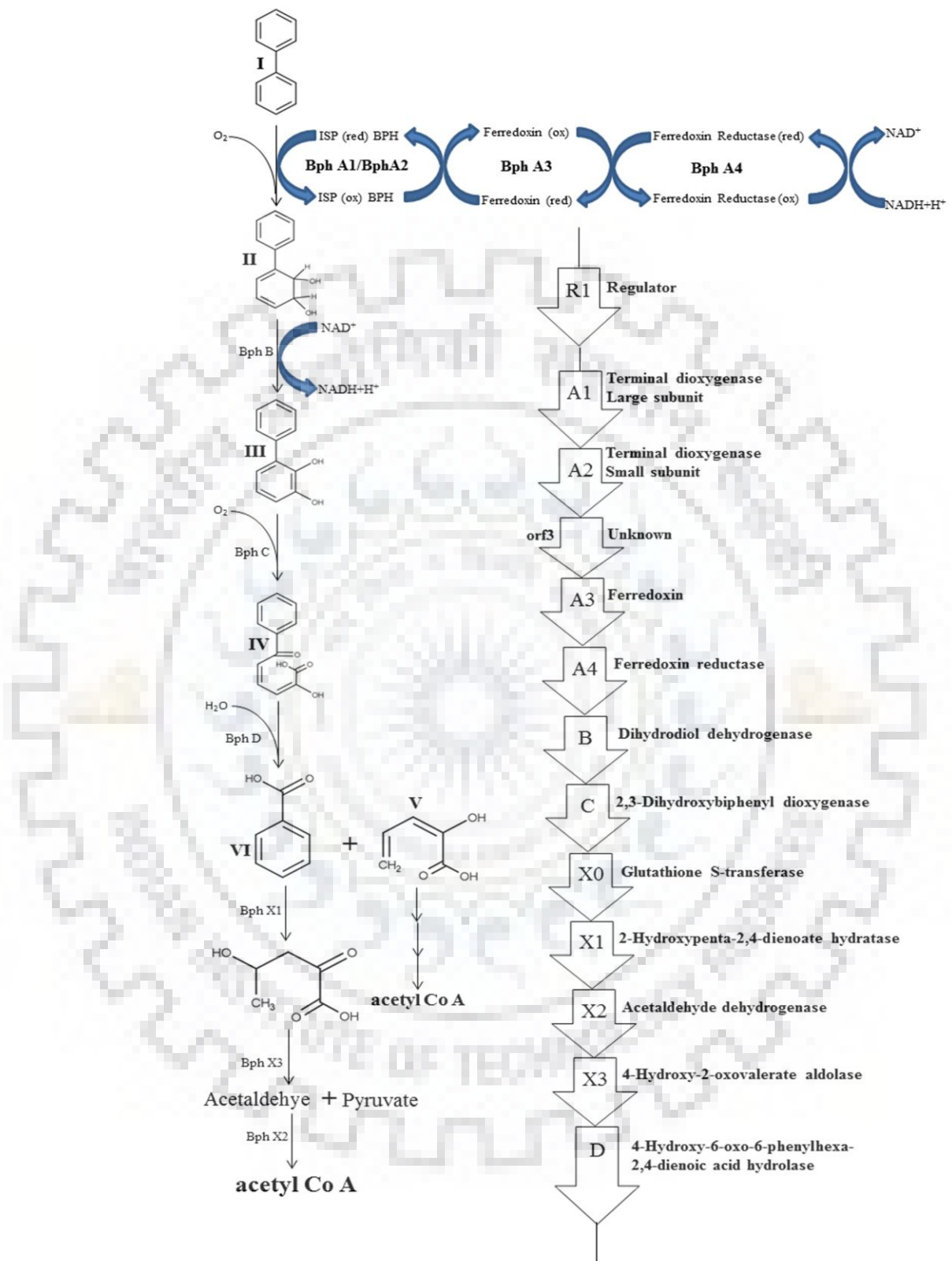


**Figure 1.5. The metabolic pathway involved in PCB degradation.** Compound I corresponds to biphenyl which is degraded to 2, 3-dihydroxy-4-phenylhexa-4.6-diene (II),



by the action mediated by enzymes (BphA) from the gene products from A1 to A4. Then this, dihydrodiol compound is degraded to 2,3 dihydroxybiphenyl (III) by dihydrodiol dehydrogenase (BphB). It is further degraded to 2-hydroxy-6-oxo-6-phenylhexa-2,4-dienoic acid (IV), mediated by Bph C. The latter is converted by benzoic acid (V), by the action of BphD. Further, degradative steps involved in complete degradation of benzoic acid, leads to the formation of acetyl CoA are also shown.

In brief, it can be seen the insertion of molecular oxygen occurs at 2,3 of less chlorinated or non-chlorinated PCB ring which led to the formation of (2,3-dihydroxy-4-phenylhexa-4,6-diene) cis-dihydrodiol compound by the action of oxygenase, encoded by genes for biphenyl 2,3-dioxygenase (bphA1A2A3A4), in *Pseudomonas putida* LB400. The first reaction of the degradation is initiated by biphenyl 2,3-dioxygenase, which belongs to the superfamily of Rieske non-heme iron dioxygenase. This enzyme consists of terminal oxygenase composed of large  $\alpha$ - and smaller  $\beta$ -subunit, a ferredoxin component and ferredoxin reductase. The latter two act as an electron transport system and mediate the transfer of electrons from NADH to terminal oxygenase. Subsequently, these dihydrodiols are dehydrogenated by cis-2,3-dihydro-2,3-dihydroxybiphenyl dehydrogenase (dihydrodiol dehydrogenase, bphB) to give 2,3-dihydroxy biphenyl. Then by the action of 2,3-dihydroxy biphenyl dioxygenase (bphC), 2,3-dihydroxy biphenyl is cleaved to yield 2-hydroxy-6-oxo-6-phenylhexa-2,4-dienoate, a meta cleavage product. Then, this meta-cleavage product is hydrolyzed by 2-hydroxy-6-oxo-6-phenylhexa-2,4-dienoate hydrolase (HOPDA Hydrolase, bphD) to chlorobenzoic acid [150].

The complete biodegradation of PCBs requires the contribution from mixed type of microbial population along with their specific congener preferences. It is to be noted that, position and number of chlorine substitutions on particular PCB congener also influence the rate of biodegradation [162]. It has been reported that, accession to enzyme's active site is hampered by the bulkiness of chlorine substitutions in higher PCBs [163]. The position of a chlorine atom is also very crucial, as it is observed that, many aerobic PCB degrading bacteria have the ability to initiate the degradation process by initial attack of oxygenase for 3,4 dihydroxylation instead of 2,3-dihydroxylation, as shown in **Figure 1.6** [164]. This has been observed in the case of *Pseudomonas putida* LB400 and *Pandoraea pnomenusa* B356 . It is to be noted that no single organism can biodegrade polychlorine substituted biphenyls



as such, therefore, a mixed microbial consortium is needed for complete microbial synergism and cometabolism based degradation. This strategy increases the rate of overall degradation, as in mixed cultures complete degradation is the result of the mutual attack at different sites of concerned PCB congener [150].

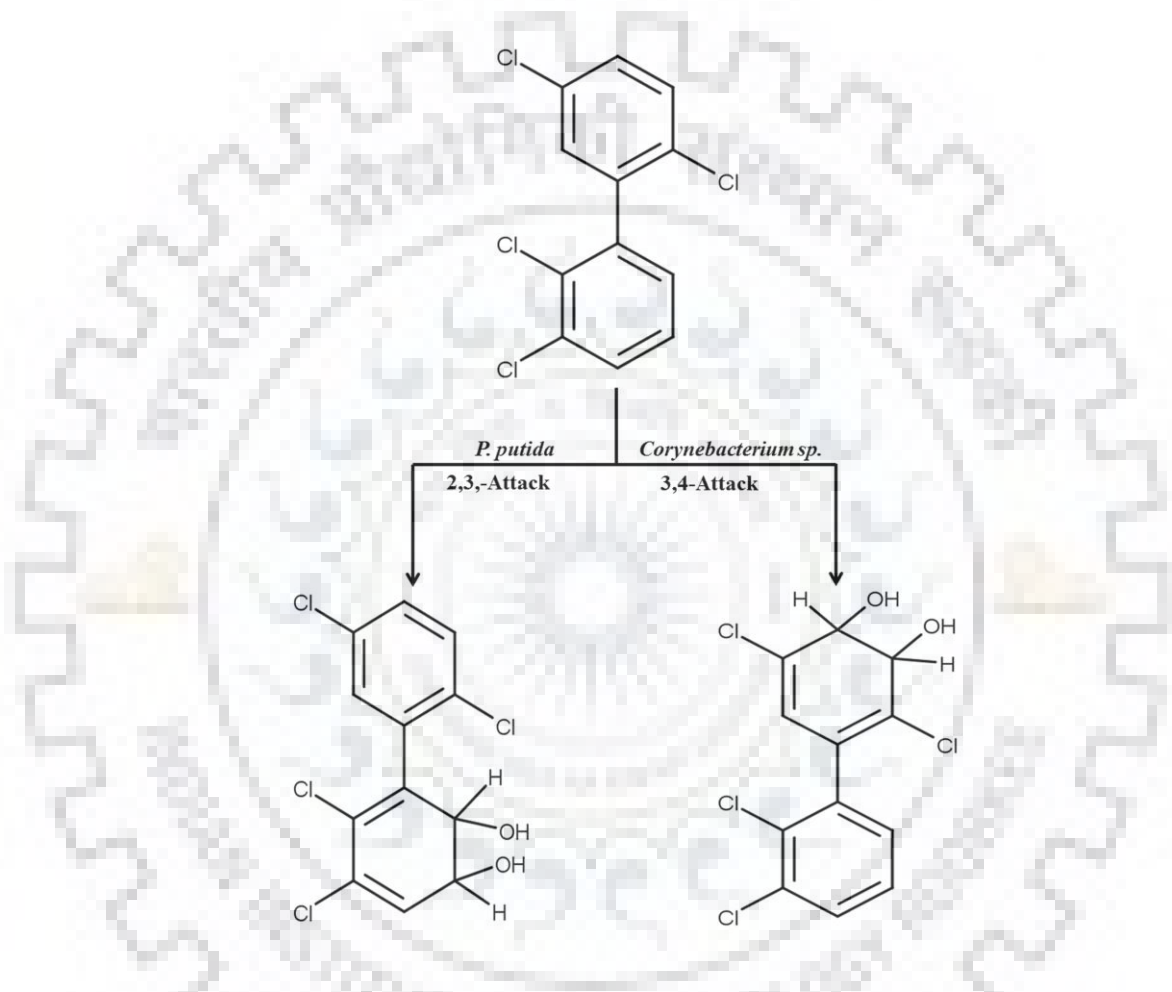


**Figure 1.6. The specific nature of PCB degradation in different microorganisms (adapted from [65]).** *P. putida* degrades PCB congener, a tetrachlorobiphenyl via 2, 3-attack; and a *Corynebacterium sp.* degrade the same congener via 3, 4-attack.

On the basis of the analysis of various biphenyl-degrading isolates, it could be illustrated that lower chlorinated PCB congeners are more readily transformed as compared to their higher chlorinated PCB congeners counterparts, and congeners with chlorine substitutions only on one aromatic ring only are more easily degraded than those having chlorine substituents on both PCB aromatic rings [165].







**CHAPTER 2**

**IN-SILICO APPROACH FOR ELUCIDATING TOXIC EFFECTS OF HIGH  
MOLECULAR WEIGHT PHTHALATE DICYCLOHEXYL PHTHALATE (DCHP)  
IN GLUCOCORTICOID RECEPTOR MEDIATED ADIPOGENESIS**

## 2.1 Introduction

Over the past few decades, the occurrence of the metabolic disorders related to obesity, high blood pressure and diabetes in humans has significantly increased [166-168]. Around the globe, within the same course, a parallel increase in the production and usage of xenobiotic compounds has also increased [169, 170]. Many xenobiotic compounds present in the environment such as genistein, bisphenol A, organotin (TBT, TPT), and phthalates exhibit endocrine disrupting properties [171-175]. Several reports have shown that regular exposure to these xenobiotic chemicals may lead to the alteration in metabolic programming linked to adipose biology and obesity [176-179]. These generalizations have been included in the hypothesis of obesogen theory, revolving around the existence of chemical “obesogens” molecules that inappropriately regulate lipid metabolism and adipogenesis and eventually promotes obesity [180, 181].

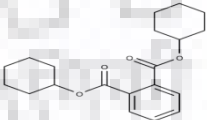
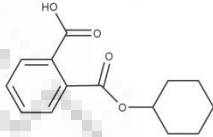
Phthalates or phthalic acid esters (PAEs) are commonly used in a variety of industrial and household products including lubricants, paints, and flexibility agent in PVC plastics, etc. [182-184]. Several microbial studies have elucidated, the role of microorganisms in the degradation of these harmful xenobiotic compounds [85, 115, 116, 185-187]. It has been reported that phthalates have teratogenic and anti-androgenic properties and interfere with male reproductive development [188-190]. Several computational studies have shown that phthalates can interact with nuclear hormone receptors such as peroxisome proliferator-activated receptor gamma (PPAR $\gamma$ ), androstane receptor, estrogen receptor, progesterone receptor and important enzyme systems such as human  $\alpha$ -amino- $\beta$ -carboxymuconate- $\epsilon$ -semialdehyde decarboxylase (hACMSD) in tryptophan metabolism pathway [84, 191-195]. In different case studies, measurable phthalate concentration in urine and breast milk samples, have been linked to genital alterations and changes in reproductive hormone levels [196-198]. Their omnipresence and continuous exposure have prompted concern over their enduring endocrine disrupting properties.

A precise link has been established between specific urinary phthalate metabolite concentration and increased waist circumference along with insulin resistance, which shows the obesogenic nature of phthalates [199-201]. Several studies propose that such phenotypic changes are mediated by the capability of phthalates such as mono-(2-ethylhexyl) phthalate (MEHP), monoethyl phthalate (MEP), butyl benzyl phthalate (BBzP),

and monobenzyl phthalate (MBzP) etc. acting as an agonist for PPAR $\gamma$  mediated adipogenesis [202]. Generally, phthalates are considered to disrupt lipid metabolism, by activation of PPAR $\gamma$  mediated adipogenesis in preadipocytes [171, 203]. Therefore, phthalates, with their ubiquitous existence can be linked to unregulated stimulation of PPAR $\gamma$  and induction of an associated adipogenic response.

The second aspect of adipogenesis deals with glucocorticoid signaling which is essential for adipocyte differentiation [204, 205]. The glucocorticoid receptor (GR) is activated by steroid hormone and generally controls the regulation of genes related to glucose homeostasis, cell differentiation and bone turnover [206]. Regulation of glucocorticoid hormone levels is also an important feature in the hypothalamic-pituitary-adrenal alliance, which coordinates and monitors metabolism in peripheral and stress responses [207]. It has been shown that the varieties of endocrine disrupting chemicals (EDCs) were checked for their glucocorticoid-like activity by means of a luciferase reporter assay in 3T3-L1 preadipocytes. Four of the tested EDCs i.e. bisphenol A (BPA), endrin, tolylfluanid (TF) and dicyclohexyl phthalate (DCHP) activate GR, without significant PPAR $\gamma$  activation [208]. From here, it is interesting to unravel the fact that phthalates can efficiently utilize another pathway in a synergistic manner for activation of glucocorticoid receptor-mediated adipogenesis. In this particular study, DCHP a high molecular weight phthalate has been shown to stimulate adipogenesis in 3T3-L1 preadipocytes in the low picomolar range concentration. Properties of DCHP and its monophthalate metabolite mono-cyclohexyl phthalate (MCHP) are mentioned in **Table 2.1**.

**Table 2.1. General properties and uses of DCHP and MCHP.** Molecular structure of DCHP and MCHP have been shown along with their respective molecular weight.

Properties	DCHP	MCHP
Molecular weight	330.424 g/mol	248.278 g/mol
Molecular formula	C <sub>20</sub> H <sub>26</sub> O <sub>4</sub>	C <sub>14</sub> H <sub>16</sub> O <sub>4</sub>
Molecular Structure		
Uses	<ol style="list-style-type: none"> <li>1. Used in cosmetic products</li> <li>2. Plasticizer ingredient in nitrocellulose, ethyl cellulose, vinyl cellulose, and resins</li> <li>3. Added with poly (methyl Methacrylate) in amorphous thermoplastics</li> </ol>	

Although, this study has revealed that DCHP is involved in glucocorticoid-mediated adipogenesis in 3T3-L1 cells, but the elucidation of the binding mode and important interactions of DCHP with human glucocorticoid receptor (hGR) has not been accounted yet. Therefore, this computational study highlights the toxic effects of DCHP and its monophthalate metabolite, MCHP with human glucocorticoid receptor which may eventually lead to the initiation of glucocorticoid-mediated adipogenesis pathway. The crystal structure of the hGR ligand binding domain with agonist dexamethasone (DEX) (PDB ID: 4UDC) is available [209]. The overall structure of the hGR ligand binding domains has 11  $\alpha$  helices as well as 4  $\beta$  strands that are folded into a three-layered helical domain.

Therefore, in this study, computational techniques like molecular docking and simulation were used to investigate the binding mode and stability of DCHP-hGR and its monophthalate metabolite MCHP-hGR complexes. Overall results illustrate that DCHP and MCHP can efficiently bind and can activate hGR mediated adipogenesis.

## 2.2 Material and methods

### 2.2.1 System preparation and Molecular docking of ligands

The crystal structure of human glucocorticoid receptor (hGR) is used as a model to investigate binding modes of high molecular weight phthalate DCHP and its monophthalate metabolite MCHP. For that purpose, crystal coordinates of the hGR ligand binding domain (from residues 500- 777), in complex with bound agonist dexamethasone (DEX) was retrieved from RCSB Protein Data Bank (PDB ID: 4UDC) [209]. The receptor was geometrically optimized by utilizing the Clean Geometry module of Discovery Studio (DS) 4.0 suite provided by Accelrys (San Diego, CA, USA). The structure was energy minimized for 1000 steps by using a smart-minimizer algorithm with 0.1 RMS gradient cutoff [210]. The initial 3D structures of DCHP and MCHP were sketched using Marvin suite 17.13 [<http://www.chemaxon.com/marvin/sketch/index.jsp>] and minimized using DS suite.

To envisage the interaction of hGR with phthalates, automated ligand-receptor docking calculations were carried out by using AutoDock Tools 4.0 and AutoDock Vina 1.1.2 [211, 212]. Receptor and ligand molecules were prepared by adding hydrogen molecules and associated Kollman and Gasteiger charges, respectively. The spacing of 0.375 Å was used for the generation of atomic potential grid map. Catalytic key residues, such as Asn564, Gln570, Arg611, Gln642, Cys736, and Thr739 were used for constructing docking receptor grid box. The final dimensions of the grid box were 70 Å × 70 Å × 70 Å and the center point coordinates were set as X = 0.56, Y = -12.94 and Z = 2.77. Lamarckian genetic algorithm and grid supported energy evaluation method were adopted for docking purpose with total 100 GA runs. The pose having the maximum binding affinity score and corresponding interaction with the key residues was selected and further analyzed in PyMol 1.3 [213]. Important hydrophobic interactions involved during complex formation were analyzed and compared using Maestro 11.2 (Schrödinger Release 2017-4: Maestro, Schrödinger, LLC, New York, NY, 2017).

### **2.2.2 Molecular dynamics simulation**

Molecular simulation studies were performed in order to evaluate the stability and flexibility of the phthalates-hGR complexes within a precise hydration environment. The associated structural and dynamic changes occurring at the atomistic level in glucocorticoid receptor on the binding of DCHP and MCHP were analyzed. All the simulation-based study was performed with Gromacs 5.1.4 suite with GROMOS96 54A7 force field on a



LINUX based workstation [214, 215]. Automated Topology Builder (ATB) was used for the generation of ligand topology files [216, 217]. The protein complexes were solvated in a cubic box of volume 534.76 nm<sup>3</sup> with simple point charge (SPC) waters and three Na<sup>+</sup> counterions were added by using “genion” tool for ensuring the neutrality of the system. In the next step of energy minimization, the steepest descent algorithm was used for 50,000 iteration steps with cut-off up to 1000 kJmol<sup>-1</sup>. The system was equilibrated in two different phases and LINCS algorithm was used for covalent bond constraints. The NVT phase of equilibration was performed with a constant number of particles, volume, and temperature, each step 2 fs. In a similar manner, the NPT phase of equilibration was done with a constant number of particles, pressure, and temperature, at 300 K with Parrinello-Rahman pressure coupling method. For calculation of short-range interactions, such as Lennard-Jones and Coulomb interactions, 1.4 nm radius cut-off was used. Particle Mesh Ewald (PME) method was employed for long-range electrostatics with Fourier grid spacing of 1.6 Å was utilized. The constant temperature of the system was maintained by using V-rescale, a modified form of Berendsen temperature coupling method. The final production step of molecular dynamics simulation was carried out for 20 ns, each step of 2 fs. The results of MD simulations were analyzed in terms of the stability of the trajectory, hydrogen bond analysis, and conformational flexibility of DEX-hGR and PAEs-hGR complexes.

### 2.2.3 MMPBSA binding free energy calculations

The Molecular Mechanic/Poisson-Boltzmann Surface Area (MMPBSA) method was utilized for the computation of binding energies of the complexes which employ ensembles derived from molecular dynamics (MD) simulation [218]. The trajectories related to stable equilibrium state were selected for the calculation of corresponding binding energy. In the GROMACS module, the g\_mmpbsa application is used for the estimation of different components of the binding free energy of DEX-hGR and PAEs-hGR complexes.

In general, the binding free energy,  $\Delta G_{\text{bind}}$ , was computed using Equation (1) from the free energy of the receptor-ligand complex ( $G_{\text{rlc}}$ ) with respect to the unbound receptor ( $G_{\text{rec}}$ ) and ligand ( $G_{\text{lig}}$ ):

$$\Delta G_{\text{bind}} = G_{\text{rlc}} - (G_{\text{rec}} + G_{\text{lig}})$$

On the basis of a complete thermodynamic cycle, MM-PBSA allows the calculation of the binding free energy, including ligand and protein desolvation energies. Here, the binding energy involves the average of potential energy in the vacuum, polar-solvation energy, and non-polar solvation energy, respectively. In the present study, at equilibration state, snapshots for every 10 ps between 15 and 20 ns were assembled and MMPBSA was performed to predict the binding energy.

## 2.3 Results

### 2.3.1 Molecular docking of the ligands

As shown in **Figure 2.1**, high molecular weight diphtalate DCHP and its monophthalate counterpart MCHP, were successfully docked into the active site pocket (volume 599 Å<sup>3</sup>) of the human glucocorticoid receptor. Best binding poses were clustered and selected according to their binding affinity score, and the orientation within the active site. The AutoDock and AutoDock Vina results are shown in **Table 2.2**. Autodock and Autodock Vina binding affinity scores for DCHP are -7.17 (kcal/mol) and -8.6 (kcal/mol), respectively. Similarly, MCHP has a lower binding affinity as compared to DCHP and its Autodock and Autodock Vina binding affinity scores are -5.24 (kcal/mol) and -7.5 (kcal/mol), respectively.

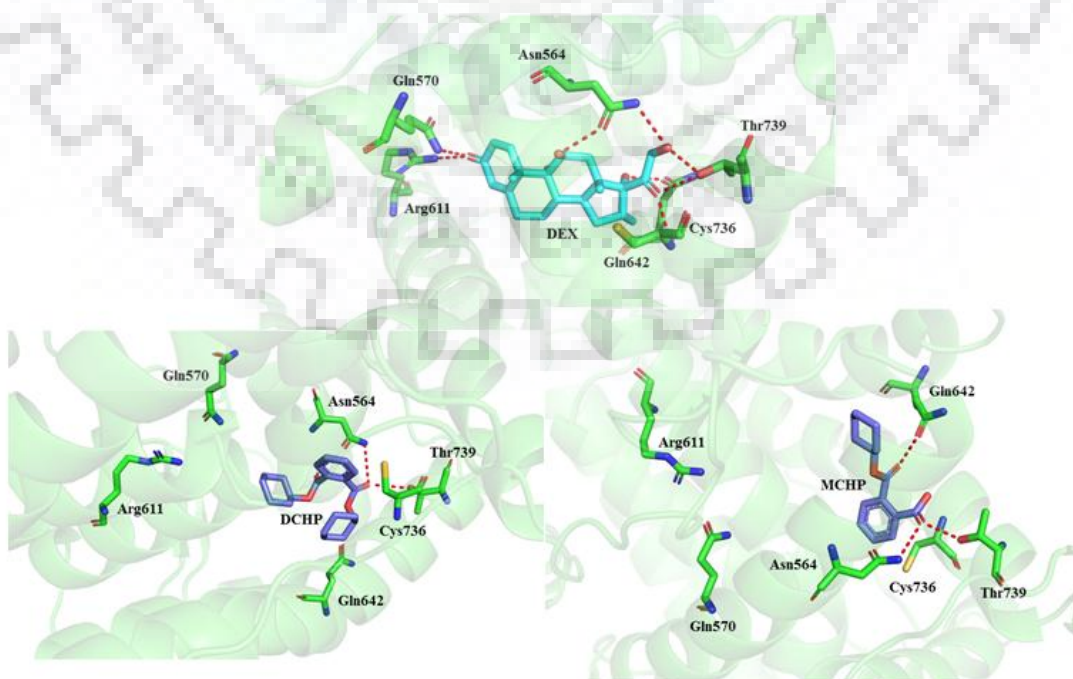


**Figure 2.1.** The ribbon diagram of human glucocorticoid receptor (hGR)-ligand binding domain, active site cavity with DEX, DCHP and its metabolite MCHP. A) DEX (cyan color), B) DCHP (red color), C) MCHP (yellow color). DCHP and MCHP occupy the active site cavity in the same manner as that of DEX. Interacting residues of the hGR are shown in stick form and the red dotted line represents intermolecular hydrogen bond interactions.

**Table 2.2.** Molecular docking results showing binding affinities of DEX, DCHP and MCHP. Binding affinities (kcal/mol) and the important interactions of the high m.wt DCHP and its metabolite MCHP with human glucocorticoid receptor are shown.

S.no	Compound	Binding affinity (kcal/mol) (Autodock)	Binding affinity (kcal/mol) (Autodock Vina)	Important interactions
1	DEX	-10.2	-12.4	Asn(564) OD1- 2.9Å- O2 Arg(611) NH2- 2.9Å- O2 Gln(642) OE1- 3.0 Å- O3 Thr(739) OG2- 2.8 Å- O5
2	DCHP	-7.17	-8.6	Asn(564) ND2- 3.4Å- O4 Thr(739) OG1- 3.1 Å- O4
3	MCHP	-5.24	-7.5	Asn(564) ND2- 3.2Å- O4 Gln(642) OE1- 3.0 Å- O3 Thr(739) OG1- 3.0 Å- O4

It is to be noted that the binding affinity of DEX is higher than that of DCHP and MCHP as shown in table 2.2. Phthalate ring of DCHP and MCHP have shown hydrophobic interactions with important active site residues such as Met560, Leu563, Trp600, Met601, Met604, Phe623, Leu732, Tyr735, and Cys736, as shown in **Figure 2.2**.

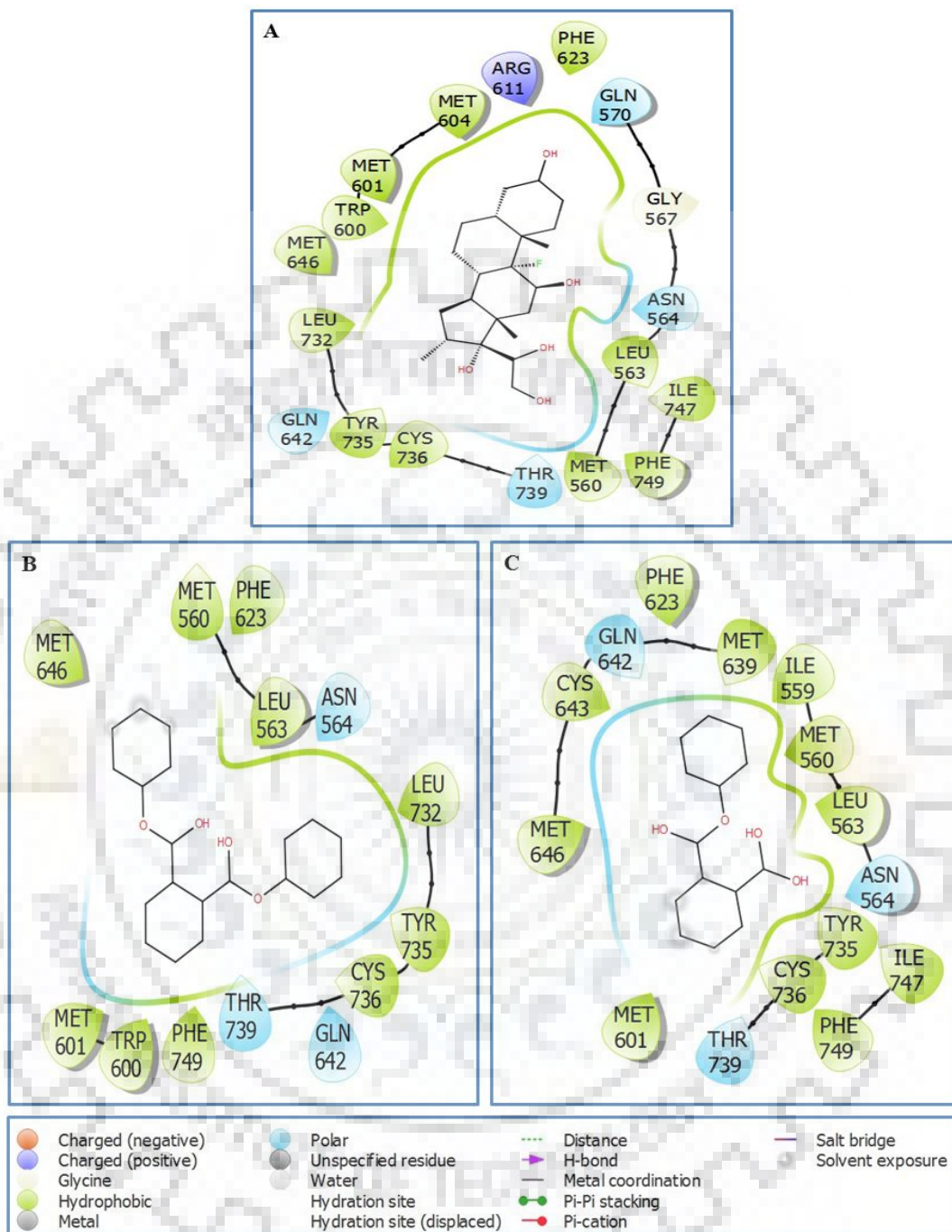


**Figure 2.2. Pictographic representation of hydrophobic interaction involved in DEX-hGR, DCHP- hGR and its metabolite MCHP-hGR complex formation using Maestro 11.2.** A) DEX, B) DCHP, and C) MCHP. All the aromatic rings of DCHP and MCHP are deeply embedded into the hydrophobic pockets of hGR. Hydrophobic interactions are shown in green color.

### 2.3.2. Molecular simulation results

Molecular dynamics simulation was performed to evaluate the stability and flexibility of the docking complexes of hGR with high molecular weight phthalate, DCHP, and its monophthalate MCHP.

#### 2.3.2.1 Root-mean-square deviation (RMSD)

In the present study, time-dependent RMSD graphs were plotted for protein C $\alpha$  backbone of DEX-hGR and PAEs-hGR complexes. RMSD results indicate that the complex formation between hGR and high molecular weight phthalate DCHP and its monophthalate metabolite MCHP is stable and less flexible. In each case, ligand-hGR complexes reached equilibrium during the initial phase of the simulation and tend to remain stable during the course of 20 ns simulation study. RMSD values of DEX-hGR and PAEs-hGR complexes gradually increased up to 11 ns and started to converge between 15 to 20 ns, as shown in **Figure 2.3**. It is to be noted that, complexes of MCHP with hGR showed higher average RMS variation as compared to their corresponding diphtalate counterpart, DCHP, as shown in **Table 2.3**. Overall RMSD results suggest that there is no significant variation in the protein backbone RMSD patterns of PAEs-hGR complexes as compared to DEX-hGR complex. These results imply that the binding of these PAEs at the active site of hGR is stable.

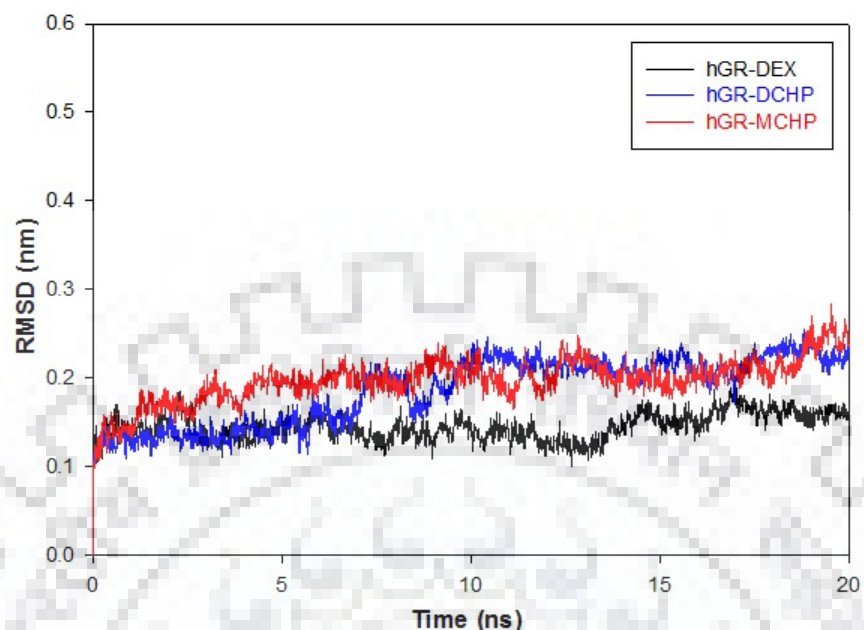


**Figure 2.3. RMSD graphs of hGR with DEX, DCHP, and MCHP.** RMSD profile of DEX, DCHP and its metabolite MCHP depicting the  $C\alpha$  backbone stability of hGR during the 20 ns of the simulation at 300 K.

**Table 2.3. Average RMSD and RMSF of hGR-DEX, hGR-DCHP, and hGR-MCHP complexes.** Resultant average RMSD and RMSF values of the variation in hGR backbone on the binding of DEX, DCHP, and MCHP are mentioned.

S.no	Compound	Average RMSD (nm)	Average RMSF (nm)	Average Rg (nm)
1.	DEX	0.144	0.093	1.836
2.	DCHP	0.186	0.101	1.835
3.	MCHP	0.197	0.097	1.829



### 2.3.2.2 Root-mean-square fluctuation (RMSF)

In this study, root mean square fluctuation (RMSF) for each residue of hGR complexes with DEX, DCHP, and MCHP was analyzed, as shown in **Figure 2.4**. RMSF results show that the active residues of hGR involved in the interaction with ligands have shown lesser fluctuation (within the range of 0.05 to 0.15 nm). RMSF result depicting residue mobility suggests that the reference position of hGR active site residues was not significantly varied on the binding of ligands. These results also demonstrate that the RMSF fluctuation profiles of PAEs-hGR complexes were almost comparable to DEX-hGR complex, which implies that these high molecular weight PAEs, DCHP, and MCHP form stable complexes with hGR and can activate the glucocorticoid receptor in a synergistic manner.

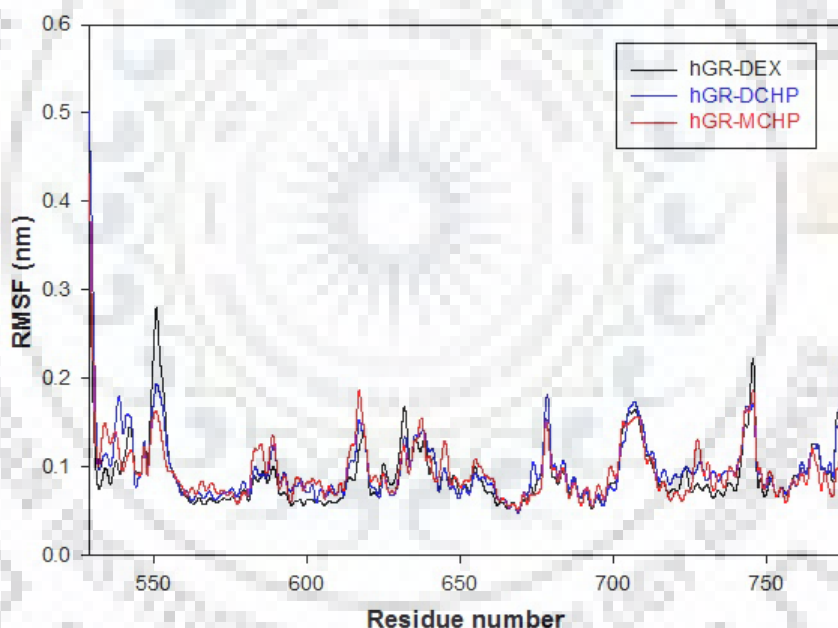


**Figure 2.4.** RMSF plots of molecular dynamics simulation study of hGR-DEX, hGR-DCHP and hGR-MCHP complexes for 20 ns. Fluctuation in protein residues upon binding of DEX, DCHP and its metabolite MCHP is shown.

### 2.3.2.3 Radius of gyration (Rg)

The protein backbone Rg was calculated for 20 ns trajectory and plotted in **Figure 2.5**. The radius of gyration results shows that variation in Rg value of PAEs-hGR complexes is analogous to DEX-hGR complex. Rg results suggest that all the complexes were stable in nature and the secondary structures of protein are densely packed during the course of the simulation.

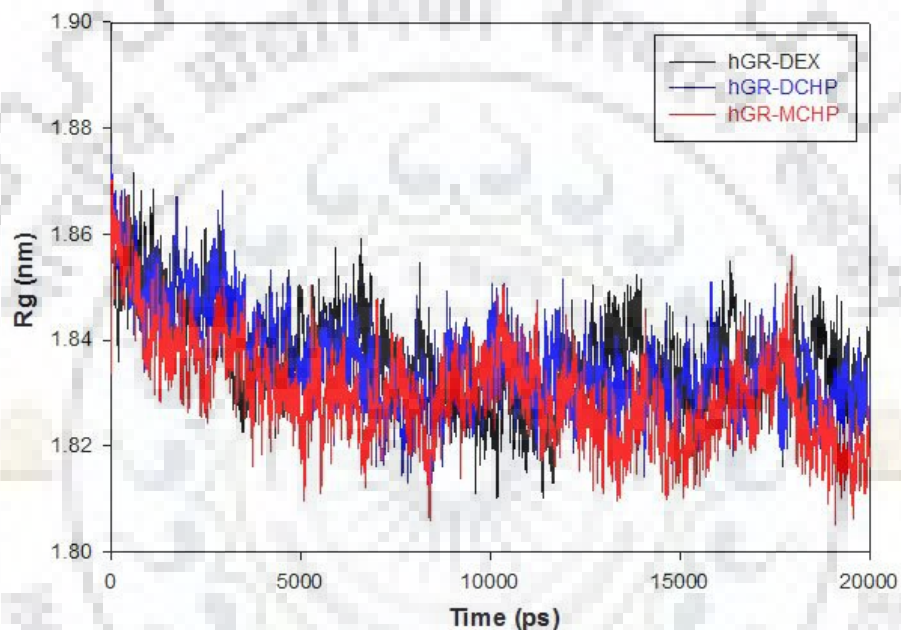


**Figure 2.5. Radius of gyration (Rg) graphs of DEX-hGR, DCHP-hGR and MCHP-hGR complexes.** The radius of gyration factor is related to the compactness of the hGR protein complex, during the course of the simulation of the 20 ns study.



### 2.3.2.4 Hydrogen bond analysis

The protein-ligand complex binding interactions were studied by H-bond analysis during the time period of 20 ns simulation. Hydrogen-bond number analysis of DEX, DCHP and its corresponding monophthalate MCHP with hGR is shown in **Figure 2.6**. The distribution of hydrogen bond lengths results is shown in **Figure 2.7**. These results indicate that the affinity of inter-molecular hydrogen bonds of PAEs-hGR complexes is comparable to DEX-hGR complex.

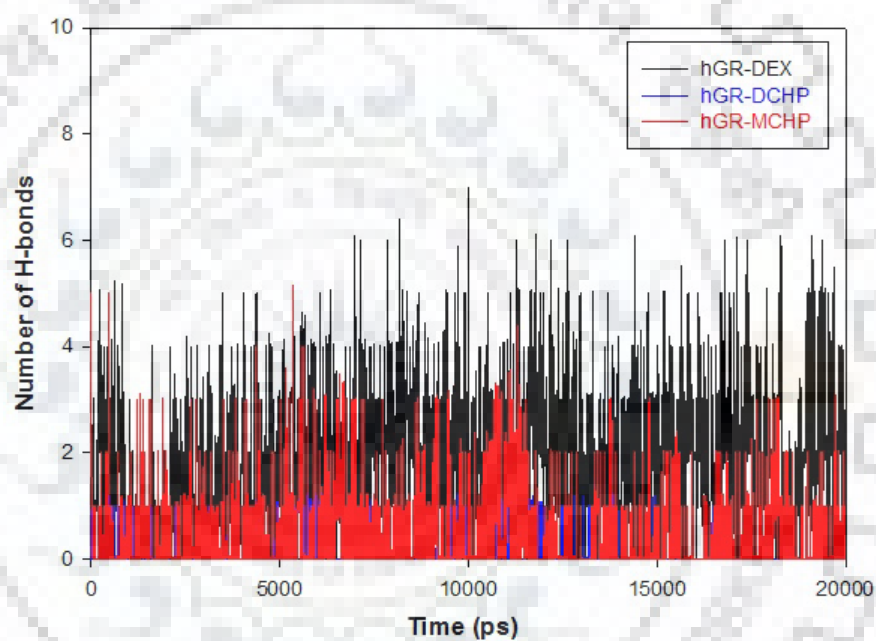


**Figure 2.6. Hydrogen bond number results of DEX-hGR, DCHP-hGR and MCHP-hGR complexes.** Average number of H-bonds formed during the 20 ns of simulation are mentioned.

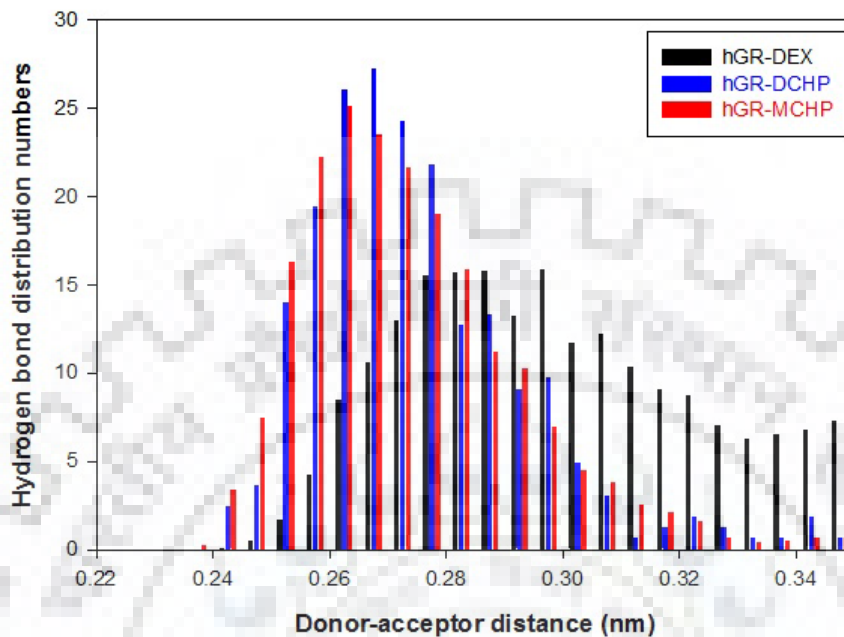


**Figure 2.7. Bar representation of the hydrogen bond number distribution of hGR with DEX and PAEs.** Hydrogen bond distribution profiles w.r.t to donor-acceptor distance, in case of DEX-hGR, DCHP-hGR and MCHP-hGR complexes during the course of 20 ns simulation at 300 K are shown.

### 2.3.3 MMPBSA Binding free energy calculation

The binding free energy ( $\Delta G_{\text{bind}}$ ) of the DEX-hGR and PAEs-hGR complexes were calculated using MMPBSA method and corresponding individual energy components ( $\Delta E_{\text{vdW}}$ ,  $\Delta E_{\text{elec}}$ ,  $\Delta G_{\text{polar}}$ , and  $\Delta G_{\text{non-polar}}$ ) are mentioned in **Table 2.4**. MMPBSA results provide a quantitative inference of the binding free energy. It has been shown that the binding free energies of the studied PAEs are lesser as compared to the DEX, a potent agonist for the human glucocorticoid receptor. Binding free energy results illustrate that PAEs-hGR complexes are stable and these high molecular weight PAEs, DCHP, and MCHP can effectively activate the glucocorticoid receptor-mediated adipogenesis in a synergistic approach.

Compound	Vander Waals energy (kJ/mol)	Electrostatic energy (kJ/mol)	Polar solvation energy (kJ/mol)	SASA energy (kJ/mol)	Binding energy (kJ/mol)
DEX	-234.153±0.412	-17.873±0.260	84.199±0.392	-19.163±0.035	-187.004±0.462
DCHP	-156.703±3.497	-4.745±0.210	63.397±0.785	-14.769±0.340	-113.01±3.294
MCHP	-139.202±0.474	-10.236±0.417	80.944±0.284	-24.351±0.269	-92.845±0.582

**Table 2.4. Binding energies of hGR-DCHP and hGR-MCHP complexes calculated by MMPBSA.** Different energy components such as Van der Waals energy, electrostatic energy, polar solvation energy and SASA energy contributing to the total binding free energy are mentioned.

### 2.4 Discussion

Generally, glucocorticoids have a vital role in adipocyte differentiation, and variation in glucocorticoid levels affects long-term metabolic programming and homeostasis maintaining pathways [219-221]. GR belongs to the family of nuclear receptors (NRs) and arranged in three domains: first is towards N-terminal, an activation function-1 domain (AF-1), second is a central DNA binding domain, and the third is at C-terminal, a ligand binding domain (LBD) [209, 222]. LBD also contains a ligand-dependent activation function domain (AF-2) which is directed by hormone binding. As it is already reported that, DCHP have a synergistic role in glucocorticoid receptor-mediated adipogenesis [223]. Here in glucocorticoid receptor, LBD folds into a canonical three-layer helical pack having

a hydrophobic pocket for ligand binding. Dexamethasone (DEX) is a powerful agonist for hGR that helps in the binding of coactivators to hGR. Here, in this study, the manner in which DCHP and its metabolite MCHP interact with the receptor active site is elucidated and compared with agonist DEX. Side chains of DCHP and MCHP enabled them to make resembling interactions with the hGR active site residues such as Gln570, Asn564, Arg611, and Thr739. Therefore, this study illustrates the binding efficiency of commonly used high molecular weight phthalate DCHP and its monophthalate metabolite MCHP and highlights their synergistic effect on the activation of glucocorticoid receptor-mediated adipogenesis.

To gain insights into the interaction between DCHP, MCHP and human glucocorticoid receptor, the best poses were selected from molecular docking studies. The crystal structure of hGR with dexamethasone (PDB ID:4UDC) shows that DEX is present in the bottom half cavity of the LBD of hGR. In a similar manner, DCHP and MCHP also occupy the bottom cavity of LBD of hGR. It is known that the presence of an outward tilt at the interface of helix (H6 and H7), is often correlated to the expanded ligand binding pocket in case of glucocorticoid receptor. Therefore, binding pocket of hGR can accommodate high molecular weight DCHP and MCHP.

Molecular docking results show that DCHP and MCHP have similar hydrogen bond interaction profile as compared to DEX with hGR active site residues. Further, hydrophobic interactions of DCHP-hGR and MCHP-hGR complexes are analogous to DEX-hGR complex. Such observation is in coordination with the report asserting synergistic effects of DCHP along with agonist DEX, in glucocorticoid-mediated adipogenesis. Likewise, as seen in the binding pattern of DEX, phthalate ring of high DCHP and MCHP occupies the central active site cavity and carboxylate groups form hydrogen bonds with key amino acids such as Asn564 and Thr739. Hence, activation of hGR by DCHP and MCHP can lead to glucocorticoid receptor-mediated adipogenesis.

Molecular dynamics simulation studies help in recognition of the changes occurring at the atomistic level in the ligand-protein complex. In the present study, different parameters associated with simulation studies such as RMSD, RMSF, radius of gyration (Rg), and the hydrogen bond formation and length distribution were analyzed.

This RMS deviation predicts the conformational changes occurring in the protein backbone during the course of the molecular simulation. Overall RMSD results illustrate that there is

no significant variation in the protein backbone RMSD patterns of PAEs-hGR complexes as compared to DEX-hGR complex. These results imply that the binding of these PAEs at the active site of hGR is stable and efficient. Root mean square fluctuation (RMSF) aspect of simulation study deals with the fluctuation of protein C $\alpha$  atom coordinates from their average position during the course of the simulation. As it is shown that, constant backbone atom RMSF value with such small or minor fluctuations signifies the stability of the PAEs-hGR complexes. Radius of gyration (Rg) determines the compactness of protein complexes in a given time frame during the molecular simulation. In general, a stably folded protein tends to maintain a relatively less variation in Rg value which determines its dynamic stability. Rg results analysis also shows that the DCHP-hGR and MCHP-hGR complexes are stable as that of DEX-hGR complex. The total average number of H-bonds formed during the simulation phase provide stability to the ligand-protein complex. The overall H-bond contribution by protein active site residues with DEX, DCHP, and MCHP were analyzed. The PAEs-hGR complexes were stable throughout the 20 ns simulation period. The stability of complexes was also contributed by non-bonded interactions such as electrostatic and Van der Waals forces. The hydrogen bond results help in understanding the stability of PAEs-hGR complexes and they may play a pivotal role in synergistically activating glucocorticoid-mediated adipogenesis in humans. Overall, molecular dynamics results DCHP-hGR and MCHP-hGR complexes were stable and less flexible during the course of the simulation.

Free binding energy calculations were used for estimation of the binding affinity of the ligand (DCHP and MCHP) with a protein receptor (hGR). In this study, MMPBSA, a plug-in utility of GROMACS was used for the computation of the binding free energy of PAEs-hGR complexes. The ligand binding affinity was analyzed based on the free binding energy calculations, evaluated for snapshots of trajectories from last 5 ns obtained from the MD simulation. Overall binding free energy results show that the DCHP-hGR and MCHP-hGR complexes were stable as compared to DEX-hGR complex.

## 2.5 Conclusion

Endocrine disrupting chemicals (EDCs) can modulate the activity of steroid hormone via disruption of nuclear hormone receptors and vary sexual development and normal cellular physiological conditions. Phthalates are the ubiquitous environmental contaminants that have established endocrine disrupting and teratogenic properties. Appropriate activation of hGR is a critical controller of adipocyte differentiation. The in-silico techniques of molecular docking and simulation were utilized to analyze the important interactions of DCHP and its metabolite MCHP with hGR. This computational study shows that the PAEs-hGR complexes have good binding affinities and form stable complexes. Hence, DCHP and MCHP, from a class of high molecular weight phthalates can efficiently bind to hGR and activate the glucocorticoid-mediated adipogenesis in a synergistic manner. Our computational study emphasizes that the DCHP and MCHP can bind to hGR and concurrently provides a regulatory connection between the rate of rising obesity with that of the alarming rate of increase in phthalate production. The rise in rates of metabolic disorder is related to increase in exposure, usage, and production of xenobiotic compounds. A large variety of environmental endocrine disrupting substances influence adipogenesis and obesity. "Obesogens" are chemical agents that improperly regulate the genes involved in glucose metabolism and adipocyte differentiation and promote lipid accumulation and adipogenesis. The human glucocorticoid receptor (hGR) is a steroid hormone triggered transcriptional factor and it regulates target genes important in basal glucose homeostasis. Molecular docking analysis was performed in order to assess in-silico structure based toxic effects of high molecular weight phthalate dicyclohexyl phthalate (DCHP) and its monophthalate metabolite mono-cyclohexyl phthalate (MCHP). DCHP and MCHP were docked within the active site cavity of human glucocorticoid receptor (hGR). Molecular docking results show that the binding affinities of DCHP and MCHP lie in the comparable range (-7.17 kcal/mol and -5.24 kcal/mol) with Dexamethasone (-10.2 kcal/mol), a potent agonist for hGR. These two PAEs occupy the active site of hGR and have shown interaction with the key residues such as Met560, Asn564, Trp600, Met604, Phe623, Gln642, Leu732, Tyr735, Cys736, and Thr739. Molecular dynamics and stability of the DCHP-hGR and MCHP-hGR complexes were determined by molecular simulation using GROMACS 5.14. Molecular dynamics simulation results infer that DCHP-hGR and

MCHP-hGR complexes were stable. Binding free energy calculations of the DCHP-hGR and MCHP-hGR complexes were estimated by using Molecular Mechanic/Poisson-Boltzmann Surface Area (MMPBSA) method. Molecular Docking and simulation results emphasize that DCHP and MCHP can efficiently bind to hGR, which further leads to glucocorticoid-mediated adipogenesis in a synergistic manner.









**CHAPTER 3**

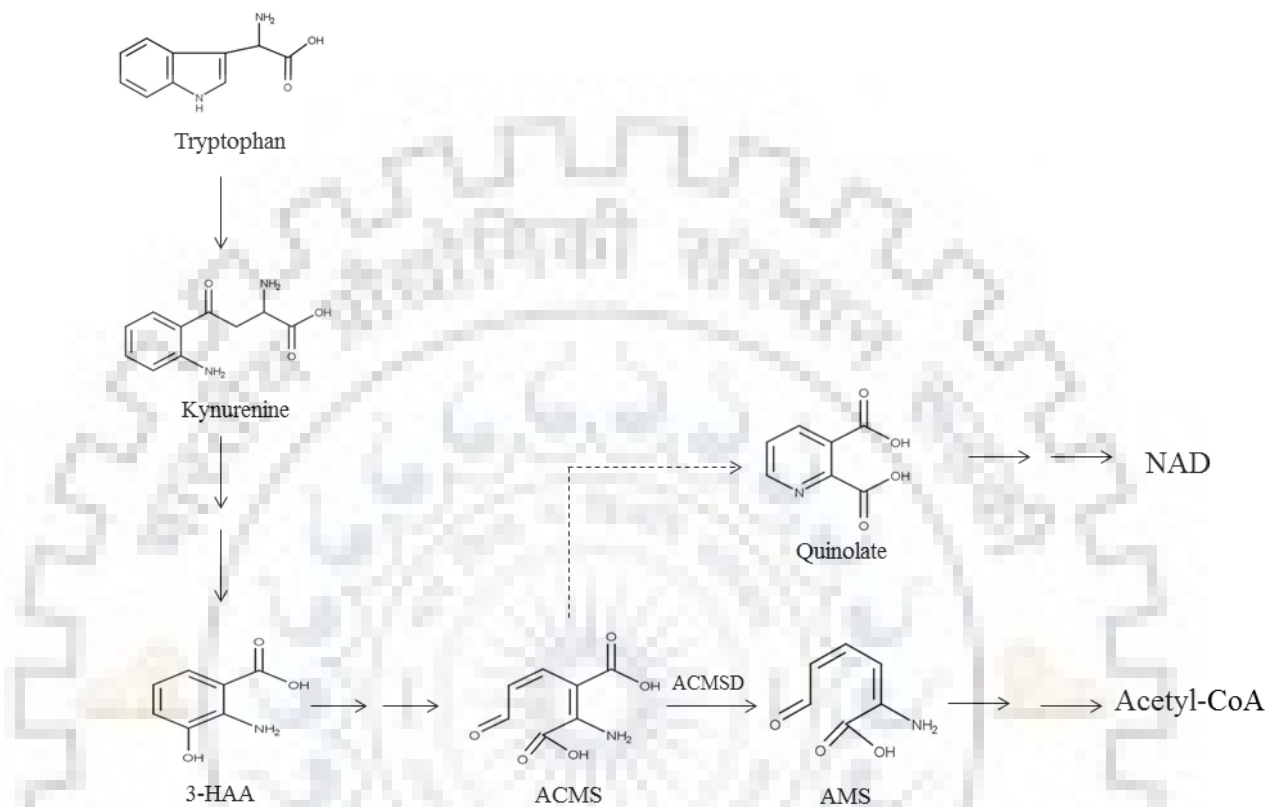
**STRUCTURE-BASED MIMICKING OF PHTHALIC ACID ESTERS (PAES) AND  
INHIBITION OF hACMSD, AN IMPORTANT ENZYME OF THE TRYPTOPHAN  
KYNURENINE METABOLISM PATHWAY**

### 3.1 Introduction

In the brain, elevated levels of quinolinic acid (QA) are often associated with the pathogenesis of different neurodegenerative disorders including Alzheimer's and Huntington's disease [224-226]. In the kynurenine pathway of tryptophan metabolism,  $\alpha$ -amino- $\beta$ -carboxymuconate- $\epsilon$ -semialdehyde (ACMS) is metabolized to  $\alpha$ -amino- $\beta$ -muconate- $\epsilon$ -semialdehyde (AMS) via the action of important enzyme ACMS decarboxylase, further AMS converted to acetyl CoA as shown in **Figure 3.1** [227, 228]. To maintain the basal Trp-niacin ratio, ACMS is non-enzymatically metabolized to quinolate (QA) which further leads to the NAD formation [229]. Thus, the presence of key enzyme ACMSD prevents the accumulation of quinolate [230]. Various studies related to ACMSD show that enzyme is zinc-dependent amidohydrolase maintaining quinolinic acid (QA) and NAD homeostasis [231]. Disturbance in the basal levels of QA is associated with many physiological and pathological conditions related to the central nervous system (CNS) [232]. Thus, ACMSD act as a checkpoint and regulates the balance between the relative QA levels.

Several studies have reported that ACMSD is a critical enzyme for tryptophan metabolism [233, 234]. Phthalic acid esters (PAEs) are commonly used for the industrial manufacturing of lubricants, various adhesives, pest repellents, and plastics [183, 235]. Several PAEs are long-established environmental endocrine disruptors, peroxisome proliferators and induce reproductive and developmental toxicities [191, 236-239]. It has been reported that PAEs can imbalance the Trp-niacin basal ratio in the tryptophan metabolism pathway. In rats, it has been reported that the conversion ratio of tryptophan to niacin has increased with the increase in the dietary concentration of di-(2-ethyl hexyl) phthalate (DEHP) [240]. This study shows that the increase in the amount of quinolinic acid with an increase in DEHP concentration is associated with the inhibition of enzymatic activity of ACMSD. Similarly, di-n-butyl phthalate (DnBP) is reported to be linked with alteration in trp to niacin ratio in the weaning rats, which were fed with niacin-free and tryptophan limited diet [241]. It has been shown that DEHP degrades to phthalic acid via an intermediate mono-(2-ethyl hexyl) phthalate (MEHP) [115]. In another report, it has been shown that DEHP and its metabolite MEHP increased QA production in the rats [242]. This study reveals that the structural

similarity of DEHP and MEHP to tryptophan metabolites is responsible for the noticeable



changes in normal tryptophan metabolism and caused the inhibition of ACMSD activity.

**Figure 3.1. Kynurenine pathway of tryptophan metabolism.** Tryptophan is metabolized to kynurenine and further to 3-Hydroxy anthranilic acid (3-HAA). Then, ACMSD participates in a reaction (marked with a solid arrow) and directs the conversion of  $\alpha$ -amino- $\beta$ -carboxymuconate- $\epsilon$ -semialdehyde (ACMS) to  $\alpha$ -amino- $\beta$ -muconate- $\epsilon$ -semialdehyde (AMS), which is further metabolized to Acetyl-CoA. ACMS is also non-enzymatically converted to quinolate (marked with a dotted arrow), which further leads to nicotinamide adenine dinucleotide (NAD) biosynthesis.

Although, numerous studies have shown that phthalates are involved in disturbing the basal trp to niacin ratio, but the elucidation of the binding mode and important interactions of PAEs with hACMSD have not been reported yet. This study highlights the important interactions of phthalates with human  $\alpha$ -amino- $\beta$ -carboxymuconate- $\epsilon$ -semialdehyde decarboxylase (hACMSD) which eventually inhibit the hACMSD activity and leads to the accumulation of quinolate. The crystal structure of the hACMSD along with substrate analog Dipicolinic acid, PDC (PDB ID: 4IH3) is available [231]. PDC binds in the zinc-containing active site of hACMSD and shows the interaction with Arg47 and Trp191. In this study, five commonly used PAEs and their corresponding monophthalates used for the docking studies with hACMSD are: dimethyl phthalate (DMP), diethyl phthalate (DEP), di-n-butyl phthalate (DnBP), di-isobutyl phthalate (DIBP), di-(2-ethylhexyl) phthalate (DEHP), monomethyl phthalate (MMP), monoethyl phthalate (MEP), mono-n-butyl phthalate (MBP), mono-iso butyl phthalate (MIBP), and mono-(2-ethylhexyl) phthalate (MEHP), mono-(2-ethyl-5-hydroxyhexyl) phthalate (MEHHP), mono-(2-ethyl-5-oxyhexyl) phthalate (MEOHP). Molecular docking and simulation studies were used to investigate the binding mode and stability of these PAEs to human ACMSD. The results conclude that these phthalates can efficiently bind and can inhibit the activity of hACMSD. Hence, the binding of PAEs with hACMSD affect the basal trp to niacin ratio which further accumulates the quinolate in the tryptophan metabolism pathway.

### **3.2 Material and methods**

#### **3.2.1 Protein and ligand preparation**

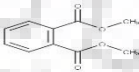
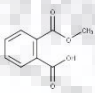
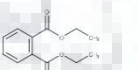
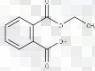
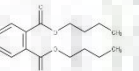
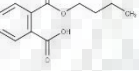
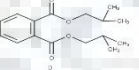
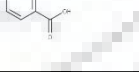
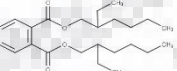
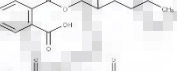
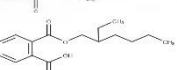
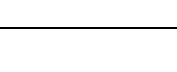
Computational docking and simulation studies were performed in order to assess the interaction of the phthalates with hACMSD. The coordinates of hACMSD were retrieved from the crystal structure of hACMSD bound to a substrate analog Dipicolinic acid (PDC) (PDB ID: 4IH3) from the RCSB database [231]. Geometric optimization of the protein was done by using the Clean Geometry module of Discovery Studio (DS) 4.0 suite by Accelrys (San Diego, CA, USA). Side-chain torsion angles varying more than 30° from the ideal values were corrected. The conformational quality was checked using the Minimize and refine protein module of DS suite, in which water molecules were eliminated and the CHARMM27 force field was used for the protein receptor [243]. The structure was

minimized for 1000 steps by utilizing the smart-minimizer algorithm with 0.1 RMS gradient cut-off to remove the steric overlaps.

### 3.2.2 Molecular docking of ligands

AutoDock 4.2.6 was used to perform the docking of PAEs with hACMSD [211]. Autodock utilizes a semiempirical free energy forcefield to calculate the binding free energy of a small molecule to a macromolecule. Receptor molecule was prepared by adding explicit hydrogen molecules and associated Kollman charges (16.0) by utilizing the AutoDock Tools 1.5.6 and saved in .pdbqt file format. Five commonly used diphtalates and their corresponding monophthalates used for the docking studies with hACMSD are: dimethyl phthalate (DMP), diethyl phthalate (DEP), di-n-butyl phthalate (DnBP), di-isobutyl phthalate (DIBP), di-(2-ethylhexyl) phthalate (DEHP), monomethyl phthalate (MMP), monoethyl phthalate (MEP), mono-n-butyl phthalate (MBP), mono-iso butyl phthalate (MIBP), mono-(2-ethylhexyl) phthalate (MEHP), mono-(2-ethyl-5-hydroxyhexyl) phthalate (MEHHP), and mono-(2-ethyl-5-oxyhexyl) phthalate (MEOHP). As a positive control, substrate analog of hACMSD, dipicolinic acid (PDC) was docked and compared with binding affinity scores of PAEs. The 3D structures of all the phthalates were drawn using Marvin suite 17.13 [<http://www.chemaxon.com/marvin/sketch/index.jsp>] and minimized using DS suite. The properties of phthalate compounds and their structures are shown in **Table 3.1**. The ligands were prepared by adding hydrogen atoms and Gasteiger charges and then saved in .pdbqt format. The ligand flexibility was used to specify the torsional degrees of freedom in ligand molecule. The atomic potential grid map was generated with a spacing of 0.375 Å by using AutoGrid 4. The docking receptor grid was created by choosing the catalytic key residues which show interaction with substrate analog, PDC i.e. Arg47 and Trp191 and His174, present in the proximity of zinc metal. The dimensions of the grid box were as follows 70 Å × 70 Å × 70 Å and the center point coordinates were set as X = 0.56, Y = -12.94 and Z = 2.77. For docking purpose, Lamarckian genetic algorithm and grid supported energy evaluation method were adopted. The number of total GA runs was increased from 10 to 100. Other docking parameters were used as default. The pose with the maximum binding affinity score and the corresponding interactions was selected and further visually inspected and analyzed in PyMol 1.3 [213].

**Table 3.1. Commonly used Phthalates and their usage.** The details of Phthalic acid esters (PAEs) such as DMP, DEP, DBP, DIBP, DEHP and their metabolites along with their different uses.

S.no.	Phthalate category	Phthalates	Molecular weight (g/mol)	Structure	Usage
1	Low Molecular weight	DMP	194.18		Used as plasticizer, also used in insect repellents
		MMP	180.15		
		DEP	222.4		Solvent in personal care products, cellulose acetate plasticized films for food packaging
		MEP	194.18		
		DBP	278.34		An enteric coating of medications and food supplements and nitrocellulose-coated regenerated cellulose film (RCF) used in plasticized coatings.
		MBP	222.24		
DIBP	278.34		Used as a substitute for DBP due to the similarity in their application properties		
	MIBP	222.24			
2	High molecular weight	DEHP	390.56		Production of polyvinyl chloride (PVC) plastics, Used in PVC based, medical products, retail packed food items
		MEHP	278.34		
		MEHHP	294.34		
		MEOHP	292.33		

### 3.2.3 Molecular dynamics simulation

The associated structural and dynamic changes occurring at the atomistic level in hACMSD on the binding of PAEs were analyzed by molecular dynamics simulation. The simulation study was performed with Gromacs 5.1.4 suite with GROMOS96 43a1 force field on the LINUX based workstation [214, 215]. PDC and phthalates topology files were generated using Automated Topology Builder (ATB) [216, 217]. The protein complexes were solvated in a cubic box with simple point charge (SPC) waters and counter-ions were added for the overall electrostatic neutrality of the system [244]. Energy minimization was performed to minimize the steric clashes by using Steepest descent algorithm for 50,000 iteration steps and cut-off up to 1000 kJmol<sup>-1</sup>. Then the system was equilibrated in two different phases for 50,000 steps. The first phase of equilibration was done with a constant number of particles, volume, and temperature (NVT), each step 2 fs. The second phase of equilibration was performed with a constant number of particles, pressure, and temperature (NPT), the ensemble at 300 K. LINCS algorithm was utilized for covalent bond constraints in the equilibration steps. For the calculation of Lennard-Jones and Coulomb interactions, 1.4 nm radius cut-off was used. Long-range electrostatics were calculated by using Particle Mesh Ewald (PME) method with Fourier grid spacing of 1.6 Å. The temperature inside the box was regulated by using V-rescale, a modified Berendsen temperature coupling method. Parrinello-Rahman pressure coupling method was utilized in NPT equilibration. The final production step of molecular dynamics simulation was carried out for 20 ns, each step of 2 fs. Trajectories were saved and results were analyzed using XMGRACE. Root mean square deviation (RMSD) variation in protein backbone was calculated by using g\_rms tool which utilizes the least-square fitting method. Overall root mean square fluctuation (RMSF) in the atomic positions of protein C $\alpha$  backbone was calculated by using the g\_rmsf tool. A rough measure of compactness factor of protein during the course of the simulation was estimated by using the g\_gyrate tool of GROMACS. gmx\_sasa was used for computation of the total solvent accessible surface area (SASA). Hydrogen bonds were calculated with 3.5 Å distance cut-off by using g\_hbond and the distribution of inter-molecular hydrogen bond lengths throughout the simulation were also analyzed.



### 3.2.4 MMPBSA binding free energy calculation

The binding free energy of the interaction between ligand-protein complexes were obtained by utilizing the Molecular Mechanic/Poisson-Boltzmann Surface Area (MMPBSA) method which employs ensembles derived from molecular dynamics (MD) simulation [245]. In the GROMACS module, the `g_mmpbsa` application is used for the calculation of different components of the binding free energy of PDC-hACMSD and PAEs-hACMSD complexes. Here, the binding energy is an average of three energetic terms, i.e. potential energy in the vacuum, polar-solvation energy, and non-polar solvation energy, respectively. In the present study, the snapshots at every 10 ps between 15 and 20 ns were collected and MMPBSA was performed to predict the binding energy.

## 3.3 Results and discussion

Due to the structural similarity of the benzene ring of PAEs with natural substrate analog, PDC, they are expected to mimic the binding mode at the active site of hACMSD. Side chains of PAEs enabled them to make analogous interactions with the important residues such as Arg47 and Trp191 and they occupy the active site of hACMSD within the 4 Å vicinity of zinc metal. Therefore, this study illustrates the binding efficiency of commonly used PAEs comparable to that of PDC, a substrate analog of hACMSD.

### 3.3.1 Molecular docking of ligands

Molecular docking is an extensively used computational approach to validate the binding of the suitable orientation of small molecule with the receptor protein. In order to characterize the molecular interactions, molecular docking of co-crystallized substrate analog, Dipicolinic acid (PDC) along with PAEs was performed within the binding pocket of hACMSD using AutoDock 4.2.6. All the generated binding poses were ranked and clustered according to their root mean- standard deviation (RMSD) value, binding affinity score, and the vicinity of the zinc metal. The AutoDock results show that the diphtalates and their monophthalates have a binding affinity in the range of -4.9 to -7.48 kcal/mol which is comparable to a substrate analog, PDC (-6.21 kcal/mol) as shown in **Table 3.2**. All phthalates have shown interaction with the key amino acid residues such as Arg47 and Trp191, similar to substrate analog, PDC as shown in **Figures 3.2-3.4**. Moreover, the monophthalates of DEHP such as MEHP, MEHHP, and MEOHP have shown maximum

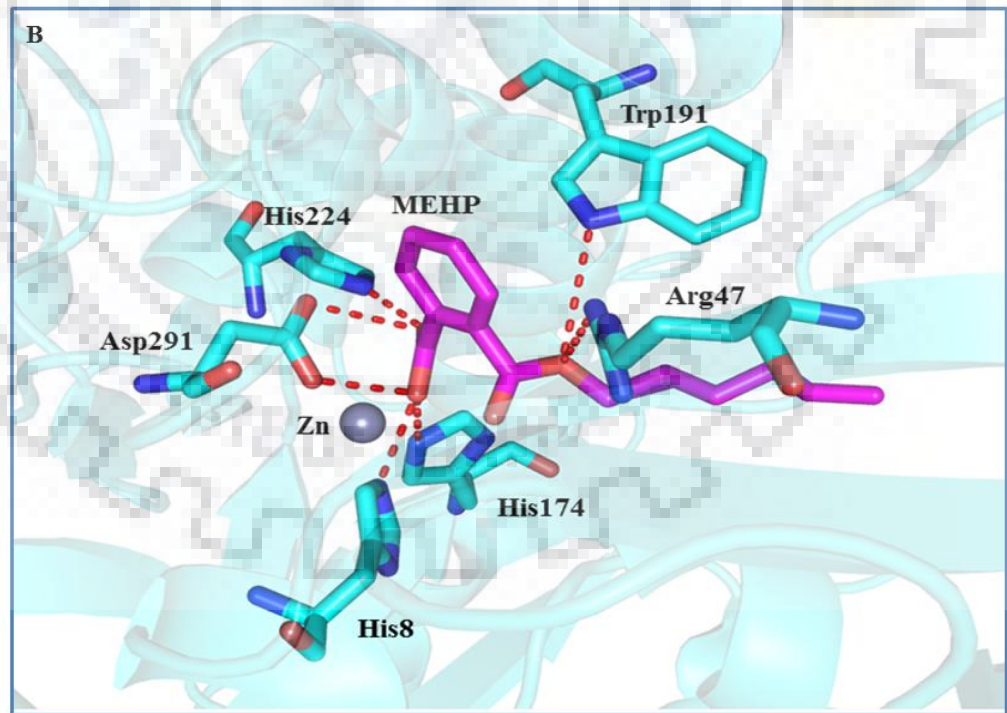
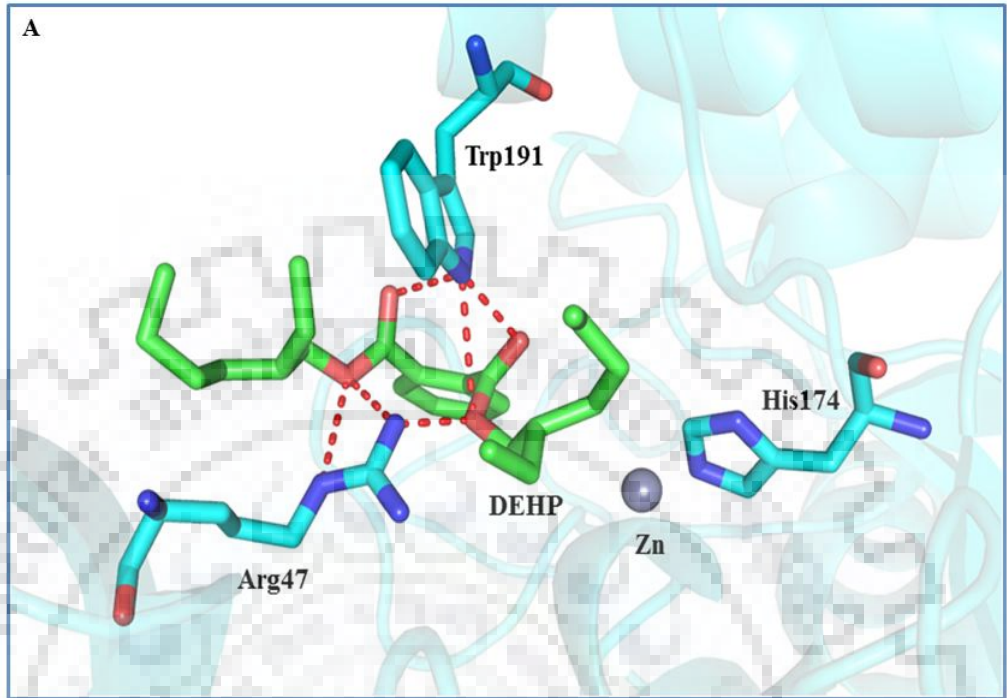


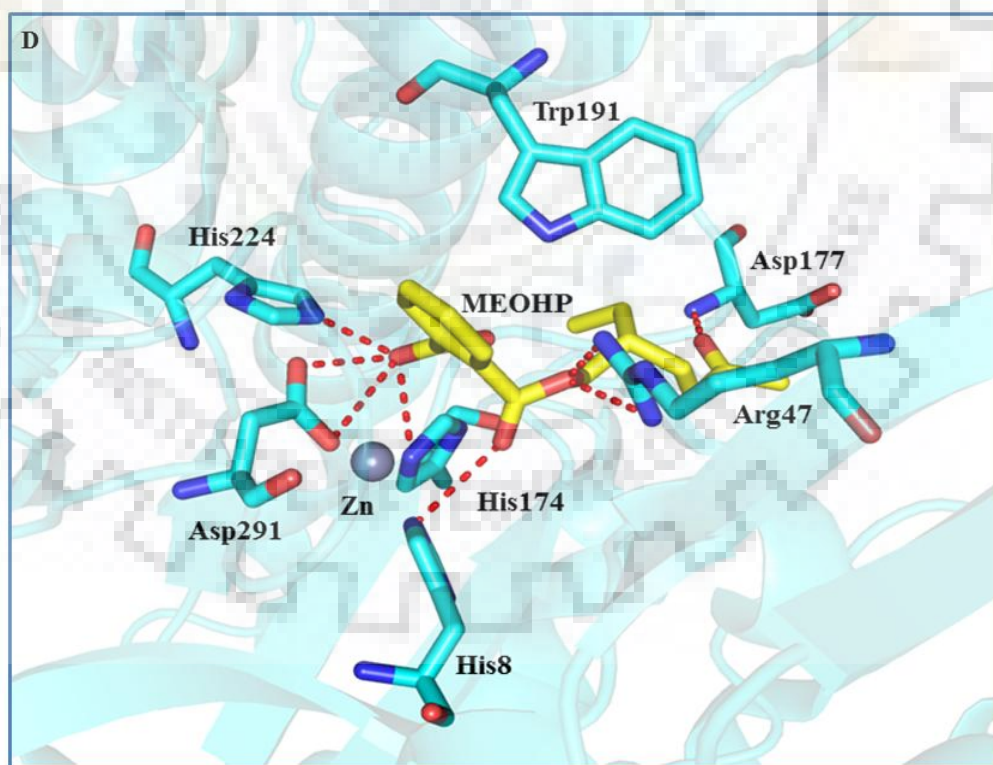
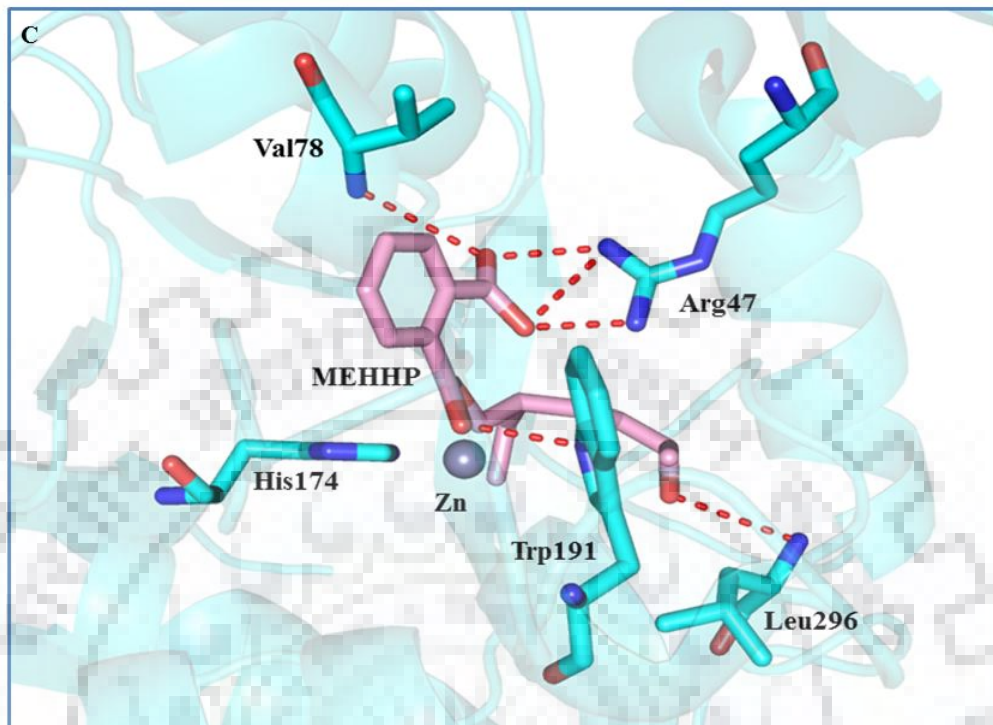
binding affinities with hACMSD. PAEs are present within the range of 4 Å from the zinc metal and occupied the active site cavity comprising of residues such as His8, Val76, His174, Asp291, Phe294, and Leu296, in the same manner as that of PDC. MEHP and MEOHP also have shown interaction with other active site residues such as His8, His224, His174, Asp177, and Asp291. The crystal structure of hACMSD in complex with 1,3-dihydroxyacetone phosphate (DHAP) (PDB ID: 2WM1), a glycolytic intermediate which is a potent inhibitor of the enzyme also shows interaction with key residues such as Arg47, Asp291, and Trp191. These results suggest that all the studied PAEs can efficiently bind in the active site of hACMSD. Moreover, DEHP along with its monophthalates seems to be a potent inhibitor for hACMSD. Hence, inhibition of hACMSD by PAEs can disbalance the basal ratio of Trp-niacin in the kynurenine pathway.

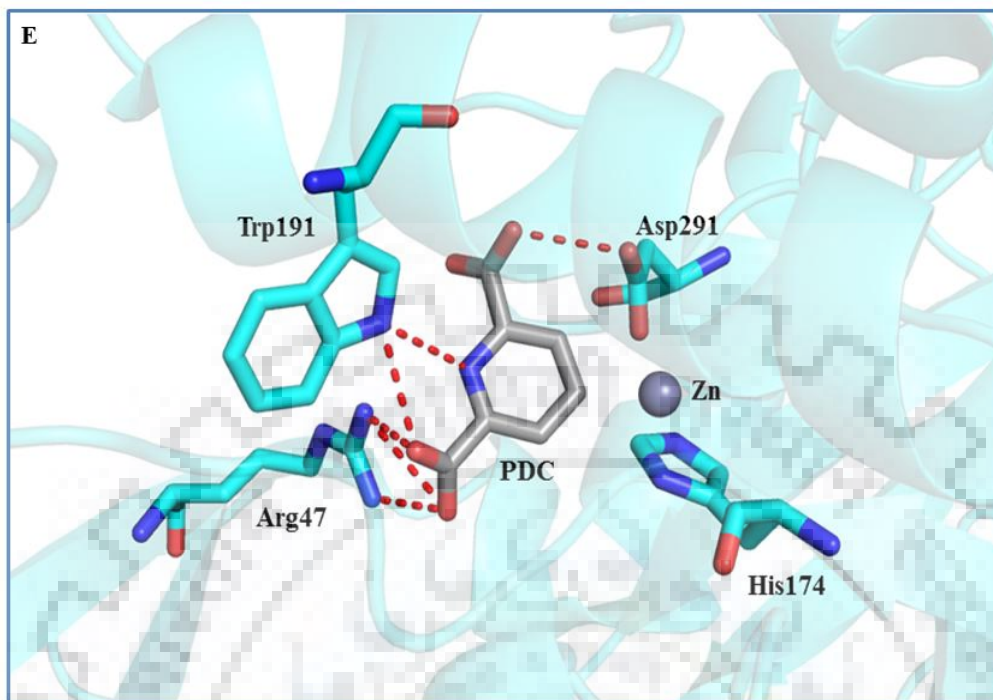
**Tables 3.2. Details of molecular docking results of PAEs-hACMSD complexes.** The summary of binding affinities (kcal/mol) and the polar interactions of the PAEs-hACMSD complexes

S.no	Ligand	Binding affinity (kcal/mol)	Interactions
1.	Dipicolinic acid (PDC)	-6.21	Arg47 (NH1) - O <sub>3</sub> (2.8 Å) Arg47 (NH2) - O <sub>3</sub> (3.4 Å) Arg47 (NH2) - O <sub>3</sub> (3.1 Å) Trp191 (NE1) - O <sub>4</sub> (3.2 Å) Trp191 (NE1) - N <sub>1</sub> (3.3 Å) Asp291 (OD2) - O <sub>2</sub> (3.1 Å)
2.	DEHP	-5.77	Arg47 (NH2) - O <sub>4</sub> (2.4 Å) Arg47 (NH2) - O <sub>1</sub> (2.7 Å) Arg47 (NE) - O <sub>3</sub> (3.4 Å) Trp191 (NE1) - O <sub>4</sub> (2.4 Å) Trp191 (NE1) - O <sub>4</sub> (2.7 Å) Trp191 (NE1) - O <sub>4</sub> (3.5 Å)
3.	MEHP	-7.48	His8 (NE2) - O <sub>3</sub> (2.7 Å) Arg47 (NH2) - O <sub>1</sub> (3.5 Å) His174 (NE2) - O <sub>3</sub> (2.5 Å) Trp191 (NE1) - O <sub>1</sub> (3.8 Å) His224 (NE2) - O <sub>3</sub> (2.7 Å) Asp291 (OD1) - O <sub>3</sub> (2.6 Å) Asp291 (OD2) - O <sub>4</sub> (3.2 Å)
4.	MEHHP	-6.94	Arg47 (NH1) - O <sub>4</sub> (3.0 Å) Arg47 (NH1) - O <sub>5</sub> (3.0 Å) Arg47 (NH2) - O <sub>4</sub> (3.2 Å) Val78 (N) - O <sub>5</sub> (3.6 Å) Trp191 (NE1) - O <sub>3</sub> (2.9 Å) Leu296 (N) - O <sub>3</sub> (3.5 Å)
5.	MEOHP	-7.42	His8 (NE2) - O <sub>3</sub> (3.4 Å)

			Arg47 (NH1) - O <sub>1</sub> (3.4 Å) Arg47 (NH2) - O <sub>1</sub> (2.8 Å) His174 (NE2) - O <sub>3</sub> (3.2 Å) Asp177(N) - O <sub>3</sub> (2.7 Å) Trp191 (NE1) - O <sub>1</sub> (3.6 Å) His224 (NE2) - O <sub>3</sub> (2.7 Å) Asp291 (OD1) - O <sub>3</sub> (3.5 Å) Asp291 (OD2) - O <sub>4</sub> (3.1 Å)
6.	DMP	-4.96	Arg47 (NH1) - O <sub>2</sub> (2.7 Å) Arg47 (NH2) - O <sub>2</sub> (3.3 Å) Arg47 (NH2) - O <sub>3</sub> (2.8 Å) Trp191 (NE1) - O <sub>4</sub> (3.1 Å) Trp191 (NE1) - N <sub>1</sub> (2.9 Å)
7.	DEP	-4.90	Arg47 (NH1) - O <sub>4</sub> (2.9 Å) Arg47 (NH1) - O <sub>3</sub> (3.1 Å) Arg47 (NH2) - O <sub>2</sub> (2.8 Å) Arg47 (NH2) - O <sub>3</sub> (3.0 Å) Arg47 (NH2) - O <sub>4</sub> (3.5 Å) Trp191 (NE1) - O <sub>2</sub> (3.3 Å)
8.	DBP	-5.65	Arg47 (NH1) - O <sub>3</sub> (3.0 Å) Arg47 (NH2) - O <sub>3</sub> (2.9 Å) Val78 (N) - O <sub>5</sub> (2.5 Å) Trp191 (NE1) - O <sub>2</sub> (3.2 Å)
9.	DIBP	-5.13	Arg47 (NH1) - O <sub>4</sub> (2.9 Å) Arg47 (NH1) - O <sub>2</sub> (3.2 Å) Arg47 (NH2) - O <sub>1</sub> (2.9 Å) Val78 (N) - O <sub>3</sub> (3.7 Å) Trp191 (NE1) - O <sub>1</sub> (3.2 Å)
10.	MMP	-5.10	His8 (NE2) - O <sub>11</sub> (2.7 Å) Arg47 (NH2) - O <sub>1</sub> (3.1 Å) His174 (NE2) - O <sub>11</sub> (2.6 Å) Trp191 (NE1) - O <sub>1</sub> (3.3 Å) His224 (NE2) - O <sub>12</sub> (3.0 Å) Asp291 (OD1) - O <sub>11</sub> (2.5 Å) Asp291 (OD2) - O <sub>12</sub> (3.4 Å)
11.	MEP	-5.03	Arg47 (NH1) - O <sub>4</sub> (2.8 Å) Arg47 (NH2) - O <sub>4</sub> (3.3 Å) Arg47 (NH2) - O <sub>1</sub> (3.0 Å) Val78 (N) - O <sub>2</sub> (3.4 Å) His174 (NE2) - O <sub>3</sub> (3.5 Å) Trp191 (NE1) - O <sub>1</sub> (2.8 Å)
12.	MBP	-5.83	Arg47 (NH1) - O <sub>3</sub> (3.2 Å) Arg47 (NH2) - O <sub>4</sub> (3.2 Å) Arg47 (NH2) - O <sub>3</sub> (3.0 Å) Val78 (N) - O <sub>4</sub> (3.6 Å) Trp191 (NE1) - O <sub>2</sub> (2.8 Å)
13.	MIBP	-5.25	Arg47 (NH1) - O <sub>4</sub> (2.9 Å) Arg47 (NH2) - O <sub>3</sub> (3.0 Å) Arg47 (NH2) - O <sub>2</sub> (2.6 Å) Trp191 (NE1) - O <sub>2</sub> (2.7 Å)

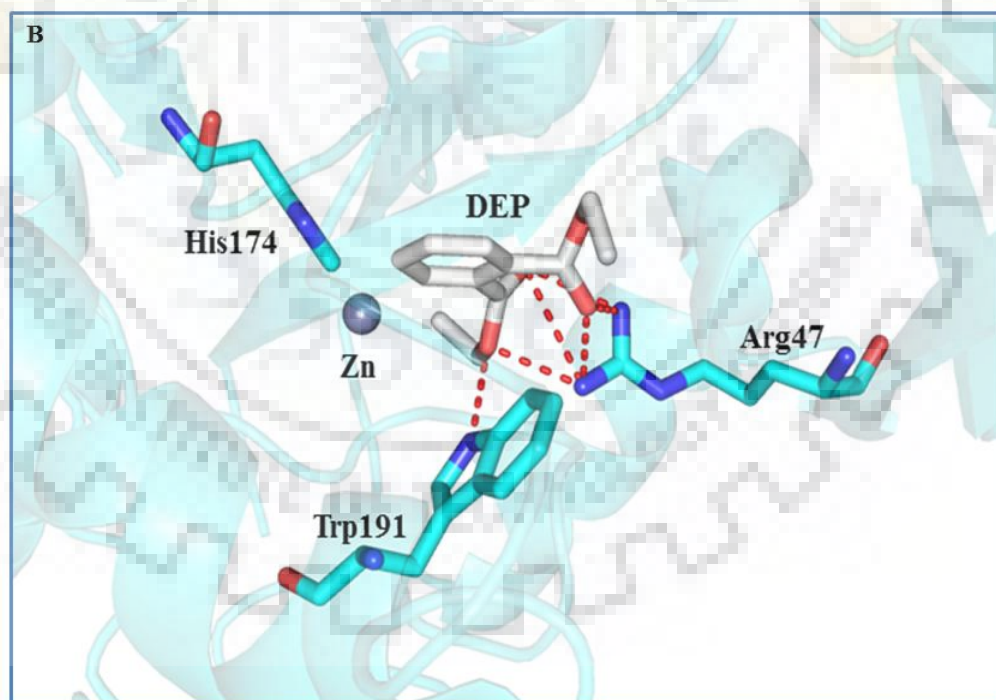
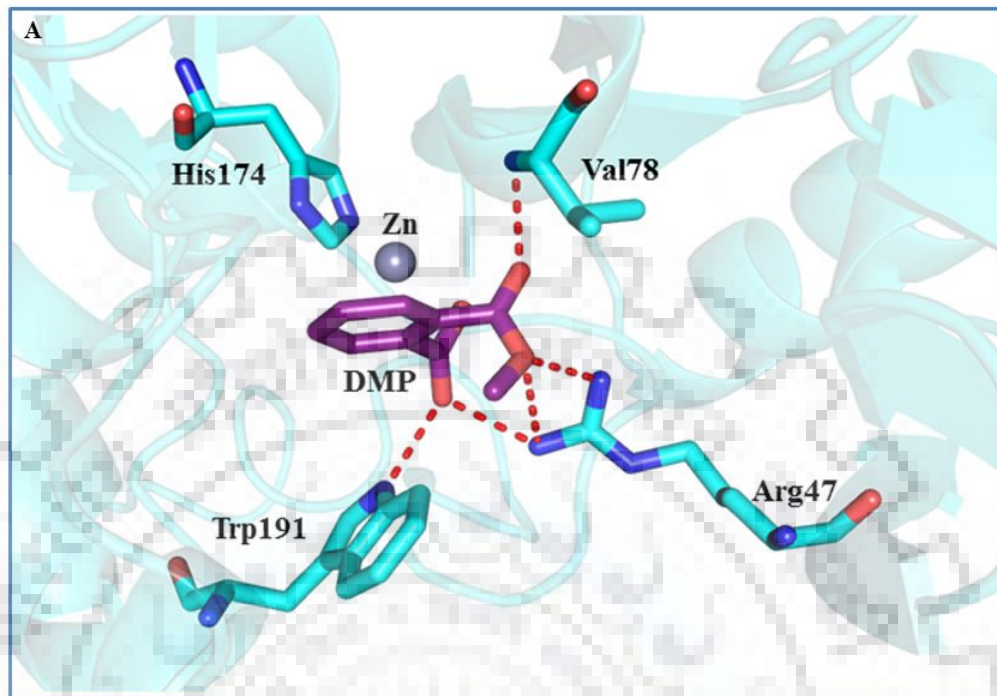


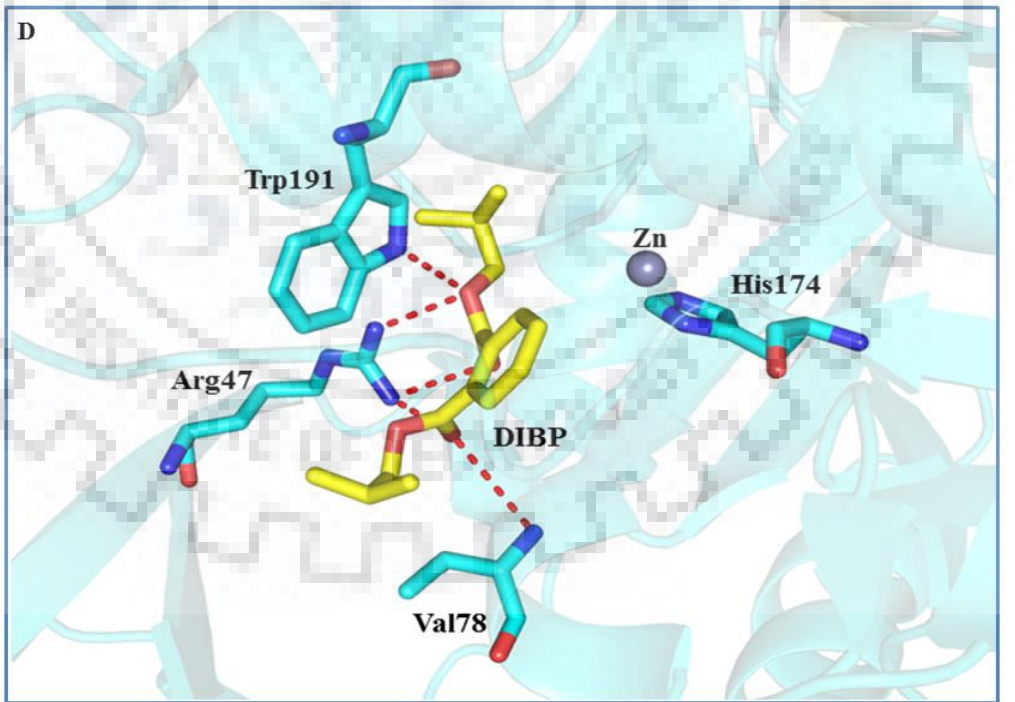
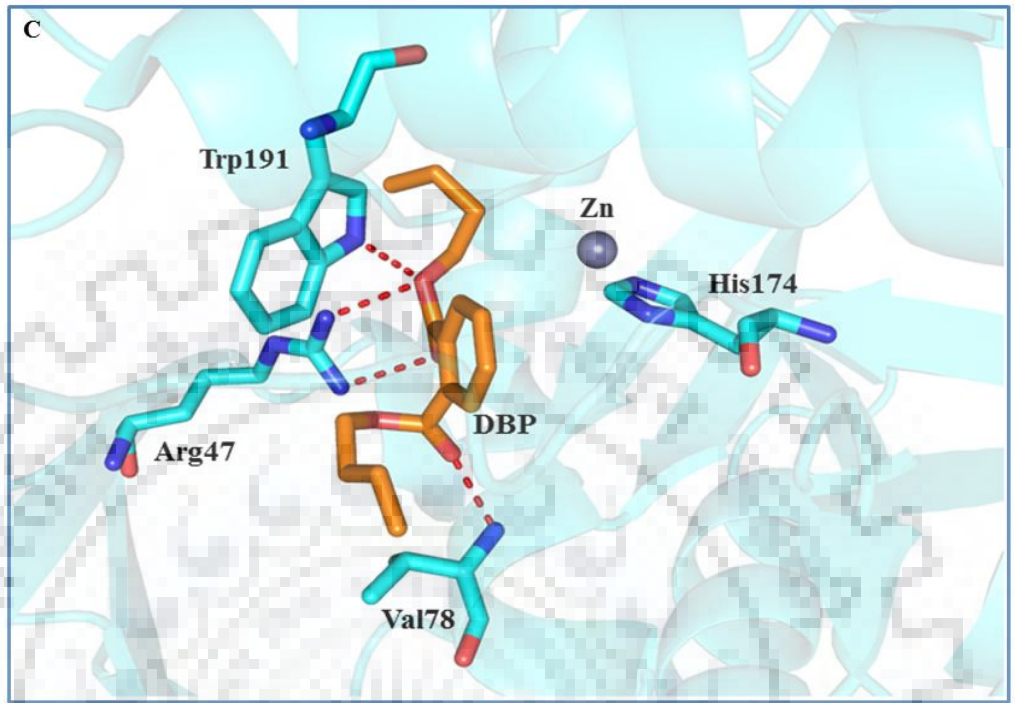




**Figure 3.2. The ribbon diagram of hACMSD binding active site cavity with PDC, DEHP and its metabolites.** A) DEHP (green color), B) MEHP (magenta color), C) MEHHP (pink color), D) MEOHP (pale yellow color) and E) PDC (grey color). All the PAEs occupy the active site cavity within the 4 Å vicinity of zinc metal. Residues of the hACMSD are shown in stick form, zinc metal is shown as a sphere in metallic blue color and the red dotted line represents intermolecular hydrogen bond interactions.

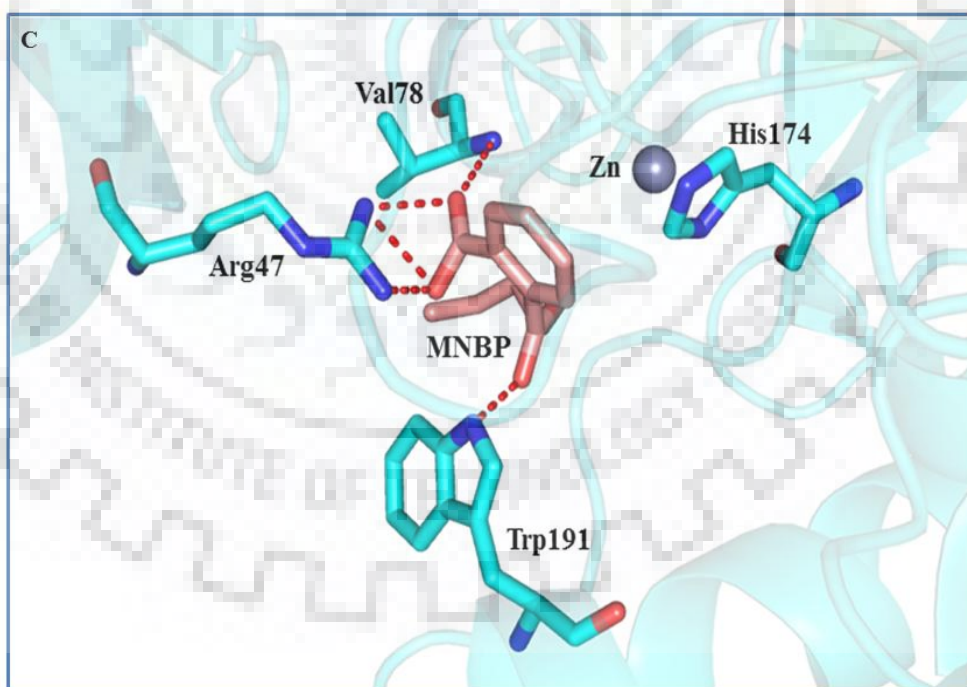
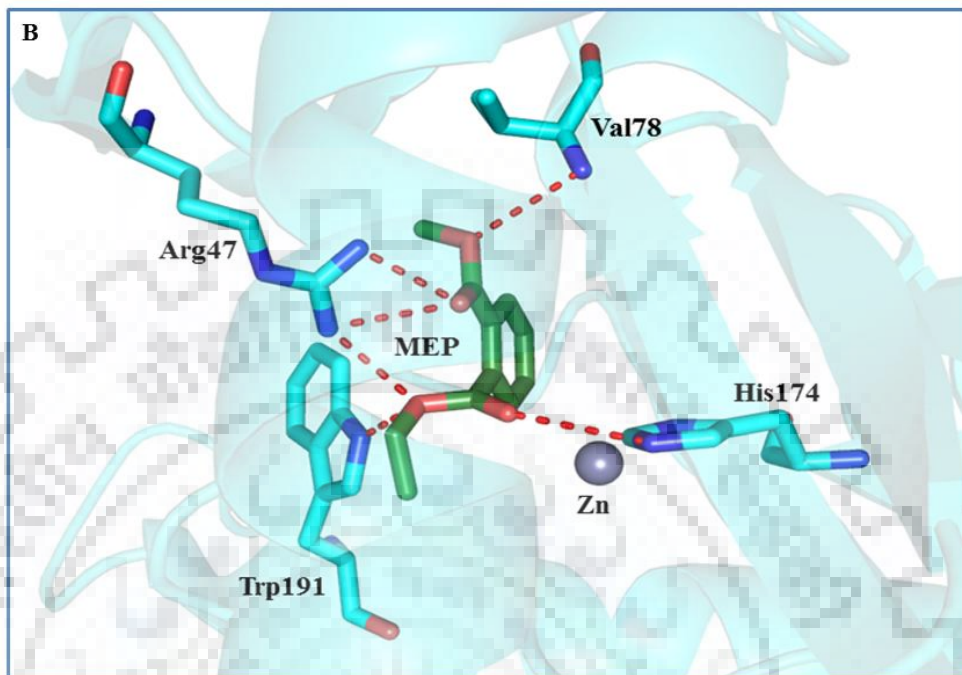












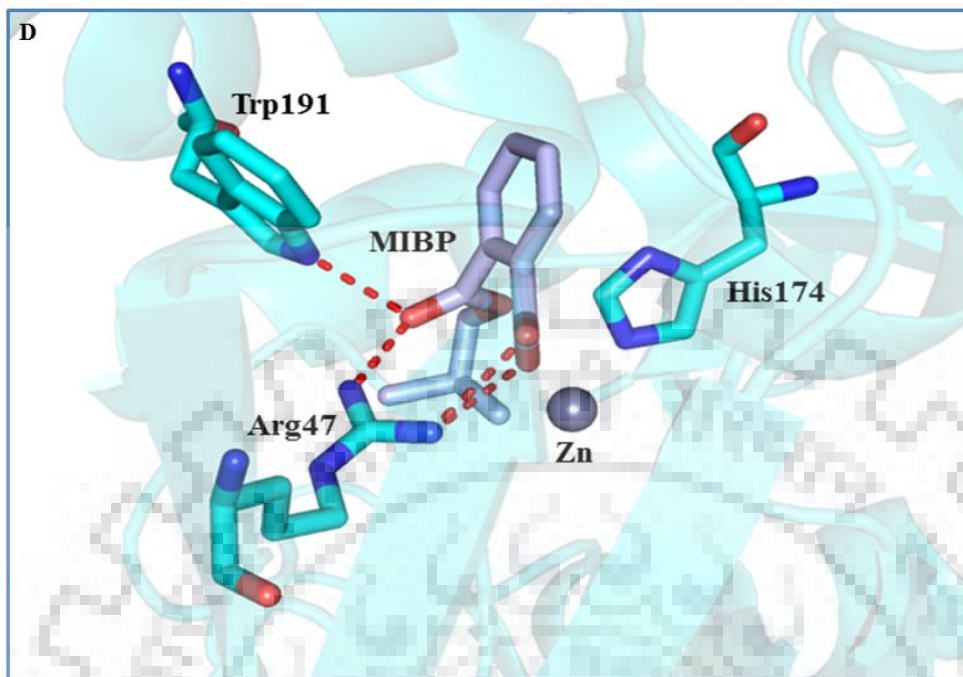


**Figure 3.4. The binding interaction of low molecular weight Monophthalates with hACMSD.** A) MMP (pale green color), B) MEP (forest green color), C) MBP (light red color) and D) MIBP (light blue color). The interacting residues of hACMSD residues are represented in stick form, zinc metal is shown as a sphere in metallic blue color and the red dotted line shows the intermolecular hydrogen bonds.

### 3.3.2 Molecular simulation results

Molecular dynamics simulation studies provide suitable means to understand the changes occurring at the atomistic level in the protein-ligand system and emphasizes on the stability of the complex. Therefore, a simulation study was performed in order to understand the dynamics involved in binding of phthalates to hACMSD. In the present study, different parameters such as RMSD, RMSF, radius of gyration (Rg), solvent accessible surface area (SASA) and the hydrogen bond formation and length distribution during the course of the simulation have been studied.

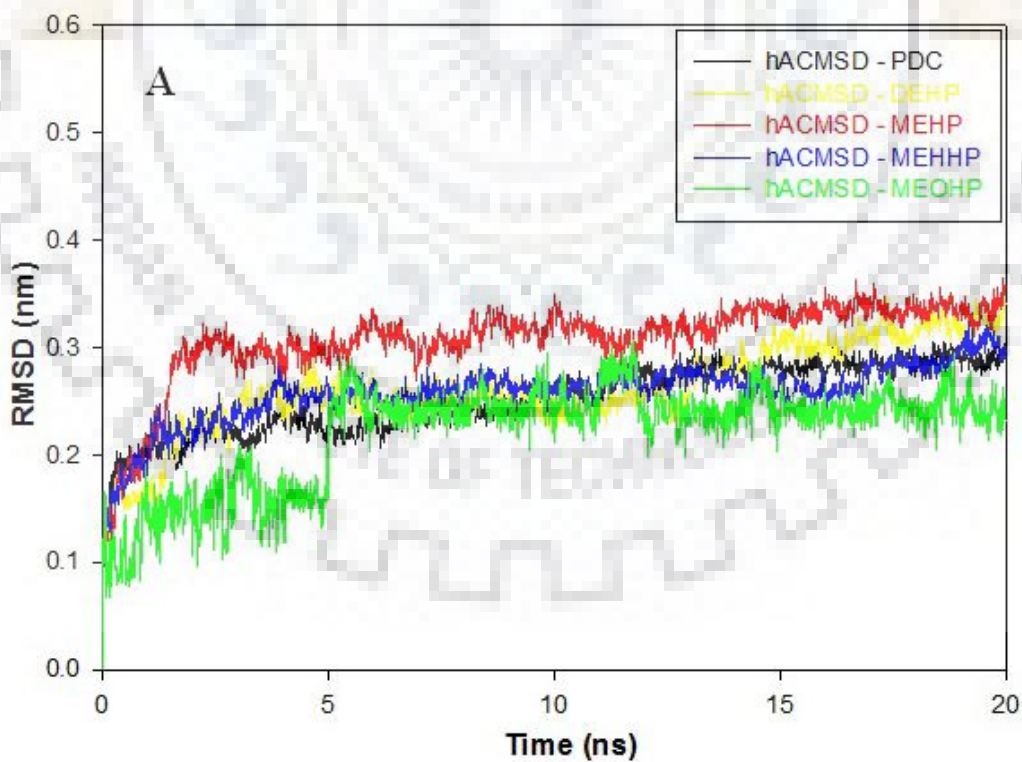
### 3.3.2.1 Root-mean-square deviation (RMSD)

It represents the dynamic stability of the protein and predicts the conformation changes occurring in the protein backbone during the simulation. Here, in the present study, RMSD values of PDC-hACMSD and PAEs-hACMSD complexes were analyzed. RMSD plots show that most of the system acquires equilibrium within 10-12 ns during the course of the simulation and were stable up to 20 ns as shown in **Figure 3.5**. The average RMSD values of the PAEs-hACMSD complexes were compared with the reference ligand PDC-hACMSD complex as shown in **Table 3.3**. The high fluctuation of the RMSD values for all the complexes lies within the range of 2 Å to 3 Å. Complexes of lower molecular weight monophthalates with hACMSD showed less average RMSD as compared to their corresponding diphthalates. Complexes of hACMSD with DEP and MEP show initial fluctuations and attained equilibrium after 7 ns of simulation. RMSD results suggest that there is no major change in the backbone RMSD patterns of PAEs-hACMSD complexes as compared to PDC-hACMSD complex. Moreover, results reveal that lower molecular weight monophthalates have a less average root mean square deviation and are more stabilized as compared to their corresponding diphthalates. The RMSD results analysis implies that the binding of phthalates at the catalytic site of hACMSD is stable and does not vary the protein backbone stability.

**Tables 3.3. Average values of RMSD and RMSF of hACMSD-PAEs complexes.**

Average RMSD and RMSF values corresponding to variation in hACMSD backbone on the binding of PAEs and PDC.

S.No	Compound	Average RMSD (nm)	Average RMSF (nm)
1.	PDC	0.252	0.112
2.	DEHP	0.261	0.126
3.	MEHP	0.307	0.115
4.	MEHHP	0.257	0.125
5.	MEOHP	0.221	0.125
6.	DMP	0.278	0.127
7.	DEP	0.275	0.117
8.	DBP	0.255	0.118
9.	DIBP	0.295	0.111
10.	MMP	0.231	0.102
11.	MEP	0.262	0.136
12.	MBP	0.223	0.110
13.	MIBP	0.279	0.132



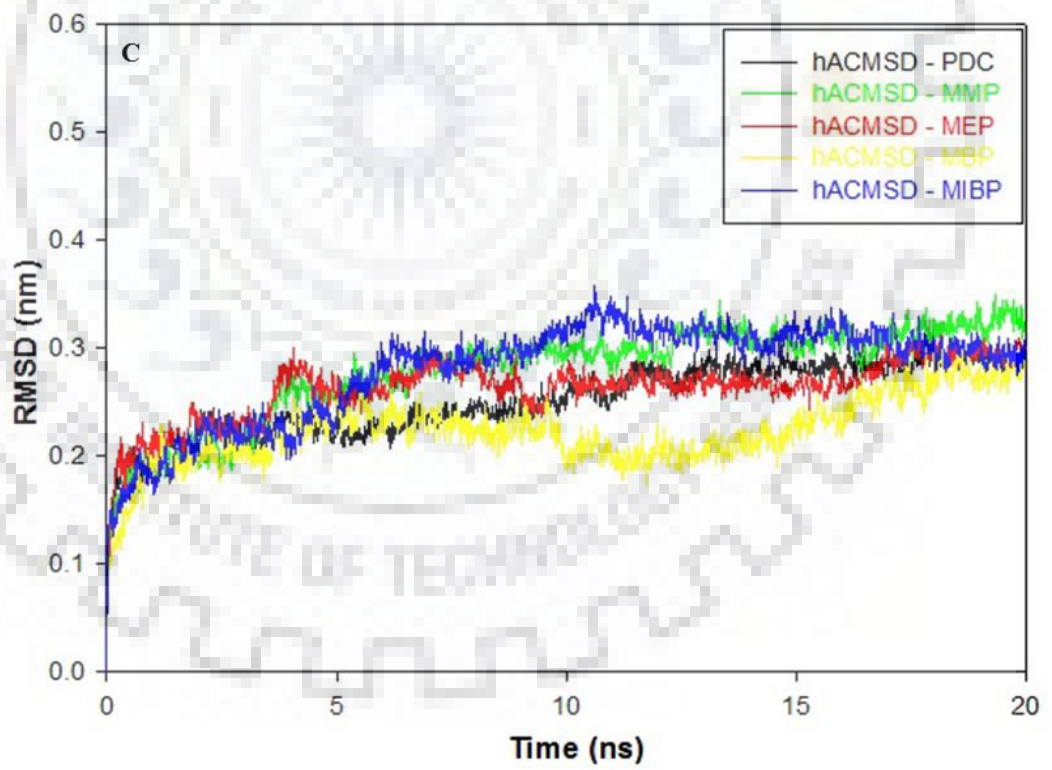
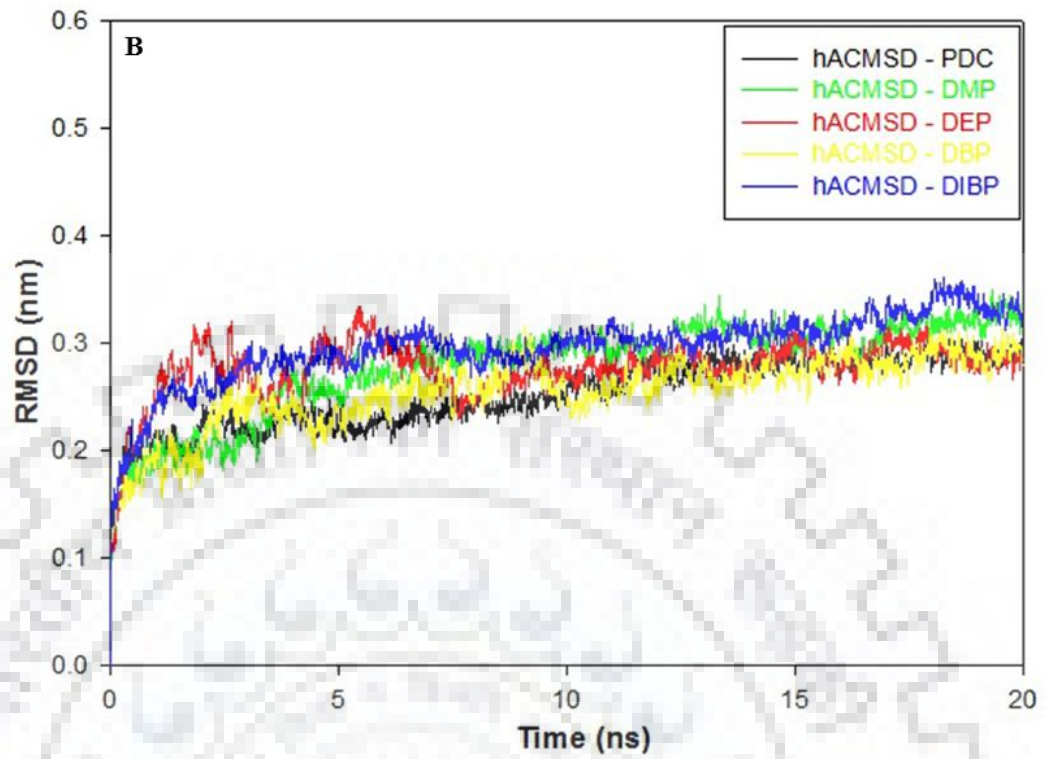
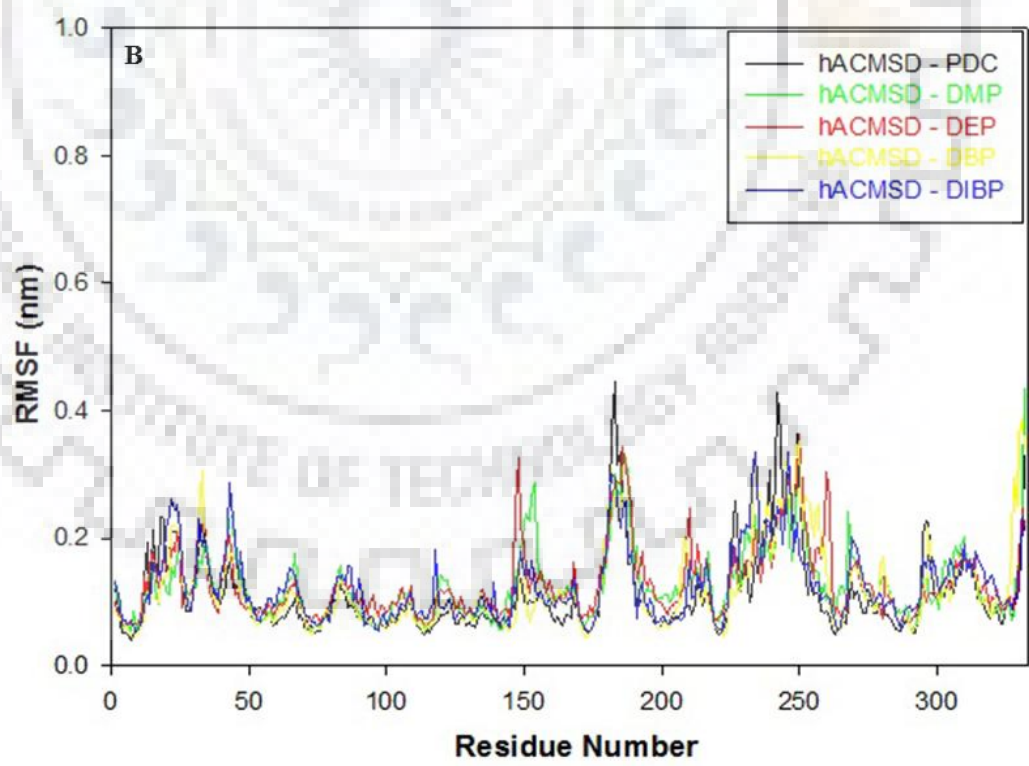
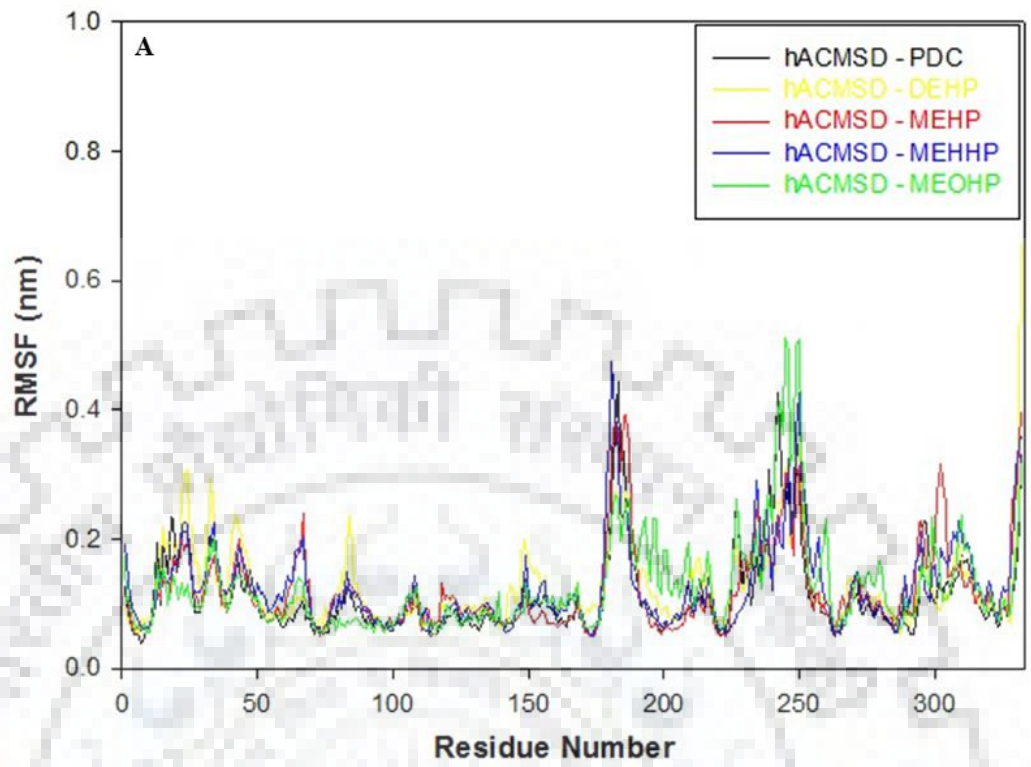




**Figure 3.5. RMSD graph of hACMSD with PDC and PAEs.** RMSD profile of the C $\alpha$  backbone of hACMSD during the 20ns of simulation at 300 K: A) PDC, DEHP and its metabolites, B) PDC and low molecular weight diphthalates such as DMP, DEP, DBP and DIBP, and C) PDC and low molecular weight monophthalates such as MMP, MEP, MBP and MIBP.

### 3.3.2.2 Root-mean-square fluctuation (RMSF)

RMSF determines the flexibility of the polypeptide chain after fitting it to a reference frame. It is the fluctuation of C $\alpha$  atom coordinates from their average position during the simulation. Generally, in proteins loosely organized loops are characterized by high RMSF values while secondary structural elements show less flexibility. In the present context, residue mobility was calculated for each of the PAEs-hACMSD complexes and was plotted against the residue number based on the trajectory of MD simulation. Results show a higher RMSF peak in the residues range of 180–193, a loop region, which facilitates the entry of ligands into the active site of hACMSD as shown in **Figure 3.6**. The partial helical region from the residue 232–250, present towards the C terminal of hACMSD also shows the higher RMSF fluctuation. These results suggest that active site residues were not considerably perturbed upon binding of the ligands. Results illustrate that the RMSF fluctuation profiles of PAEs-hACMSD complexes were almost similar to PDC-hACMSD complex. RMSFs results imply that the atomic mobility of PAEs-hACMSD complexes is in consent with PDC-hACMSD complex. Thus, the PAEs form stable complexes with hACMSD and can inhibit this important enzyme of tryptophan metabolism pathway.



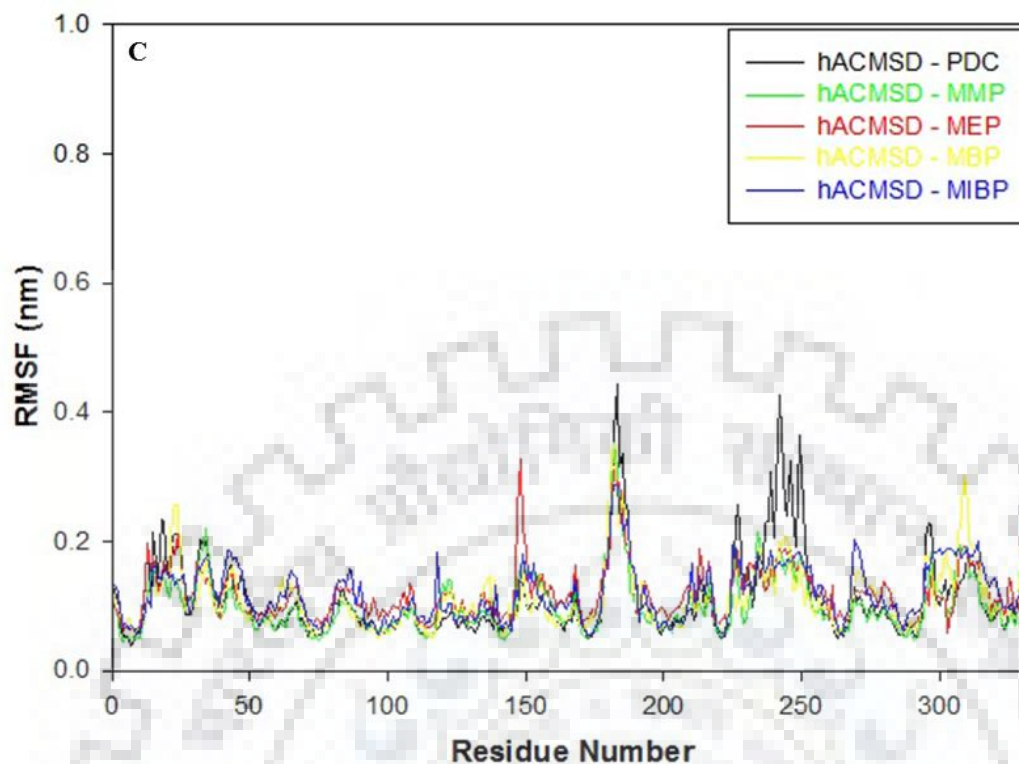
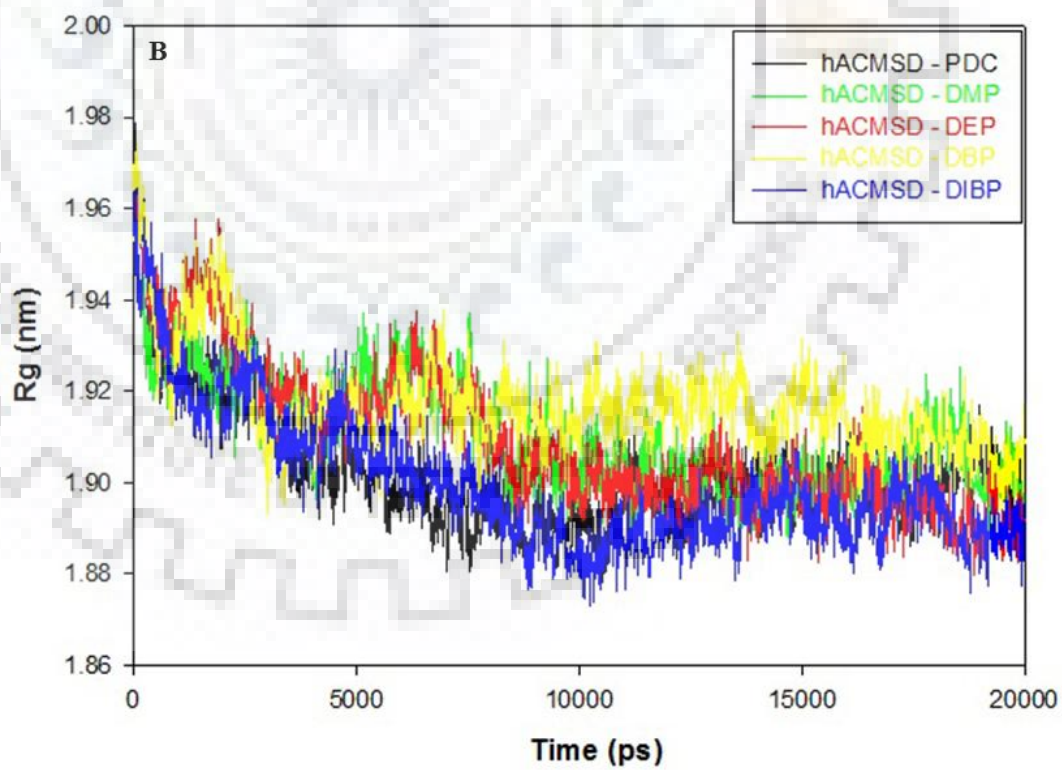
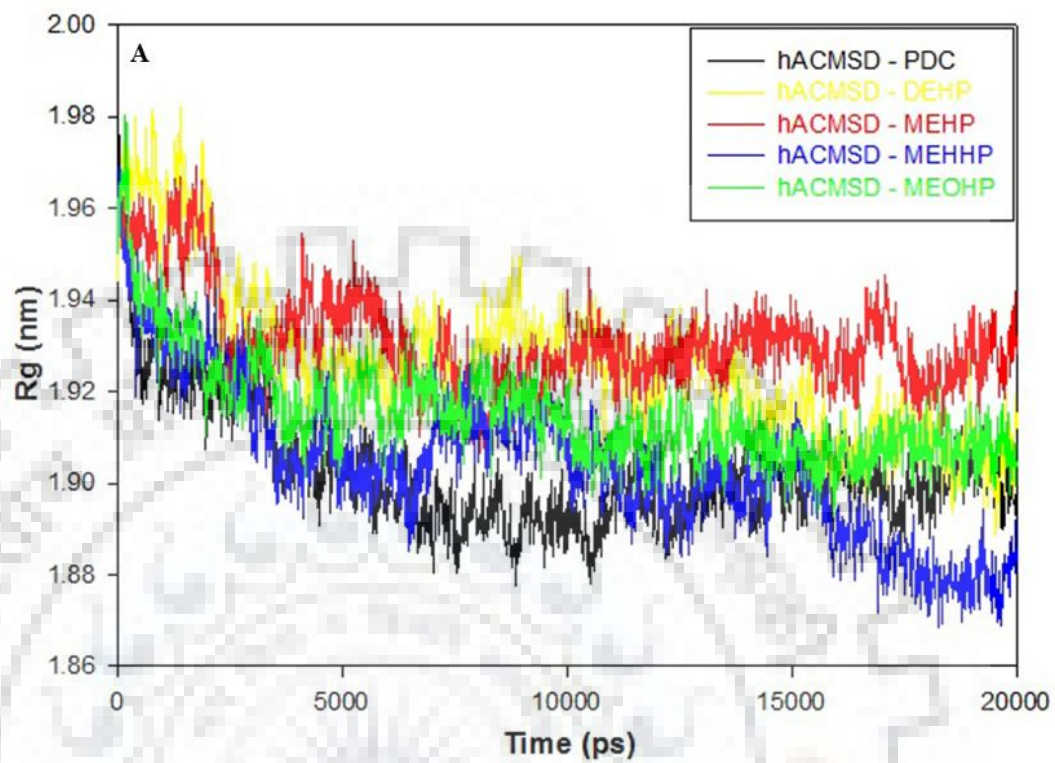


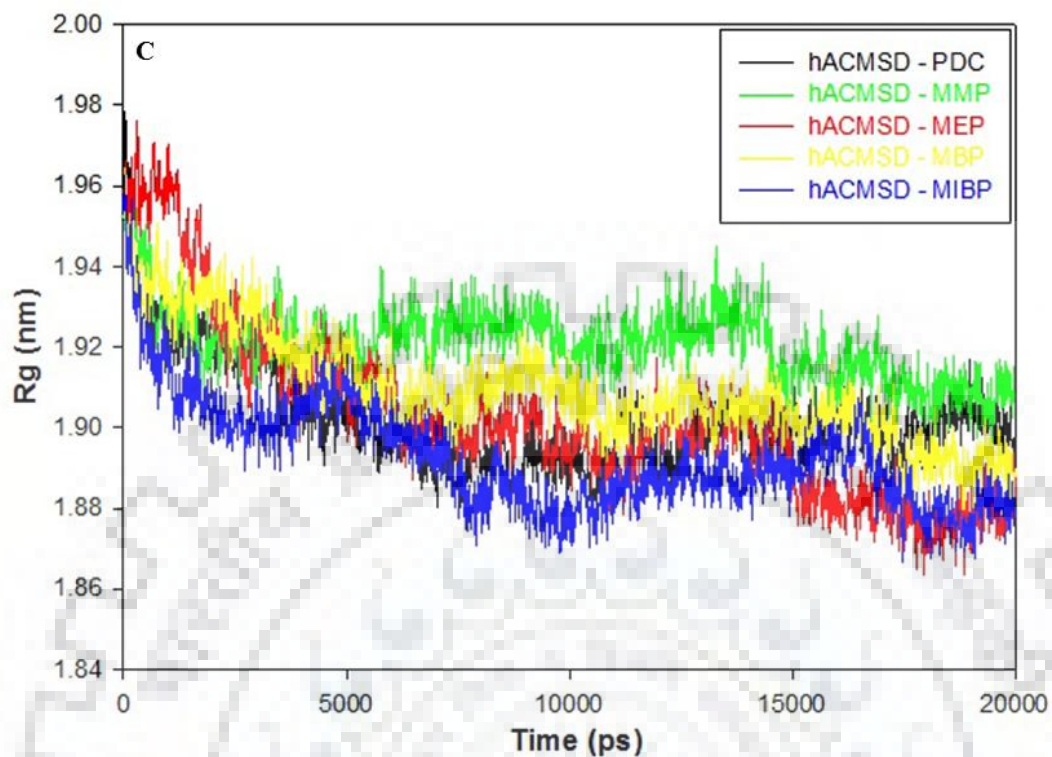
**Figure 3.6. RMSF molecular dynamics simulation results of hACMSD for 20ns.** A) PDC, DEHP and its metabolites with hACMSD, B) PDC and low molecular weight diphthalates such as DMP, DEP, DBP and DIBP with hACMSD, and C) PDC and low molecular weight monophthalates such as MMP, MEP, MBP, and MIBP.

### 3.3.2.3 Radius of gyration (Rg)

Radius of gyration (Rg) factor is associated with the compactness of protein during the molecular simulation. It is simply a measure of the distance between the center of mass of the protein atoms and its terminal in a given time step. In general, a stably folded protein tends to maintain a relatively less variation in Rg value which determines its dynamic stability. In the present study, variation occurring in Rg value is plotted against time as shown in **Figure 3.7**. The radius of gyration results shows that compactness of phthalate-hACMSD complexes is comparable to the PDC-hACMSD complex. Rg results reveal that secondary structures are compactly packed in the case of diphthalates and their metabolites to form stable complexes with hACMSD.



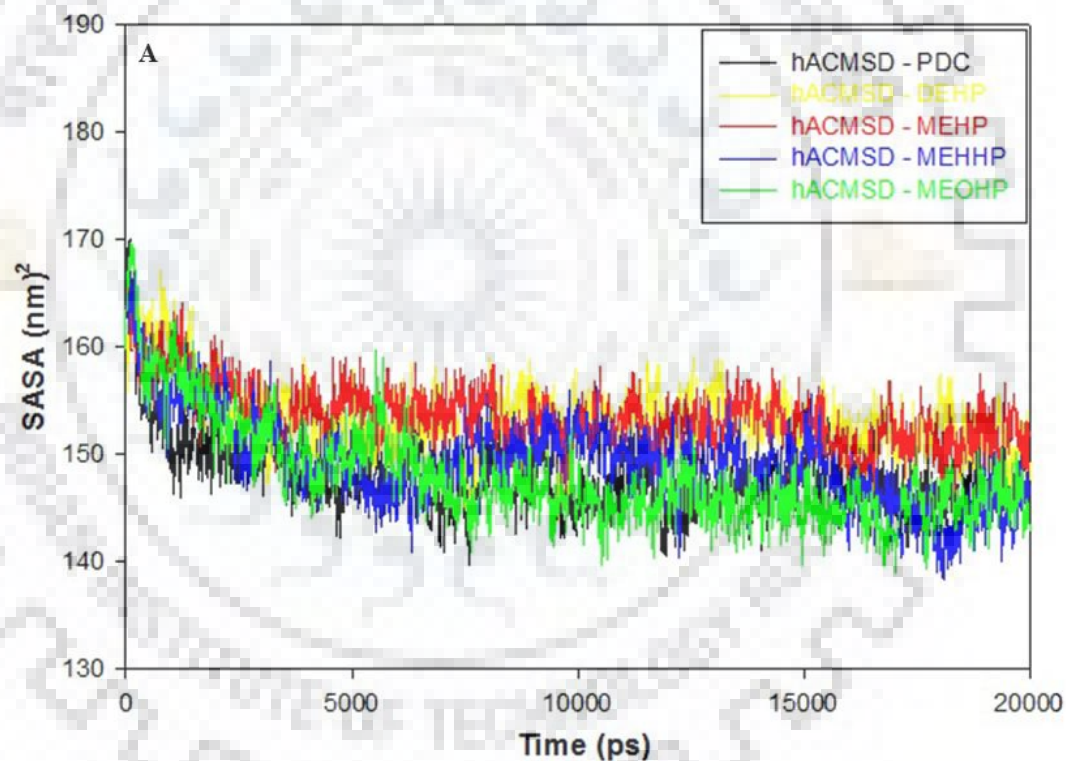




**Figure 3.7. Radius of gyration (Rg) plots of PDC-hACMSD and PAEs-hACSMD.** The radius of gyration results associated with the compactness of the hACMSD protein for the simulation of 20 ns: A) PDC, DEHP and its metabolites, B) PDC and low molecular weight diphtalates such as DMP, DEP, DBP and DIBP, and C) PDC, low molecular weight monophthalates such as MMP, MEP, MBP and MIBP.

### 3.3.2.4 Solvent accessible surface area (SASA)

The solvation free energy of each atom in a protein is contributed by its polar and non polar residue interactions. Solvent accessible surface area (SASA) is the surface area monitored by the probe of the solvent molecule when it traces the Van der Waals surface of the receptor molecule. Mostly structural alterations are monitored in the residues forming the loop region in the vicinity of the active site cavity. In general, hydrophobic residues mostly contribute to the rise of SASA value. This is also apparent by the raised value of the solvent accessible surface area (SASA) in that region. SASA results of PAEs-hACMSD complexes are similar to PDC-hACMSD complex as shown in **Figure 3.8**.



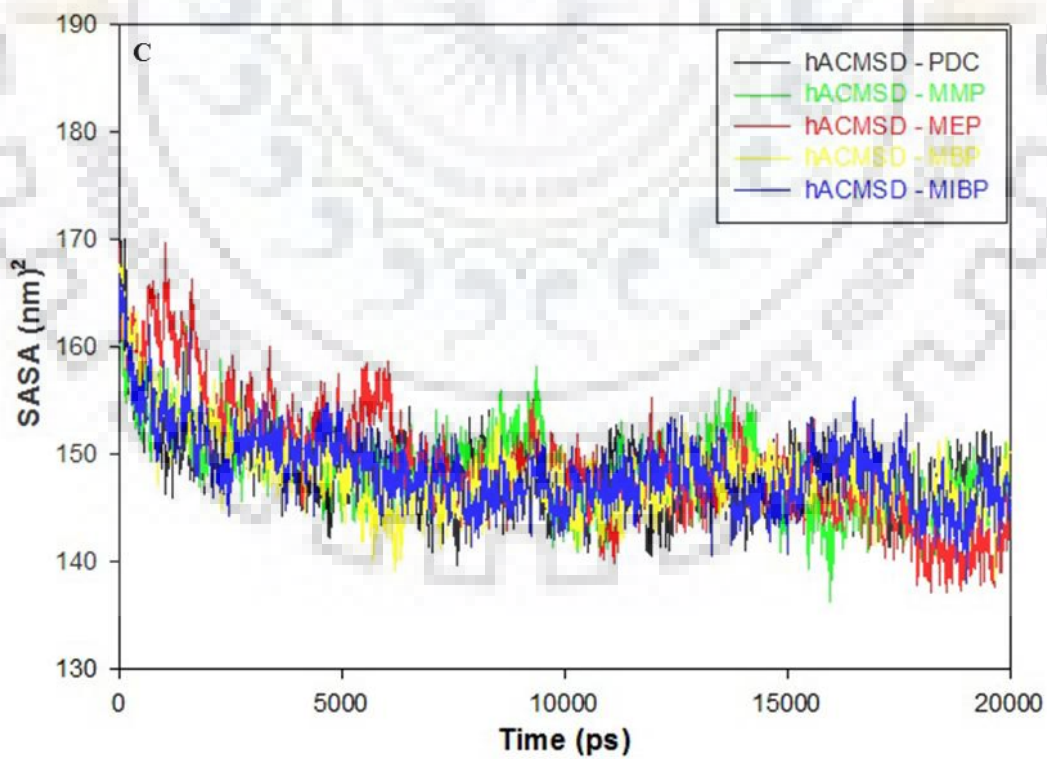
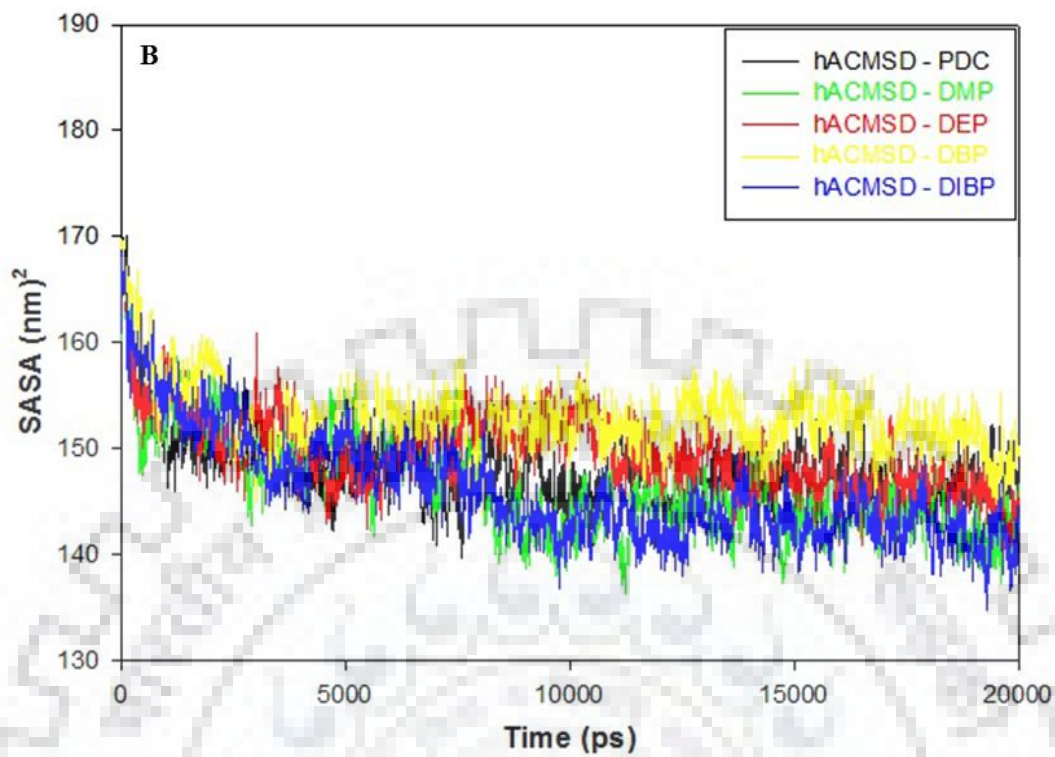
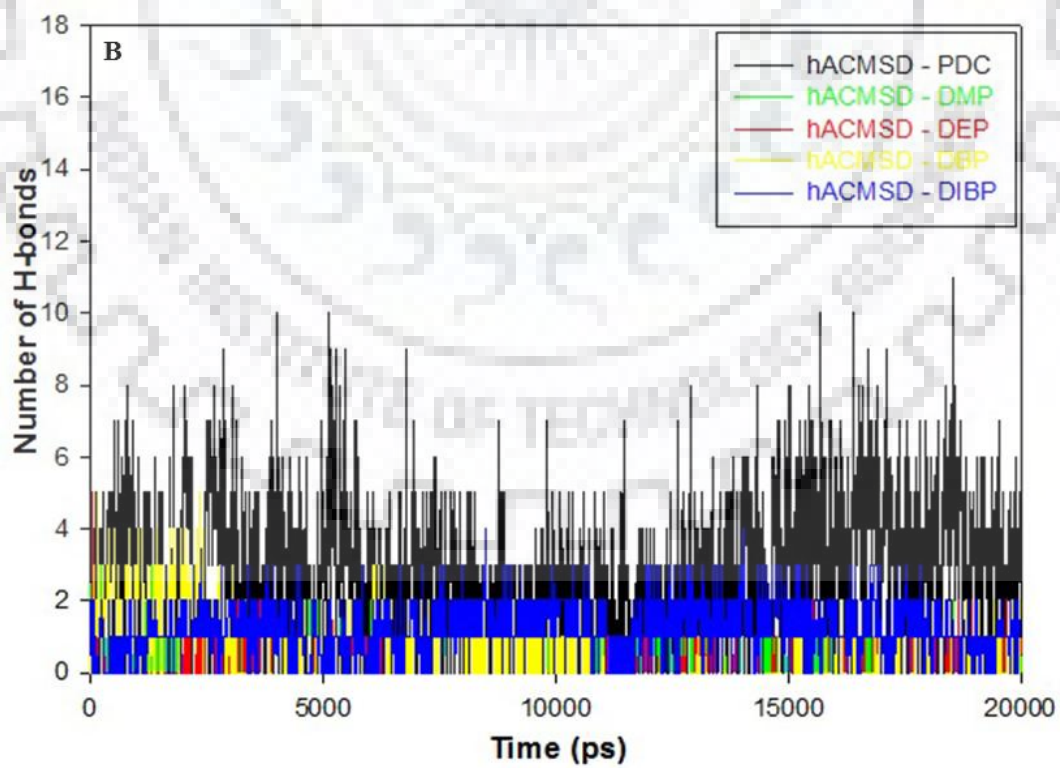
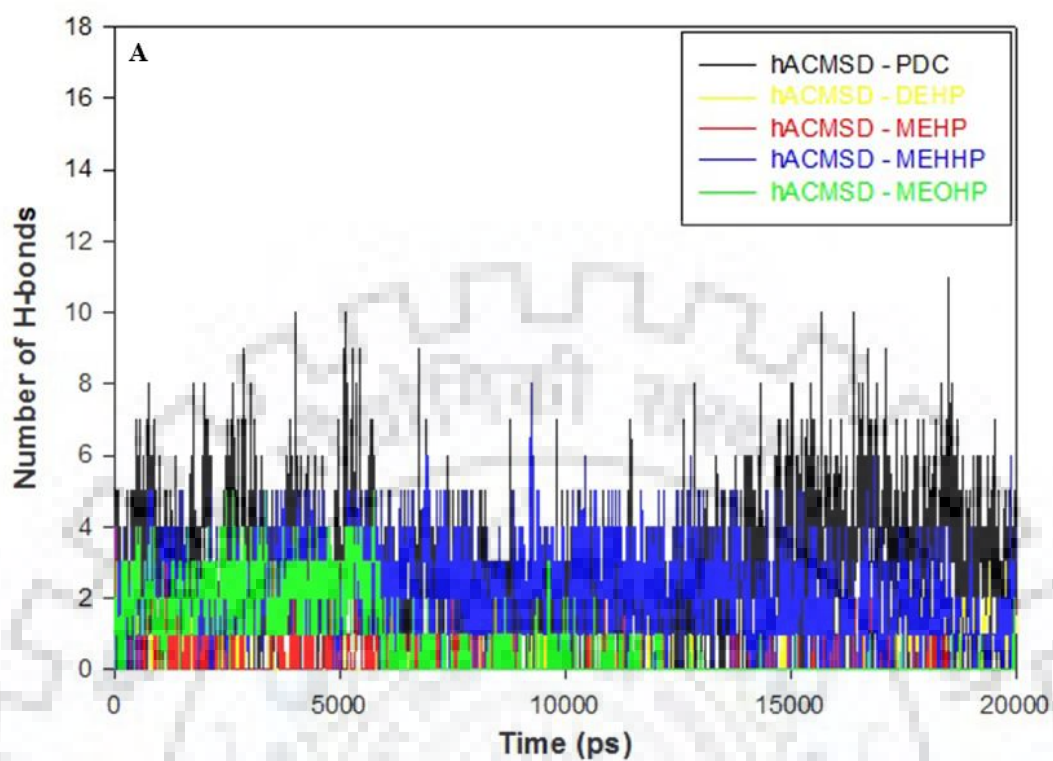


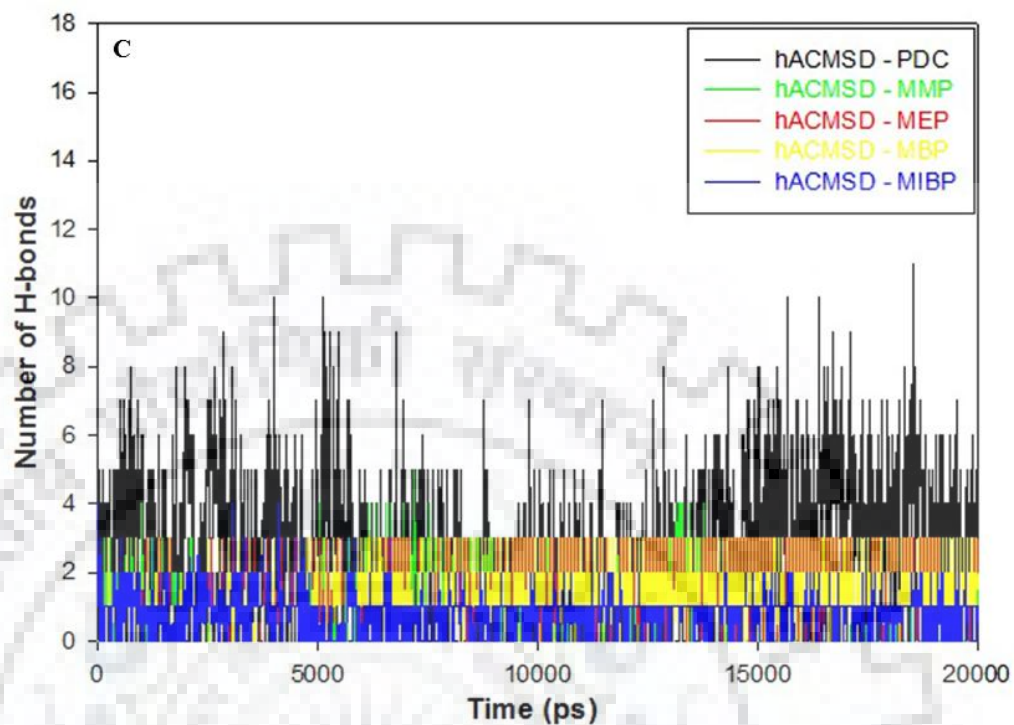
**Figure 3.8. Solvent accessible surface area profile of hACMSD with PDC and PAEs.** SASA results of hACMSD-PDC and hACMSD-PAEs complexes during the simulation of 20 ns: A) PDC, DEHP and its metabolites, B) PDC and low molecular weight diphthalates such as DMP, DEP, DBP and DIBP, and C) PDC and low molecular weight monophthalates such as MMP, MEP, MBP, and MIBP.

### 3.3.2.5 Hydrogen bond analysis

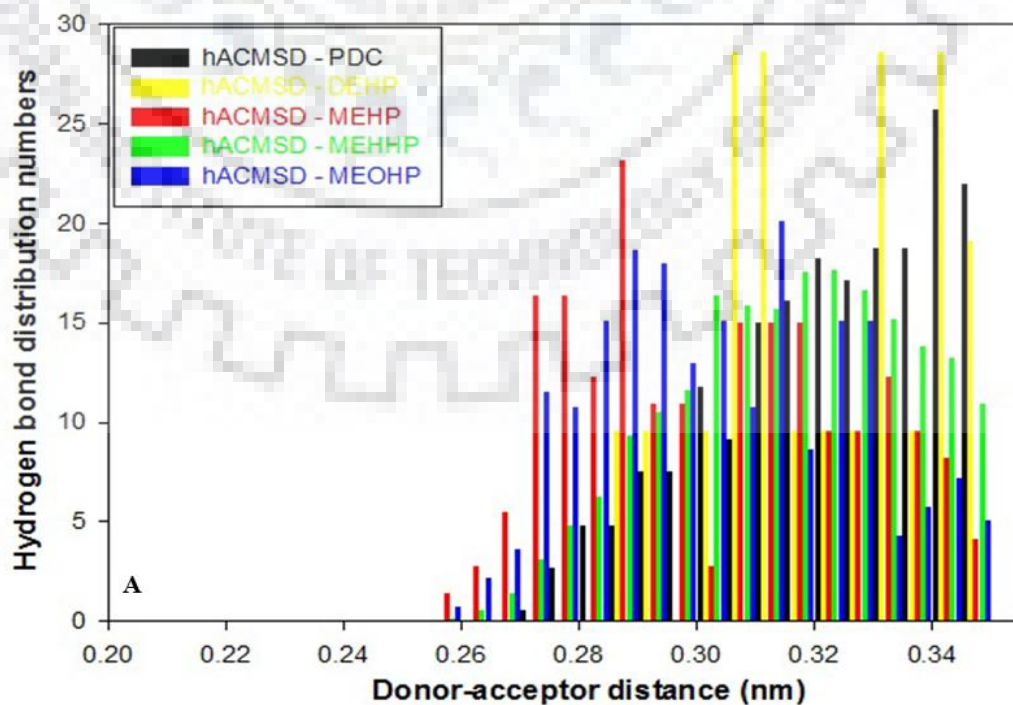
Hydrogen bond number and distribution in the PAEs-hACMSD complexes were studied to determine the stability of the system during the 20 ns simulation period. The `g_hbond` utility of GROMACS was employed to compute the hydrogen bond numbers and distribution profiles of the complexes. Hydrogen bond numbers results show that the most of the PAEs-hACMSD complexes have maintained a minimum of two hydrogen bonds throughout the course of simulation as shown in **Figure 3.9**. Moreover, monophthalate metabolites of DEHP such as MEHP, MEHHP, and MEOHP form a maximum number of hydrogen bonds with the hACMSD during the course of 20 ns simulation. The average number of h bonds during the MD phase shows their continuous contribution in providing stability to the complex. The results of the distribution of hydrogen bond lengths also indicate that the PAEs-hACMSD complexes have form high to low-affinity hydrogen bonds, which is in consent with PDC-hACMSD complex as shown in **Figure 3.10**. The hydrogen bond results help in understanding the functionality and ability of these harmful phthalate compounds to effectively hinder the activity hACMSD in the kynurenine pathway.







**Figure 3.9. Hydrogen bond number results of PDC-hACMSD and PAEs-hACMSD complexes during the 20ns of simulation.** A) PDC, DEHP and its metabolites, B) PDC and low molecular weight diphthalates such as DMP, DEP, DBP and DIBP, and C) PDC and low molecular weight monophthalates such as MMP, MEP, MBP, and MIBP.



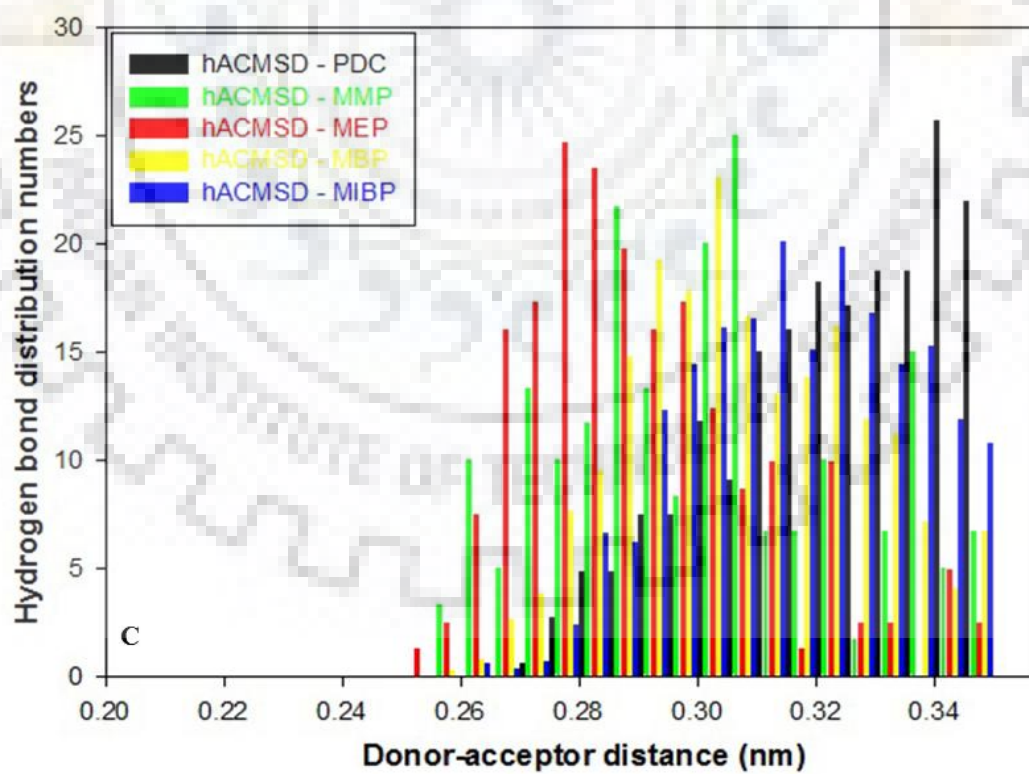
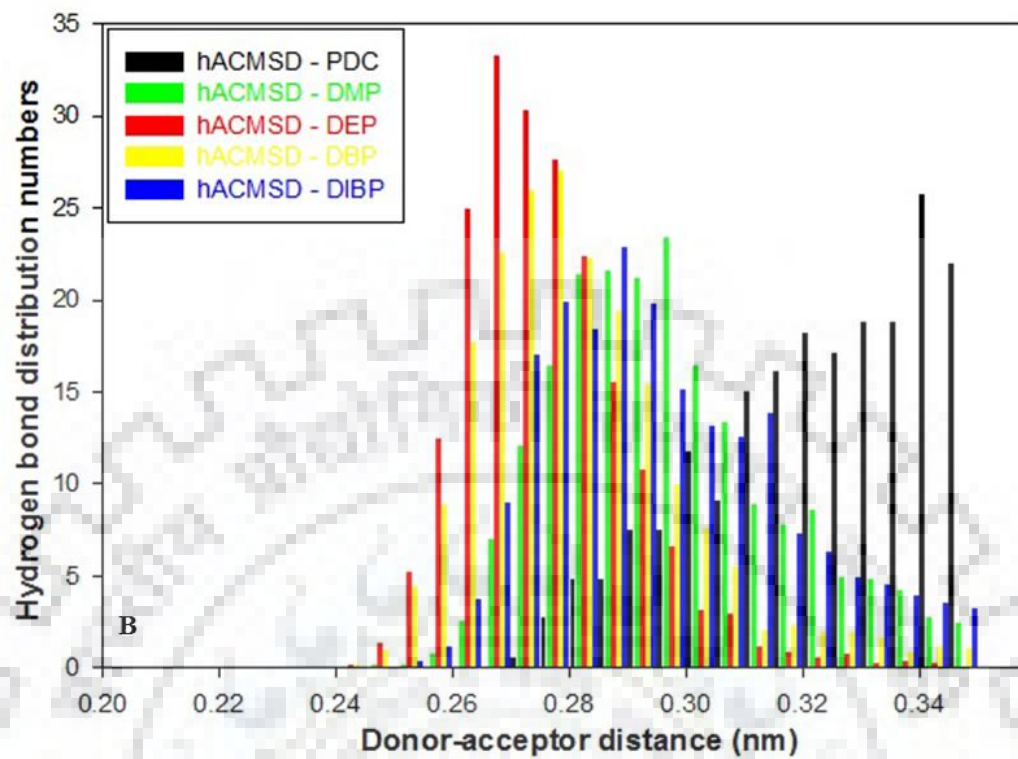




**Figure 3.10. Bar representation of the hydrogen bond number distribution of hACMSD with PDC and PAEs.** Hydrogen bond distribution profile of PDC-hACMSD and PAEs-hACMSD complexes for the course of 20ns simulation at 300 K, A) PDC, DEHP and its metabolites, B) PDC and low molecular weight diphthalates such as DMP, DEP, DBP and DIBP, and C) PDC and low molecular weight monophthalates such as MMP, MEP, MBP and MIBP.

### 3.3.3 MMPBSA binding free energy calculation

The free energy calculation analysis is useful in assessing the binding potential of ligands as it provides a quantitative estimation of the binding free energy. MMPBSA, a utility within GROMACS was utilized to calculate the binding free energy of PAEs-hACMSD complexes. The trajectories of the last 5 ns of PAEs-hACMSD complexes were generated and the MMPBSA was utilized for the prediction of the binding energy of the complexes. MMPBSA results show that the binding free energies of the PAEs are comparable to the PDC while the monophthalates metabolites of DEHP have higher binding free energy than other PAEs as shown in **Table 3.4**. Binding free energy results of MMPBSA indicate that PAEs-hACMSD complexes are stable. MMPBSA results confirm that these phthalates can efficiently bind to the active site of hACMSD and inhibit enzymatic activity. Highest binding free energies of DEHP and its metabolites reveal that they can bind with high affinity to hACMSD as compared to PDC.

**Tables 3.4. Binding energies of hACMSD-PAEs complexes by MMPBSA.** Van der Waals energy, electrostatic energy, polar solvation energy and SASA energy components contributing to the total binding free energy of hACMSD-PAEs and hACMSD-PDC complexes.

S.No	Compound	Van der Waals energy (kJ/mol)	Electrostatic energy (kJ/mol)	Polar solvation energy (kJ/mol)	SASA energy (kJ/mol)	Binding energy (kJ/mol)
1	PDC	-139.405 +/- 0.329	-9.747 +/- 0.331	67.745 +/- 0.423	-11.127 +/- 0.027	-92.546 +/- 0.567
2	DEHP	-213.316 +/- 0.602	-12.924 +/- 0.346	157.375 +/- 1.362	-20.392 +/- 0.056	- 89.257 +/- 1.515
3	MEHP	-182.956 +/- 0.609	-35.861 +/- 0.383	104.625 +/- 0.742	-15.679 +/- 0.045	-129.888 +/- 0.686
4	MEHHP	-201.045 +/- 0.928	-10.651 +/- 0.404	78.052 +/- 0.629	-15.373 +/- 0.059	-149.068 +/- 0.806
5	MEOHP	-228.297 +/- 0.522	-22.370 +/- 0.309	118.271 +/- 0.579	-17.246 +/- 0.043	-149.646 +/- 0.847
6	DMP	-158.565 +/- 0.343	-25.771 +/- 0.241	122.446 +/- 0.451	-12.060 +/- 0.029	- 73.961 +/- 0.507
7	DEP	-142.667 +/- 0.468	-42.500 +/- 0.454	135.593 +/- 1.449	-12.310 +/- 0.040	-61.884 +/- 1.347
8	DBP	-167.730 +/- 0.465	-27.721 +/- 0.459	124.417 +/- 0.716	-14.253 +/- 0.042	-85.287 +/- 0.810
9	DIBP	-183.035 +/- 0.477	-9.031 +/- 0.340	125.265 +/- 0.891	-17.092 +/- 0.041	-83.893 +/- 0.910
10	MMP	-149.449 +/- 0.410	-65.586 +/- 0.430	139.931 +/- 0.756	-10.851 +/- 0.026	-85.955 +/- 0.990
11	MEP	-145.130 +/- 0.379	-23.799 +/- 0.557	103.311 +/- 1.398	-12.793 +/- 0.039	-78.411 +/- 1.385
12	MBP	-182.239 +/- 1.320	-20.841 +/- 0.394	108.814 +/- 0.860	-13.533 +/- 0.098	-107.794 +/- 1.402
13	MIBP	-196.513 +/- 0.367	-9.160 +/- 0.191	122.351 +/- 0.323	-13.708 +/- 0.029	-97.022 +/- 0.489

### 3.4 Conclusion

Human  $\alpha$ -amino- $\beta$ -carboxymuconate- $\epsilon$ -semialdehyde decarboxylase (hACMSD) is a zinc-containing amidohydrolase which is a vital enzyme of the kynurenine pathway in tryptophan metabolism. It prevents the accumulation of quinolinic acid (QA) and helps in the maintenance of basal Trp-niacin ratio. To assess the structure based inhibitory action of PAEs such as DMP, DEP, DBP, DIBP, DEHP and their metabolites, these were docked into the active site cavity of hACMSD. Docking results show that the binding affinities of PAEs lie in the comparable range (-4.9 kcal/mol -7.48 kcal/mol) with Dipicolinic acid (-6.21 kcal/mol), a substrate analog of hACMSD. PAEs interact with the key residues such as Arg47 and Trp191 and lie within the 4 Å vicinity of zinc metal at the active site of hACMSD. Dynamics and stability of the PAEs-hACMSD complexes were determined by performing molecular dynamics simulations using GROMACS 5.14. Binding free energy calculations of the PAEs-hACMSD complexes were estimated by using MMPBSA method. The results emphasize that PAEs can structurally mimic the binding pattern of tryptophan metabolites to hACMSD, which further leads to inhibition of its activity and accumulation of the quinolate in the kynurenine pathway of tryptophan metabolism. In kynurenine pathway, human  $\alpha$ -amino- $\beta$ -carboxymuconate- $\epsilon$ -semialdehyde decarboxylase (hACMSD) controls the level of quinolinic acid. The inhibition of hACMSD activity may lead to the elevation of quinolate levels, which is often associated with several neurological disorders. PAEs are the ubiquitous environmental pollutants which have endocrine disruption and teratogenic properties. The in-silico techniques such as molecular docking and simulation studies were done to analyze the interactions of commonly used PAEs with hACMSD. This computational study shows that the PAEs-hACMSD complexes are stable and have binding affinities similar to natural substrate analog complex i.e. PDC-hACMSD. Hence, PAEs and their metabolites can efficiently bind to hACMSD and inhibit its activity in the kynurenine pathway of tryptophan metabolism. Our study emphasizes on the inhibitory effects of phthalates on hACMSD activity and simultaneously provides a regulatory link between disturbances in trp to niacin ratio on the administration of PAEs in the diet. Further studies should focus on the in-vitro assessment of phthalate toxicity and correlation needs to establish between the elevations of quinolinic acid level in urine along with corresponding phthalate exposure.



**CHAPTER 4**

**BIODEGRADATION OF PHTHALIC ACID ESTERS (PAES) AND IN SILICO  
STRUCTURAL CHARACTERIZATION OF MONO-2-ETHYLHEXYL  
PHTHALATE (MEHP) HYDROLASE ON THE BASIS OF CLOSE STRUCTURAL  
HOMOLOG**



## 4.1 Introduction

Phthalates are the dialkyl or alkyl aryl esters of o-phthalic acid, which are ubiquitous environmental pollutants. They are frequently used as plasticizers to provide stability and flexibility to the plastic products [182, 184]. Phthalates have many different properties which depend on the composition and the type of alcohol that usually makes up the alkyl chain of phthalates [183]. Several experimental and in silico molecular docking studies have highlighted the toxic effects related to phthalate exposure. This may eventually lead to inhibition of normal activities of various receptors such as peroxisome proliferator-activated receptors, glucocorticoid receptors, estrogen receptors and progesterone receptors [191, 246-250]. Six PAEs namely Dimethyl phthalate (DMP), Diethyl phthalate (DEP), Di-n-butyl phthalate (DnBP), Benzyl butyl phthalate (BBzP), Di-(2-ethylhexyl) phthalate (DEHP) and Di-n-octyl phthalate (DnOP) are in the priority pollutants list of United States Environmental Protection Agency (USEPA) and European Union (EU), due to their explored toxicological, teratogenic and mutagenic properties [86, 88, 251].

Bioremediation is an effective and important method for removal of these harmful phthalates from the environment. There are numerous studies related to PAEs degradation pathways using pure cultures [85, 108, 186, 187, 252-255]. Under aerobic and anaerobic environmental conditions, the different type of pathways such as de-esterification or dealkylation,  $\beta$ -oxidation, and trans-esterification lead to the primary degradation of phthalate diesters to phthalate monoesters [116]. Further, phthalate monoesters are serially degraded to yield phthalic acid (PA) [256]. In aerobic condition, dioxygenase mediated reaction degrades PA to protocatechuate which is further degraded to oxaloacetate and pyruvate [257-259]. In anaerobic degradation, PA is decarboxylated to benzoate, which is then cleaved and degraded via  $\beta$ -oxidation to hydrogen,  $\text{CO}_2$ , and acetate [260]. Likewise, in the DEHP degradation pathway, MEHP is an intermediate which is further reduced to PA [261]. It is to be noted that, degradation of MEHP to PA is mediated by MEHP hydrolases, belonging the serine hydrolases family. The primary sequences of MEHP hydrolase characterized from *Gordonia* sp. P8219 and *Rhodococcus* EG-5 have conserved catalytic triad and pentapeptide motif ( $\text{GX}_1\text{SX}_2\text{G}$ ) which are distinctive features of this class of serine hydrolases [124, 262].

Three-dimensional structural knowledge of MEHP hydrolase is important to understand the interactions involved in the binding of phthalate monoesters to MEHP hydrolase. The present study focuses on the isolation and characterization of efficient PAEs degrading strains. The tentative DEHP degradation pathway was generated from the identification of intermediate metabolites which were formed during DEHP degradation. In addition, a 3D homology model of MEHP hydrolase from *Pseudomonas mosselii* was predicted. The phthalate monoesters such as mono-2-ethylhexyl phthalate (MEHP), mono-n-hexyl phthalate (MHP), mono-n-butyl phthalate (MBP) and mono-n-ethyl phthalate (MEP) were docked with MEHP hydrolase to understand the interactions between protein receptor and ligand.

## **4.2 Materials and Methods**

### **4.2.1 Chemicals and Media**

DMP, DEP, DEHP, *n*-hexane all with  $\geq 97\%$  purity were procured from Sigma-Aldrich (St. Louis, MO, USA). Analytical grade chemicals were used. Agar, antibiotics (kanamycin, ampicillin, and chloramphenicol) were purchased from HiMedia Chemicals (Mumbai, India). Luria-Bertani medium (LB) composed of ( $L^{-1}$ ): 10 g of tryptone, 5 g of yeast extract and 10 g of NaCl. Modified minimal salt media (MSM) contained ( $L^{-1}$ ) 6.0 g of Tris-HCl, 1.07 g of  $NH_4Cl$ , 4.68 g of NaCl, 0.2 g of  $MgCl_2 \cdot 2H_2O$ , 1.49 g of KCl, 0.43 g of  $Na_2SO_4$ , 30 mg of  $CaCl_2 \cdot 2H_2O$  and 1X trace elements solution [263]. The final pH of the media was adjusted to 7 using HCl.

### **4.2.2 Isolation and characterization of bacterial strains**

The microorganisms were isolated by an enrichment culture technique where DEHP served as the only carbon and energy source. 5 g of soil sample was collected from local landfill site and mixed with 50 mL of autoclaved MSM. The cells were dislodged from the soil matrix using ultrasonic sonication bath (Bio Technics BTI- 48 50 W, Mumbai, India) for 10 minutes at  $20^\circ C$ . 100 mL of fresh MSM having DEHP ( $200\text{ mg } L^{-1}$ ) was inoculated with the 1 mL of soil culture and the suspension was kept for 5 days at  $30^\circ C$  and 180 rpm. 100  $\mu L$  of the culture was used to inoculate fresh MSM having a higher concentration of DEHP ( $300\text{ mg } L^{-1}$ ). Likewise, an enrichment procedure was followed for 15 days (3 cycles) with the gradual increase in the concentration of DEHP up to  $500\text{ mg } L^{-1}$ . 50  $\mu L$  of the final



enrichment culture was spread on the MSM agar plates provided with DEHP (500 mg L<sup>-1</sup>). The pure colonies were obtained and the plates were incubated at 30°C for 36 hours. Finally, DEHP utilizing strains were isolated and designated as *Pseudomonas* sp. PKDM2, *Pseudomonas* sp. PKDE1 and *Pseudomonas* sp. PKDE2. Morphological features of the isolated strains were examined by scanning electron microscopy (LEO 435VP SEM, SEMTech Solutions, USA).

#### **4.2.3 16S rRNA gene amplification and phylogenetic analysis**

For 16S rRNA gene amplification, genomic DNA was isolated using the QIAamp DNA Mini Kit (QIAGEN, Germany), following the manufacturer's protocol. The amplification was performed using universal bacterial primers 27F (5'-AGAGTTTGATCMTGGCTCAG-3') and 1492R (5'-CGGTTACCTTGTTACGACTT-3'). The 50 µL of PCR mixture had 5 µL of 10X reaction buffer, 1 µL of dNTP mixture (each dNTP, 2.5 mmol/ µL), 1 µL of each primer (10 pmol/ µL), 2 µL of the template DNA (100 ng/µL) and 0.5 µL of Taq DNA polymerase (New England BioLabs, USA). The PCR cycle parameters were as follows: initial denaturation at 94°C for the duration of 5 min which is followed by 30 cycles at 94°C for the duration of 1 min, at 56°C for 45 sec, at 72°C for 90 sec, and final extension carried out at 72°C for 10 min and final storage at 4°C. The PCR products obtained were further purified using a QIAquick Gel Extraction Kit (QIAGEN, Germany) and subsequently sequenced (Eurofins Scientific India Pvt Ltd, Bengaluru, India).

#### **4.2.4 Antibiotic susceptibility test**

All the isolated strains were checked for their susceptibility towards the tested antibiotics (i.e. kanamycin, ampicillin, and chloramphenicol) using the agar disc diffusion technique. 20 µL of each antibiotic (30 µg mL<sup>-1</sup>) solution was transferred into the respective well of the nutrient agar plate. 20 µL of sterile water served as a control. The plates were incubated at 30°C for 24 hours and the resultant zone of inhibition was observed.

#### **4.2.5 Biodegradation of DMP, DEP, and DEHP**

For assessing the biodegradative capabilities, the isolated bacterial strains were grown on enriched media (LB Broth) at 30°C for 24 hours at 180 rpm. Bacterial cells were pellet



down at 6,000 rpm for 8 min. Pellets were washed thrice with 0.1 mM phosphate buffer saline (PBS), pH 7.2. Cells were suspended in the PBS buffer and used as inoculum (with  $OD_{600}$  of 0.2) in further experiments. 30 mL of fresh MSM was supplemented with either of DMP, DEP, and DEHP ( $500 \text{ mg L}^{-1}$ ) and was inoculated with 0.3 mL of cell suspension. Non-inoculated MSM medium with carbon source was used as a control. All the experiments were performed in triplicate. After every 5 hours, the samples were collected and Gas chromatography and mass spectrometry (GC-MS) (7890A GC system, 5975C MS system, Agilent Technologies, California, USA) was used to analyze the residual amount of DMP, DEP, and DEHP in the culture. An equal amount of n-hexane was added to the 30 mL of culture media having degraded PAEs. To determine the residual amount, the resultant heavy emulsion was centrifuged for 8 min at 6,000 rpm and the aqueous phase was extracted. Later on, the hexane was evaporated close to dryness and reconstituted for further study. The extract was passed through  $0.22 \mu\text{m}$  membrane filter and  $1.0 \mu\text{l}$  of it was used for GC-MS analysis. The following program conditions of GC-MS were used: DB-5MS (Agilent J&W GC) column ( $30 \text{ m}/0.25 \text{ mm}/0.25 \mu\text{m}$ ) with helium acting as a carrier gas at the flow rate maintained at  $1.0 \text{ ml min}^{-1}$ . The analysis conditions were as follows: an injection temperature of  $250 \text{ }^\circ\text{C}$ , and an ion source temperature of  $220 \text{ }^\circ\text{C}$ , column temperature was  $80^\circ\text{C}$  for the duration of 5 min and it was increased to  $200^\circ\text{C}$  at the rate of  $10^\circ\text{C}/\text{min}$  in split ratio mode (1:20). The mass spectrometer was used in the electron ionization energy mode of  $70\text{eV}$  (mass range of 40-600 a.m.u) with 3 microscans. The scans were collected and the corresponding peaks of the DMP, DEP, and DEHP were identified by matching and comparing them with standard mass spectra peaks available in the National Institute of Standards and Technology (NIST) library (Agilent Technologies, USA) attached to MS system. The residual amount of respective phthalate was estimated with the help of corresponding peak area.

#### **4.2.6 Identification of DEHP degradation pathway intermediates**

*Pseudomonas* sp. PKDE1 was cultured in 10 mL of LB broth at  $30^\circ\text{C}$  and 180 rpm. The cells were pellet down at 6,000 rpm for 8 min. The pellet was washed and suspended in the PBS buffer, pH 7.2. 1% of the culture inoculum was added to 50 mL of MSM having DEHP ( $500 \text{ mg L}^{-1}$ ) and incubated at  $30^\circ\text{C}$  and 200 rpm. Samples were collected at the regular interval of 5 hours and intermediate metabolites were extracted using hexane

extraction procedure. GC-MS study of DEHP degradation intermediates was performed using DB 5MS capillary column and MS detector. The intermediate metabolites produced during the biodegradation of DEHP were tentatively identified by comparing the resultant spectra with standard mass spectra peaks available in the NIST library attached to the MS system.

#### **4.2.7 Comparative molecular modeling and structure validation**

Isolated strains *Pseudomonas* sp. PKDE1 has 99% 16S rRNA sequence identity with *Pseudomonas mosselii*. The sequence of MEHP hydrolase from *Gordonia* sp. P8219 having accession no. BAE78500 was used for searching MEHP hydrolase sequence an  $\alpha/\beta$  hydrolase from *Pseudomonas mosselii* ATCC BAA-99 [124]. The sequence with accession no. WP\_023629646.1 was obtained from NCBI as an  $\alpha/\beta$  hydrolase from *Pseudomonas mosselii*. A suitable template for homology modeling was searched by using NCBI BLAST search tool against PDB database [264]. The crystal structure of a hydrolytic enzyme (PDB ID:4F0J) from *Pseudomonas aeruginosa* PAO1 having a sequence identity of 67% and query coverage of 93% was selected as a template.

Modeller 9.17 was used to build the comparative 3D model of MEHP hydrolase from *Pseudomonas mosselii* [265]. Twenty models were sorted according to their DOPE scores. Model with the lowest DOPE score was selected and assessed for its stereochemical quality using PROCHECK [266]. The PROCHECK evaluates the overall stereochemical property of the predicted model. ModLoop program was used for refining the disordered loop regions of the structure [267]. Swiss PDB Viewer 4.10 was used for the energy minimization of the selected model [268].

The ProSA integrated web server (<https://prosa.services.came.sbg.ac.at/prosa.php>) was utilized for the estimation of statistical Z-score deviation of the predicted model from highly resolved PDB deposited structures [269]. The refined model was also validated by VERIFY-3D [270]. It determines the compatibility between generated 3D model and its primary amino acid sequence, assigns a structural class on the basis of environment and location and comparison with refined crystal structures. The multiple sequence alignment of MEHP hydrolase from *Pseudomonas mosselii* with other C-C hydrolases from different bacteria was generated by Clustal Omega [271]. The ESPript 3.0 server was used for illustration of the sequence alignment of query sequence [272].

#### **4.2.8 Molecular docking**

AutoDock 4.2.6 was used for performing the docking of PME's (MEHP, MHP, MBP and MEP) with the MEHP hydrolase model [211]. After selecting the MEHP hydrolase, hydrogen atoms and Kollman charges (Kollmann charges 7.0) were added by using AutoDock MGL Tools version 1.5.6. Then the receptor protein was saved in .pdbqt file format. Phthalate monoesters utilized for the docking studies were retrieved from PubChem compound database in the SDF format and converted to the PDB format using an Open Babel [273, 274]. For ligand preparation, hydrogen atoms and Gasteiger charges (-1.0, -1.0, -1.0001 and -1.0001) for MEHP, MHP, MBP, and MEP were added, respectively and saved in .pdbqt format. Ligand flexibility was used to specify the torsional degrees of freedom in ligand molecule. The atomic potential grid map was generated with a spacing of 0.375 Å by using AutoGrid 4. The docking receptor grid was created by choosing the conserved catalytic triad residues and pentapeptide motif. The dimensions of grid box were as follows 40 Å × 40 Å × 40 Å. The center point coordinates were set as X= 39.439, Y= 14.124 and Z= 13.708. For docking purpose, Lamarckian genetic algorithm and grid supported energy evaluation method were adopted. The number of total GA runs was increased from 10 to 100. Other docking parameters were used as default. The pose with the minimum binding energy score was selected and further visually inspected and analyzed using PyMol [213]. Active site volume was also calculated for MEHP hydrolase using DoGSiteScorer, an automated tool for pocket volume detection and analysis [275].

### **4.3. Results and discussion**

#### **4.3.1 Isolation and characterization of bacterial strains**

Three bacterial strains proficiently utilizing DEHP as sole carbon and energy source were isolated from the plastic contaminated soil sample. Cells of the isolated strains *Pseudomonas* sp. PKDM2, *Pseudomonas* sp. PKDE1 and *Pseudomonas* sp. PKDE2 were observed to be rod-shaped gram-negative and aerobe with 1-1.5 µm × 0.4-0.7 µm dimensions as shown in **Figure 4.1**.

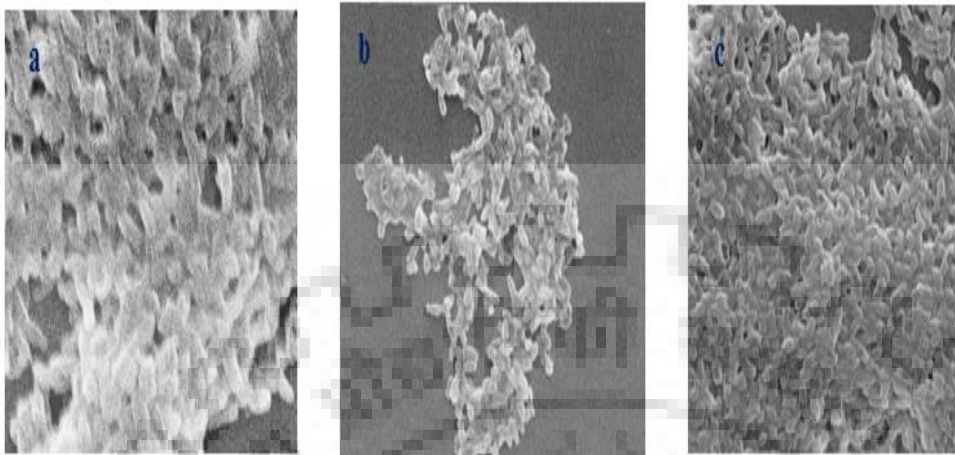


**Figure 4.1. SEM micrographs of the isolates at 5000X magnification. A:** *Pseudomonas* sp. PKDM2; **B:** *Pseudomonas* sp. PKDE1; **C:** *Pseudomonas* sp. PKDE2.

The physiochemical properties of the isolated strains are summarized in **Table 4.1**.

**Table 4.1.** General characteristics of the isolated strains

Strain: 1: *Pseudomonas* sp. PKDM2; 2: *Pseudomonas* sp. PKDE1; 3: *Pseudomonas* sp. PKDE2.

(a) *Pseudomonas* sp. PKDM2 (b) *Pseudomonas* sp. PKDE1 (c) *Pseudomonas* sp. PKDE2.

Characteristics	1	2	3
pH for growth	6.0-8.0	6.0-8.0	6.0-8.0
Growth at 4°C	-	-	-
Growth at 37°C	+	+	+
Maximum tolerable concentration of DEHP (ppm)	1000	1000	800
Utilization of			
Glucose	+	+	+
Acetate	+	+	+
Sucrose	+	+	+
16 S rDNA gene similarity (%)			
with <i>Pseudomonas mosselii</i> (T) ATCC BAA-99	99	-	-
with <i>Pseudomonas monteilii</i> (T) ATCC 700476	-	99	-
with <i>Pseudomonas pseudoalcaligenes</i> (T) ATCC 17440	-	-	99

### 4.3.2 16S rRNA gene amplification and phylogenetic analysis

Phylogenetic analysis of 16S rRNA gene sequences shows that the isolated strains were positioned close to the members of genus *Pseudomonas*, which are previously reported to degrade persistent organic pollutants [276-278]. The 16S rRNA gene sequence of *Pseudomonas* sp. PKDM2 shows 99% sequence similarity with *Pseudomonas aeruginosa* ATCC 10145, as shown in **Figure 4.2**. the sequence of *Pseudomonas* sp. PKDE1 and *Pseudomonas* sp. PKDE2 shows 99% homology with *Pseudomonas mosselii* ATCC BAA-99 and *Pseudomonas monteilii* ATCC 700476, respectively. In the previous studies, *Pseudomonas aeruginosa* and *Pseudomonas monteilii* have been reported to degrade recalcitrant organic compounds such as anthracene, benz[*a*]anthracene, benzo[*b*]fluoranthene, fluorene, naphthalene and phenanthrene [277, 279]. *Pseudomonas mosselii* has not been reported to degrade phthalates, but it has ferredoxin-NADP<sup>+</sup> reductase gene, which is having 34% sequence identity with Phthalate dioxygenase reductase gene from *Burkholderia cepacia* [280]. Likewise, *Pseudomonas fluorescens* B-1 isolated from activated sludge reported to degrade PAEs efficiently [281]. These findings highlight the utility and extensive role played by the members of *Pseudomonas* genus in degradation of PAEs and other organic pollutants.

The 16S rRNA gene sequences of three strains were deposited in the GenBank database with accession numbers KX949578, KX949579, and KX949580 for the strains *Pseudomonas* sp. PKDM2, *Pseudomonas* sp. PKDE1 and *Pseudomonas* sp. PKDE2, respectively.



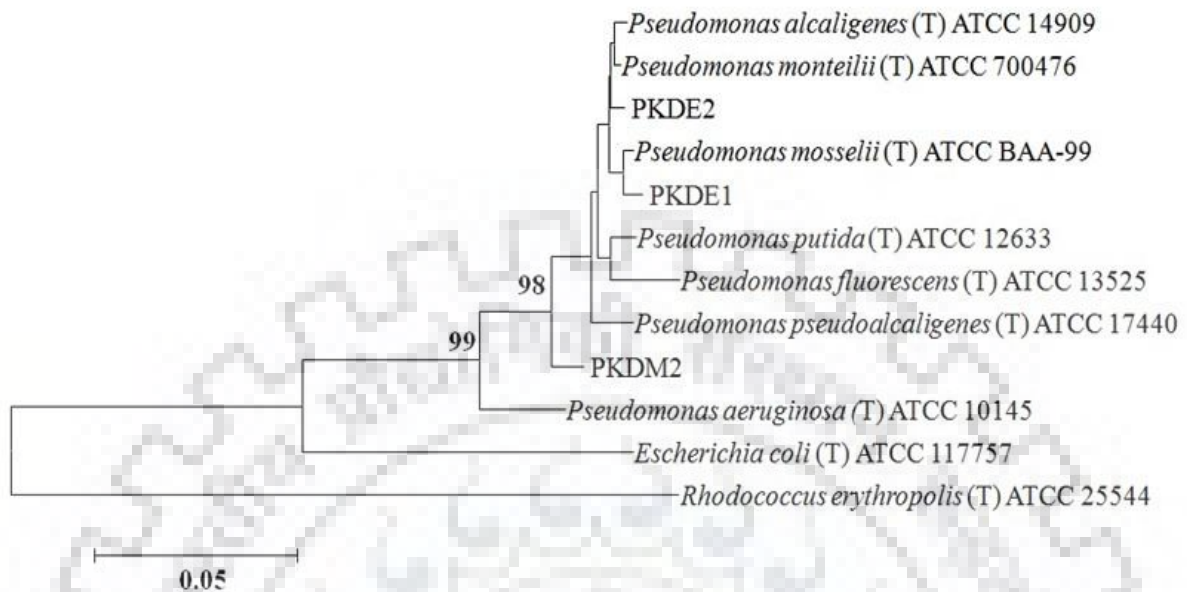


**Figure 4.2. Phylogenetic tree analysis of 16S rRNA gene sequences.** The tree shows that *Pseudomonas* sp. PKDM2, *Pseudomonas* sp. PKDE1 and *Pseudomonas* sp. PKDE2 are related with the members of genus *Pseudomonas*. Distances were calculated by using the neighbor-joining method and bootstrap values at the nodes were calculated from 1,000 samplings. The major branch points having significant ( $\geq 90\%$ ) bootstrap values are shown. *Rhodococcus erythropolis* strain ATCC 25544 was used as an outgroup. The scale bar 0.05 indicates 5% nucleotide sequence substitution. Sequences of related strains procured from RDP database are mentioned with T.

### 4.3.3 Antibiotic susceptibility test

Antibiotic susceptibility test result indicates that isolated bacterial strain may be pathogenic or not, but are non-drug resistant. From the results, it can be inferred that using these susceptible strains for *in-situ* bioremediation of PAEs may cause low risk of spreading drug-resistant factor to other native bacterial species. The test results of the isolated strains are summarized in **Table 4.2**.

**Table 4.2. Antibiotic susceptibility tests.** Antibiotics (each 30  $\mu\text{g mL}^{-1}$ ) used in the antibiotic susceptibility tests and associated presence of an interpretative zone of inhibition.

S.NO	STRAIN	KANAMYCIN	AMPICILLIN	CHLORAMPHENICOL
1.	<i>Pseudomonas</i> sp. PKDM2	+	-	+
2.	<i>Pseudomonas</i> sp. PKDE1	+	+	+
3.	<i>Pseudomonas</i> sp. PKDE2	+	-	+

+ : SUSCEPTIBLE to the respective antibiotic; - : RESISTANT to the respective antibiotic



#### 4.3.4 Biodegradation of DMP, DEP, and DEHP

The isolated bacterial strains were grown in different PAEs and their substrate utilization profiles were analyzed. GC-MS results showed no significant decrease in the initial amount of respective PAEs in sterile control as shown in **Figure 4.3**. All three isolated strains prefer DMP as carbon source compared to DEP and DEHP as shown in **Table 4.3**. DMP degradation was observed to be comparatively higher (77.4% - 84.4%) than that of DEP (75.0% - 75.7%) and DEHP (71.7% - 74.7%). Similarly, in the case of *Arthrobacter* sp. C21, the rate of degradation of DMP (99.5%) was higher than that of DEHP (51.4%) [110]. The observed pattern in the degradation of PAEs is possibly due to the steric hindrance caused by the phthalate side ester chains. The phthalate ester side chain hampers the binding site of hydrolytic enzymes and thus inhibits the hydrolysis reaction. In this study, *Pseudomonas* sp. PKDE1 was observed to be more efficient in terms of phthalate degradation as compared to the other two isolated strains. These isolated strains seem to be potential candidates for the efficient remediation of the PAEs contaminated site as compared to already reported *Pseudomonas* species isolated from various environmental sites, as shown in **Table 4.4**.

**Table 4.3.** Residual amount (%) of PAEs after 44 hours of bacterial incubation at 30°C and 180 rpm.

STRAIN	Residual amount (%)		
	DMP	DEP	DEHP
<i>Pseudomonas</i> sp. PKDM2	15.6 ± 5	25.0 ± 5	28.3 ± 4
<i>Pseudomonas</i> sp. PKDE1	14.5 ± 5	25.0 ± 5	25.3 ± 4
<i>Pseudomonas</i> sp. PKDE2	22.6 ± 5	24.3 ± 5	26.3 ± 3

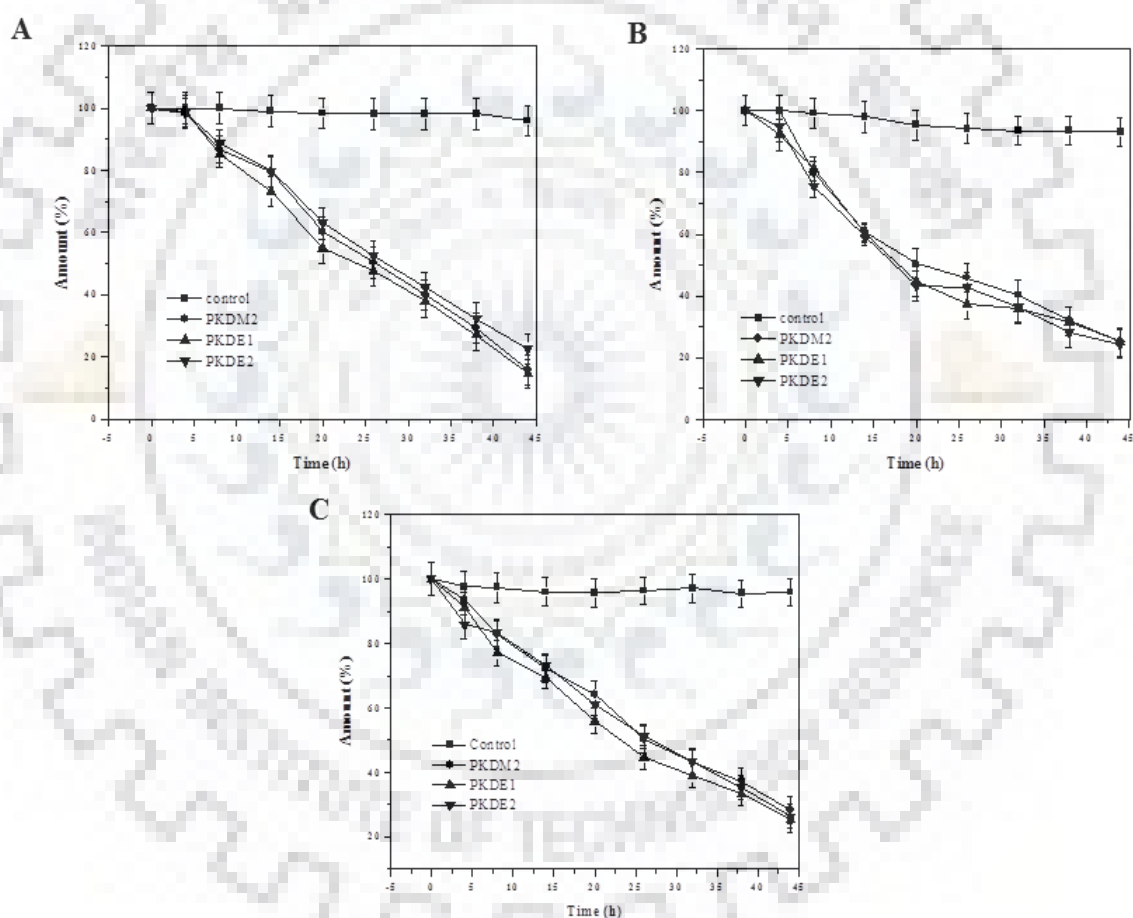


**Figure 4.3.** Degradation of PAEs by the isolated strains. Residual amount profile (in percentage) of PAEs after 44 hours of incubation: (a) DMP degradation (b) DEP degradation (c) DEHP degradation. Error bars represent the overall distribution of data (n=3).

**Table 4.4.** Overview of metabolization of different PAEs by *Pseudomonas* species isolated from

different environments.

Organism	Isolated Environment	Phthalates metabolized	Conc. (mg L <sup>-1</sup> )	Time taken for metabolizing phthalates	Intermediates involved	Ref.
<i>Pseudomonas</i> sp. Strain P136 (anaerobic metabolism)	Garden soil	Phthalate isomers (PA, IA, TA)	2000	50-60 h	CoA esters of phthalate, benzoate, cyclohex-1-ene-carboxylate, 2-hydroxycyclohexane carboxylate pimelate	[118]
<i>Pseudomonas Pseudoalcaligenes</i> B20b1 (anaerobic metabolism)	Sewage effluent	DBP	100	20 Days	MnBP and PA	[282]
<i>Pseudomonas aureofaciens</i> , <i>Pseudomonas fluorescens</i> , <i>Sphingomonas paucimobilis</i> - [in consortium]	Activated sludge	DMP	400	2 Days	MMP, PA	[283]
<i>Pseudomonas aeruginosa</i> PP4	Oil and plastic contaminated soil	PA, IA, TA	150-450	Degradation rate: t <sub>1/2</sub> =7.91 h (IA); t <sub>1/2</sub> =3.45 h(TA); t <sub>1/2</sub> =5.43 h (PA)	PA, 3,4-DHB	[284]
<i>Pseudomonas</i> sp. PPD	Oil and plastic contaminated soil	PA, IA, TA	150-450	Degradation rate: t <sub>1/2</sub> =4.64 h(IA); t <sub>1/2</sub> =2.73 h(TA); t <sub>1/2</sub> =4.52 h (PA)	PA, 3,4-DHB	[285]
<i>Pseudomonas aeruginosa</i> P1	Garden soil	DBP	1-60 mg/g	96 h	PA, dihydroxybenzoic acid	[286]
<i>Pseudomonas fluorescens</i> B-1	Mangrove sediment	DBP	2.5-10.0	4 Days	For DBP degradation- MBP and PA	[281, 286]
		BBP	2.4-20.8	6 Days	For BBP degradation- MBP, mono-benzyl phthalate PA, BA	
<i>Pseudomonas fluorescens</i>	activated sludge at a	DMP	25-400	25 mg/L t ½ 16.17 h	-	

FS-1	petrochemical factory	DEP	25-400	400 mg/L	t	[287]
				$\frac{1}{2}$ 10.39 h		
		DBP	25-400	25 mg/L	t	
				$\frac{1}{2}$ 7.75 h		
		DiBP	25-300	400 mg/L	t	
				$\frac{1}{2}$ 12.49 h		
		DnOP	12.5-200	25 mg/L	t	
				$\frac{1}{2}$ 10.34 h		
		DEHP	12.5-200	400 mg/L	t	
				$\frac{1}{2}$ 15.40 h		
		25 mg/L	t			
		$\frac{1}{2}$ 15.00 h				
		300 mg/L	t			
		$\frac{1}{2}$ 23.25 h				
		12.5 mg/L	t			
		$\frac{1}{2}$ 6.85 Days				
		200 mg/L	t			
		$\frac{1}{2}$ 13 Days				
		12.5 mg/L	t			
		$\frac{1}{2}$ 9.59 Days				
		200 mg/L	t			
		$\frac{1}{2}$ 16.99 Days				
<i>Pseudomonas</i> sp. PKDM2 <i>Pseudomonas</i> sp. PKDE1 <i>Pseudomonas</i> sp. PKDE2	Plastic contaminated soil	DMP, DEP, and DEHP	500	40-44 h	For DEHP degradation- MEHP and PA	

#### 4.3.5 Identification of DEHP degradation pathway intermediates

To study the biodegradation pathway of DEHP in *Pseudomonas* sp. PKDE1, intermediates were extracted from culture and characterized by GC-MS. In sterile control, only a single peak of DEHP was obtained at the retention time of 21.70 min as shown in **Figure 4.4**. After 26 hours of bacterial incubation, several peaks corresponding to pathway intermediates were observed. Analysis of m/z peaks with the available database (NIST library) shows that the spectra with retention time of 21.63 min and 19.38 min correspond to MEHP and PA, respectively as shown in **Table 4.5**. Similar DEHP degradation pathway intermediates were also obtained in the case *Agromyces* sp. MT-O, *Microbacterium* sp. strain CQ0110Y, and *Bacillus subtilis* [187, 288, 289]. In the present study, it is observed that the breakdown of DEHP to PA occurs via an intermediate MEHP as shown in **Figure 4.5**. Degradation of MEHP to phthalate is mediated by MEHP hydrolases, belonging to a serine hydrolases family [290-292].

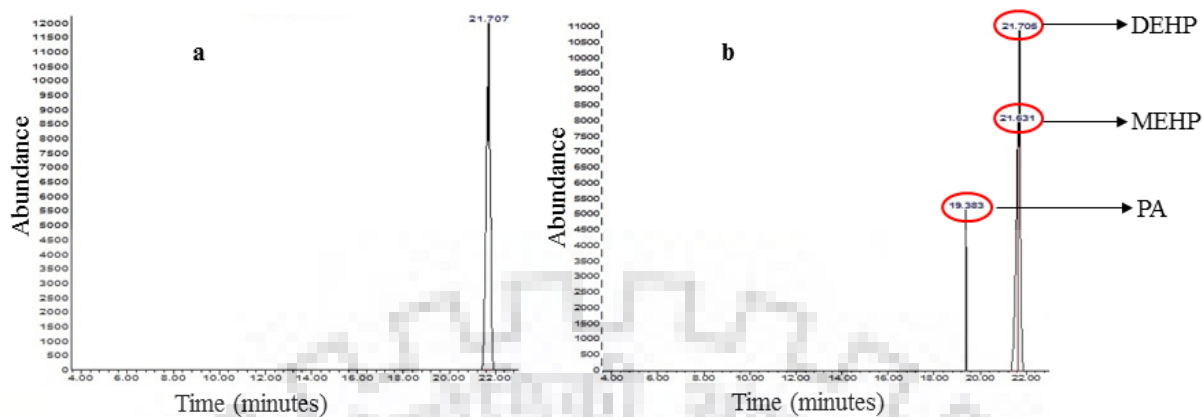


**Figure 4.4.** GC-MS chromatograms of DEHP and its biodegradation intermediates. (a) Control (b) DEHP degradation intermediates after 26 hours of bacterial incubation in MSM.

**Table 4.5.** Identification of DEHP and its intermediate metabolites by gas chromatography-mass spectrometry

COMPOUND	MOLECULAR ION ( $M/Z$ ) PEAKS	RETENTION TIME (MIN)
PA	149, 177	19.38
MEHP	104, 131, 149, 167, 279	21.63
DEHP	104, 149, 168, 279	21.70

DEHP: Bis(2-ethylhexyl) phthalate; MEHP: Mono-(2-ethylhexyl) phthalate; PA: Phthalic acid; IA: Isophthalic acid, TA: Terephthalic acid; MMP: Monomethyl phthalate; 3,4-DHB: 3,4- Dihydroxybenzoate; DBP: Dibutyl phthalate; MBP: Monobutyl phthalate; BA: Benzoic acid; DIBP: Diisobutyl phthalate; DnOP: Di-n-octyl phthalate; MEHP: Mono-(2-ethylhexyl) phthalate).

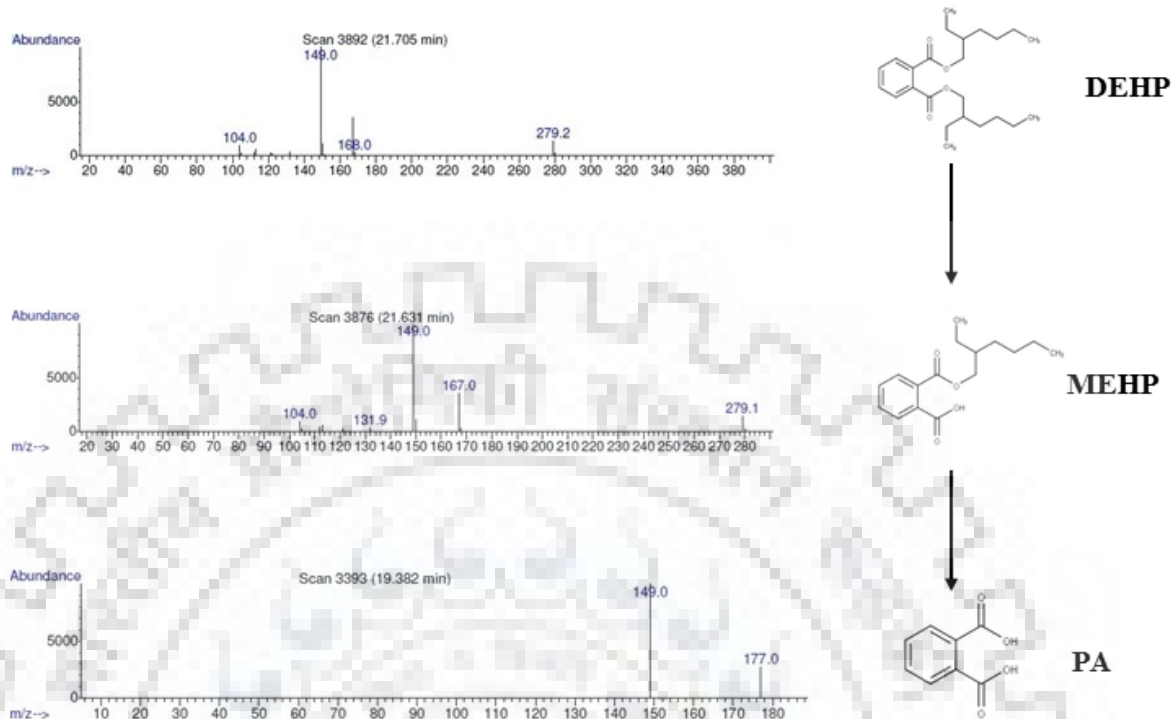


**Figure 4.5. GC-MS spectra of DEHP degradation pathway.** Di-(2-ethylhexyl) phthalate (DEHP) is degraded to phthalic acid (PA) via an intermediate mono-ethylhexyl phthalate (MEHP).

### 4.3.6 Comparative molecular modeling and structure validation

The 3D homology model of MEHP hydrolase from *P. mosselii* was generated in accordance with The crystal structure of the hydrolytic enzyme from *P. aeruginosa* (PDB ID: 4F0J) as shown in **Figure 4.6**. The structural superposition of MEHP hydrolase and template 4F0J shows the RMSD value of 0.098 Å for 276 C<sub>α</sub> atoms. Twenty models were generated and the model with a minimum DOPE score of -38961.66 was selected for further analysis. After loop refinement, energy minimization of MEHP hydrolase was done by Swiss PDB Viewer.

Ramachandran plot of MEHP hydrolase produced by PROCHECK illustrates that 95.5% amino acid residues are in the core region, 4.2% residues in the allowed region, 0.4% amino acid residues are in generously allowed and disallowed region, respectively. Cartoon diagram of MEHP hydrolase showing α helices (α1- α15, blue color) in cylindrical spiral ribbons, β- sheets (β1-β8, orange color) by arrows and loops (green color).

The results obtained indicate that the protein model is reliable. ProSA analysis further confirmed the validation of the modeled structure as the Z scores obtained for the model protein and the template were -8.7 and -8.68, respectively as shown in **Figure 4.7**. The closeness of this parameter suggests that the predicted model is much closer to the experimentally determined structure. Verify 3D result shows that 97.44% of the amino acid residues had an average 3D-1D score  $\geq 0.2$ . This result demonstrated that the folding energy pattern of the modeled protein structure is in complete agreement and lies within the expected range. Multiple sequence alignment result shows that the catalytic triad and pentapeptide motif (GX<sub>1</sub>SX<sub>2</sub>G) of MEHP hydrolase is well conserved, as found in the other bacterial C-C MCPs (meta cleavage product) hydrolases, as shown in **Figure 4.8**.



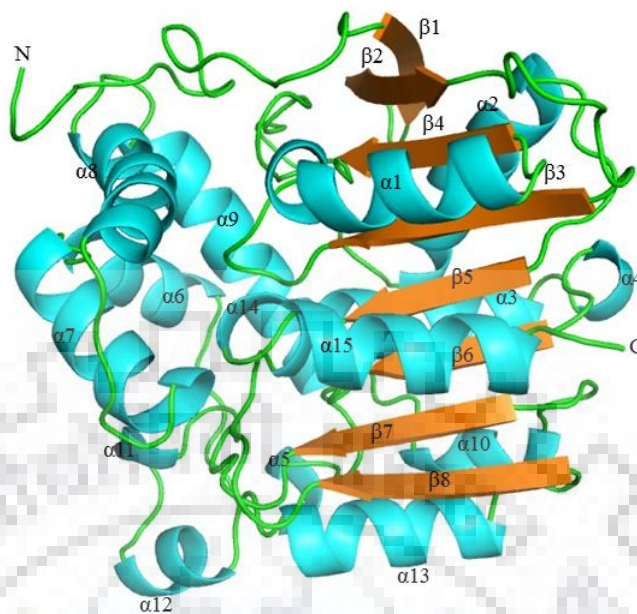


**Figure 4.6. Modeled structure of mono-2-ethylhexyl phthalate (MEHP) hydrolase.** Three dimensional homology model structure of MEHP hydrolase is shown. Helices are shown in cyan color, sheets in brown color and loops are shown in green color.

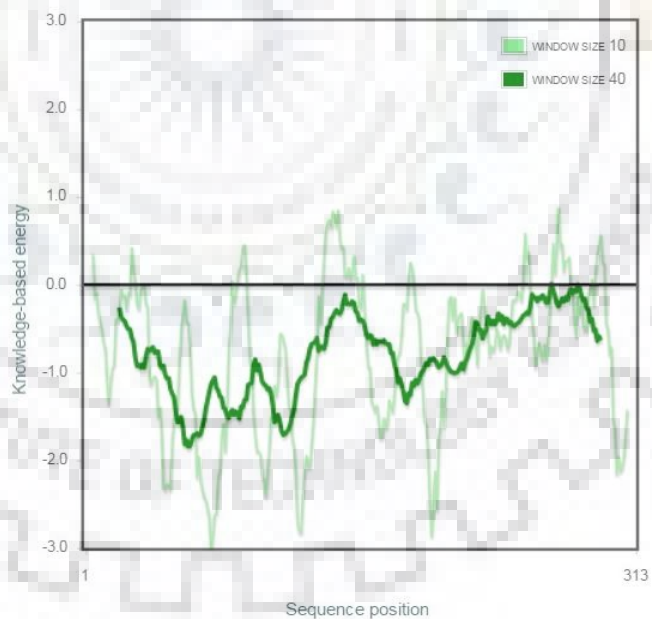


**Figure 4.7. ProSA energy profile of MEHP hydrolase model structure.** ProSA plot shows the folding energy of MEHP hydrolase is in good agreement.

```

1      10      20      30      40      50
ALBEH_PMOS MLRATALALACLITGA..ATAAEPPTYGKQLEGFAYPYPLQHFDFQSOGQALOMCYMVDVP
MEHPH_GORS .....MNCISIVIVHRKALSVPSSII.....T...QKFTT.VDVKGVQTRYFDDG
MEHPH_RHOS .....MNT.....D...LSVNYI.SVGGIRTRYIDOG
HADH_PSES .....MLNKAEQISEK.SES.....A...YVERF.VNAGGVETRYLEAG
HODH_RALS .....MT.NAN.....A...EVGRM.VLAGGIDTNLHDVVG
HOHH_BURL .....M.SSN.....P...EIGRR.IVAGGIDTNVHDAAG
HOSH_DELT .....MSTT.SSN.....P...EIGHS.IEAGGIRTNVHDSG

```

```

60      70      80      90      100     110
ALBEH_PMOS AKGTANQHNVVLMHCKNFC...AAATWQTTLDAISQAGYRVIAVDQIGFCTSSKPAH
MEHPH_GORS ....QDKDPILLIHGGHFGFFIPVGIESWGNVLEDFGEYG.RVLAVDKLGGGETGLPLND
MEHPH_RHOS ....EG.PVILLIHGGHSGMSMPVGGDGWAPVIAPLVDKGRVVTFDKLGGGETGLPETH
HADH_PSES ....KQPVILLIHGGGGAES...EGNWRNVIP.IILARHYRVIAMMLGFGKTAKP.D.
HODH_RALS ....ACKPVVILVHGGSPGVT...WANWRTVMP.ELSRRRRVIAFDMVGFGTORP.QG
HOHH_BURL ....DGPVILLIHGGSPGVT...YANWRLTMP.ATARQFVIAFDMAGFGGETERP.AR
HOSH_DELT ....AOCAPVILLIHGGSPGVS...WANWRLVMP.ATLAQNARVIAFDMVGFGTDRP.QG

```

```

120     130     140     150     160     170
ALBEH_PMOS YQYSFQOLADNTHALIASLGVN.KAIVIGHSTGGLATRYALMYPQVERIAMVNPIGLE
MEHPH_GORS EDWTVDAVAEHWANFATQLGK.NITLVGHSRGGMTAVLLALKYPEMVKRIVITSSATAA
MEHPH_RHOS AEWTFDAVVKHARGFIDALGLE.DMILVGHSGGLASKLALDMPSTKGIIVYSSATLA
HADH_PSES IEYTDQRRIRHLHDFIKAMNFDGKVISVGNMGGATGLGVSVLHSELVNALVLMGSAATLV
HODH_RALS IRYGVDAWVAHLAGILDALDLD.RVDLVGNSFGGALSIAFAIRFPHRRVRLVLMGAGVH
HOHH_BURL YRYSMDHVVHAGLGLDLDLIE.RAHVVGNSFGGALALALAIRAPERVGRVLMGAGATR
HOSH_DELT FAYGMDAWVRQAVGLDLDALGTE.RTDLVGNFGGLALALAIRAPERVGRVLMGAGVGS

```

```

180     190     200
ALBEH_PMOS DWKALGVPYRTVDQW..YARELKLDAEGVRYER.....
MEHPH_GORS PAPPVGTDMDFYERVERTAFGGSAE..LIRHYHAAQAVNEGDLPEYIGIATKWLESEKQ
MEHPH_RHOS GTDAKFRDVEFYDAITRSLPADASPEEIGGAYFR..ALYVTPVPEQINAAAAKYVKNENH
HADH_PSES VELHEDLR.....PIINYDFETREGMVHLVK.AL...TNDGYKIDAMINSRYTATDEAT
HODH_RALS FKLTDGLD.....AVWGYEPESVANMRKVM.D.YE...AYDRSLVSDLAELRYASASIRPGF
HOHH_BURL FTLTEGLD.....AVWGYTPESIANMRLD.IE...AFDRALVNDLAKLRYDASVRPGY
HOSH_DELT FPIITEGLD.....AVWGYTESVENMRSIMD.YE...AFNKGLMSDDLARLRFEEASARPGV

```

```

210     220     230     240     250
ALBEH_PMOS ATVYAG.....RWKPEY...ERWVQMLVGLNKGPGEAVAWNSALIIDMIFTQPVVHE
MEHPH_GORS LDAVAGYARNAEEHWLPSLSEGRRWVQE.....RLA.....
MEHPH_RHOS QNALKTYPMVEKKEYWEPSPQAQKDDIRA.....RLF.....
HADH_PSES RKAYVAT.....MQWIREQG.....GLFYDPEF.....
HODH_RALS QEAFASMFPPAPR.....QRWVD.....ALASDPDQ.....
HOHH_BURL QEAFANMFPPAPR.....QRWVD.....ALASDEAK.....
HOSH_DELT QESYAMFPPAPR.....QRWVD.....AMASREED.....

```

```

260     270     280     290     300
ALBEH_PMOS FKLQKMP TLLIICDODTITAGSDIATPEVKAMLGRYKTLGPQVAGLIP...KGE LVTPE
MEHPH_GORS DAGLIPVPTLVVVGVDNRSAFVS.....MGKGLFDLIIAANTLDSL LYLIN
MEHPH_RHOS AGEVNTPEVVVGRDDRSAPVD.....LGI AFYQKLALVSETSLHILG
HADH_PSES IRKVPVPTLVVHGRDDKVPVVE.....TAYKFLDLID...DSWGYIIF
HODH_RALS IRLAIRHETLIVHGRDDRVIPLE.....TSLRLNQLIE...PSRLHVFEG
HOHH_BURL LRLALTHDTLIVHGRDDRVIPLE.....SSSLKLELLP...NAQLHVFEG
HOSH_DELT IRLALPHOTLIVHGRDDRVIPLE.....TSLTLSSWIA...RSLHVFYGG

```

```

310     320     330
ALBEH_PMOS GIGHAPQIEQPERFHKALIDWIGR.....
MEHPH_GORS NAGHVFSDQREKFNAAVGFISL.....
MEHPH_RHOS TAGHNVFAERTEDFVRILADYAGRRSASAYATRR
HADH_PSES HCGHWAMIEHPEDFANATLSFLSRRADITRAAA
HODH_RALS RCGHWAQIEQNQGFIRLVDDFLATED.....
HOHH_BURL RCGHWTQIEHAARFNQLVIEHFSAKP.....
HOSH_DELT QCGHWTQIEHAARFARLVGDFLAEASADEPQPL

```

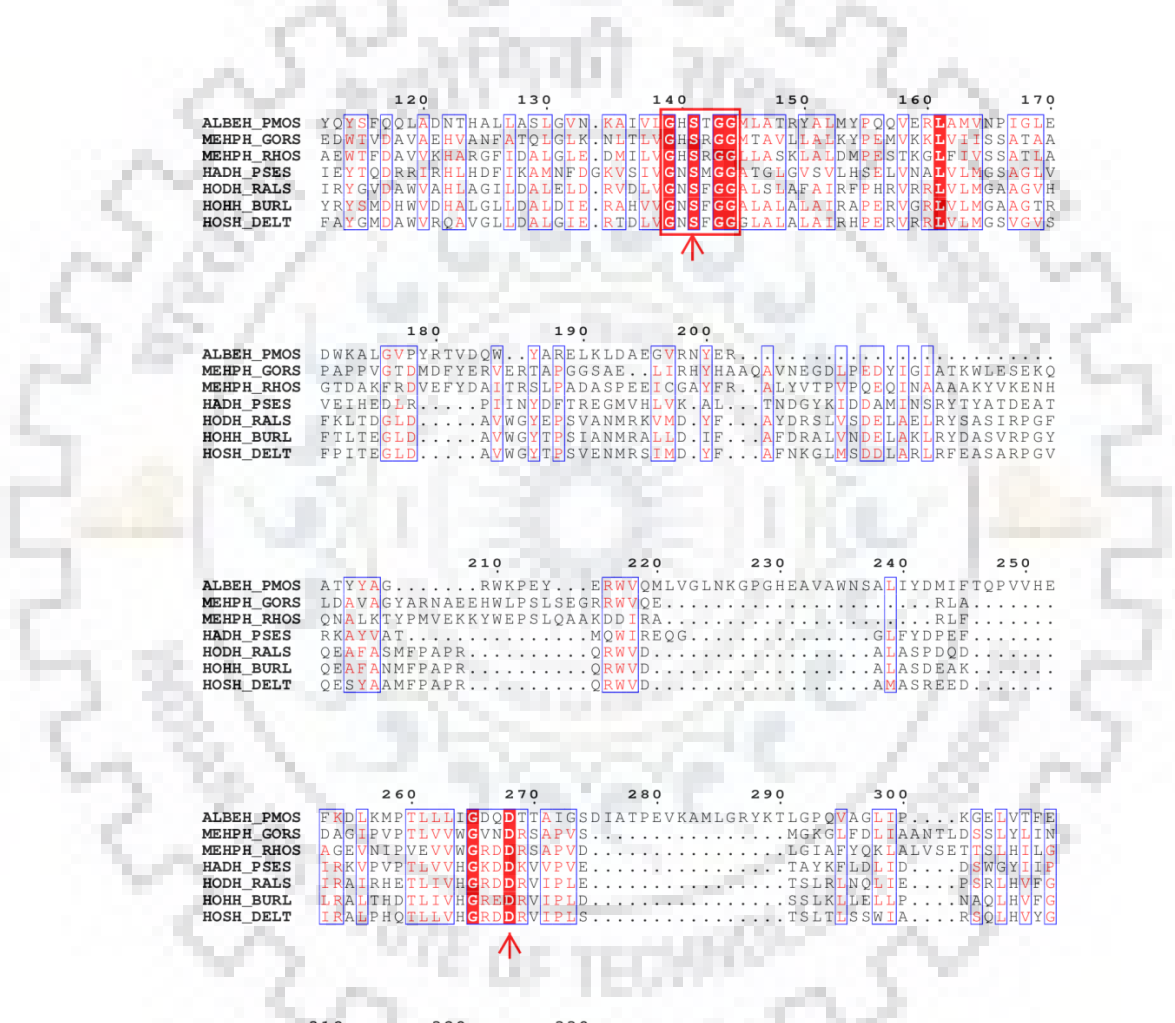
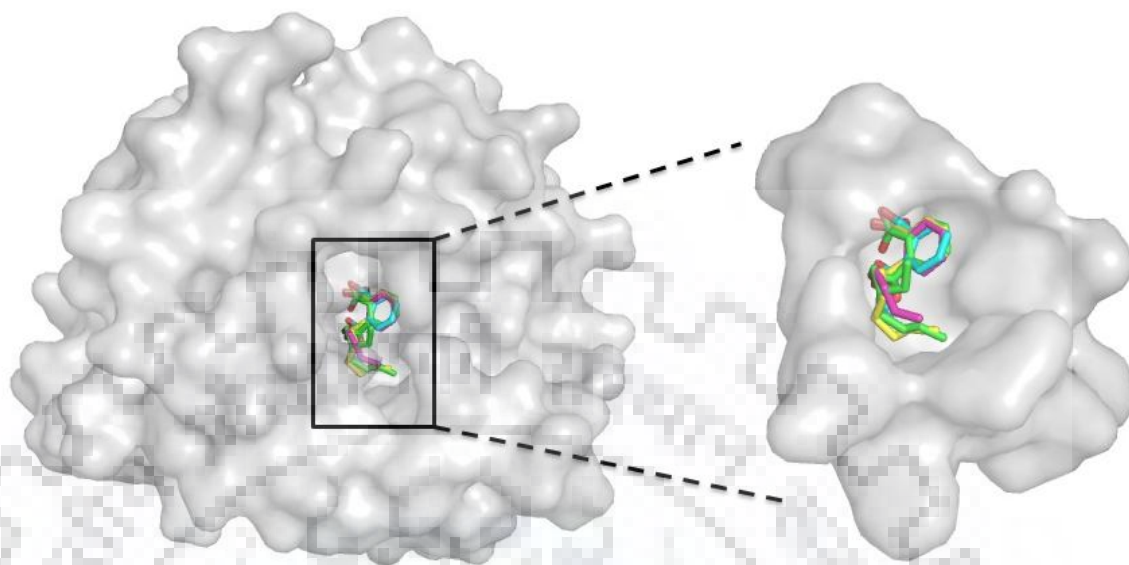


**Figure 4.8. Multiple sequence alignment of MEHP hydrolase from *P. mosselii* with homologs from the C-C hydrolases from different bacteria.** The sequence alignment was done using Clustal Omega and the ESPript 3.0s was used for figure generation. The conserved catalytic triad residues (His-Asp-Ser) are shown by red arrows towards the bottom of the alignment. Identical residues among all the bacterial hydrolases are highlighted in white against a red background. A conserved pentapeptide (GX<sub>1</sub>SX<sub>2</sub>G) motif is shown in the red box. The sequences aligned are as follows (top to bottom) 1. ALBEH\_PMOS:  $\alpha/\beta$  hydrolase from *Pseudomonas mosselii* (WP\_023629646.1), 2. MEHPH\_GORS: MEHP hydrolase from *Gordonia* sp. P8219 (BAE78500), 3. MEHPH\_RHOS: MEHP hydrolase from *Rhodococcus* sp. EG-5, 4. HADH\_PSES: 2-hydroxy-6-oxo-6-(20-aminophenyl)hexa-2, 4-dienoate hydrolase from *Pseudomonas stutzeri* (BAA31270), 5. HODH\_RALS: 2-hydroxy-6-oxohepta-2,4-dienoate hydrolase from *Ralstonia* sp. JS705 (CAA06969), 6. HOHH\_BURL: 2-hydroxy-6-oxo-2,4-heptadienoate hydrolase from *Burkholderia lata* (WP\_011356546), 7. HOSH\_DELT: 2-hydroxymuconic semialdehyde hydrolase from *Delftia tsuruhatensis* (AAX47253).

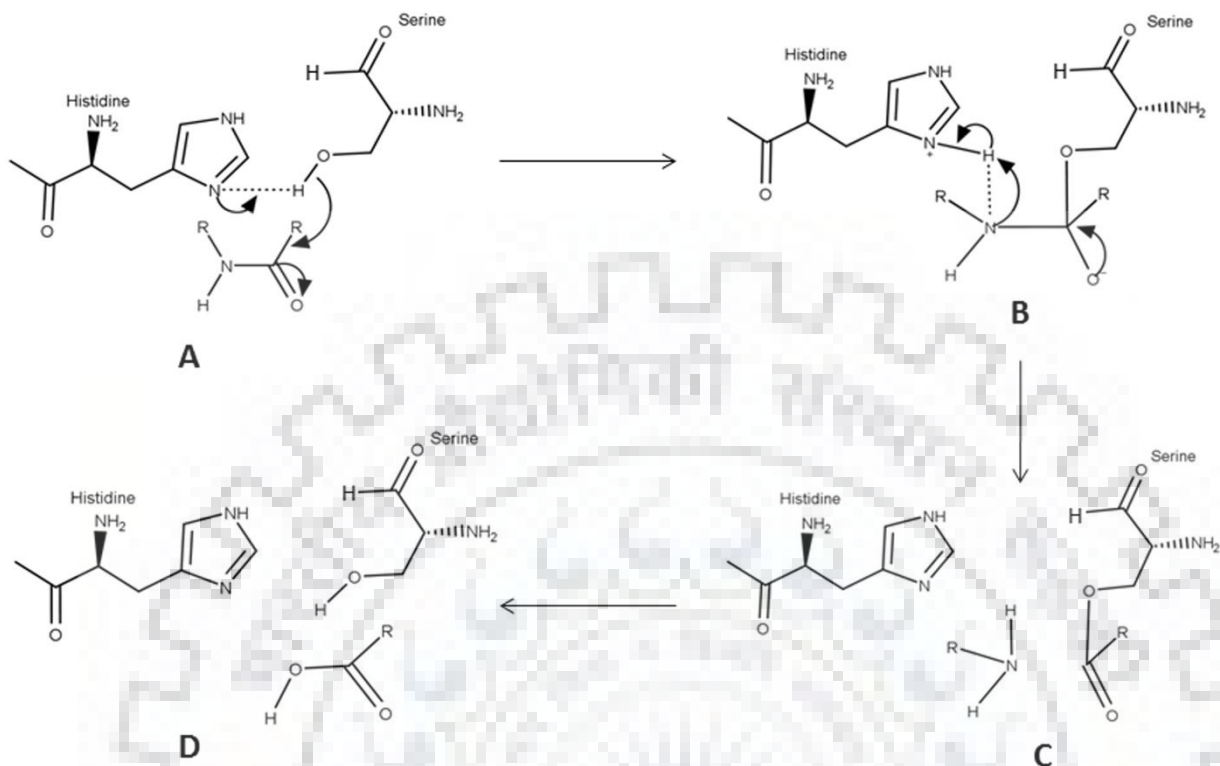
### 4.3.7 Molecular docking

Docking studies were performed using phthalate monoesters (MEHP, MHP, MBP, and MEP) as ligands and surface view of the ligand-binding pocket is shown in **Figure 4.9**. It is reported that serine hydrolases have conserved catalytic triad (Ser-His-Glu), where serine O $\gamma$  acts as a nucleophilic center for hydrolyzing ester, amide or the thioester bonds [293]. Histidine residue act as general base or acid, a carboxylate group of aspartic acid helps in the proper orientation and charge neutralization of the imidazole ring of histidine in the tetrahedral intermediate state [294, 295]. Further, deprotonated catalytic serine attacks the carbonyl carbon of the substrate which leads to the formation of covalent intermediate as shown in **Figure 4.10**.

In order to analyze the ligand binding and interactions, molecular docking of the ligand in close proximity of catalytic serine of the MEHP hydrolase model was performed. The binding energy and ligand efficiency of different PMEs into the active pocket of MEHP hydrolase are shown in **Table 4.6**. The results show that all the docked PMEs are efficiently binding to the MEHP hydrolase. The binding energy and ligand efficiency scores of the docked PMEs illustrate the substrate preference of the MEHP hydrolase in the following manner: MEP > MBP > MHP > MEHP. The phthalate side ester chain of MEP causes less steric hindrance as compared to other PMEs. All PMEs are stabilized in the active site of MEHP hydrolase by forming 4 hydrogen bonds with the Asn56, Ser122, and Tyr186 while MEP, MBP, and MHP interact with His 293 as well, shown in **Figure 4.11**.

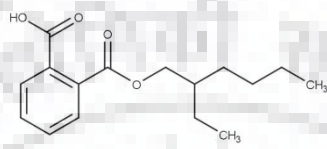
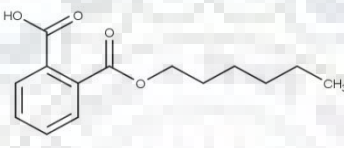
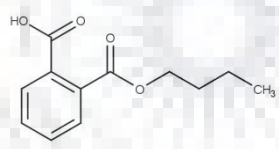
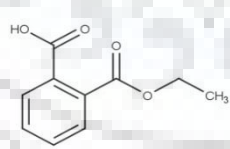


**Figure 4.9. Surface view of the MEHP hydrolase binding pocket.** Zoom window shows that MEHP (green color), MHP (yellow color), MBP (magenta color) and MEP (cyan color) are buried in the pocket of MEHP hydrolase. The volume of this cavity is 1044.22 Å<sup>3</sup> (DoGSiteScorer).



**Figure 4.10. Proposed mechanism of catalysis mediated by MEHP hydrolase.** A. shows the MEHP hydrolase and MEHP complex. The  $\gamma$ -hydroxyl group of serine acts as a nucleophilic center and attacks the carbonyl group of MEHP as shown by black curved arrows. B. Carbonyl carbon accepts the electron and tetrahedral intermediate is formed which is stabilized by oxyanion hole (not shown) C. Tetrahedral intermediate disintegrates to form an aryl-enzyme intermediate. D. Finally, water attacks the aryl-enzyme complex to form the second tetrahedral intermediate (not shown) and rearrangement occurs to give the product.

**Table 4.6.** Docking results showing details of ligands used for the molecular docking. Ligand binding energies and ligand efficiencies score obtained and the distance between the carbonyl carbon of PME<sub>s</sub> and O<sub>γ</sub> of serine (Å) of MEHP hydrolase.

LIGAND NAME	PUBCHEM ID	LIGAND STRUCTURE	BINDING ENERGY (kcal/mol)	LIGAND EFFICIENCY (kcal/mol)	DISTANCE BETWEEN C=O OF PME <sub>s</sub> AND O <sub>γ</sub> OF SER (Å)
MEHP	20393		-4.43	-0.22	3.3
MHP	20269373		-5.01	-0.28	3.3
MBP	8575		-5.86	-0.37	3.3
MEP	71750793		-6.31	-0.45	2.9



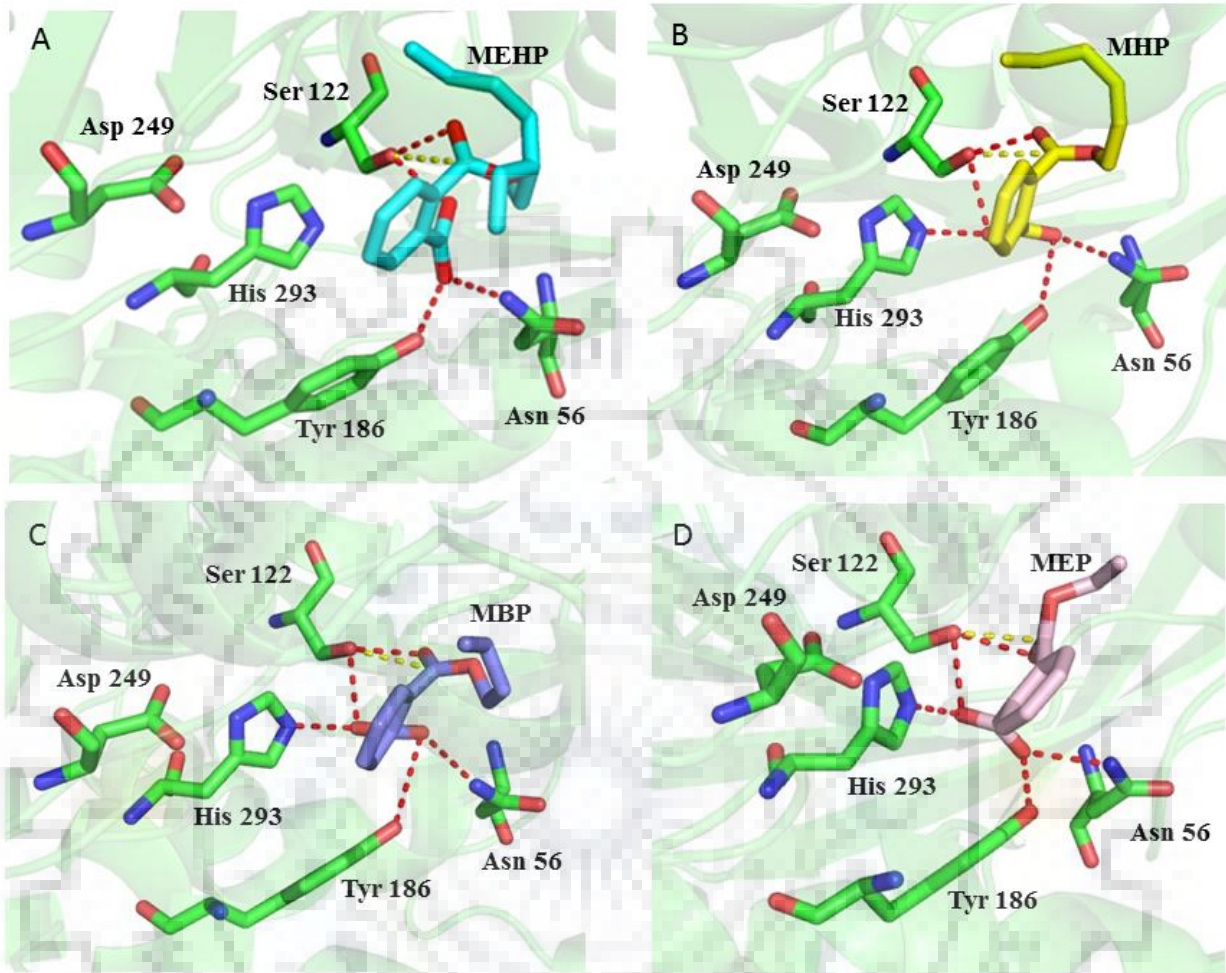


**Figure 4.11. Ribbon diagram of MEHP hydrolase binding cavity.** The ligand A. MEHP (cyan color), B. MHP (yellow color), C. MBP (blue color) and D. MEP (light pink color), and the interacting residues of MEHP hydrolase (green color) are shown in stick forms. Polar interactions of ligand and receptor are shown in red dotted lines. The distance between catalytic Serine  $\gamma$ -hydroxyl group and carbonyl carbon of MEHP is shown in yellow dotted line.

The results of molecular docking infer that the distance between the carbonyl carbon of PMEs and the O $\gamma$  of catalytic Serine is in the range of 2.9 to 3.3 Å which is similar to the Michaelis–Menten ES complex of other known serine hydrolases [296]. These PMEs are found in the close proximity of catalytic serine as reported in the crystal

structures of serine hydrolase complex with their substrates [297-299]. Several crystal structures of serine hydrolases highlight the role of active site residues which are responsible for the adaptability of these hydrolases to catalyze the wide range of substrates. Superposition of catalytic triad residues (Ser-Asp-His) of MEHP hydrolase and crystal structures of various serine hydrolases is shown in **Figure 4.12**.

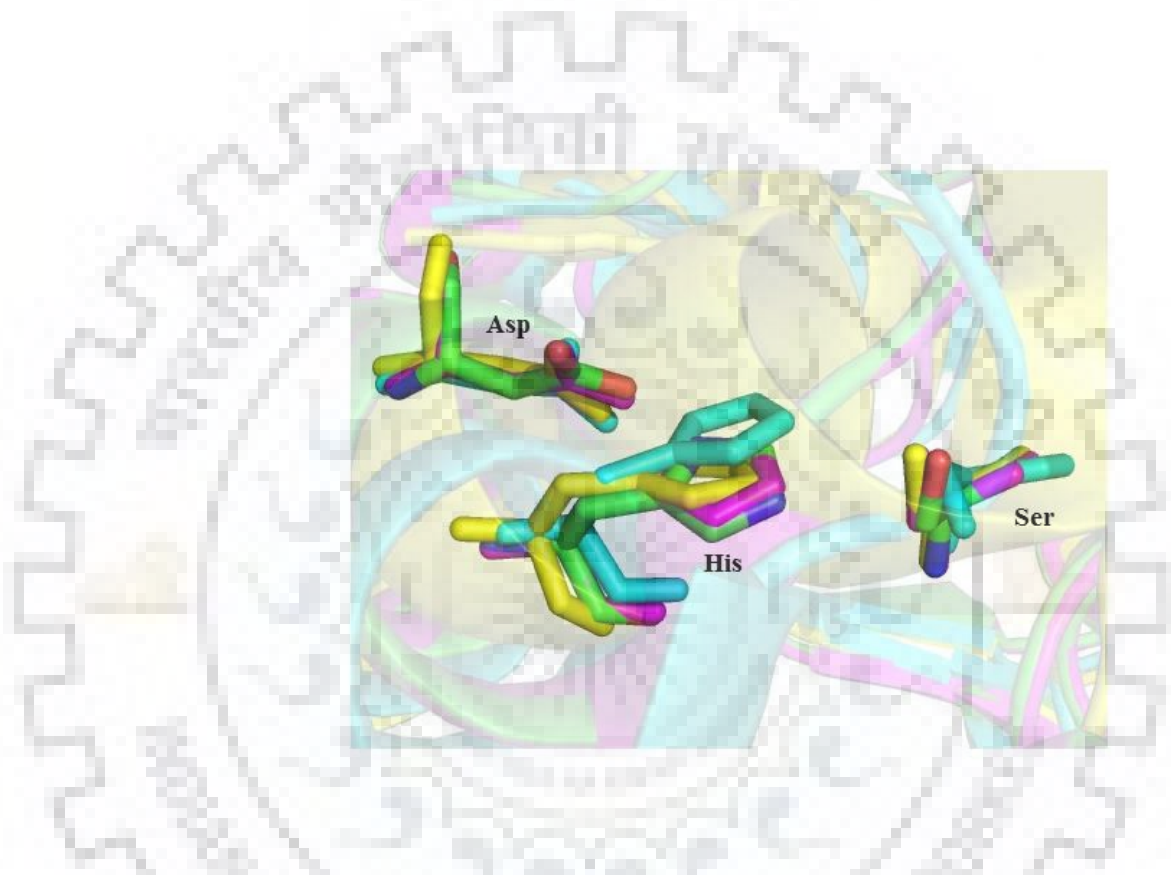


**Figure 4.12. Superposition of catalytic triad residues (His-Asp-Ser) of MEHP hydrolase and crystal structures of various serine hydrolases.** Crystal structure of a probable hydrolytic enzyme from *Pseudomonas aeruginosa* PAO1 at 1.50 Å resolution (PDB ID: 4F0J, pink color); *Pseudomonas fluorescens* esterase complexed to the R-enantiomer of a sulfonate transition state analog (PDB ID: 3IA2, yellow color); Crystal structure of a His-tagged Serine Hydrolase Involved in the Carbazole Degradation (CarC enzyme) from *Janthinobacterium* sp. strain J3 (PDB ID: 1IJ1, cyan color); Model structure of mono-2-ethylhexyl phthalate (MEHP) hydrolase from *Pseudomonas mosselii* (green color).

#### 4.4 Conclusion

Three bacterial strains capable of degrading phthalates namely *Pseudomonas* sp. PKDM2, *Pseudomonas* sp. PKDE1 and *Pseudomonas* sp. PKDE2 were isolated and characterized for their degradative potential. These strains efficiently degraded 77.4 % - 84.4 % of DMP, 75.0 % - 75.7 % of DEP and 71.7 % - 74.7 % of DEHP, the initial amount of each phthalate is 500 mg L<sup>-1</sup> of each phthalate, after 44 hours of incubation. GC-MS results reveal the tentative DEHP degradation pathway, where hydrolases mediate the breakdown of DEHP to phthalic acid (PA) via an intermediate MEHP. MEHP hydrolase is a serine hydrolase which is involved in the reduction of the MEHP to PA. The predicted 3D model of MEHP hydrolase from *Pseudomonas mosselii* was docked with phthalate monoesters (PMEs) such as MEHP, mono-n-hexyl phthalate (MHP), mono-n-butyl phthalate (MBP) and mono-n-ethyl phthalate (MEP), respectively. Docking results show the distance between the carbonyl carbon of respective phthalate monoester and the hydroxyl group of catalytic serine lies in the range of 2.9 to 3.3 Å, which is similar to the ES complex of other serine hydrolases. This structural study highlights the interaction and the role of catalytic residues of MEHP hydrolase involved in the biodegradation of PMEs to phthalate.

Phthalate degrading three bacterial strains *Pseudomonas* sp. PKDM2, *Pseudomonas* sp. PKDE1 and *Pseudomonas* sp. PKDE2 were isolated and characterized for their degrading abilities. The overall results suggest that all isolated bacterial strains may act as a strong candidate for the proficient remediation of PAEs-polluted sites. Future aspect should focus upon the performance of these isolated strains in mixed co-culture for PAEs degradation. Validated molecular model of MEHP hydrolase was used for studying the binding interactions with phthalate monoesters such as mono-2-ethylhexyl phthalate (MEHP), mono-n-hexyl phthalate (MHP), mono-n-butyl phthalate (MBP) and mono-n-ethyl phthalate (MEP). It was observed that the docked ligand is in good coordination with the catalytic serine residue. This work could be further utilized to elucidate the binding mechanism of other hydrolases for the efficient degradation of PAEs. Future studies based on structural and functional aspects of other enzymes involved in PAE biodegradation will help to optimize the biodegradation process.







## 5.1 Introduction

Phthalates are persistent chemicals which are primarily used as an additive in plastic-based products to provide flexibility and durability to the plastic products. These are basically dialkyl or aryl esters of 1,2-benzene-dicarboxylic acid [300]. As phthalates are not covalently bound to their plastics counterparts, they have a propensity to be easily released into the environment via migration, abrasion or leaching processes [301]. Di(2-ethylhexyl) phthalate (DEHP) is generally used as a flexibility agent in polyvinyl chloride (PVC) polymer formulations [302]. Such flexible PVCs are routinely used in the medicated consumer products like blood transfusion bags, catheter tubings etc. [17]. Many reports have established a link between the presence of PAEs metabolites in urine and serum samples of several individual populations to increased waist circumference and decreased insulin sensitivity [199, 303, 304]. Such findings have substantiated the ubiquitous nature and exposure to these harmful phthalates, which are directly correlated to their extensive usage and production [305-308].

As photodegradation and hydrolysis rates of these chemical contaminants are often very slow under natural conditions, therefore, microbial degradation is a natural way to combat these hazardous chemicals [85, 86]. Numerous studies have been reported related to isolation and characterization of phthalate degrading bacteria and respective pathways involved in such processes. Several reports have shown that bacterial strains from *Arthrobacter* sp., *Pseudomonas* sp., *Rhodococcus* sp., *Sphingomonas* sp., *Acinetobacter* sp., are able to degrade several classes of phthalates [116, 254, 309-311]. In this study, *Ralstonia eutropha* strain CH34, an aerobic Gram-negative, non-pathogenic bacteria is considered on the basis of its bioremediating capabilities [312]. It is known to have heavy metal resistance ability and is able to degrade chlorinated aromatic (chloro-aromatic) compounds. [313]. This strain acts as an indicator of heavy metal pollution. Its genome has been fully sequenced and used in bioremediation of heavy metals [314].

Microbial aerobic biodegradation of phthalates involves several steps catalyzed by various enzymes such as esterases, permeases, dioxygenases, dehydrogenases etc [116, 117]. The most crucial step in the degradation of phthalate is the hydroxylation step, which is mediated by dioxygenase in the degradation of phthalates [259]. Phthalate dioxygenase has been categorized as Rieske dioxygenases (RDOs), which catalyze the initial step in the



microbial aerobic degradation of phthalates [315]. This two-component enzyme system has two important proteins: first is phthalate dioxygenase reductase (PDR), a flavo-iron-sulfur protein with NADH-dependent oxidoreductase activity, and the second is phthalate dioxygenase oxygenase (PDO), a non-heme iron protein having oxygenase activity [127]. Crystal structure of phthalate dioxygenase reductase from *Burkholderia cepacia* in both oxidized and reduced form has been analysed at 2.0 and 2.7Å resolution data respectively [128]. In this case, it is reported that PDR is folded into three domains, towards N-terminal is FMN binding domain, the central one is NAD(H) binding domain and lastly, [2Fe-2S] domain is present at the C-terminal. The phthalate dioxygenase has featured two iron-containing important sites, one of them is a Rieske-type [2Fe-2S] cluster, an electron-transferring cofactor, and another is a mononuclear iron binding site, crucial for aromatic ring substrate oxygenation. Several kinetic studies have recognized the subsequent sequential steps occurring during the reaction of Phthalate dioxygenase reductase with NADH, as shown in **Figure 5.1**.

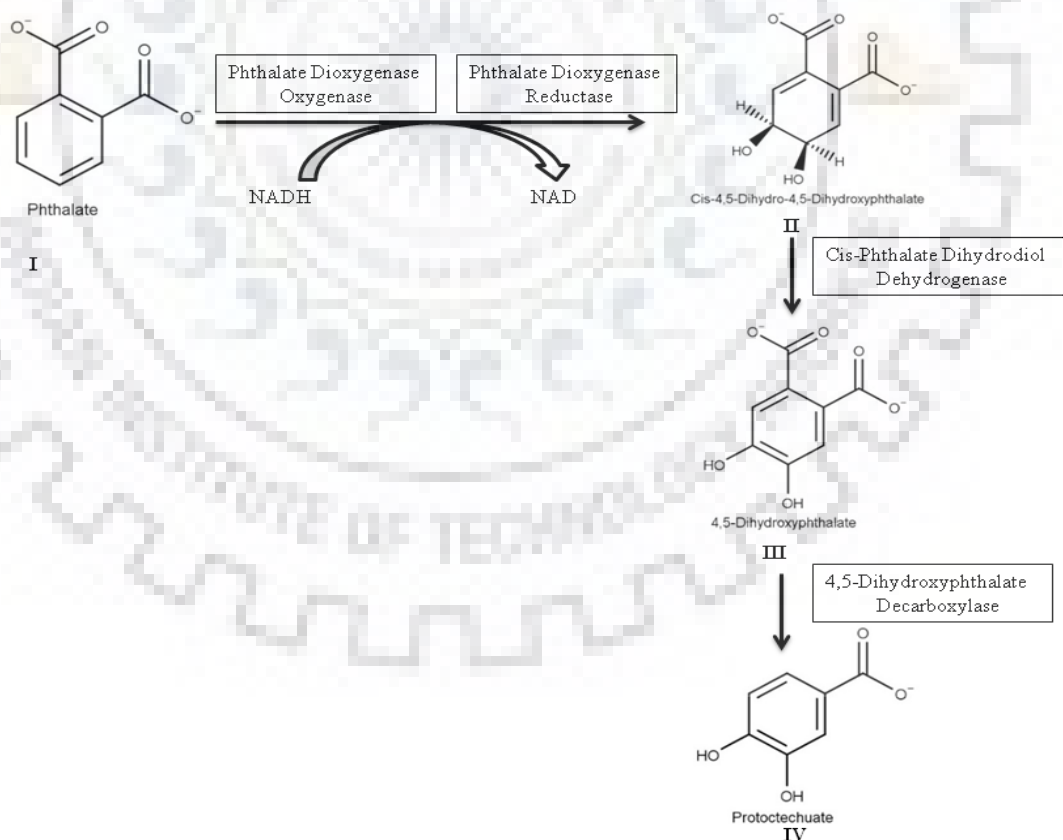


**Figure 5.1. Sequential steps for initial phthalate degradation.** The enzymes involved in the first step of phthalic acid degradation are Phthalate dioxygenase reductase, phthalate dioxygenase. The second step is mediated by phthalate dihydrodiol dehydrogenase and the third step is mediated by dihydroxyphthalate decarboxylase.

It is known that PDR utilizes flavin mononucleotide (FMN) as a cofactor for mediating the electron transfer from NADH to  $[2Fe-2S]$  center, a one-electron acceptor. In phthalate degradation, PDR is an important protein and the final product formation is firmly coupled to electron delivery in steady-state kinetic reactions, with a rate of 1 dihydrodiol (DHD) of phthalate produced from every 2 electrons transported from NADH of PDR [316]. It is to be noted that, the binding of substrate and PDR to PDO shows synergistic effect, and once they bind to PDO, it becomes fully catalytically active [317].

In the present study, PDR an important protein in PDO system has been cloned, expressed and purified from *Ralstonia eutropha* CH34. Further, to investigate the important interaction occurring between *RcPDO* and *RcPDR*, protein-protein docking has been done using HADDOCK. Model structures of the individual proteins serve as an input for protein-protein docking and it helps in the prediction of the structure of the complex. Molecular docking provides a means for fundamental structural studies of protein interactions during complex formation. Important interface residues from both the individual counterparts, i.e. *RcPDO* and *RcPDR* have been elucidated. The evolutionary relationship between important interface residues of *RcPDO* and *RcPDR* has also been established.

## **5.2 Material and Methods**

### **5.2.1 Chemicals**

Luria-broth (LB) broth and other media components were acquired from Himdeia (Mumbai, India) and Merck (USA). All other chemicals of analytical were purchased from Sigma-Aldrich (St. Louis, MO, USA).

### **5.2.2 Molecular biology kits and enzymes**

For molecular biology experiments Plasmid DNA isolation kit, Genomic DNA isolation kit, PCR purification and gel extraction kits were procured from Qiagen (Hilden, Germany). Enzymes such as DNA polymerase, different restriction enzymes, and T4-DNA

ligase were obtained from New England Biolabs (NEB-USA). *E. coli* strains such as (DH5 $\alpha$  and BL21 (DE3) were purchased from Novagen. Standard methods were adopted for molecular cloning procedures. Ni-NTA columns used for protein purification were purchased from GE healthcare. Primer ordering and DNA sequencing was carried out by using services from Eurofins (India). Bacterial strain *Ralstonia eutropha* strain CH34 was purchased from MTCC, Chandigarh, India and has MTCC identifier number-2487, India.

### **5.2.3 Cloning, expression of *RePDR***

Full-length coding region gene ID gi|499839221| encoding putative *RePDR* protein was amplified by using PCR. Forward and reverse primers were designed to amplify the *RePDR* gene (966 bp nucleotides) having 5'NdeI and 3'XhoI restriction sites. Megaplasmid from *Ralstonia eutropha* strain CH34 was used as a template for amplification. The sequences of primers were presented in 5' to 3' orientation.

#### ***RePDR* Forward Primer with NdeI site Sequence**

5'-AAT ACA TAT GAT GAG CAT GAA CAC C-3'

#### ***RePDR* Reverse Primer with XhoI site Sequence**

5'AAT ACT CGA GTC AAA GGT CTA GCA C-3'

The PCR amplified fragment was digested with both the restriction enzymes and ligated into pET-28c vector with a 6xHIS tag at N-terminal. One TEV protease site was there in between 6xHIS tag and *RePDR* which used for the tag removal. The recombinant plasmid having *RePDR* was then transformed into *E. coli* DH5 $\alpha$  cells. The clone was confirmed by PCR, restriction digestion with NdeI and XhoI and further automated DNA sequencing was done (Eurofins Genomics India Pvt Ltd. Bangalore, India).

After sequencing, the clone was confirmed and it was transformed into *E. coli* B21 (DE3) expression host. For newly constructs, the expression analysis and optimization was conducted on the small scale culture pattern. For that purpose, single pure colony was used for the inoculation of 10ml of the Luria Bertini (LB) broth having 30  $\mu$ g/ml of kanamycin as an antibiotic. 100  $\mu$ l from overnight grown culture was used for the inoculation of a fresh 10ml LB tube having the same concentration of antibiotic, at 37°C at 200 rpm. The culture was kept until the optical density at 600 nm (O.D. 600) reached up to 0.6-0.7. The culture was induced with varying concentrations of IPTG (from 0.3 mM to 1.0 mM) and

kept at different temperatures ranges like 18°C, 25°C and 37°C temperatures and growth was monitored for 16 hours, 6 hours and 4 hours respectively. After that cells were harvested at 5,000 rpm for 10 minutes and kept for storage in -80°C. The cell pellet was suspended in Tris buffer, pH 7.5 and lysis was done using a cell disruptor. Cell debris was removed and protein expression profile was further analyzed with 12% SDS polyacrylamide gel electrophoresis.

#### **5.2.4 Purification of *RePDR* protein**

For purification, the overnight grown culture tube was used to inoculate 1 liter of LB containing 30 µg/ml kanamycin concentration. The culture was kept at 37°C at 200 rpm until the optical density (O.D. 600nm) reached to ~0.7. Then, induction was done by the addition of 0.4mM isopropyl-1-thio-β-D-galactopyranoside (IPTG), followed by the incubation at 18°C at 200 rpm for 16 hours. The cells were pelleted down and stored at -80°C.

For protein purification, the cell pellet was suspended in 20 ml of binding buffer (25mM Tris buffer pH 8.0, 20mM imidazole, 500mM NaCl, 1 mM Dithiothreitol and 5% glycerol). The resuspended cells were lysed on ice using cell disruptor. Cell debris was removed and the lysate was centrifuged at 12,000 rpm for 60 minutes at 4°C. Then, the supernatant was applied on Ni<sup>2+</sup>-NTA agarose column pre-equilibrated with binding buffer. After binding the column was washed with 50 ml of binding buffer (25mM Tris buffer pH 8.0, 20mM imidazole, 300mM NaCl, 1 mM dithiothreitol and 10% glycerol). The Ni<sup>2+</sup> bound protein was eluted with 0-100% linear gradient of elution buffer (25mM Tris buffer pH 8.0, 250mM imidazole, 200mM NaCl, 1 mM dithiothreitol and 5% glycerol). The purity of the protein was checked by running the fractions on 12% sodium dodecyl sulfate-polyacrylamide gel electrophoresis (SDS-PAGE). Bradford method was used for determination of protein concentration. The protein concentration was calculated by interpolating the absorbance reading into a standard BSA curve.

#### **5.2.5 In-silico prediction of *RePDR* and *RePDO* interaction**

In our study, we have utilized the computational method for *RePDR* and *RePDO* model prediction. HADDOCK based precise prediction of *RePDR* and *RePDO* docking and

related interaction of the interface residues have been studied [318]. The evolutionary relationship between the conserved interface residues has also been established.

#### **5.2.5.1 Comparative molecular modeling and validation of *RePDR* and *RePDO***

To gain insights into the important interaction of *RePDR* with phthalate dioxygenase (*RePDO*) an important enzyme system in the degradation of phthalates, both were modeled and protein-protein docking was performed.

For the preparation of homology models of PDR and PDO from *Ralstonia eutropha* CH34, homology modeling program PHYRE 2.0 was used [319]. ModLoop program was utilized for refining the disordered loop regions in the models [267]. Swiss PDB Viewer 4.10 was used for the energy minimization of the selected *RePDR* and *RePDO* models [268]. The resultant models were verified and assessed by means of Ramachandran plot and Verify-3D scores [266, 320].

Molecular dynamics simulations studies were employed for estimating the dynamic variation taking place at the atomistic level in the *RePDR* and *RePDO* models. Molecular simulation studies were conducted by using Gromacs 5.1.4 suite along with AMBER 99SB forcefield based on LINUX based Fujitsu workstation [214, 321]. Both the protein models were solvated within a cubic box along with addition of counter-ions for overall stability and neutrality of the respective model system. The system was equilibrated with constant number of particles, volume, and temperature (NVT) and constant number of particles, pressure, and temperature (NPT) phases for 50,000 steps in each phase, at 300K. The final simulation production step for both the models was carried out for 10 ns and each step of 2 fs. Resultant trajectories were acquired and the final results were evaluated. Stability of the models were assessed on the basis of root mean square deviation (RMSD) variation which was calculated by using least-square fitting method for the protein backbone of *RePDR* and *RePDO* models.

#### **5.2.5.2 Determination of *RePDR* and *RePDO* interface residues**

In this study, with a goal for correct prediction of the interfacial residues, a program termed as WHISCY an acronym for “What information does surface conservation yield” has been used [322]. This program gives sufficiently reliable predictions related to interfacial residues, which were later used for *RePDR* and *RePDO* docking using HADDOCK. The

predicted active (cut-off 0.18Å) and passive (cut-off 6.5Å) interfacial residues were used for the generation of ambiguous interatomic restraints values in HADDOCK 2.2 web server used for *RePDR* and *RePDO* docking.

Another program called “Consensus Prediction Of interface Residues in Transient complexes” (CPORT) was also used for the prediction of interface residues in *RePDR* and *RePDO* protein [323]. In CPORT six interface prediction web servers are integrated and combined. It gives more stable and reliable predictions and was developed to be integrated with data-driven docking HADDOCK program.

### 5.2.5.3 *RePDR-RePDO* docking using HADDOCK

For elucidation of important protein-protein interaction, HADDOCK web server 2.2 is used for protein-protein docking. It is used for the depiction of changes occurring in the side chains of proteins as well as in the protein backbone, during complex formation.

The methodology used by HADDOCK for such protein-protein interactions are mentioned in flow chart diagram **Figure 5.2**.

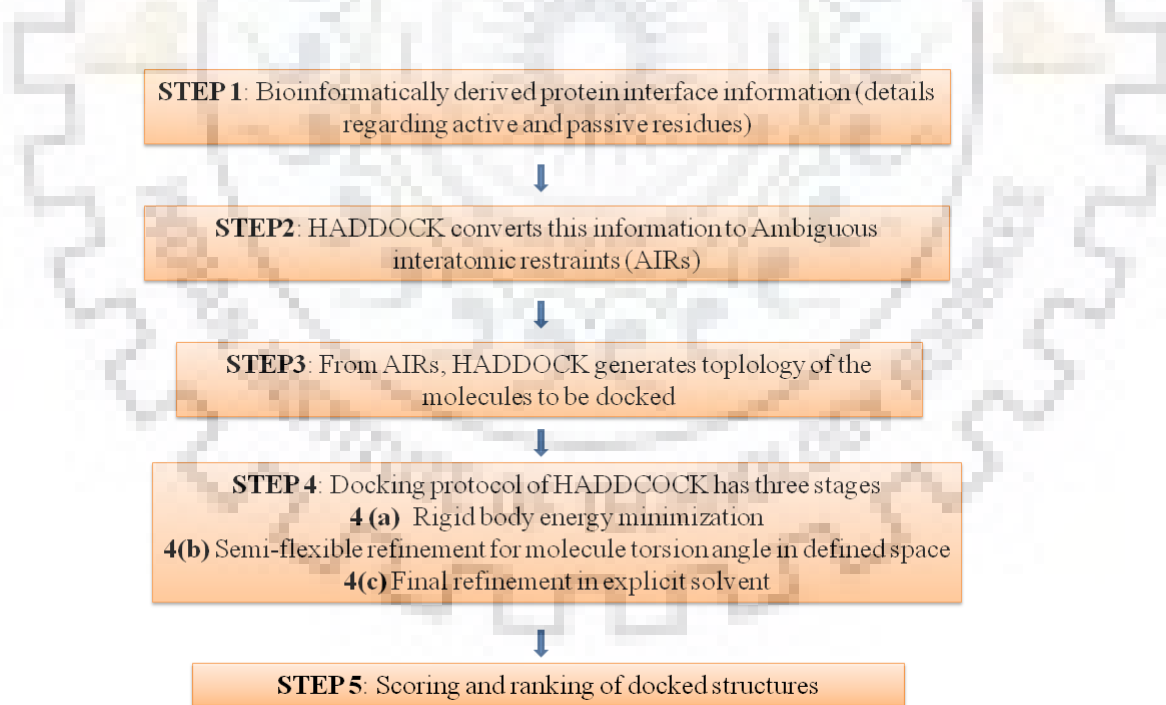


**Figure 5.2.** The steps used for *RePDR-RePDO* docking in HADDOCK. HADDOCK 2.2 web server was used for *RePDR* and *RePDO* docking.



Residues which were common in both the predictions (WHISCY and CPORT) were used for defining the active and passive residues for the generation of ambiguous interatomic restrains (AIRs) in HADDOCK. HADDOCK utilizes this information for the generation of topology files. The final score of HADDOCK is the sum of four components such as van der Waals, desolvation, electrostatic, and restraint violation energies altogether within the total surface area.

#### 5.2.5.4 Evolutionary relationship between conserved *RePDR* and *RePDO* residues

ConSurf web server (<http://consurf.tau.ac.il>) is an extensively used tool which helps in elucidating the functional regions in protein molecules, that are analyzed on the basis of the evolutionary dynamics of amino acids substitutions in the accessible homologous sequences [324]. In our case, as there are no crystal structures available for *RePDR* and *RePDO* proteins, therefore, site-specific description of the buried/exposed status of individual amino acid residues, and interrelated evolutionary significance is important for determining properties of interfacial residues. ConSurf estimates the evolutionary rates, which are based on the status of phylogenetic relationships between the homologous sequences and the specific dynamics associated with the analyzed sequence utilizing advanced probabilistic evolutionary models. ConSurf also allocates confidence intervals for the calculated evolutionary rates, which also estimate the reliability of the outcome. Steps utilized for determining evolutionary relationships between interface residues of *RePDR* and *RePDO* proteins using the ConSurf program are represented schematically in **Figure 5.3**.

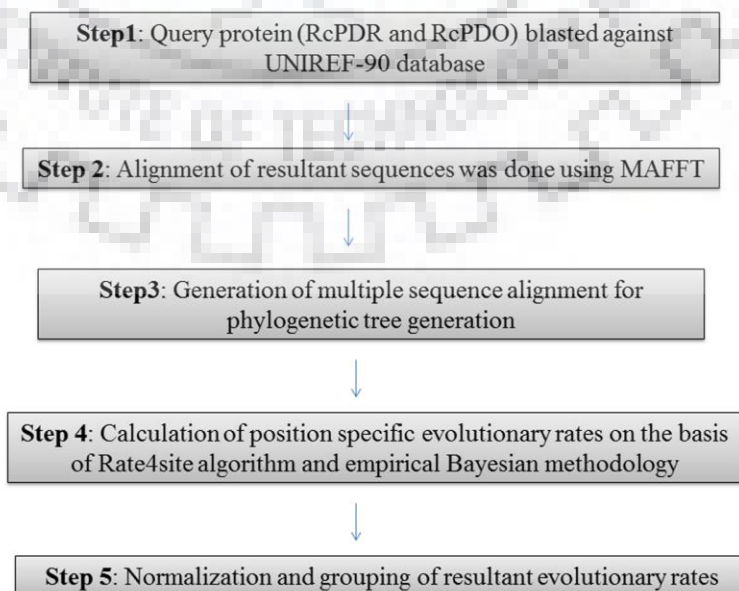




### **Figure 5.3. Steps utilized for determining evolutionary relationships using CONSURF.**

For determination of conservation between interface residues of *RePDR* and *RePDO* proteins, Consurf web server was used.

### **5.3 Results and discussion**

Microbial degradation of PAEs involves the participation of several classes of enzymes, including esterases/hydrolases, permeases, phthalate dioxygenase and many more. In this study, our focus is on the important phthalate dioxygenase (PDO) system. This enzyme system is composed of two proteins, first is Phthalate oxygenase reductase (PDR), a flavo iron-sulfur protein with NADH-dependent oxidoreductase activity and the second is phthalate dioxygenase oxygenase (PDO), a non-heme iron protein having oxygenase activity. In this study, PDR gene was cloned, expressed and purified from *Ralstonia eutropha* mega-plasmid. To explore the functional aspect of *RcPDR* and its counterpart *RcPDO*, homology model structures of both the proteins were predicted. The stability of the models was assessed by means of the molecular simulation study. Protein (*RcPDR*)-protein (*RcPDO*) docking was utilized for the prediction of the interaction between this important enzyme system. Interfacial residues participating in the interaction were identified and evolutionary aspect associated with them was illustrated.

#### **5.3.1 Cloning and expression of *RePDR***

In *Ralstonia eutropha* CH34 genome, phthalate reductase (*RePDR*) protein is coded by gene gi|499839221|. Megaplasmid from *Ralstonia eutropha* CH34 was isolated, which served as a template for PCR based amplification of *RePDR* gene. The amplified gene was cloned in *E.coli* based expression vector, pET-28c, along with N-terminal based 6xHIS tag. 1% agarose gel was used for the confirmation of an amplification band of size approximately, 966 bp, which corresponds to phthalate reductase (*RePDR*) gene. For ligation purpose, firstly the vector pET-28c and amplified PDR gene product were double-digested with restriction enzymes, *NdeI* and *XhoI* and ligated into the recombinant product by T<sub>4</sub> DNA ligase and finally transformed into *E.coli* DH5a cells), as shown in **Figure 5.4**. The automated DNA sequencing results were further used for the confirmation of the cloned DNA fragment (*RePDR*).

After confirmation of the clone, it was successfully transformed into *E. coli* BL21 (DE3) cells. Expression of *RePDR* was assessed at a small scale by varying concentrations of IPTG and varying the temperature. The optimum expression and solubility was obtained at induction with 0.4mM concentration of IPTG, at 18°C.

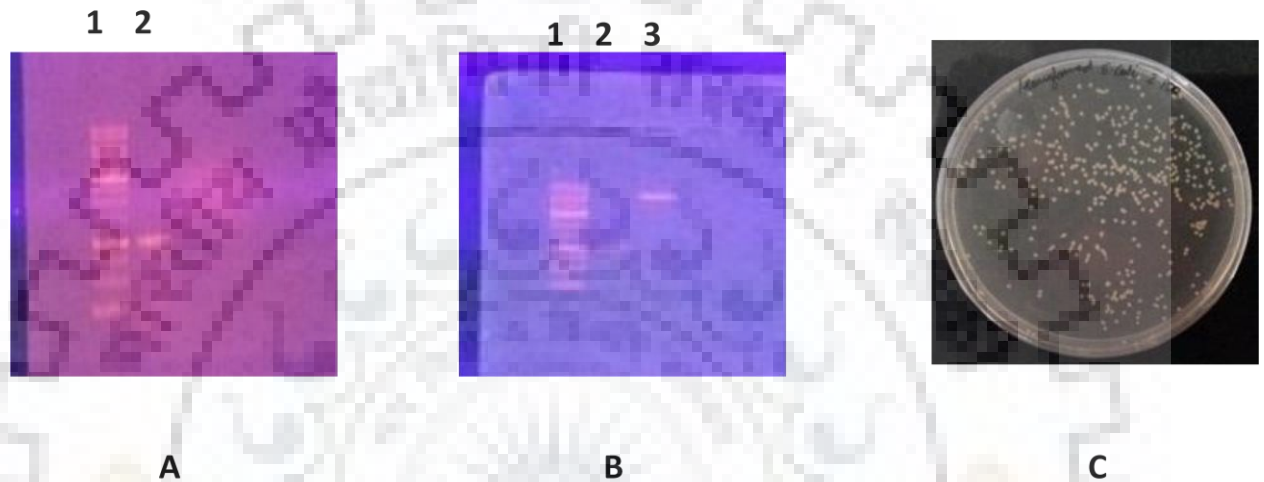


**Figure 5.4. Amplification and cloning of *RcPDR* gene.** Agarose gel electrophoresis (A) PCR products. Lane 1 shows the DNA marker; lane 2 shows *RcPDR* amplified from *Ralstonia eutropha*. (B) Agarose gel showing plasmid pET-28c and *RcPDR* digested with *NdeI* and *XhoI*. Lane 1 shows the DNA marker, lane 2 and lane 3 shows digested *RcPDR* gene and pET-28c respectively. (C) DH5 $\alpha$  cell colonies after transformation on LB agar plate is shown.

### 5.3.2 Purification of *RePDR*

A high level expression level of *RePDR* protein was obtained by inducing the *E. coli* BL21 (DE3) cells harboring pET-28c(+)-*RcPDR* with 0.4 mM of IPTG. The immobilized (Ni-NTA agarose) affinity chromatography was utilized for the purification of *RcPDR*. The *RcPDR* protein was purified with homogeneity and more than 95% purity. The SDS PAGE profile of samples from each stage of the purification is shown in **Figure 5.5**. From 1 liter of induced culture, the yield is around 10-12 mg for *RcPDR* protein with near 95% homogeneity.

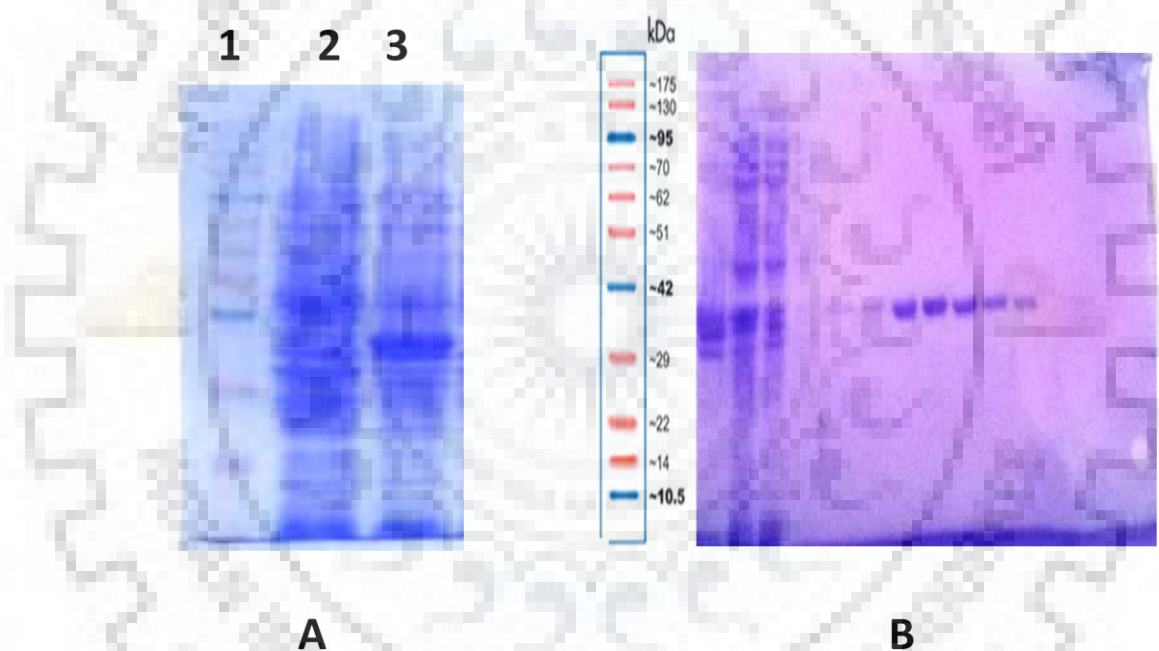


**Figure 5.5. Optimized purification of recombinant *RcPDR*.** A) 12% SDS-PAGE gel showing expression of PDR protein at 18°C in the pellet. Lane 1 is protein molecular weight depicting protein ladder, lane 2 shows uninduced pellet, kept at 18°C for 16 hours. Lane 2 shows induced pellet at 18°C for 16 hours. B) Analysis of the purification of *RcPDR* by SDS-PAGE (12%) stained with Coomassie Blue. Lane 1: Pellet sample, lane 2: supernatant, lane 3: flow through, lane 4-6 washes, lane 7-11: eluted fractions.

### 5.3.3 In-silico prediction of *RePDR* and *RePDO* interaction

In most of the cellular processes, proteins of basic cellular machinery and metabolism rarely carry out the function all alone. They tend to interact with other proteins present in the cellular environmental vicinity for carrying out important functions. Since the techniques of conventional NMR and X-ray crystallography are not sufficient enough to prevail over the need of hour associated with an increase in the total number of protein-protein complexes in the cellular processes. As taking into consideration, the huge number of protein-protein interactions, there is a need for the development of computational based methods that can precisely and adequately predict the protein complex structures as well as important interactions associated with complex formation. In this study, *RePDR* and *RePDO* homology models were predicted and HADDOCK was used for the elucidation of precise prediction of *RePDR* and *RePDO* docking interactions. Extensive illustration of the interaction of the interface residues of both the proteins has been studied. The evolutionary relationship between the conserved interface residues has also been established.

#### 5.3.3.1 Comparative molecular modeling and validation of *RePDR* and *RePDO*

Homology modeling is a constructive approach utilized for the prediction of three-dimensional structure from the homologous protein structure template. Here in this study, three-dimensional homology structure of *RePDR* and *RePDO* were constructed by using different homology modeling methods. It can be seen in pairwise sequence alignment that *RePDR* shares 42% sequence identity and 97% query coverage with phthalate dioxygenase reductase from *Burkholderia cepacia*, as shown in **Figure 5.6**. Likewise, *RePDO* shares 27% sequence identity and 48% query coverage with carbazole 1,9a-dioxygenase [325].

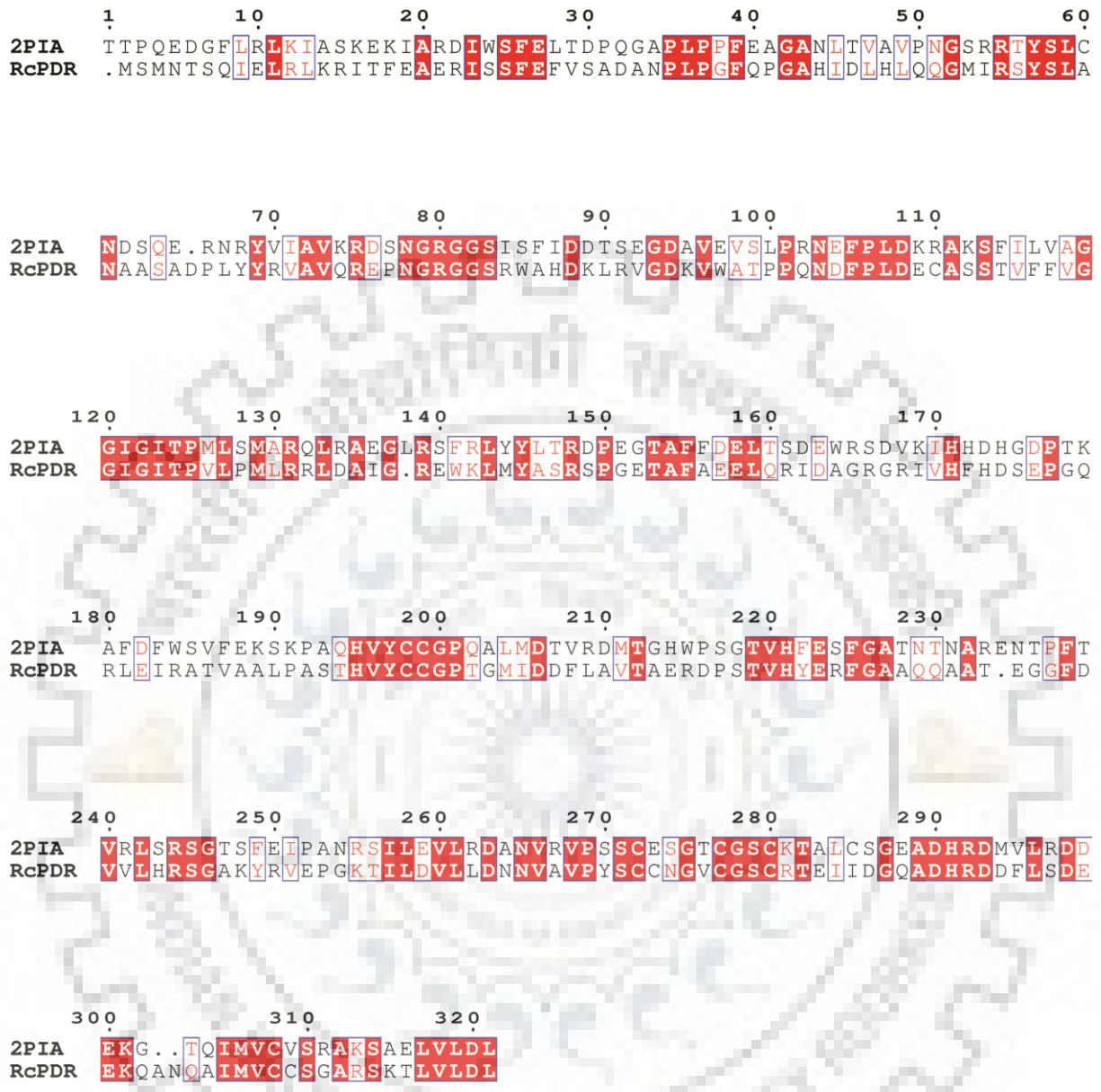


**Figure 5.6. Pairwise sequence alignment.** Pairwise alignment of phthalate dioxygenase reductase (*RcPDR*) from *Ralstonia eutropha* with PDR from *Burkholderia cepacia* (PDB ID: 2PIA) is shown.

In case of PDO, it was difficult to identify the template for homology modeling. Therefore, for both the cases, construction of accurate and reliable model was done by using PHYRE 2.0 tool. ModLoop program was used for refining the disordered loop regions of the structure. Resulting models were aligned to the template for evaluation of variation in the backbone residues from the template. Final homology models for *RePDR* and *RePDO* are shown in **Figure 5.7**.

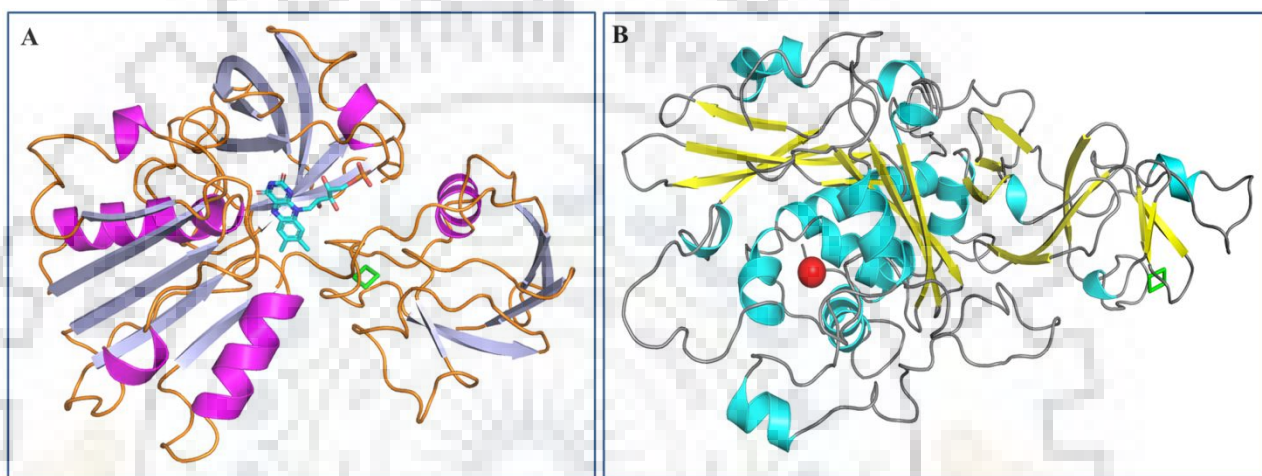


**Figure 5.7. Homology models of *RePDR* and *RePDO*.** The modeled structure of both proteins is shown in cartoon diagram A) *RePDR*, the helices are shown in pink color, sheets in grey color and loops in orange color. FMN is shown in stick form (cyan color). B) *RePDO*, helices are shown in cyan color, sheets in yellow color and loops in grey color. Active site iron is shown as a sphere (red color). FES moiety in both the models is shown in green color.



Precise analysis of Psi/Phi angles from Ramachandran plot evaluation confirmed the quality of the predicted *RePDR* and *RePDO* models, as shown in **Figure 5.8** and **Table 5.1**.

**Table 5.1. Ramachandran plot statistics for *RePDO* and *RePDR* models.**

Model	Favored residues (%)	Additionally allowed residues (%)	Number of Outlier residues (%)
<i>RePDO</i>	92.4	7.0	0.6
<i>RePDR</i>	98.4	1.3	0.3

The results obtained indicate that the protein models are reliable. Verify 3D result shows that in case of *RePDR* and *RePDO* models 95.56% and 86.46% respectively of the amino acid residues had an average 3D-1D score  $\geq 0.2$ . These results demonstrated that the folding energy pattern of the modeled protein structure is in complete agreement and lies within the expected range. The precise proximity of this factor advocates that the predicted models are much closer to the experimentally determined structure.

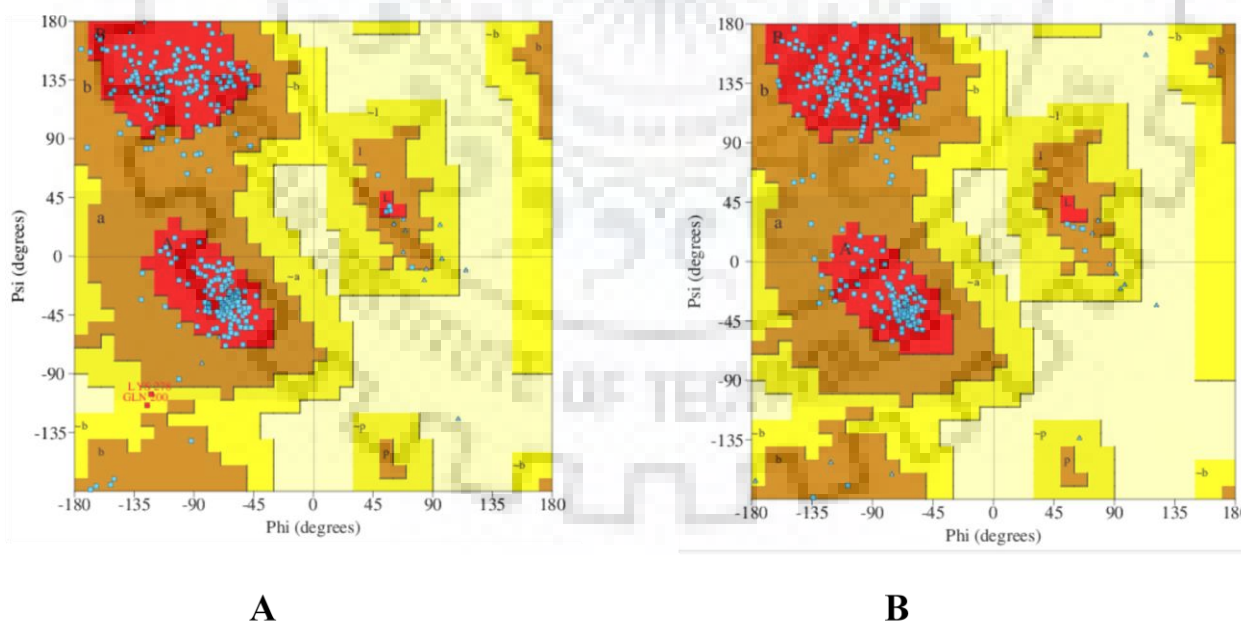


**Figure 5.8. The Ramachandran plot of the finalized *RePDR* and *RePDO* models. A) Ramachandran plot of *RePDO* model B) Ramachandran plot of *RePDR* model**



Stability of the predicted *RePDR* and *RePDO* models was also assessed on the basis of molecular dynamics studies. Here, in the current study, variation in the backbone RMSD values of *RePDR* and *RePDO* models is compared with crystal structure of phthalate dioxygenase reductase from *Burkholderia cepacia* (PDB ID: 2PIA) and carbazole 1,9a-dioxygenase (PDB ID: 2DE7) respectively, as shown in **Figure 5.9**. It has been shown that average RMSD variation in between predicted models and corresponding templates lies within a comparable range. It can be observed that the system attains equilibrium in initial 4-5 ns and was stable up to 10 ns during the course of the simulation.

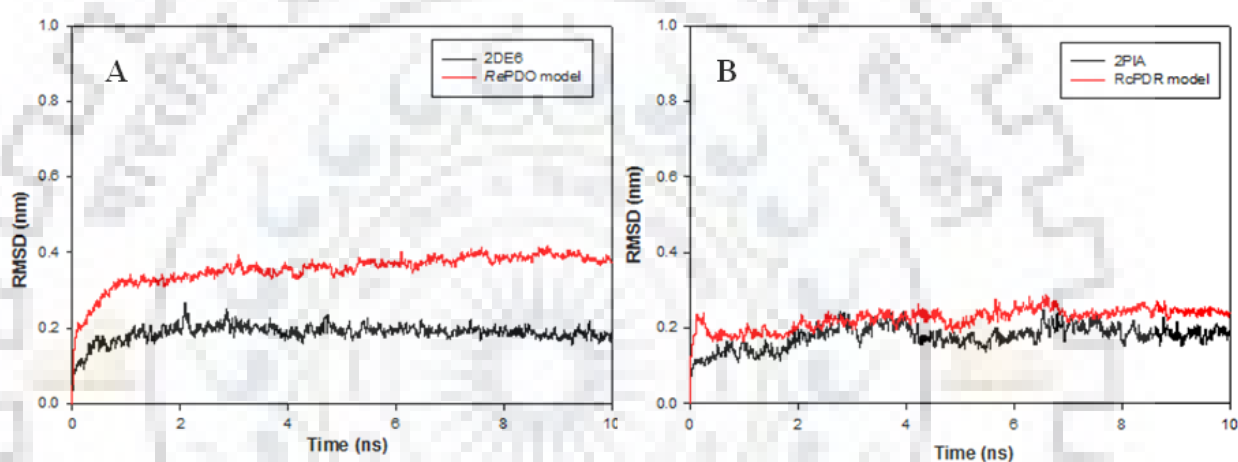


**Figure 5.9.** RMSD graph of *RePDO* and *RePDR* models. A) *RePDO* model and carbazole 1,9a-dioxygenase (PDB ID: 2DE7); B) RMSD profile of the C $\alpha$  backbone of *RePDR* and PDR from *Burkholderia cepacia* (PDB ID: 2PIA), during the 10ns of simulation at 300 K.

The average RMSD values of the *RePDR* and *RePDO* models, as well as template structures, are shown in **Table 5.2**. An overall analysis of the models shows that predicted homology models are reasonable enough for subsequent protein-protein docking studies. The final *RePDR* and *RePDO* models were validated and analyzed in terms of geometric analysis as well as RMSD validation. All these results indicate that, these models are suitable and reliable for further molecular protein-protein docking studies.

**Table 5.2. The average RMSD values of the *RePDR* and *RePDO* models as well as of the template structures**

<b>S.no</b>	<b>Component</b>	<b>Average RMSD (nm)</b>
1.	<i>RcPDR</i>	0.22
2.	2PIA	0.18
3.	<i>RcPDO</i>	0.3
4.	2DE7	0.18

### 5.3.3.2 Determination of *RePDR* and *RePDO* interface residues

Protein-protein interactions play an important role in biological processes. The first step in understanding these interactions at a structural level revolves around basic identification of important interface residues participating complex formation. “What information does surface conservation yield” (WHISCY) a protein interface prediction program, uses surface conservation and associated structural information for the precise prediction of protein-protein interface residues. WHISCY computes a prediction score for every residue present at the surface in *RePDR* and *RePDO* protein, and it can be matched to the alignment. In sorting the initial scoring file, a high prediction score means a high probability of that residue to be in a protein-protein interface. Predicted active and passive residues derived from the WHISCY program are shown in **Table 5.3**. For defining the active surface residue cut-off of 0.18 Å is used, whereas for passive residue radius of 6.5 Å is used. Theoretically, it means that a residue which has surface accessibility larger than 40% within these defined cut-offs will be used for categorizing the *RePDR* and *RePDO* residues as active and passive residue present on the surface of the protein.

Another consensus interface prediction program “Consensus Prediction Of interface Residues in Transient complexes” (CPORT) was also used for the prediction of *RePDR* and *RePDO* protein interfacial residues. Residues predicted by CPORT are also mentioned in Table 5. Further, the residues which were common in both the predictions were sorted out and these common predictions were used as input for the docking of *RePDR* and *RePDO* using HADDOCK.

**Table 5.3. Predicted active and passive residues of *RePDR* and *RePDO* derived from the WHISCY and CPORT program**

S.no	Program used	Residue category	<i>RePDO</i>	<i>RePDR</i>
1.	WHISCY	Active	78, 90, 72, 233, 185, 71, 45, 46, 89, 263, 79, 87, 80, 181, 234, 2, 367, 235	224, 275, 120, 199, 321, 294, 270, 285, 283, 56, 289, 200, 121, 264, 276, 291, 223, 101
		Passive	375, 390, 265, 38, 70, 57, 3, 175, 4, 73, 74, 75, 77, 97, 348, 364, 366, 368, 369, 230, 231, 232, 105, 106, 22, 40, 41, 42, 43, 44, 49, 180, 182, 68, 81, 184, 82, 83, 84, 187, 188	201, 202, 205, 221, 225, 227, 241, 228, 242, 229, 243, 244, 245, 261, 262, 263, 265, 267, 281, 268, 284, 286, 36, 37, 39, 300, 8, 100, 102, 103, 104, 274, 277, 279, 295, 296, 297, 298, 313, 80, 316
2.	CPORT	Active	51, 68, 70, 71, 72, 73, 74, 75, 77, 78, 79, 87, 89, 90, 106, 159, 174, 175, 176, 178, 180, 181, 182, 184, 185, 186, 187, 188, 190, 193, 197, 198, 224, 230, 231, 232, 233, 234, 235, 245, 246, 247, 249, 255, 272, 284, 287, 331, 333, 334, 335, 341, 344, 345, 347, 348, 350, 351, 352, 355, 366	15, 45, 47, 49, 50, 51, 55, 56, 83, 85, 87, 90, 91, 92, 97, 99, 101, 102, 104, 107, 108, 109, 110, 120, 121, 156, 161, 165, 167, 168, 169, 170, 178, 180, 181, 183, 184, 185, 187, 199, 200, 201, 202, 203, 205, 206, 208, 209, 212, 216, 217, 219, 220, 221, 223, 224, 225, 257, 260, 265, 267, 268, 269, 270, 272, 274, 275, 276, 277
		Passive	32, 42, 43, 44, 45, 46, 49, 50, 80, 81, 86, 105, 107, 109, 113, 117, 118, 120, 127, 128, 129, 150, 157, 158, 160, 161, 162, 163, 165, 166, 171, 177, 189, 192, 194, 195, 196, 200, 222, 223, 225, 226, 227, 228, 229, 236, 248, 250, 251, 252, 253, 273, 275, 279, 280, 281, 282, 283, 285, 332, 336, 338, 339, 340, 343, 354, 356, 357, 358, 361, 363, 364, 365, 367, 368, 369, 371, 378,	5, 6, 7, 8, 9, 11, 13, 14, 16, 17, 18, 21, 26, 36, 37, 39, 74, 75, 76, 77, 79, 80, 84, 88, 89, 93, 94, 95, 100, 103, 106, 112, 115, 132, 136, 138, 140, 141, 147, 148, 151, 155, 157, 159, 160, 162, 163, 164, 166, 171, 172, 173, 174, 175, 176, 177, 179, 188, 189, 190, 192, 210, 211, 213, 214, 215, 226, 227, 228, 252, 253, 254, 258, 261, 262, 263, 264, 266, 279, 290, 291, 294, 295, 309, 321,
3.	Common residues identified from both the programs	Active	71, 72, 78, 79, 87, 89, 90, 181, 185, 233, 234, 235	56, 101, 120, 121, 199, 200, 223, 224, 270, 275, 276
		Passive	42, 43, 44, 49, 81, 105, 364, 368, 369	8, 36, 37, 39, 80, 100, 103, 227, 228, 261, 262, 262, 279, 295

**5.3.3.3 *RePDR* - *RePDO* docking using HADDOCK**

In general, docking studies are based on the modeling of the protein complex structure and prediction of its important interactions with the constituents of the complex structure. HADDOCK is a useful docking method which is based on the experimental driven prior knowledge related to the interface region between the two participating molecular components w.r.t their relative acquired orientations. When experimental information, from NMR or mutagenesis is not available, then interface predictions derived from the bioinformatics interface can also be used. HADDOCK is used to analyze the conformational changes occurring in the protein molecules during the course of complex formation.

The docking procedure in HADDOCK 2.2 web server is usually carried out by using ambiguous interaction restraints (AIRs). These AIRs are usually obtained from either experimental or bioinformatically predicted residue interface data and helps in the precise prediction of intermolecular macromolecule interaction. For this purpose, common interface active and passive residues, derived from WHISCY and CPORT predictions, were provided along with the homology models of *RePDR* and *RePDO* proteins. The docking protocol for HADDOCK has three steps: during the first step random orientations are subjected to rigid body energy minimization, in the second step, simulated annealing is done in a semi-rigid manner in available torsion angle and in the last step final refinement with explicit solvent is done in Cartesian space. In the initial docking stage, random orientations were subjected to rigid body refinement. After refinement, best 200 docking orientation solutions were selected on the basis of the lower intermolecular energies. Then semi-flexible simulated annealing is done on these solutions in torsion angle space. Finally, the resulting structures were refined in explicit water. The final results were clustered and grouped on the basis of a relative pairwise RMSD variation in the protein backbone at the interface. Final clusters were sorted and categorized according to the average interaction energy of the complex. Best docking results obtained by the HADDOCK are clusters of structures, falling within an overall protein backbone RMSD of approximately 1.5Å. This lowest energy structure shows least AIRs violation (within a threshold of 0.3Å), have Z score of -0.9. HADDOCK results for *RePDR* and *RePDO* docking are shown in **Table 5.4**. The selected *RePDR* and *RePDO* docked complex has a buried surface area 2397.0 Å<sup>2</sup>,

which shows that the complex is compact enough during the course of protein-protein docking.

**Table 5.4. Final statistical analysis of *RePDR-RePDO* complex docking result acquired by HADDOCK**

S.no	Analysis Component	Value
1.	HADDOCK score	-146.1 +/- 17.4
2.	RMSD from the overall lowest-energy structure	1.5 +/- 1.1
3.	Van der Waals energy (kcal mol <sup>-1</sup> )	-79.0 +/- 9.4
4.	Electrostatic energy (kcal mol <sup>-1</sup> )	-308.4 +/- 90.2
5.	Desolvation energy (kcal mol <sup>-1</sup> )	-21.8 +/- 18.3
6.	Restraints violation energy (kcal mol <sup>-1</sup> )	29.4 +/- 26.23
7.	Buried surface area (Å <sup>2</sup> )	2397.0 +/- 45.7

Important intermolecular interactions occurring at the interface of the final docked *RePDR-RePDO* structure complex are evaluated by PDBsum are also shown in **Table 5.5**.

**Table 5.5. *RePDR-RePDO* docking results showing details of important interactions occurring at the interface of the complex.**

Nature of interaction	Participating residues		Distance (Å)
Hydrogen bond	<i>RePDO</i>	<i>RePDR</i>	
	OG1-THR (68)	NZ-LYS (299)	2.82
	O-PRO (70)	NH2-ARG(279)	2.82
	N-HIS (71)	OE2-GLU (297)	2.61
	NH1-ARG (72)	OD1-ASP (205)	2.63
	NH2-ARG (72)	OD2-ASP (205)	2.69
	N-GLY (73)	OE2-GLU (297)	2.97
	O-TYR (90)	OH-TYR (221)	2.75
	NH2-ARG (116)	O-ARG (279)	2.70
	NH1-ARG (407)	O-ALA (209)	2.74
Salt bridges	NH2-ARG (407)	O-ALA (209)	3.21
	OE2-GLU (50)	NZ-LYS (299)	2.66
	NH1-ARG (72)	OD1-ASP (205)	2.63
	OE1-GLU (393)	NZ-LYS (299)	2.68

Important interactions such as salt bridges are observed between oppositely charged interface residues as shown in **Figure 5.10**. Hydrogen bonding and non-covalent interactions such as Vander Waal interactions play a crucial role in the stability of the *RePDR* and *RePDO* complex.



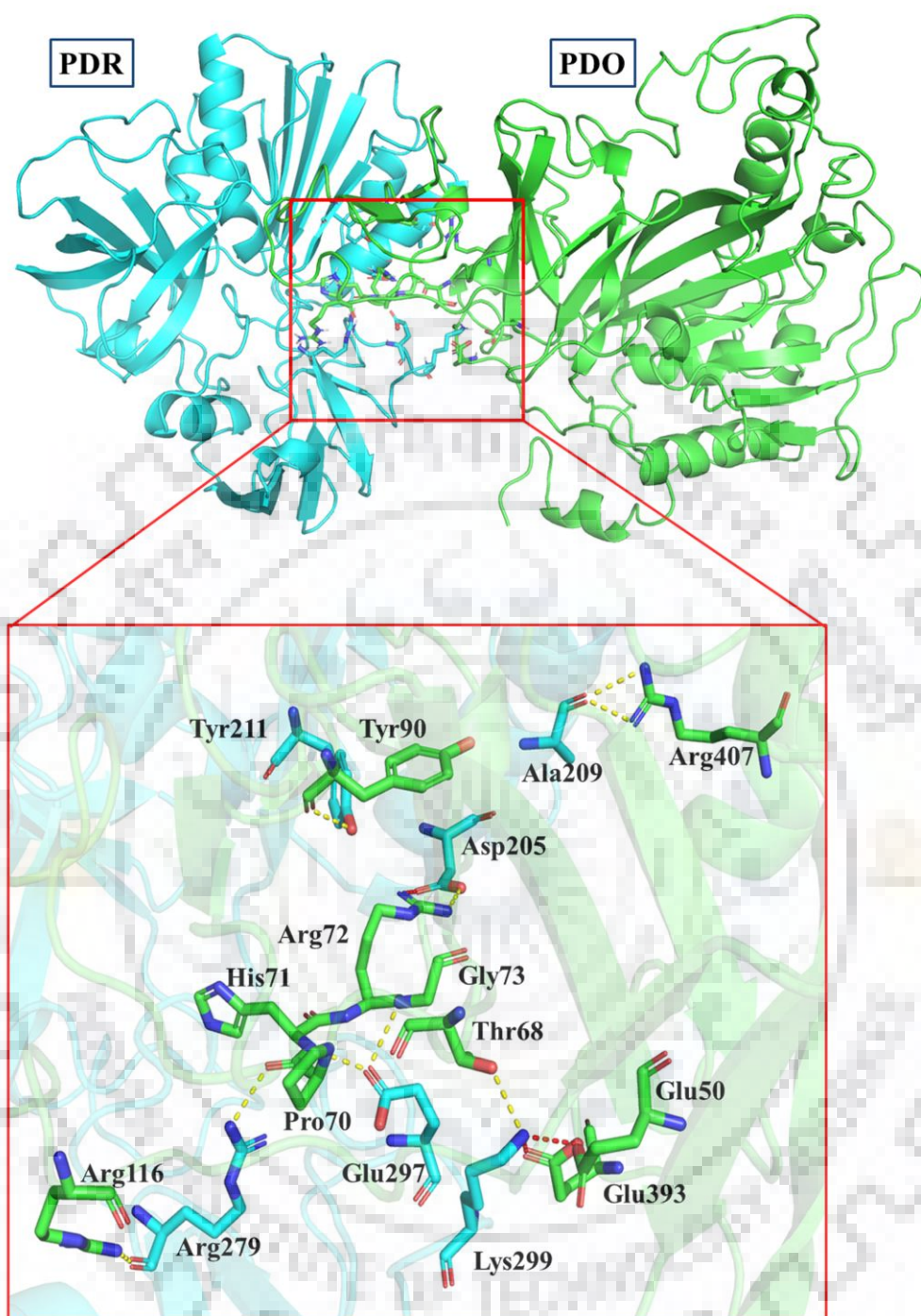


**Figure 5.10.** The important interactions at the interface of *RePDR* and *RePDO* complex are shown. The interacting residues of *RePDR* (cyan color) and *RePDO* (green color) are represented in stick form and the yellow dotted line shows the intermolecular hydrogen bonds and red dotted lines shows salt bridges.

#### **5.3.4.4 Evolutionary relationship between conserved *RePDR* and *RePDO* residues**

This aspect of the analysis is important since it highlights the slowly or highly evolving sites for the query macromolecule and emphasizes on the importance of the function of important amino acid sequence. ConSurf was used for the generation of respective conservation score of the important interface residues, as shown in **Table 5.6**.

**Table 5.6.** Conservation scores of important interface interacting residues of *RePDR-RePDO* docked complex

S.no	Interacting residue	Normalized conservation scores	Residue position in Consurf map
<b><i>RePDO</i></b>			
1.	GLU (50)	-0.828	9
2.	THR (68)	-0.379	7
3.	PRO (70)	-0.746	9
4.	HIS (71)	-0.807	9
5.	ARG (72)	-0.804	9
6.	GLY (73)	-0.717	9
7.	TYR (90)	-0.770	9
8.	ARG (116)	0.149	4
9.	GLU(393)	2.278	1
10.	ARG (407)	-0.807	3
<b><i>RePDR</i></b>			
1.	ASP (205)	-0.497	7
2.	ALA (209)	0.152	4
3.	TYR (221)	0.740	2
4.	ARG (279)	0.996	1
5.	GLU (297)	0.300	4
6.	LYS (299)	0.189	6

Initially, in ConSurf, homologous sequences were retrieved from the UNIREF-90 database, using the HMMER homolog search algorithm. This information is used for the generation of a multiple sequence alignment for PDO and PDR sequences using CLUSTALW of top 20 sequences selected. For calculation of conservation scores, a Bayesian method of calculation is used. Resulting conservation scores of important interface residues of *RcPDO* and *RcPDR* are shown. It can be seen that, according to the relative conservation score, a grading pattern is observed on the basis of which slow or fast evolutionary rate of interacting residues is shown. Evolutionary grades are normalized and grouped from 1 to 9, where, 1 grade signifies the most rapidly evolving amino acid residue, upto 5th grades it is for the intermediate rate of evolutionary aspect and later on in the same manner 9 grades



shows rather evolutionary most conserved positions as shown in **Figure 5.11**. It can be observed from the conservational data that, residues such as Thr50, Pro70, His71, Arg72 and Tyr90 from *RcPDO* are very conserved and other interacting residues shown in the data have either intermediate or rapid rate of variability associated with them.

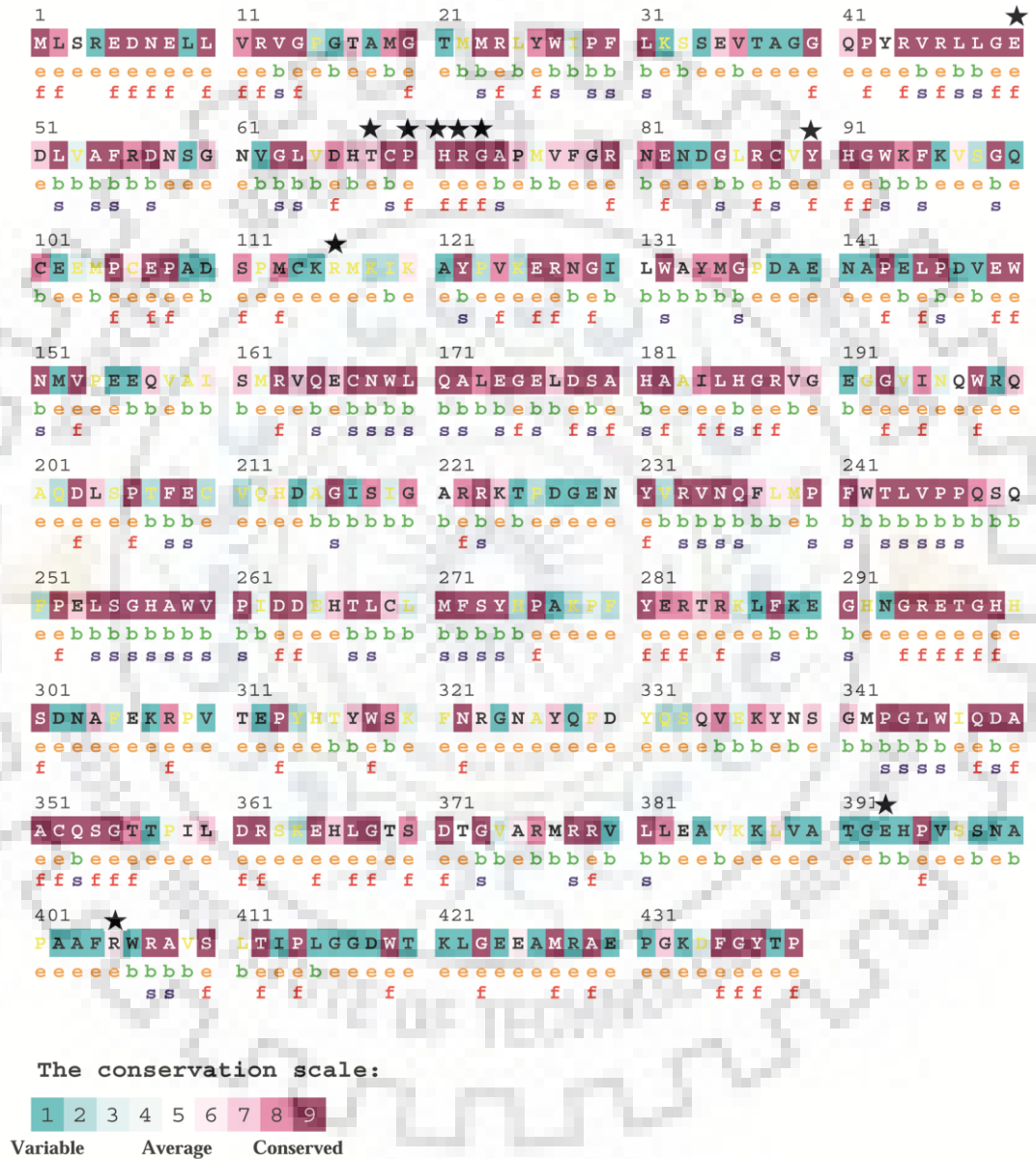


**Figure 5.11.** A) **Consurf** results for *RcPDO*. The residues highlighted with a star are highly important for the interaction with *RcPDR*. Description as “e” and “b” represent the exposed and buried status of the amino acid residue.



aerobic degradation of aromatic phthalic acid esters (PAEs). Two separate proteins phthalate dioxygenase (PDO) and phthalate dioxygenase reductase (PDR) are required for phthalate dioxygenase activity. In our study, *RcPDR* protein has been successfully cloned, expressed and purified. In order to assess the important interaction between *RcPDR* and *RcPDO*, both the important proteins have been modeled and protein-protein docking has been conducted. It has been shown that the interface residues which play an important part in interactions are highlighted. Moreover, conservation score has been allotted to the residues participating in the interfacial interaction.







**CHAPTER 6**

**STRUCTURE DETERMINATION OF BIPHENYL DIOXYGENASE FROM  
*PANDORAEA PNOMENUSA* B-356 IN COMPLEX WITH 2, 3', 5'  
TRICHLOROBIPHENYL**



## 6.1 Introduction

Polychlorinated biphenyls (PCBs) are synthetic toxic aromatic compounds which pose an enormous threat to human health and the surroundings due to their continuous exposure and persistence. These compounds have two benzene rings in which hydrogen atoms are replaced with by one-ten chlorine atoms. Theoretically, there are total of 209 PCB congeners, that generally vary in the respective position and number of chlorine atoms [326, 327]. These PCBs are generally thermostable and recalcitrant from degradation viewpoint [328]. PCB congeners are lipophilic in nature and this aspect of lipophilicity generally increases with increment in the degree of chlorination. Due to this behavior of PCBs, they tend to have very low water solubility property [8, 329]. Basic backbone structure and nomenclature of the biphenyl ring w.r.t chlorine substituent is shown in **Figure 6.1**.

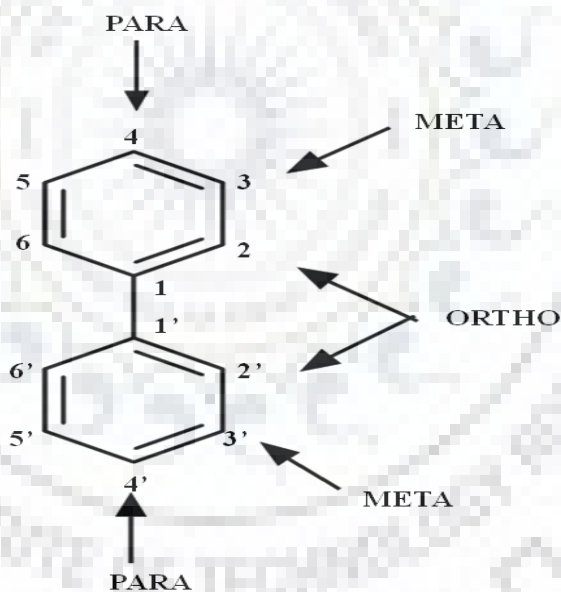


**Figure 6.1. The Basic chemical structure of Biphenyl and IUPAC based nomenclature.** Hydrogen atoms present in positions 2,2' and, 6,6' are (*ortho*), 3,3', and 5,5' are (*meta*) and/or 4,4' (*para*) may be substituted by chlorine atoms.

Like many, persistent organic pollutants (POPs) many PCB congeners are highly persistent, chemically inert and have a propensity to accumulate within the food chains [330, 331].



PCBs have been reported to have similar toxic effects as caused by 2,3,7,8-tetrachlorodibenzo-*p*-dioxin (TCDD) and other correlated halogenated polycyclic aromatic hydrocarbons such as polychlorinated dibenzofuran (PCDF), polychlorinated dibenzo-*p*-dioxin (PCDD) and they all are reported to generally act through the activation of aryl hydrocarbon receptor signal transduction mechanism [332-334]. A major structural distinction amid PCBs and related PCDDs/PCDFs is associated with conformational mobility. It is to be noted that, though PCDDs and PCDFs are relatively rigid and less flexible compounds, however, PCBs are present in a variety of conformations that generally occur due to rotation around the important bond linking the two aromatic biphenyl rings [335].

Microbial mediated bioremediation approach seems to be a potential route for management of PCB contaminated soils [336, 337]. Many species of aerobic bacteria have been reported to oxidatively degrade polychlorinated biphenyls. These bacteria predominantly belong to the genera of *Pseudomonas* sp., *Rhodococcus* sp., *Burkholderia* sp., *Arthrobacter* sp. [338-343]. These bacterial strains show substantial differences in their relative congener preferences depending on the chlorine substitution pattern on the biphenyl ring [150, 344]. These bacteria aerobically transform PCBs via *bph* pathways. In this pathway, initial catabolism of biphenyl to benzoate and then to 2-hydroxypenta-2,4-dienoate occurs [344, 345]. In the next step of degradation, the latter is converted to the Krebs cycle intermediates, as shown in **Figure 6.2**.

To envisage the molecular basis of PCBs biodegradation, *bph* pathway, an important pathway for catabolic activities for degradation was extensively studied. Biphenyl dioxygenase (BPDO) is first and an important enzyme of *bph* pathway and has a crucial role in determining of substrate specificity in biphenyl as well as PCB congener degradation [346, 347]. It has been shown that it is a ring-hydroxylating dioxygenase that generally mediates the attack of molecular oxygen onto biphenyl ring, and forms *cis*-(2*R*,3*S*)-dihydroxy-1-phenylcyclohexa- 4,6-diene. This oxygenase component (BPDO) has an  $\alpha$ 3- $\beta$ 3 arrangement and each of its  $\alpha$ -subunit contains a Rieske-type  $\text{Fe}_2\text{S}_2$  iron-sulfur center and mononuclear iron center is present at the active site. The reductase subunit (BphG) and a ferredoxin subunit (BphF) play an important role in the transfer of electrons from NADH to  $\text{Fe}_2\text{S}_2$  center of the oxygenase component. In the presence of  $\text{O}_2$  and

electrons, BPDO mediates the catalysis and dihydroxylation of the biphenyl aromatic ring at mononuclear iron center [348, 349].

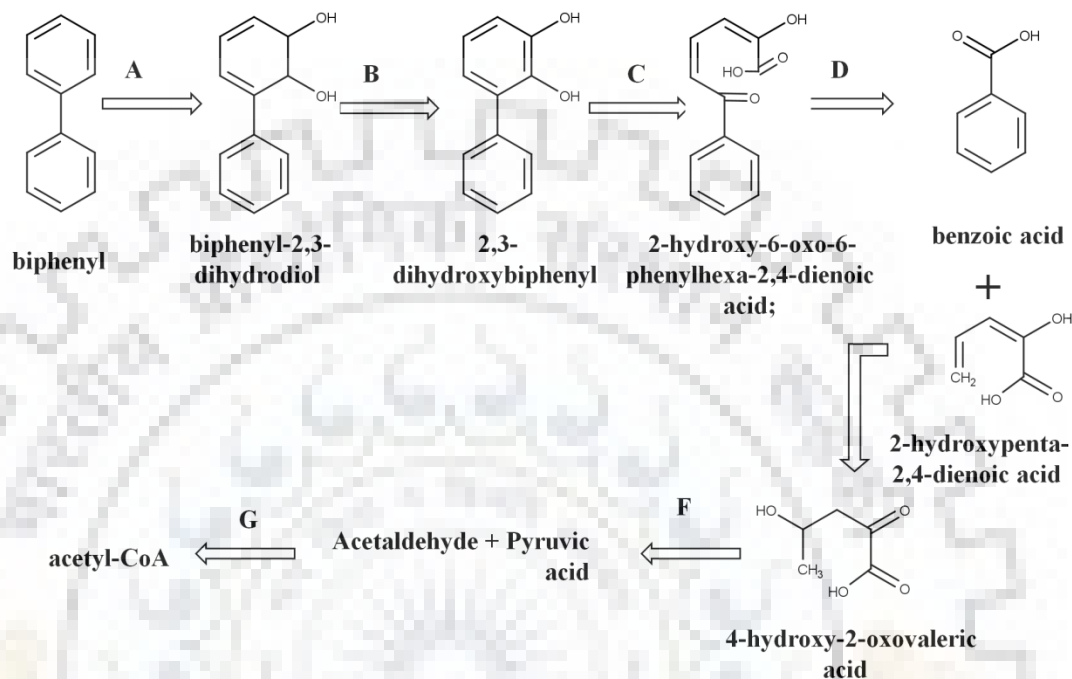


**Figure 6.2. Biphenyl degradation pathway in *Pandoraea pnomenusa* B-356.** Different Enzymes involved are mentioned (A) biphenyl-2,3-dioxygenase; (B) biphenyl-2,3-dihydrodiol-2,3-dehydrogenase; (C) 2,3-dihydroxybiphenyl-1,2-dioxygenase; (D) 2-hydroxy-6-oxo-6-phenylhexa-2,4-dienoate hydrolase; (E) 2-hydroxypenta-2,4-dienoate hydratase; (F) 4-hydroxy-2-oxovalerate aldolase; (G) acetaldehyde dehydrogenase.

Biphenyl dioxygenase (BPDO) is an important determinant in PCB-transforming capabilities of a particular bacterial species. Several studies from various bacterial populations reveal that diverse organisms have noteworthy variation in congener preference and associated regiospecificity, due to different selectivity mechanism of species-specific biphenyl dioxygenase [163, 350, 351]. The relationship between the selectivity of a particular congener and its biodegradability under the same concentration is extensively studied. For example, BPDO<sub>KF707</sub> from *Pseudomonas alcaligenes* KF707 and BPDO<sub>LB400</sub> from *Burkholderia xenovorans* LB400, show incredibly diverse reactivities, even though they have been shown to have more than 95% sequence identity. Several studies have

substantiated the relevance of the active site residues in influencing the enzyme's congener preference and related regiospecificity aspects [352-354]. It has been shown that BPDO<sub>B356</sub> from *Pandoraea pnomenusa* have about 70% sequence identity with other BPDOs from *Pseudomonas alcaligenes* KF707 and *Burkholderia xenovorans* LB400 [355]. Recently, various enzyme engineering attempts have yielded BPDO with improved PCB-degrading capabilities, as well as provide an insight into the molecular origin of specific congener preference. It has been reported that BphAEII9, a variant of BPDO<sub>LB400</sub> has a region from BPDO<sub>B356</sub>, and it possessed improved PCB-degrading properties than both of the parental enzyme [356].

It is to be noted that, specificity of biphenyl dioxygenase is an important aspect for determination of biphenyl analogs fate that will be metabolized by a particular microorganism in the biphenyl catabolic pathway. Significant efforts have been made for characterization and crystallization of this important enzyme. The three-dimensional crystal structure of its oxygenase part (BphAE) from the various strains such as *Pandoraea pnomenusa* B-356, *Burkholderia xenovorans* LB400 and many more have been resolved [357, 358]. It is an established that significantly diverse ranges of biphenyl analogs are degraded by *Pandoraea pnomenusa* B-356 and *Burkholderia xenovorans* LB400. Although *B. xenovorans* LB400 is regarded as one of the best naturally occurring PCB-degrading bacterial species, but many latest reports have revealed that BphAE from B356 (BphAEB356) also degrades several biphenyl analogs considerably more efficiently as compared to BphAE from the strain LB400 (BphAELB400) [358-361].

In this study, with an objective to understand the influence of the pattern and degree of chlorination on the catalytic activity of BPDO from *Pandoraea pnomenusa* B-356, a systematic computational study on chlorinated biphenyls has been conducted. Although such aspects of study can invariably be conducted experimentally, but the high number as well as the availability of all the congeners, makes it less feasible. Therefore, for that purpose, PCB congener library of 209 compounds was made and screened to elucidate the enhanced degradation abilities of BPDO. The important feature related to congener specificity has been highlighted. Through docking studies the binding ability of BPDO from *Pandoraea pnomenusa* B-356 w.r.t. PCB congeners were measured and important residues of active site residues involved in the interaction were acknowledged. Moreover,

the geometrical properties of the congeners such as aromatic benzene dimer ring offset, and the angle of rotation in between the two aromatic biphenyls influencing the rate of catalysis are also highlighted. Moreover, structure determination of BPDO with congener 2,3',5'-trichlorobiphenyl was also done. The results related to the geometry and electrostatic properties of chlorinated biphenyls can be useful to rationalize their selective toxicities.

## **6.2 Material and methods**

### **6.2.1 System preparation**

Computational studies were conducted with the purpose to assess the interaction of PCB congeners with BPDO<sub>B356</sub> from *Pandoraea pnomenusa* B-356. For that purpose, coordinates of biphenyl dioxygenase were taken from the available crystal structure of BPDO bound to substrate biphenyl (PDB ID: 3GZX) from the RCSB protein databank [357]. Protein was geometrically optimized by utilizing Clean Geometry module from Discovery Studio (DS version 4.0) suite, the service provided by Accelrys (San Diego, CA, USA). The protein was minimized in order to remove steric overlaps and clashes, using a smart minimizer algorithm, for 1000 steps with cut-off of 0.1 RMS gradient [243].

### **6.2.2 PCB Library preparation**

Three-dimensional structure of 209 PCB congeners was drawn using Marvin suite 17.13 [<http://www.chemaxon.com/marvin/sketch/index.jsp>]. Congener files were saved in Sybyl Mol2 format.

### **6.2.3 Screening of library using PyRx**

In order to understand the influence of substitution pattern of chlorination in PCBs in interaction with BPDO<sub>B356</sub>, a virtual molecular screening of the PCB congener library was done. For that purpose PyRx, a virtual screening software which provides an easy-to-use interface was used for the screening of PCB congener library. PyRx ensembles, several softwares such as AutoDock Vina, AutoDock 4.2, Open Babel, etc. in this study, AutoDock Vina is used for the docking purpose. Firstly, ligand library was uploaded, and protein molecule is provided into the PyRx workspace. Then protein and ligand files were converted to .pdbt AutoDock file format and minimized for the docking purpose. The docking receptor grid box was constructed within the vicinity of active site iron by

selecting the active site residues such as Gln226, Phe227, Asp230, His233, Ala234, Gly319, His321, Leu331, and Phe376. All these residues show important hydrophobic interactions in case of biphenyl as well. The dimensions of the grid box were as follows  $25 \text{ \AA} \times 25 \text{ \AA} \times 25.76 \text{ \AA}$  and the center point coordinates were set as  $X = -27.44$ ,  $Y = 92.94$  and  $Z = 3.56$ . It is to be noted that, grid box size is big enough to allow the PCB congener to move freely in the search space and the exhaustiveness factor was increased to 10. Once the calculations are done, the results appeared depicting the binding affinity (kcal/mol) values of the ligands. Final results were exported to Pymol (version 1.3) for further visual analysis [213].

Top 15 congeners along with biphenyl were selected for further analysis. Compounds showing maximum binding affinity and proper orientation within the active site vicinity were sorted, selected and docked using AutoDock 4.0 as well [211]. AutoDock utilizes a semi-empirical free energy forcefield to calculate the binding free energy of a small molecule to a macromolecule. Receptor molecule was prepared by adding explicit hydrogen molecules and associated Kollman charges using the AutoDock Tools 1.5.6 and saved in .pdbqt file format. A grid spacing of  $0.375 \text{ \AA}$  was used. The dimensions of the grid box were as follows  $60 \text{ \AA} \times 60 \text{ \AA} \times 60 \text{ \AA}$  and the center point coordinates were set as  $X = -30.187$ ,  $Y = 91.916$  and  $Z = 3.328$ . Lamarckian genetic algorithm and grid supported energy evaluation method were adopted. All other docking parameters were set as default. General properties of selected congeners have been shown in **Table 6.1**.

#### **6.2.4 Determination of pi-stacking interactions**

The determination of important interactions in the protein-ligand complex is very important for deep structural analysis. Here, a web service called protein-ligand interaction profiler (PLIP) ([projects.biotec.tu-dresden.de/plip-web](http://projects.biotec.tu-dresden.de/plip-web)) was used for the detection and visualization of important non-covalent interactions i.e. pi-stacking interactions, involved in protein-ligand complexes [362]. It also provides with important parameters related to the orientation of aromatic ring during complex formation and the values obtained are compared with that of the PCB-BPDO<sub>B356</sub> complex.

**Table 6.1.** General properties of best scoring PCBs. molecular weight, the characteristic dipole moment of selected top 15 PCBs, including biphenyl are mentioned.

S.no	Compound		Mwt	Dipole moment (D)
1.	Biphenyl	BP0	154.208	0
2.	2-Chlorobiphenyl	BP1	188.653	0.764
3.	3-Chlorobiphenyl	BP2	188.653	0.765
4.	2,3-Dichlorobiphenyl	BP5	223.098	1.306
5.	2,5-Dichlorobiphenyl	BP9	223.098	0.056
6.	3,4-Dichlorobiphenyl	BP12	223.098	1.283
7.	2,2',3-Trichlorobiphenyl	BP16	257.543	1.238
8.	2,2',4-Trichlorobiphenyl	BP17	257.543	1.060
9.	2,3,4-Trichlorobiphenyl	BP21	257.543	1.490
10.	2,4,4'-Trichlorobiphenyl	BP28	257.543	0.766
11.	2,4,5-Trichlorobiphenyl	BP29	257.543	0.779
12.	2,3',4'-Trichlorobiphenyl	BP33	257.543	1.851
13.	2,3',5'-Trichlorobiphenyl	BP34	257.543	1.289
14.	2,2',3,4-Tetrachlorobiphenyl	BP41	291.988	1.606
15.	2,2',3,4,5-Pentachlorobiphenyl	BP86	306.015	2.141



### 6.2.5 Chemicals

2,3',5' trichlorobiphenyl was a kind gift from Professor Michel Sylvestre from the prestigious Institut National de la Recherche Scientifique, INRS-Institut Armand-Frappier, Laval, QC, Canada. Crystallization chemicals were purchased from Himedia (Himedia, Mumbai), and Sigma-Aldrich (St. Louis, MO, USA). All chemicals and reagents used in this study were of ACS grade.

### 6.2.6 Structure determination of BPDO<sub>B356</sub>-2,3',5' trichlorobiphenyl complex

Purified and concentrated BPDO protein samples were provided by Professor Michel Sylvestre. Initial crystallization trials for the complex of BPDO<sub>B356</sub>-2,3',5' trichlorobiphenyl were carried out in Macromolecular Crystallography Unit, IIT Roorkee, and the final crystallization was done at Purdue University, USA.

Initial crystallization trials for the complex formation were carried out as per the earlier published purification protocol with few modifications [357]. For initial crystallization trials, 12 mg/ml of the purified enzyme, in 25 mM HEPES, pH 7.3; 1 mM DTT; 0.25 mM ferrous ammonium sulfate and 10% v/v glycerol was taken. The crystallization reservoir solution has 100 mM MES buffer, pH 5.80; PEG 4,000 (15–20% w/v); 10-15% v/v 2-propanol, 3.5 mM ferrous ammonium sulfate and 12.5 mM NaCl. Final crystallization was carried out in anaerobic condition. The 96 well sitting-drop vapor-diffusion technique was used for setting up crystallization. 2 µl of the sample drop volume had an equal protein sample and reservoir well solution in a 1:1 ratio and the tray was kept at 20°C in a vibration-free thermostat chamber.

The crystal data was collected at Advanced Photon Source (APS) synchrotron facility in Chicago, USA, 108 K and using monochromatic X-rays of 1 Å wavelength. The diffraction data was indexed, integrated and scaled using the HKL2000 program module [363]. MOLREP program of CCP4i7.0 suite was used with the initial homologous structures of BPDO with biphenyl complex [364]. Phenix refine was utilized for restrained atomic parameter refinement and COOT0.8.7 program was utilized for the electron density map analysis and suitable model building [365, 366]. The overall quality of the complex structure was evaluated by various parameters like clash score, outliers, and residues having bad angles and bad bond distances, as analyzed by Molprobit [367]. Electron density of ligand 2,3',5' trichloro biphenyl was verified using Polder maps [368]. It is



implemented in Phenix and removes the related bulk solvent effects and help in an improved illustration for ligand into the cavity of the active site. Final models of BPDO<sub>B356</sub>-2,3',5' trichlorobiphenyl complex for the structure refined using CCP4 reamac [369]. The final model was analyzed and figures were prepared by using PyMOL 2.0.5.

### 6.3 Result and Discussion

*Pandoraea pnomenusa* B-356, a biphenyl degrading bacterium was isolated from contaminated soil. It has been reported to efficiently degrade hazardous polychlorinated biphenyls (PCBs), polyhydroxylated biphenyls (PHBs) and various other compounds such as benzophenone, diphenylmethane, dihydroxybiphenyl, etc. under aerobic conditions [344, 360, 370, 371]. However, it has been shown that in case of high chlorine substitution or especially double para-substituted PCBs, the rate of degradation showed some degree of restriction. Biphenyl dioxygenase (BPDO) is an important enzyme in the degradation process of PCBs. It has been shown that the  $\alpha$ -subunit of iron-sulfur protein of biphenyl 2,3-dioxygenase (BphA1) is involved in the catalytic activities and is also an important determinant of substrate-related specificity. To envisage the enhanced degradation abilities of BPDO from *Pandoraea pnomenusa* B-356 towards various PCBs congeners, PCB congeners library was prepared, screened using PyRx. Through docking studies conducted with 209 PCB congeners, the binding affinities of total 209 PCB congeners with BPDO from *Pandoraea pnomenusa* B-356 were measured and crucial active site residues interactions were identified. The results showed that the average binding affinity of PCBs varies with a different number of chlorine substituents.

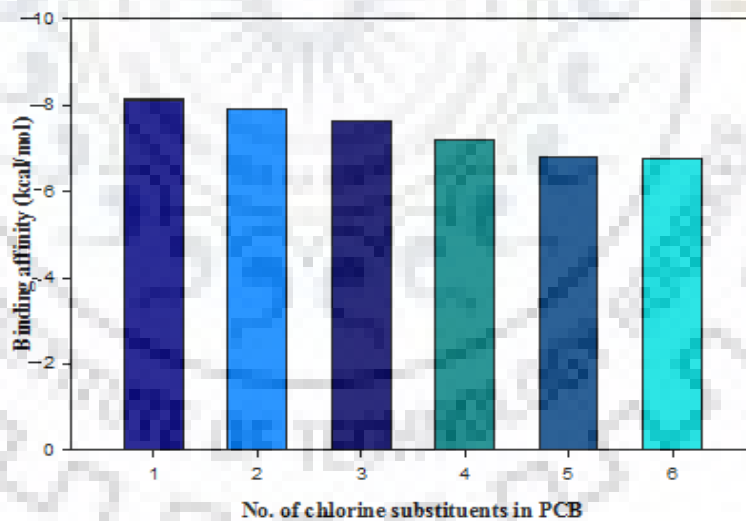
#### 6.3.1 Screening of library using PyRx

Crystal structure of native BPDO and its complex with Biphenyl from *Pandoraea pnomenusa* B-356 has been already determined (PDB ID: 3GZY and 3GZX, respectively) [357]. Structure coordinates of BPDO in complex with biphenyl were used for screening of the PCB congener library. Screening of the library was carried out by using PyRx a virtual ligand screening tool, in which AutoDock Vina 1.1.2 is used. PCBs were screened for their ability to show maximum interaction as well as proper orientation w.r.t. active site residues. In this study main objective was the evaluation of the effect of position specific chlorination influencing the binding affinity of different congeners. It has been shown

earlier that the preference of BPDO<sub>B356</sub> w.r.t. pattern and position of chlorination is as follows [349]

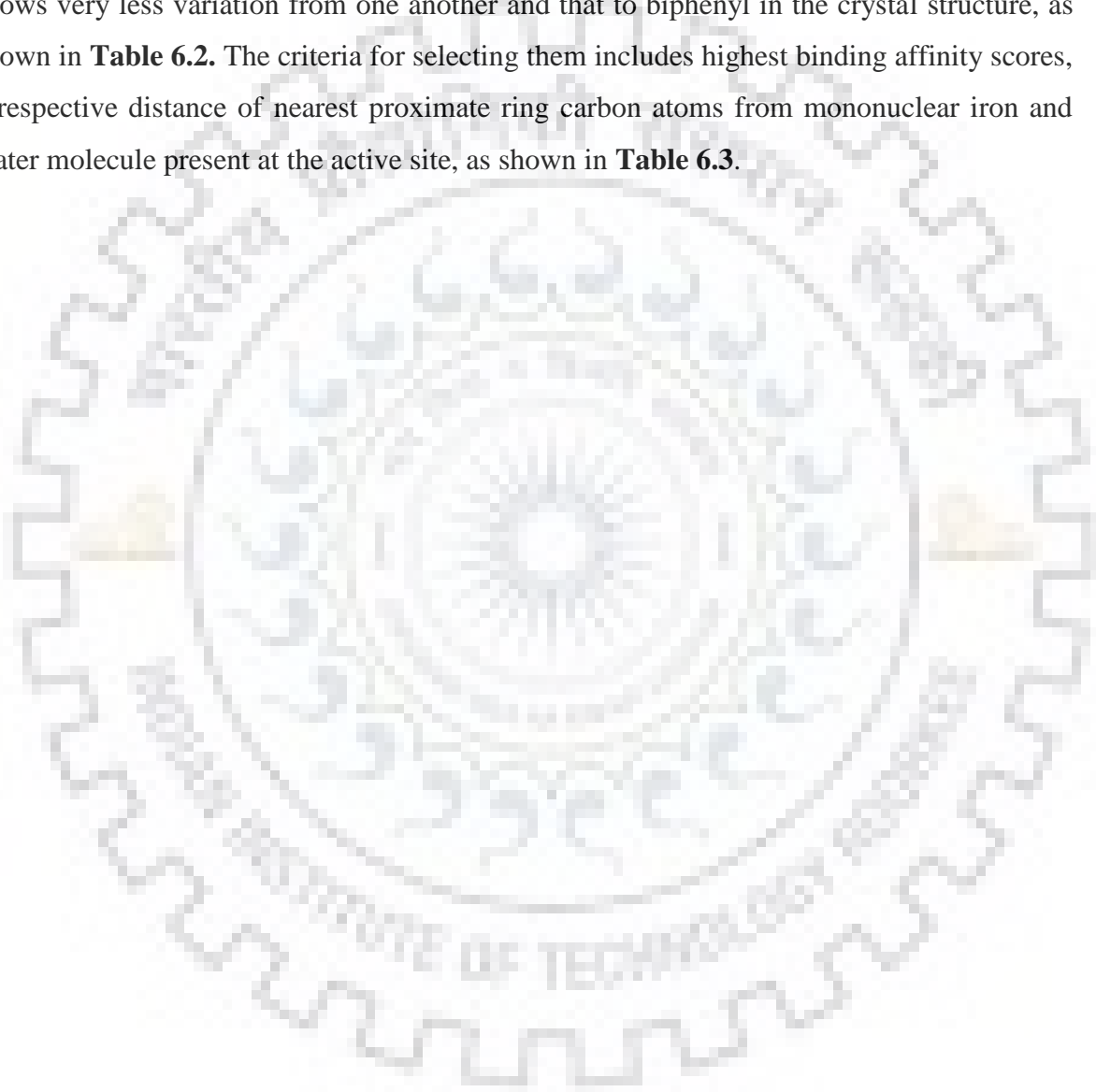
**Ortho-substituted PCBs > meta-substituted PCBs > para-substituted PCBs**

A similar pattern of preference was also observed in our study. Every docked complex of BPDO and PCB congener was aligned to the template BPDO in complex with biphenyl, and the variations in active site residues were measured. Categorization of congeners on the basis of number of chlorine *vs* binding affinity has been done. It has been seen that as the level of chlorination increases, the corresponding binding affinity of the group decreases, as shown in **Figure 6.3**. Rather, we can elucidate that as the degree of chlorination increases, the number of congener isomer giving contribution in the calculation of average binding affinity also decreases. This means that if there are 46 isomers classified in the group of pentachloro-biphenyls, then 30 isomers contribute to the average binding calculations, since all the isomers do not give possible or favorable binding pose. None of the 8, 9, or 10 chlorine substituted PCB congener showed any interaction with BPDO<sub>B356</sub>.



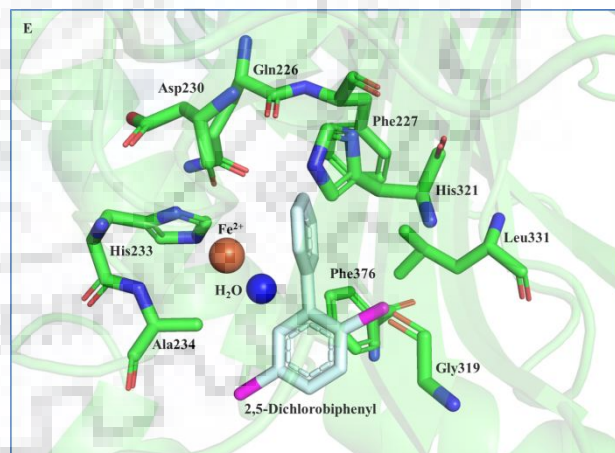
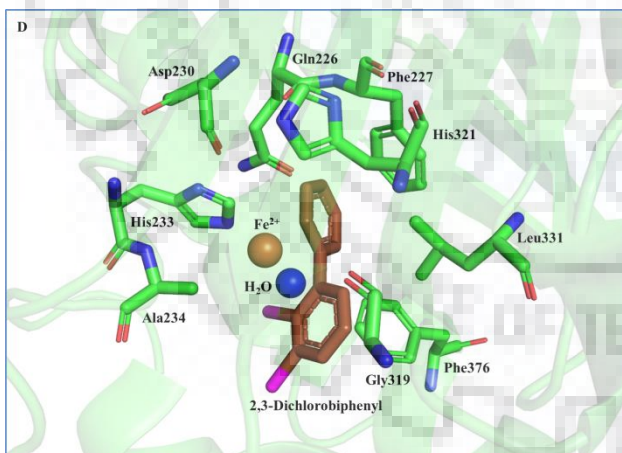
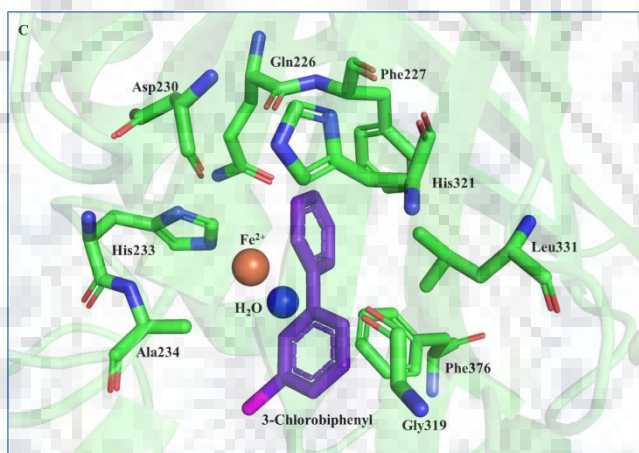
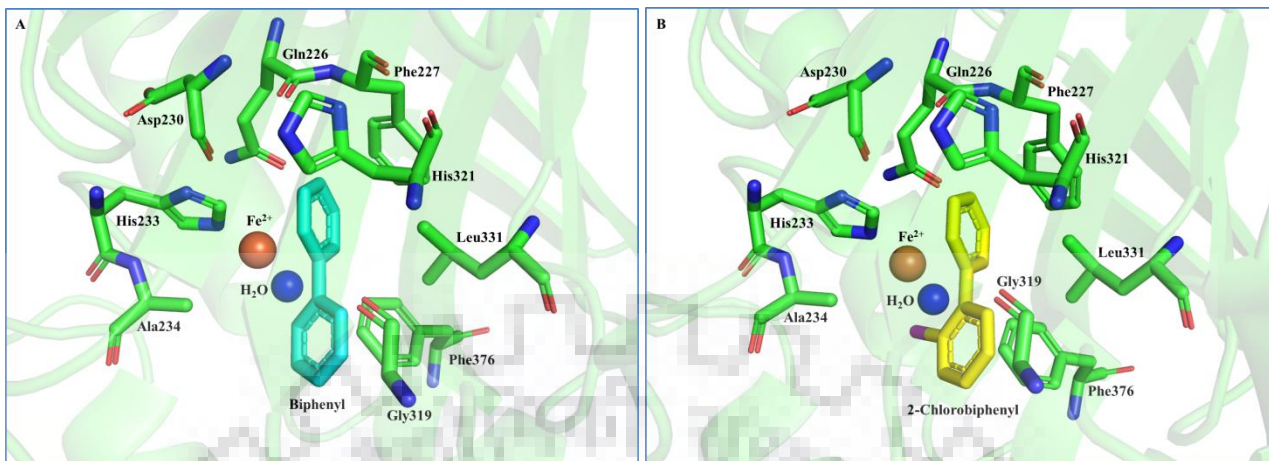
**Figure 6.3. Screening of PCB congeners and analysis.** This represents a comparison of affinities energy of PCB congeners w.r.t. different number of chlorine substituent.

It is to be noted that, top 15 compounds, including biphenyl as a substrate, have been selected for further analysis, as shown in **Figure 6.4**. 15 congeners along with biphenyl were evaluated within a cut-off range of -8.3 kcal/mol, since this the binding affinity shown by biphenyl. AutoDock 4.2.6 was used to perform the docking of top 15 congeners along with biphenyl with BPDO<sub>B356</sub>. High-ranking dockings were found with BPDO<sub>B356</sub> that shows very less variation from one another and that to biphenyl in the crystal structure, as shown in **Table 6.2**. The criteria for selecting them includes highest binding affinity scores, a respective distance of nearest proximate ring carbon atoms from mononuclear iron and water molecule present at the active site, as shown in **Table 6.3**.

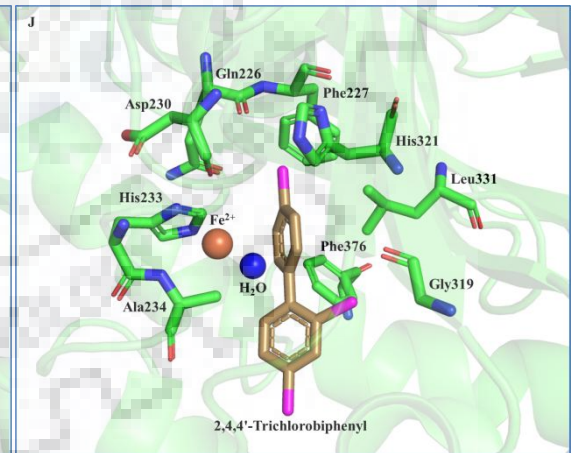
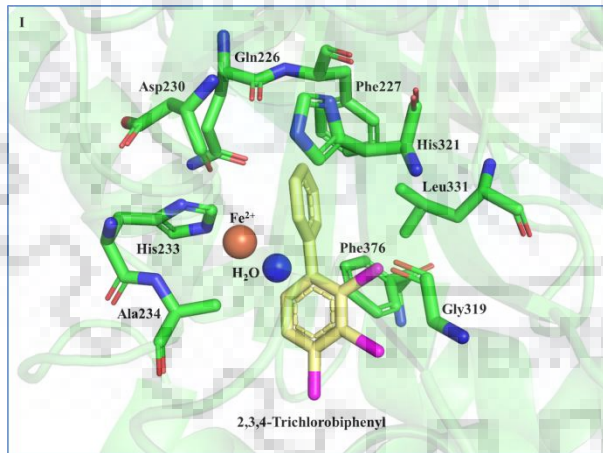
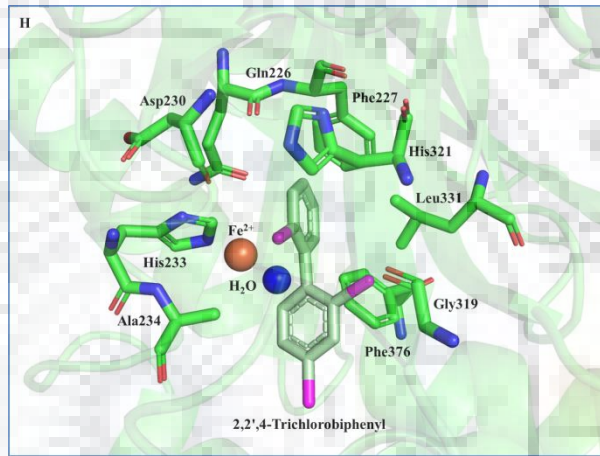
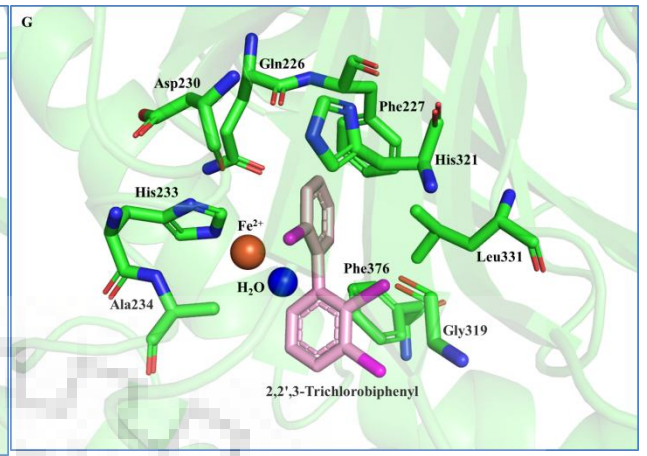
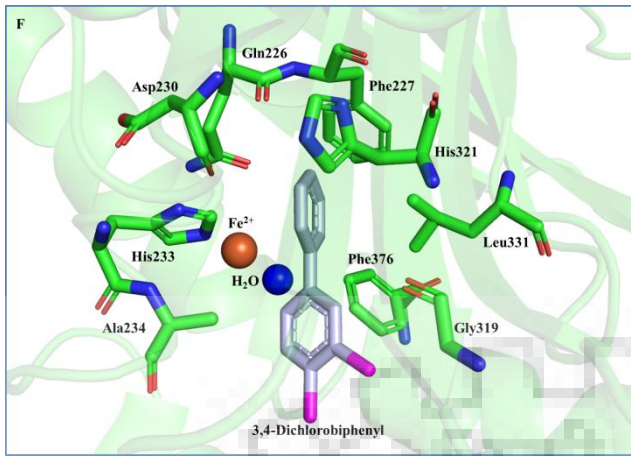


**Table 6.2. Binding affinities (kcal/mol) of PCBs.** Binding affinity (kcal/mol) details of top 15 PCBs congeners along with biphenyl are shown.

<b>S.no</b>	<b>Ligand</b>	<b>Compound</b>	<b>AutoDock Vina Binding affinity (kcal/mol)</b>	<b>AutoDock Binding affinity (kcal/mol)</b>
1.	BP0	Biphenyl	-8.3	-6.27
2.	BP1	2-Chlorobiphenyl	-8.5	-6.92
3.	BP2	3-Chlorobiphenyl	-8.4	-6.83
4.	BP5	2,3-Dichlorobiphenyl	-8.6	-7.66
5.	BP9	2,5-Dichlorobiphenyl	-8.8	-7.17
6.	BP12	3,4-Dichlorobiphenyl	-8.9	-7.58
7.	BP16	2,2',3-Trichlorobiphenyl	-9.3	-8.07
8.	BP17	2,2',4-Trichlorobiphenyl	-8.6	-7.87
9.	BP21	2,3,4-Trichlorobiphenyl	-8.4	-8.21
10.	BP28	2,4,4'-Trichlorobiphenyl	-8.3	-7.53
11.	BP29	2,4,5-Trichlorobiphenyl	-8.2	-7.53
12.	BP33	2,3',4'-Trichlorobiphenyl	-8.7	-7.82
13.	BP34	2,3',5'-Trichlorobiphenyl	-8.3	-7.62
14.	BP41	2,2',3,4-Tetrachlorobiphenyl	-9.2	-8.64
15.	BP86	2,2'3,4,5-Pentachlorobiphenyl	-8.9	-8.13







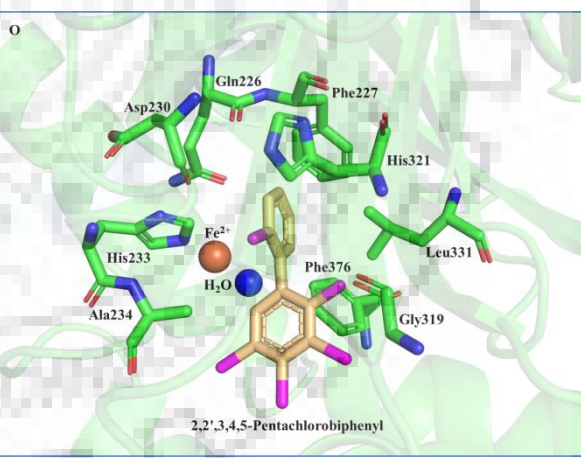
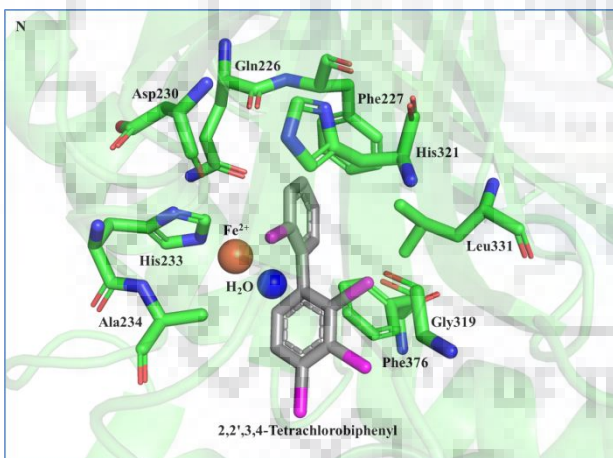
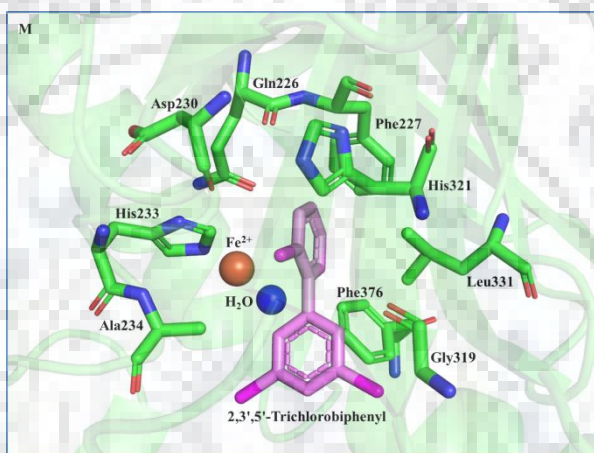
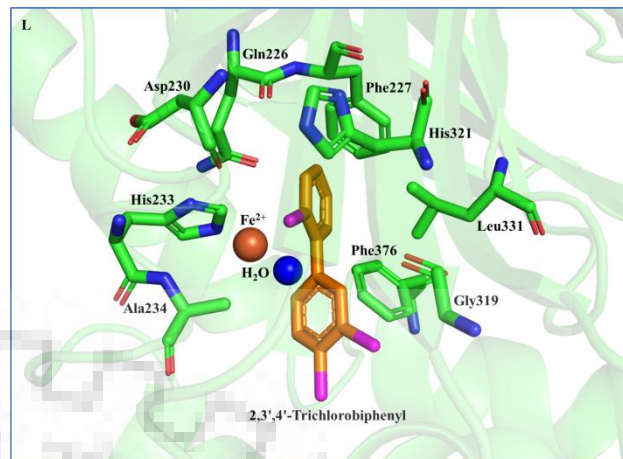
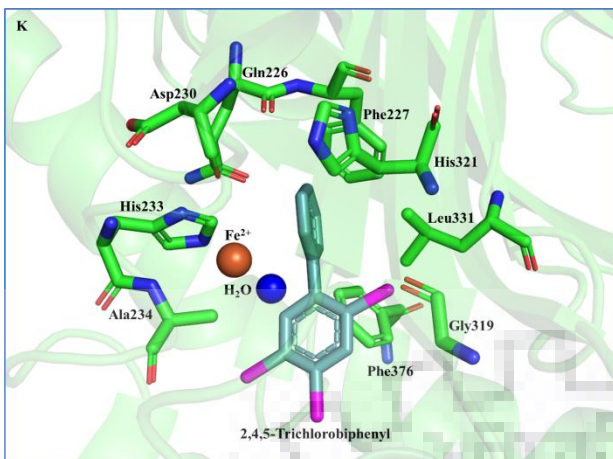




**Figure 6.4. Pictorial representation of binding of top 15 congeners along with biphenyl in the active site.** The ribbon diagram of BPDO binding active site cavity with selected PCB congeners and biphenyl. Residues of the BPDO are shown in stick form, active site Iron is shown as a sphere in metallic orange color and the water molecule is represented by a blue sphere. A) Biphenyl B) 2-Chlorobiphenyl C) 3-Chlorobiphenyl D) 2,3-Dichlorobiphenyl E) 2,5-Dichlorobiphenyl F) 3,4-Dichlorobiphenyl G) 2,2',3-Trichlorobiphenyl H) 2,2',4-Trichlorobiphenyl I) 2,3,4-Trichlorobiphenyl J) 2,4,4'-Trichlorobiphenyl K) 2,4,5-Trichlorobiphenyl L) 2,3',4'-Trichlorobiphenyl M) 2,3',5'-Trichlorobiphenyl N) 2,2',3,4-Tetrachlorobiphenyl O) 2,2',3,4,5-Pentachlorobiphenyl



**Table 6.3. The distance of mononuclear iron and active site water from proximate ligand ring carbon.** Important interactions of BPDO<sub>B356</sub> active site iron and water molecule with nearest carbon atoms of the ligand.

S.no	Ligand	Ligand	Distance (Å) of ligand from active site iron	Distance (Å) of ligand from active site water
1.	BP0	Biphenyl	C12-4.0 C17-4.0	C12-3.7 C17-3.1
2.	BP1	2-Chlorobiphenyl	C12-3.9 C17-3.9	C12-3.5 C17-2.9
3.	BP2	3-Chlorobiphenyl	C12-3.9 C17-3.9	C12-3.5 C17-2.9
4.	BP5	2,3-Dichlorobiphenyl	C12-3.8 C17-3.9	C12-3.5 C17-2.9
5.	BP9	2,5-Dichlorobiphenyl	C12-4.2 C17-4.1	C12-3.9 C17-3.2
6.	BP12	3,4-Dichlorobiphenyl	C12-4.0 C17-3.6	C12-3.7 C17-2.7
7.	BP16	2,2',3-Trichlorobiphenyl	C12-4.0 C17-3.7	C12-3.7 C17-2.8
8.	BP17	2,2',4-Trichlorobiphenyl	C12-4.1 C17-4.3	C12-3.9 C17-3.5
9.	BP21	2,3,4-Trichlorobiphenyl	C12-4.0 C17-4.0	C12-3.9 C17-3.3
10.	BP28	2,4,4'-Trichlorobiphenyl	C12-3.4 C17-3.5	C12-2.1 C17-2.6
11.	BP29		C12-4.1 C17-3.8	C12-4.0 C17-3.1

		2,4,5-Trichlorobiphenyl		
12.	BP33	2,3',4'-Trichlorobiphenyl	C12-3.9 C17-3.6	C12-3.5 C17-2.6
13.	BP34	2,3',5'-Trichlorobiphenyl	C12-3.9 C17-3.8	C12-3.5 C17-2.8
14.	BP41	2,2',3,4-Tetrachlorobiphenyl	C12-4.0 C17-3.6	C12-3.6 C17-2.7
15.	BP86	2,2',3,4,5-Pentachlorobiphenyl	C12-3.8 C17-3.9	C12-3.7 C17-3.1

### 6.3.2 Importance of pi-stacking interactions

It is to be noted that, the important interactions occurring between the protein aromatic amino acid residues have a significant influence on the overall protein structures [372]. Such non-covalent interactions, which are present in aromatic  $\pi$  systems are essential for biological events such as protein-ligand recognition [373]. It is to be noted that, on an individual note, these interactions provide a less stability to the overall protein-complex structure; on the other hand, jointly they contribute considerably to the conformational stability of the overall protein structure [374, 375]. In this study, we focused on the important aromatic amino acid residues present at the active site and their interactions with ligand compound. These pi-stacking interactions are illustrated in order to establish the extent to which their orientation and the number contribute to the stability of protein complex structures. In general, pi-stacking refers to attractive, non-covalent interactions present between aromatic rings, since these rings contain pi-bonds. These interactions are important in protein folding and molecular recognition during complex formation. In our study, the importance of these non-covalent interactions is highlighted.

For every 15 PCB congener-BPDO<sub>B356</sub> complexes, including biphenyl, different ring associated parameters were calculated and compared with the values obtained in the case of biphenyl BPDO<sub>B356</sub> complex as shown in **Table 6.4**. Ring offset is also calculated which refers to the alignment of a positive electrostatic potential on one ring with negative electrostatic potential on another ring forming a stack. In all the cases PCB congener-

BPDO<sub>B356</sub> complexes and biphenyl BPDO<sub>B356</sub> complex T type stack is formed. The geometry of these stacking interactions implies that electrostatics play a function in the attraction between these aromatic systems.

2,3',5'-trichlorobiphenyl was selected because it has 80% of its poses within the perfect orientation w.r.t. active site iron and a water molecule and it has analogous interactions like that of biphenyl with BPDO<sub>B356</sub>.

**Table 6.4. Aromatic interaction of top 15 PCBs, including biphenyl with BPDO<sub>B356</sub>.**

Important amino acids of BPDPB356 involved in aromatic interactions are shown. The angles between the ring planes and offset between the ring centers are mentioned.

S.no	Ligand	$\pi$ -Stacking				
		BPDO Residue	Distance between ring centers (Å)	Angle between ring planes	Offset between ring centers	Ligand residue involved
1.	BP0	PHE 227 HIS 233	4.67 4.89	62.28 87.19	0.30 1.08	3570, 3573, 3574, 3577, 3578, 3580
2.	BP1	PHE 227 HIS 233	4.71 4.94	61.16 85.16	0.39 1.37	3569, 3571, 3572, 3575, 3576, 3579
3.	BP2	PHE 227 HIS 233	4.63 4.88	64.61 89.22	0.31 1.11	3569, 3570, 3571, 3574, 3575, 3578
4.	BP5	HIS 233	4.95	84.17	1.35	3569, 3570, 3571, 3574, 3575, 3577
5.	BP9	PHE 227 HIS 233	4.79 4.88	66.54 88.28	0.40 1.04	3569, 3570, 3571, 3573, 3574, 3575
6.	BP12	PHE 227 HIS 233 PHE 376	4.66 4.80 5.49	74.28 78.76 86.82	0.26 0.94 1.87	3569, 3570, 3571, 3572, 3573, 3577 3574, 3575, 3576, 3578, 3579, 3580

<b>7.</b>	<b>BP16</b>	PHE 227 HIS 233 PHE 376	4.56 4.84 5.19	73.47 81.15 77.77	0.33 1.24 1.24	3570, 3571, 3573, 3575, 3576, 3578 3569, 3572, 3574, 3577, 3579, 3580
<b>8.</b>	<b>BP17</b>	PHE 227 HIS 233 PHE 376	4.55 4.83 5.38	75.02 78.46 75.42	0.42 1.24 1.58	3569, 3571, 3572, 3573, 3575, 3578 3570, 3574, 3576, 3577, 3579, 3580
<b>9.</b>	<b>BP21</b>	PHE 227 HIS 233 PHE 376	4.61 4.83 5.36	72.06 81.29 74.04	0.29 0.90 1.39	3569, 3570, 3571, 3573, 3574, 3576 3572, 3575, 3577, 3578, 3579, 3580
<b>10.</b>	<b>BP28</b>	HIS 233	4.90	85.06	1.66	3570, 3571, 3573, 3574, 3575, 3577
<b>11.</b>	<b>BP29</b>	PHE 227 HIS 233	4.68 4.86	69.10 84.72	0.34 0.83	3569, 3570, 3571, 3573, 3574, 3575
<b>12.</b>	<b>BP33</b>	PHE 227 HIS 233	4.56 4.81	75.73 77.75	0.38 1.25	3569, 3570, 3571, 3573, 3575, 3578
<b>13.</b>	<b>BP34</b>	PHE 227 HIS 233	4.63 4.90	71.43 83.55	0.54 1.34	3569, 3570, 3571, 3573, 3575, 3578
<b>14.</b>	<b>BP41</b>	PHE 227 HIS 233 PHE 376	4.52 4.83 5.35	74.81 79.38 75.83	0.37 1.31 1.51	3570, 3571, 3572, 3573, 3575, 3577 3569, 3574, 3576, 3578, 3579, 3580
<b>15.</b>	<b>BP86</b>	PHE 227 HIS 233	4.58 4.86	72.80 81.91	0.46 1.31	3569, 3570, 3571, 3572, 3574, 3577

### 6.3.3 Structure determination of 2,3',5'-trichlorobiphenyl-BPD0<sub>B356</sub> complex

Initial crystallization trials were carried out in the reservoir solution, with the composition as follows: 100 mM MES, pH 5.80; PEG 4000 (15–20% w/v); 3.5 mM ferrous ammonium sulfate; and 10-15% v/v 2-propanol and NaCl 12.5 mM. After optimizing the conditions final crystallization was carried out in anaerobic conditions (Purdue University) and the crystals grew within one to two weeks of time. The complex of BPD0<sub>B356</sub>-2,3',5'-trichlorobiphenyl complex was attained by the addition of small amounts of 2, 3', 5' trichlorobiphenyl powder to the crystals and further incubation for a period of 48 hours. The reddish-brown colored crystals have a rhombic morphology with space group R3. BPD0<sub>B356</sub> complex crystals complexed with PCB congener 2,3,5'-trichlorobiphenyl has diffracted up to 1.3 Å resolutions. The overall structure showed less variation. All the residues except first seventeen residues at the N-terminus could be efficiently built-in the electron-density map and none of the residues lies in the outlier region in the Ramachandran plot. The structural superposition of 2,3',5'-trichlorobiphenyl-BPD0<sub>B356</sub> complex with native BPD0<sub>B356</sub> (PDB ID: 3GZY) and biphenyl- BPD0<sub>B356</sub> complex (PDB ID: 3GZX) give r.m.s. deviation of 0.093 Å for 382 C $\alpha$  atoms and 0.121 Å for 407 C $\alpha$  atoms respectively. The observed structural differences between the proteins are located in the substrate binding loop region, as shown in **Figure 6.5**. Minor differences in the binding of 2,3',5'-trichlorobiphenyl congener and biphenyl to BPD0<sub>B356</sub>, are shown in **Table 6.5**. Crystallographic details of 2,3',5'-trichlorobiphenyl-BPD0<sub>B356</sub> complex, is shown in **Table 6.6**. A ligand moiety, 2,3',5'-trichlorobiphenyl was partially visible in the initial difference Fourier maps in subunit A, as shown in **Figure 6.5**. Partial occupancy of the ligand was verified by using Polder omit maps, an utility available in the Phenix. It generally removes bulk solvent effects and provides a better representation of the ligand into the active site of the protein.

Distance between (Å)	2,3',5'-trichlorobiphenyl-BPD0 <sub>B356</sub> complex (dist. in Å)	biphenyl-BPD0 <sub>B356</sub> complex (PDB ID: 3GZX) (dist. in Å)
His233(NE2)- Active site Fe <sup>2+</sup>	2.1	2.1
His239(NE2)- Active site Fe <sup>2+</sup>	2.1	2.1
Asp386(OD1)- Active site Fe <sup>2+</sup>	2.3	2.2
(OD2)- Active site Fe <sup>2+</sup>	2.3	2.5
C4 of 2,3',5' trichlorobiphenyl/biphenyl (3GZX)- Active site Fe <sup>2+</sup>	4.2	4.0
C5 of 2,3',5' trichlorobiphenyl/biphenyl (3GZX)- Active site Fe <sup>2+</sup>	3.8	4.0
C4 of 2,3',5' trichlorobiphenyl/biphenyl(3GZX) - Active site water	3.3	3.7
C5 of 2,3',5' trichlorobiphenyl/biphenyl(3GZX) - Active site water	2.4	3.1

**Table 6.5.** Differences in the binding of 2,3',5'-trichlorobiphenyl congener and biphenyl to BPD0<sub>B356</sub> are shown.

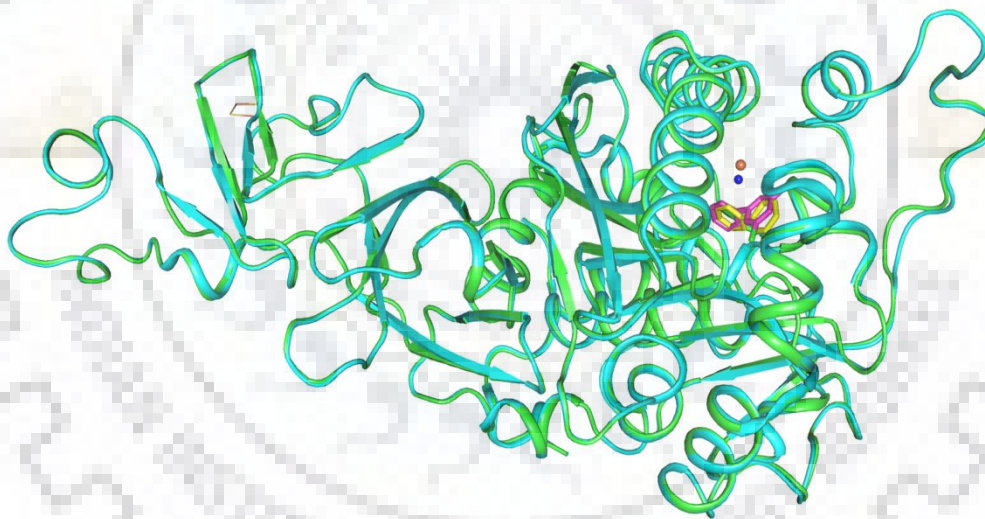


**Figure 6.5.** Structural superposition of the complex structure of 2,3',5'-trichlorobiphenyl-BPD0<sub>B356</sub> complex with biphenyl-BPD0<sub>B356</sub> complex (PDB ID: 3GZX). The ligand 2,3',5'-trichlorobiphenyl is shown in (green color) and biphenyl from 3GZX is shown in (cyan color). Active site iron is shown as a brown colored sphere and active site water is represented as a dark blue sphere.



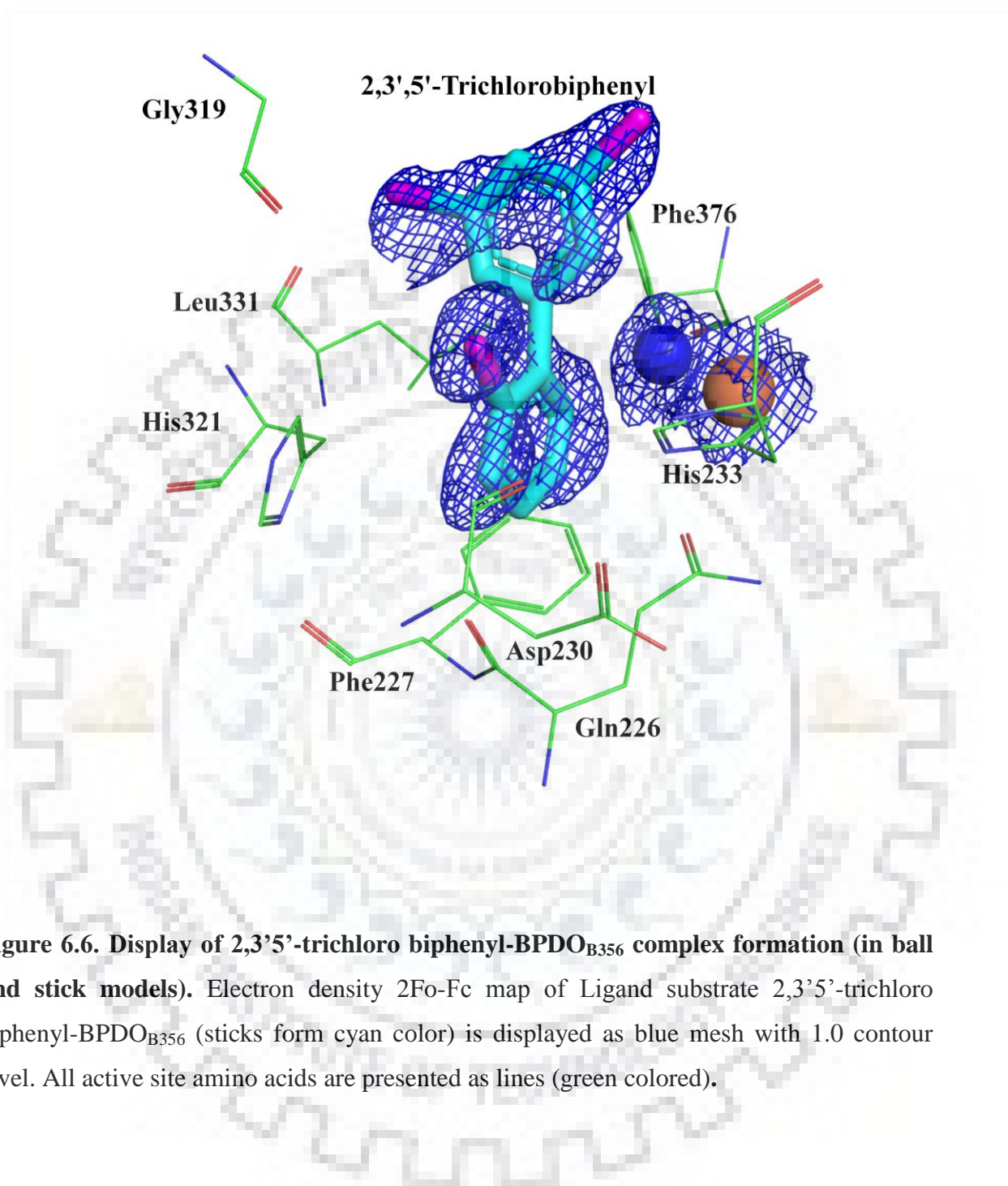


**Figure 6.6. Display of 2,3'5'-trichloro biphenyl-BPDO<sub>B356</sub> complex formation (in ball and stick models).** Electron density 2Fo-Fc map of Ligand substrate 2,3'5'-trichloro biphenyl-BPDO<sub>B356</sub> (sticks form cyan color) is displayed as blue mesh with 1.0 contour level. All active site amino acids are presented as lines (green colored).

Source	APS-CHICAGO
Resolution range (Å)	79.58-1.3
Space group	<i>R</i> 3
Cell dimensions <i>a, b, c</i> (Å), $\alpha, \beta, \gamma$ (°)	136.3, 136.3, 107.6, 90, 90, 120
Total no of Reflections	260419
Unique reflections	179483
Completeness (%)	99.6 (99.2)
Mean I/sigma(I)	17.0 (5.1)
Reflections used in refinement	170917
Reflections used for R-free	9035
R <sub>work</sub> (%)	12.8
R <sub>free</sub> (%)	16.1
RMSD (bonds)	0.017
RMSD (angles)	1.89
Number of non-hydrogen atoms	6044
Macromolecules	5163
Number of protein residues	626
Ramachandran favored (%)	96.5
Ramachandran Allowed (%)	3.5
Ramachandran outliers (%)	0
Wilson B factor	12.7
Average B-factor (Å <sup>2</sup> )	

Chain A	18.4
Chain B	15.9
Water atoms	34.4
All atoms	19.0

**Table 6.6. Crystallographic details of 2,3',5'trichlorobiphenyl-BPDO<sub>B356</sub> complex.**  
Details of the data are shown.

#### **6.4 Conclusion**

The binding ability of BPDO greatly affected the PCBs degradation abilities of BPDO. Hydrophobic interaction and pi-stacking interactions are important interactions between the active site residues site and PCB congeners as substrates. The exact number and site specificity of chlorine substituent, the orientation of ring planes, would influence and play an important role in the PCBs binding ability of BPDO<sub>B356</sub> significantly. The changes of physical, electronic and geometrical properties of the ligand molecule could influence the rate of degradation and binding affinity of PCBs as well. Different analysis pertaining to structural information, binding affinity and influences of molecular properties of ligands could be used for modification of BPDO<sub>B356</sub> to improve biodegradation capabilities of PCBs congeners and other halogenated aromatic compounds.



## 7. SUMMARY

Xenobiotic compounds such as phthalates and PCBs present in the environment have been degraded by a consortium of microbial populations. Various microorganisms have been reported which degrade these pollutants with good efficiency. Examples include different strains of aerobic degrading bacteria includes *Arthrobacter sp.*, *Pseudomonas sp.*, *Sphingomonas sp.*, *Burkholderia sp.*, *Acinetobacter sp.*, *Gordonia sp.*, *Rhodococcus sp.* etc. The genetic organization of the genes involved in degradation has been studied extensively in different model organism including *Burkholderia sp.*, *Acinetobacter sp.*, *Rhodococcus sp.* etc.

Different enzymes are involved in the phthalate degradation pathways, but the most important enzyme for phthalate degradation is Phthalate dioxygenase. This performs the hydroxylation of aromatic rings. These are categorised under Rieske dioxygenases (RDOs). This enzyme has two parts: phthalate dioxygenase reductase (PDR) a flavo iron sulphur protein with NADH-dependent oxidoreductase activity and phthalate dioxygenase oxygenase (PDO), a non heme iron protein with oxygenase activity. The 3D structure of PDR was characterized using X-ray crystallography. As the complete structural information of PDO is not there, further structural studies are needed to understand these important proteins. In our study, PDR an important protein in the PDO system has been characterized from *Ralstonia eutropha* CH34. Further, to investigate the important interaction occurring between *RcPDO* and *RcPDR*, protein-protein docking has been done, as protein-protein docking helps in the prediction of the structure of the protein complex. Molecular docking provides a means for fundamental structural studies of protein interactions during complex formation. Important interface residues from both the individual counterparts, i.e. *RcPDO* and *RcPDR* have been elucidated. The evolutionary relationship between important interface residues of *RcPDO* and *RcPDR* has also been established. This class of enzymes shows conserved structural features despite of having sequence variation. This proves that these enzymes are versatile catalysts and have been used in nature extensively for degradation of a variety of compounds.

*Pandoraea pnomenusa* B-356 is a biphenyl degrading bacterium was isolated from contaminated soil. It has been reported to efficiently degrade hazardous polychlorinated biphenyls (PCBs), polyhydroxylated biphenyls (PHBs) and various other compounds such

as benzophenone, diphenylmethane, dihydroxybiphenyl, etc. under aerobic conditions [344, 360, 370, 371]. However, it has been shown that in the case of high chlorine substitution or especially double para-substituted PCBs, the rate of degradation showed some degree of restriction. Biphenyl dioxygenase (BPDO) is an important enzyme in the biodegradation process of PCBs. It has been shown that the  $\alpha$ -subunit of iron-sulfur protein of biphenyl 2,3-dioxygenase (BphA1) is involved in catalytic activities and is also an important determinant of substrate-related specificity. To envisage the enhanced degradation abilities of BPDO from *Pandoraea pnomenusa* B-356 towards various PCBs congeners, a PCB congeners library was prepared, screened using PyRx, a virtual screening tool. Through docking studies conducted with 209 PCB congeners, the binding affinities of total 209 PCB congeners with BPDO from *Pandoraea pnomenusa* B-356 were measured and crucial active site residues interaction involved in interactions were identified. Furthermore, in order to determine and analyze the molecular properties of congener 2,3',5'-trichlorobiphenyl with BPDO, a tri-chloro substituted biphenyl is crystallized with the purified enzyme. The results showed that the average binding affinity of PCBs varies with a different number of chlorine substituents.

So we can conclude here that a better knowledge of these xenobiotic compounds occurrences and their degradation in the natural environment will help in the development of strategies to efficiently degrade these pollutants. The related degradation genes and catabolic enzymes in phthalate and PCB degrading bacteria should be further characterized to improve the efficiency of these xenobiotic removal.

## 8. Bibliography

- [1] A. Kowalczyk, T.J. Martin, O.R. Price, J.R. Snape, R.A. van Egmond, C.J. Finnegan, H. Schäfer, R.J. Davenport, G.D. Bending, Refinement of biodegradation tests methodologies and the proposed utility of new microbial ecology techniques, *Ecotoxicology and environmental safety*, 111 (2015) 9-22.
- [2] P.-G. Rieger, H.-M. Meier, M. Gerle, U. Vogt, T. Groth, H.-J. Knackmuss, Xenobiotics in the environment: present and future strategies to obviate the problem of biological persistence, *Journal of Biotechnology*, 94 (2002) 101-123.
- [3] S.D. Copley, Evolution of a metabolic pathway for degradation of a toxic xenobiotic: the patchwork approach, *Trends in biochemical sciences*, 25 (2000) 261-265.
- [4] D.B. Janssen, I.J. Dinkla, G.J. Poelarends, P. Terpstra, Bacterial degradation of xenobiotic compounds: evolution and distribution of novel enzyme activities, *Environmental Microbiology*, 7 (2005) 1868-1882.
- [5] M. Megharaj, B. Ramakrishnan, K. Venkateswarlu, N. Sethunathan, R. Naidu, Bioremediation approaches for organic pollutants: a critical perspective, *Environment international*, 37 (2011) 1362-1375.
- [6] I. Dubus, J. Hollis, C. Brown, Pesticides in rainfall in Europe, *Environmental pollution*, 110 (2000) 331-344.
- [7] X. Zhu, A.D. Venosa, M.T. Suidan, K. Lee, Guidelines for the bioremediation of marine shorelines and freshwater wetlands, US Environmental Protection Agency, (2001).
- [8] S.H. Safe, Polychlorinated biphenyls (PCBs): environmental impact, biochemical and toxic responses, and implications for risk assessment, *Critical reviews in toxicology*, 24 (1994) 87-149.
- [9] P. Kovacic, A. Kyriakis, Polymerization of benzene to p-polyphenyl, *Tetrahedron Letters*, 3 (1962) 467-469.
- [10] A. Nersasian, The Use of Toluene/Isooctane/Alcohol Blends to Simulate the Swelling Behavior of Rubbers in Gasoline/Alcohol Fuels, in: SAE Technical Paper, 1980.
- [11] H.-G. Franck, J.W. Stadelhofer, Production and uses of xylene derivatives, in: *Industrial Aromatic Chemistry*, Springer, 1988, pp. 265-290.
- [12] G. Collin, H. Höke, H. Greim, Naphthalene and hydronaphthalenes, *Ullmann's encyclopedia of industrial chemistry*, (2003).
- [13] J. Van Damme, F. Du Prez, Anthracene-containing polymers toward high-end applications, *Progress in Polymer Science*, (2018).
- [14] F. Jongeneelen, R. Anzion, C.-M. Leijdekkers, R. Bos, P.T. Henderson, 1-Hydroxypyrene in human urine after exposure to coal tar and a coal tar derived product, *International archives of occupational and environmental health*, 57 (1985) 47-55.
- [15] B.M. Lee, G.A. Shim, Dietary exposure estimation of benzo [a] pyrene and cancer risk assessment, *Journal of Toxicology and Environmental Health, Part A*, 70 (2007) 1391-1394.
- [16] P.M. Lorz, F.K. Towae, W. Enke, R. Jäckh, N. Bhargava, W. Hillesheim, Phthalic acid and derivatives, *Ullmann's encyclopedia of industrial chemistry*, (2007).
- [17] K.M. Shea, C.o.E. Health, Pediatric exposure and potential toxicity of phthalate plasticizers, *Pediatrics*, 111 (2003) 1467-1474.
- [18] P.K. Mandal, Dioxin: a review of its environmental effects and its aryl hydrocarbon receptor biology, *Journal of Comparative Physiology B*, 175 (2005) 221-230.



- [19] I. Denholm, G. Devine, M. Williamson, Insecticide resistance on the move, *Science*, 297 (2002) 2222-2223.
- [20] A. Glazer, H. Nikaido, *Biomass, Microbial biotechnology: fundamentals of applied microbiology*. New York: Freeman and Co, (1995) 662.
- [21] T.P. Curtis, W.T. Sloan, J.W. Scannell, Estimating prokaryotic diversity and its limits, *Proceedings of the National Academy of Sciences*, 99 (2002) 10494-10499.
- [22] B. Antizar-Ladislao, Bioremediation: working with bacteria, *Elements*, 6 (2010) 389-394.
- [23] M. Alexander, Aging, bioavailability, and overestimation of risk from environmental pollutants, *Environmental science & technology*, 34 (2000) 4259-4265.
- [24] P. Vasseur, M. Bonnard, F. Palais, I. Eom, J.-L. Morel, Bioavailability of chemical pollutants in contaminated soils and pitfalls of chemical analyses in hazard assessment, *Environmental toxicology*, 23 (2008) 652-656.
- [25] N. Singh, N. Sethunathan, M. Megharaj, R. Naidu, Bioavailability of sorbed pesticides to bacteria: an overview, *Developments in soil science*, 32 (2008) 73-82.
- [26] H. Harms, A. Zehnder, Bioavailability of sorbed 3-chlorodibenzofuran, *Applied and environmental microbiology*, 61 (1995) 27-33.
- [27] D.R. Shelton, M.A. Doherty, A model describing pesticide bioavailability and biodegradation in soil, *Soil Science Society of America Journal*, 61 (1997) 1078-1084.
- [28] W.-C. Tang, J. White, M. Alexander, Utilization of sorbed compounds by microorganisms specifically isolated for that purpose, *Applied microbiology and biotechnology*, 49 (1998) 117-121.
- [29] A. Büchert, O.A. Meyer, Scientific Opinion of the Panel on Plant Protection Products and their Residues on a request from EFSA on the usefulness of total concentrations and pore water concentrations of pesticides in soil as metrics for the assessment of ecotoxicological effects: Question No EFSA-Q-2008-429, (2009).
- [30] R. Ronday, V. Kammen-Polman, M. Annie, A. Dekker, N.W. Houx, M. Leistra, Persistence and toxicological effects of pesticides in topsoil: Use of the equilibrium partitioning theory, *Environmental toxicology and chemistry*, 16 (1997) 601-607.
- [31] R.J. Grosser, M. Friedrich, D.M. Ward, W.P. Inskeep, Effect of model sorptive phases on phenanthrene biodegradation: different enrichment conditions influence bioavailability and selection of phenanthrene-degrading isolates, *Applied and environmental microbiology*, 66 (2000) 2695-2702.
- [32] N. Chung, M. Alexander, Effect of soil properties on bioavailability and extractability of phenanthrene and atrazine sequestered in soil, *Chemosphere*, 48 (2002) 109-115.
- [33] S. Mas, A. de Juan, R. Tauler, A.C. Olivieri, G.M. Escandar, Application of chemometric methods to environmental analysis of organic pollutants: a review, *Talanta*, 80 (2010) 1052-1067.
- [34] S. Laha, B. Tansel, A. Ussawarujikulchai, Surfactant-soil interactions during surfactant-amended remediation of contaminated soils by hydrophobic organic compounds: a review, *Journal of Environmental Management*, 90 (2009) 95-100.
- [35] M. Rosen, *Surfactant and Interfacial phenomena*. New York, NY, John Willey and Sons, in, Inc, 1989.
- [36] M. Fu, M. Alexander, Use of surfactants and slurring to enhance the biodegradation in soil of compounds initially dissolved in nonaqueous-phase liquids, *Applied microbiology and biotechnology*, 43 (1995) 551-558.

- [37] M.-P. Otte, J. Gagnon, Y. Comeau, N. Matte, C.W. Greer, R. Smason, Activation of an indigenous microbial consortium for bioaugmentation of pentachlorophenol/creosote contaminated soils, *Applied microbiology and biotechnology*, 40 (1994) 926-932.
- [38] R.F. Lamberts, A.R. Johnsen, O. Andersen, J.H. Christensen, Univariate and multivariate characterization of heavy fuel oil weathering and biodegradation in soil, *Environmental pollution*, 156 (2008) 297-305.
- [39] M. Megharaj, R.-M. Wittich, R. Blasco, D. Pieper, K. Timmis, Superior survival and degradation of dibenzo-p-dioxin and dibenzofuran in soil by soil-adapted *Sphingomonas* sp. strain RW1, *Applied microbiology and biotechnology*, 48 (1997) 109-114.
- [40] W. Brunner, F.H. Sutherland, D.D. Focht, Enhanced Biodegradation of Polychlorinated Biphenyls in Soil by Analog Enrichment and Bacterial Inoculation 1, *Journal of Environmental Quality*, 14 (1985) 324-328.
- [41] E. Gilbert, D. Crowley, Repeated application of carvone-induced bacteria to enhance biodegradation of polychlorinated biphenyls in soil, *Applied microbiology and biotechnology*, 50 (1998) 489-494.
- [42] J. Bender, P. Phillips, Microbial mats for multiple applications in aquaculture and bioremediation, *Bioresource Technology*, 94 (2004) 229-238.
- [43] D. Wolicka, A. Suszek, A. Borkowski, A. Bielecka, Application of aerobic microorganisms in bioremediation in situ of soil contaminated by petroleum products, *Bioresource Technology*, 100 (2009) 3221-3227.
- [44] K.T. Semple, K.J. Doick, K.C. Jones, P. Burauel, A. Craven, H. Harms, Peer reviewed: defining bioavailability and bioaccessibility of contaminated soil and sediment is complicated, in, ACS Publications, 2004.
- [45] S. Duah-Yentumi, S. Kuwatsuka, Effect of organic matter and chemical fertilizers on the degradation of benthocarb and MCPA herbicides in the soil, *Soil Science and Plant Nutrition*, 26 (1980) 541-549.
- [46] A.S. Purnomo, T. Mori, I. Kamei, T. Nishii, R. Kondo, Application of mushroom waste medium from *Pleurotus ostreatus* for bioremediation of DDT-contaminated soil, *International Biodeterioration & Biodegradation*, 64 (2010) 397-402.
- [47] B. Antizar-Ladislao, J. Lopez-Real, A.J. Beck, In-vessel composting-bioremediation of aged coal tar soil: effect of temperature and soil/green waste amendment ratio, *Environment international*, 31 (2005) 173-178.
- [48] G.V. Chilingar, W.W. Loo, L.F. Khilyuk, S.A. Katz, Electrobioremediation of soils contaminated with hydrocarbons and metals: progress report, *Energy sources*, 19 (1997) 129-146.
- [49] T. Li, S. Guo, B. Wu, F. Li, Z. Niu, Effect of electric intensity on the microbial degradation of petroleum pollutants in soil, *Journal of Environmental Sciences*, 22 (2010) 1381-1386.
- [50] R.E. Saichek, K.R. Reddy, Electrokinetically enhanced remediation of hydrophobic organic compounds in soils: a review, *Critical reviews in environmental science and technology*, 35 (2005) 115-192.
- [51] L. Shi, S. Müller, H. Harms, L.Y. Wick, Effect of electrokinetic transport on the vulnerability of PAH-degrading bacteria in a model aquifer, *Environmental geochemistry and health*, 30 (2008) 177-182.
- [52] L.Y. Wick, P.A. Mattle, P. Wattiau, H. Harms, Electrokinetic transport of PAH-degrading bacteria in model aquifers and soil, *Environmental science & technology*, 38 (2004) 4596-4602.

- [53] J. Virkutyte, M. Sillanpää, P. Latostenmaa, Electrokinetic soil remediation—critical overview, *Science of the Total Environment*, 289 (2002) 97-121.
- [54] D. Sogorka, H. Gabert, B. Sogorka, Emerging technologies for soils contaminated with metals-electrokinetic remediation, *HAZARDOUS AND INDUSTRIAL WASTES*, 30 (1998) 673-685.
- [55] K.E. Gerhardt, X.-D. Huang, B.R. Glick, B.M. Greenberg, Phytoremediation and rhizoremediation of organic soil contaminants: potential and challenges, *Plant science*, 176 (2009) 20-30.
- [56] B. Ma, Y. He, H.-h. Chen, J.-m. Xu, Z. Rengel, Dissipation of polycyclic aromatic hydrocarbons (PAHs) in the rhizosphere: synthesis through meta-analysis, *Environmental Pollution*, 158 (2010) 855-861.
- [57] P.A. Holden, M.K. Firestone, Soil microorganisms in soil cleanup: How can we improve our understanding?, *Journal of Environmental Quality*, 26 (1997) 32-40.
- [58] B.-H. Kim, S.-C. Koh, J.-S.S. Ahn, E.-t. Oh, Plant terpene-induced expression of multiple aromatic ring hydroxylation oxygenase genes in *Rhodococcus* sp. strain T104, (2004).
- [59] I. Kuiper, L.V. Kravchenko, G.V. Bloemberg, B.J. Lugtenberg, *Pseudomonas putida* strain PCL1444, selected for efficient root colonization and naphthalene degradation, effectively utilizes root exudate components, *Molecular plant-microbe interactions*, 15 (2002) 734-741.
- [60] X.-D. Huang, Y. El-Alawi, J. Gurska, B.R. Glick, B.M. Greenberg, A multi-process phytoremediation system for decontamination of persistent total petroleum hydrocarbons (TPHs) from soils, *Microchemical Journal*, 81 (2005) 139-147.
- [61] J. Michels, T. Track, U. Gehrke, D. Sell, *Biologische Verfahren zur Bodensanierung*, Bonn: Grun-weise Reihe des BMBF, (2000).
- [62] C.-M. Kao, C.S. Chen, F.-Y. Tsa, K.-H. Yang, C.-C. Chien, S.-H. Liang, C.-a. Yang, S.C. Chen, Application of real-time PCR, DGGE fingerprinting, and culture-based method to evaluate the effectiveness of intrinsic bioremediation on the control of petroleum-hydrocarbon plume, *Journal of hazardous materials*, 178 (2010) 409-416.
- [63] A. Fischer, K. Theuerkorn, N. Stelzer, M. Gehre, M. Thullner, H.H. Richnow, Applicability of stable isotope fractionation analysis for the characterization of benzene biodegradation in a BTEX-contaminated aquifer, *Environmental science & technology*, 41 (2007) 3689-3696.
- [64] D. Hunkeler, R. Aravena, K. Berry-Spark, E. Cox, Assessment of degradation pathways in an aquifer with mixed chlorinated hydrocarbon contamination using stable isotope analysis, *Environmental science & technology*, 39 (2005) 5975-5981.
- [65] R.U. Meckenstock, B. Morasch, C. Griebler, H.H. Richnow, Stable isotope fractionation analysis as a tool to monitor biodegradation in contaminated aquifers, *Journal of Contaminant Hydrology*, 75 (2004) 215-255.
- [66] M. Megharaj, I. Singleton, N. McClure, R. Naidu, Influence of petroleum hydrocarbon contamination on microalgae and microbial activities in a long-term contaminated soil, *Archives of Environmental Contamination and Toxicology*, 38 (2000) 439-445.
- [67] S. Chelinho, M. Moreira-Santos, D. Lima, C. Silva, P. Viana, S. André, I. Lopes, R. Ribeiro, A.M. Fialho, C.A. Viegas, Cleanup of atrazine-contaminated soils: ecotoxicological study on the efficacy of a bioremediation tool with *Pseudomonas* sp. ADP, *Journal of soils and sediments*, 10 (2010) 568-578.
- [68] S. Park, B.-N. Kim, S.-C. Cho, Y. Kim, J.-W. Kim, J.-Y. Lee, S.-B. Hong, M.-S. Shin, H.J. Yoo, H. Im, Association between urine phthalate levels and poor attentional performance in

children with attention-deficit hyperactivity disorder with evidence of dopamine gene-phthalate interaction, *International journal of environmental research and public health*, 11 (2014) 6743-6756.

[69] I. Katsikantami, S. Sifakis, M.N. Tzatzarakis, E. Vakonaki, O.-I. Kalantzi, A.M. Tsatsakis, A.K. Rizos, A global assessment of phthalates burden and related links to health effects, *Environment international*, 97 (2016) 212-236.

[70] X.L. Cao, Phthalate esters in foods: sources, occurrence, and analytical methods, *Comprehensive reviews in food science and food safety*, 9 (2010) 21-43.

[71] F. Carlstedt, B. Jönsson, C.G. Bornehag, PVC flooring is related to human uptake of phthalates in infants, *Indoor air*, 23 (2013) 32-39.

[72] K. Chou, R.O. Wright, Phthalates in food and medical devices, *Journal of Medical Toxicology*, 2 (2006) 126-135.

[73] H. Frederiksen, J.K.S. Nielsen, T.A. Mørck, P.W. Hansen, J.F. Jensen, O. Nielsen, A.-M. Andersson, L.E. Knudsen, Urinary excretion of phthalate metabolites, phenols and parabens in rural and urban Danish mother-child pairs, *International journal of hygiene and environmental health*, 216 (2013) 772-783.

[74] R. Green, R. Hauser, A.M. Calafat, J. Weuve, T. Schettler, S. Ringer, K. Huttner, H. Hu, Use of di (2-ethylhexyl) phthalate-containing medical products and urinary levels of mono (2-ethylhexyl) phthalate in neonatal intensive care unit infants, *Environmental health perspectives*, 113 (2005) 1222.

[75] H.J. Koo, B.M. Lee, Estimated exposure to phthalates in cosmetics and risk assessment, *Journal of Toxicology and Environmental Health, Part A*, 67 (2004) 1901-1914.

[76] J. Bošnjir, D. Puntarić, A. Galić, I. Škes, T. Dijanić, M. Klarić, M. Grgić, M. Čurković, Z. Šmit, Migration of Phthalates from Plastic Containers into Soft Drinks and Mineral Water, *Food Technology & Biotechnology*, 45 (2007).

[77] S. Keresztes, E. Tatár, Z. Czégény, G. Záray, V.G. Mihucz, Study on the leaching of phthalates from polyethylene terephthalate bottles into mineral water, *Science of the total environment*, 458 (2013) 451-458.

[78] A.C. Dirtu, T. Geens, E. Dirinck, G. Malarvannan, H. Neels, L. Van Gaal, P.G. Jorens, A. Covaci, Phthalate metabolites in obese individuals undergoing weight loss: urinary levels and estimation of the phthalates daily intake, *Environment international*, 59 (2013) 344-353.

[79] H.M. Koch, M. Lorber, K.L. Christensen, C. Pälme, S. Koslitz, T. Brüning, Identifying sources of phthalate exposure with human biomonitoring: results of a 48 h fasting study with urine collection and personal activity patterns, *International journal of hygiene and environmental health*, 216 (2013) 672-681.

[80] H.-X. Sui, L. Zhang, P.-G. Wu, Y. Song, L. Yong, D.-J. Yang, D.-G. Jiang, Z.-P. Liu, Concentration of di (2-ethylhexyl) phthalate (DEHP) in foods and its dietary exposure in China, *International journal of hygiene and environmental health*, 217 (2014) 695-701.

[81] M. Gong, C.J. Weschler, Y. Zhang, Impact of clothing on dermal exposure to phthalates: observations and insights from sampling both skin and clothing, *Environmental science & technology*, 50 (2016) 4350-4357.

[82] J.A. Hoppin, R. Jaramillo, S.J. London, R.J. Bertelsen, P.M. Salo, D.P. Sandler, D.C. Zeldin, Phthalate exposure and allergy in the US population: results from NHANES 2005-2006, *Environmental health perspectives*, 121 (2013) 1129.



- [83] U. Heudorf, V. Mersch-Sundermann, J. Angerer, Phthalates: toxicology and exposure, *International journal of hygiene and environmental health*, 210 (2007) 623-634.
- [84] N. Singh, V. Dalal, P. Kumar, Structure based mimicking of Phthalic acid esters (PAEs) and inhibition of hACMSD, an important enzyme of the tryptophan kynurenine metabolism pathway, *International journal of biological macromolecules*, 108 (2018) 214-224.
- [85] D.-W. Gao, Z.-D. Wen, Phthalate esters in the environment: A critical review of their occurrence, biodegradation, and removal during wastewater treatment processes, *Science of the Total Environment*, 541 (2016) 986-1001.
- [86] S. Net, R. Sempéré, A. Delmont, A. Paluselli, B. Ouddane, Occurrence, fate, behavior and ecotoxicological state of phthalates in different environmental matrices, *Environmental science & technology*, 49 (2015) 4019-4035.
- [87] P. Zeng, B.Y.-P. Moy, Y.-H. Song, J.-H. Tay, Biodegradation of dimethyl phthalate by *Sphingomonas* sp. isolated from phthalic-acid-degrading aerobic granules, *Applied microbiology and biotechnology*, 80 (2008) 899-905.
- [88] R. Planelló, O. Herrero, J.L. Martínez-Guitarte, G. Morcillo, Comparative effects of butyl benzyl phthalate (BBP) and di (2-ethylhexyl) phthalate (DEHP) on the aquatic larvae of *Chironomus riparius* based on gene expression assays related to the endocrine system, the stress response and ribosomes, *Aquatic toxicology*, 105 (2011) 62-70.
- [89] B.-L. Yuan, X.-Z. Li, N. Graham, Aqueous oxidation of dimethyl phthalate in a Fe (VI)-TiO<sub>2</sub>-UV reaction system, *Water Research*, 42 (2008) 1413-1420.
- [90] Y. Zhang, L. Lin, Y. Cao, B. Chen, L. Zheng, R.-S. Ge, Phthalate levels and low birth weight: a nested case-control study of Chinese newborns, *The Journal of pediatrics*, 155 (2009) 500-504.
- [91] C. Philippat, M. Mortamais, C. Chevrier, C. Petit, A.M. Calafat, X. Ye, M.J. Silva, C. Brambilla, I. Pin, M.-A. Charles, Exposure to phthalates and phenols during pregnancy and offspring size at birth, *Environmental health perspectives*, 120 (2012) 464.
- [92] D. Valvi, M. Casas, D. Romaguera, N. Monfort, R. Ventura, D. Martinez, J. Sunyer, M. Vrijheid, Prenatal phthalate exposure and childhood growth and blood pressure: evidence from the Spanish INMA-Sabadell birth cohort study, *Environmental health perspectives*, 123 (2015) 1022.
- [93] S.H. Swan, K.M. Main, F. Liu, S.L. Stewart, R.L. Kruse, A.M. Calafat, C.S. Mao, J.B. Redmon, C.L. Ternand, S. Sullivan, Decrease in anogenital distance among male infants with prenatal phthalate exposure, *Environmental health perspectives*, 113 (2005) 1056.
- [94] P.-C. Huang, P.-L. Kuo, Y.-Y. Chou, S.-J. Lin, C.-C. Lee, Association between prenatal exposure to phthalates and the health of newborns, *Environment International*, 35 (2009) 14-20.
- [95] T.E. Arbuckle, K. Davis, K. Boylan, M. Fisher, J. Fu, Bisphenol A, phthalates and lead and learning and behavioral problems in Canadian children 6–11 years of age: CHMS 2007–2009, *Neurotoxicology*, 54 (2016) 89-98.
- [96] Y.-J. Lien, H.-Y. Ku, P.-H. Su, S.-J. Chen, H.-Y. Chen, P.-C. Liao, W.-J. Chen, S.-L. Wang, Prenatal exposure to phthalate esters and behavioral syndromes in children at 8 years of age: Taiwan Maternal and Infant Cohort Study, *Environmental health perspectives*, 123 (2015) 95.
- [97] P. Factor-Litvak, B. Insel, A.M. Calafat, X. Liu, F. Perera, V.A. Rauh, R.M. Whyatt, Persistent associations between maternal prenatal exposure to phthalates on child IQ at age 7 years, *PloS one*, 9 (2014) e114003.

- [98] R.W. Kobrosly, S. Evans, A. Miodovnik, E.S. Barrett, S.W. Thurston, A.M. Calafat, S.H. Swan, Prenatal phthalate exposures and neurobehavioral development scores in boys and girls at 6–10 years of age, *Environmental health perspectives*, 122 (2014) 521.
- [99] L. Trasande, T.M. Attina, Association of Exposure to Di-2-Ethylhexylphthalate Replacements With Increased Blood Pressure in Children and Adolescents Novelty and Significance, *Hypertension*, 66 (2015) 301-308.
- [100] L. Trasande, S. Sathyanarayana, A.J. Spanier, H. Trachtman, T.M. Attina, E.M. Urbina, Urinary phthalates are associated with higher blood pressure in childhood, *The Journal of pediatrics*, 163 (2013) 747-753. e741.
- [101] Y.-X. Wang, Q. Zeng, Y. Sun, P. Yang, P. Wang, J. Li, Z. Huang, L. You, Y.-H. Huang, C. Wang, Semen phthalate metabolites, semen quality parameters and serum reproductive hormones: A cross-sectional study in China, *Environmental Pollution*, 211 (2016) 173-182.
- [102] Y.-X. Wang, L. You, Q. Zeng, Y. Sun, Y.-H. Huang, C. Wang, P. Wang, W.-C. Cao, P. Yang, Y.-F. Li, Phthalate exposure and human semen quality: Results from an infertility clinic in China, *Environmental research*, 142 (2015) 1-9.
- [103] J. Jurewicz, M. Radwan, W. Sobala, D. Ligocka, P. Radwan, M. Bochenek, W. Hawuła, L. Jakubowski, W. Hanke, Human urinary phthalate metabolites level and main semen parameters, sperm chromatin structure, sperm aneuploidy and reproductive hormones, *Reproductive toxicology*, 42 (2013) 232-241.
- [104] J. Axelsson, L. Rylander, A. Rignell-Hydbom, B.A. Jönsson, C.H. Lindh, A. Giwercman, Phthalate exposure and reproductive parameters in young men from the general Swedish population, *Environment international*, 85 (2015) 54-60.
- [105] S. Sathyanarayana, E. Barrett, S. Butts, C. Wang, S.H. Swan, Phthalate exposure and reproductive hormone concentrations in pregnancy, *Reproduction*, 147 (2014) 401-409.
- [106] K. Upson, S. Sathyanarayana, A.J. De Roos, M.L. Thompson, D. Scholes, R. Dills, V.L. Holt, Phthalates and risk of endometriosis, *Environmental research*, 126 (2013) 91-97.
- [107] J. Weuve, R. Hauser, A.M. Calafat, S.A. Missmer, L.A. Wise, Association of exposure to phthalates with endometriosis and uterine leiomyomata: findings from NHANES, 1999–2004, *Environmental health perspectives*, 118 (2010) 825.
- [108] N. Wolfe, W. Steen, L. Burns, Phthalate ester hydrolysis: linear free energy relationships, *Chemosphere*, 9 (1980) 403-408.
- [109] Q. Wu, H. Liu, L.-S. Ye, P. Li, Y.-H. Wang, Biodegradation of Di-n-butyl phthalate esters by *Bacillus* sp. SASHJ under simulated shallow aquifer condition, *International Biodeterioration & Biodegradation*, 76 (2013) 102-107.
- [110] Z.-D. Wen, D.-W. Gao, W.-M. Wu, Biodegradation and kinetic analysis of phthalates by an *Arthrobacter* strain isolated from constructed wetland soil, *Applied microbiology and biotechnology*, 98 (2014) 4683-4690.
- [111] D.-C. Jin, R.-X. Liang, Q.-Y. Dai, R.-Y. Zhang, X.-L. Wu, W.-L. Chao, Biodegradation of di-n-butyl phthalate by *Rhodococcus* sp. JDC-11 and molecular detection of 3, 4-phthalate dioxygenase gene, *J. Microbiol. Biotechnol.*, 20 (2010) 1440-1445.
- [112] C.-R. Fang, J. Yao, Y.-G. Zheng, C.-J. Jiang, L.-F. Hu, Y.-Y. Wu, D.-S. Shen, Dibutyl phthalate degradation by *Enterobacter* sp. T5 isolated from municipal solid waste in landfill bioreactor, *International Biodeterioration & Biodegradation*, 64 (2010) 442-446.

- [113] X. Yang, C. Zhang, Z. He, X. Hu, J. Guo, Q. Zhong, J. Wang, L. Xiong, D. Liu, Isolation and characterization of two n-butyl benzyl phthalate degrading bacteria, *International Biodeterioration & Biodegradation*, 76 (2013) 8-11.
- [114] D. Jin, Z. Bai, D. Chang, D. Hoefel, B. Jin, P. Wang, D. Wei, G. Zhuang, Biodegradation of di-n-butyl phthalate by an isolated *Gordonia* sp. strain QH-11: genetic identification and degradation kinetics, *Journal of hazardous materials*, 221 (2012) 80-85.
- [115] N. Singh, V. Dalal, J.K. Mahto, P. Kumar, Biodegradation of phthalic acid esters (PAEs) and in silico structural characterization of mono-2-ethylhexyl phthalate (MEHP) hydrolase on the basis of close structural homolog, *Journal of hazardous materials*, 338 (2017) 11-22.
- [116] D.-W. Liang, T. Zhang, H.H. Fang, J. He, Phthalates biodegradation in the environment, *Applied microbiology and Biotechnology*, 80 (2008) 183.
- [117] C.A. Staples, D.R. Peterson, T.F. Parkerton, W.J. Adams, The environmental fate of phthalate esters: a literature review, *Chemosphere*, 35 (1997) 667-749.
- [118] T. Nozawa, Y. Maruyama, Anaerobic metabolism of phthalate and other aromatic compounds by a denitrifying bacterium, *Journal of bacteriology*, 170 (1988) 5778-5784.
- [119] C. Vamsee-Krishna, P.S. Phale, Bacterial degradation of phthalate isomers and their esters, *Indian journal of microbiology*, 48 (2008) 19.
- [120] R. Kleerebezem, L.W.H. Pol, G. Lettinga, Anaerobic biodegradability of phthalic acid isomers and related compounds, *Biodegradation*, 10 (1999) 63-73.
- [121] P. Keyser, B.G. Pujar, R.W. Eaton, D.W. Ribbons, Biodegradation of the phthalates and their esters by bacteria, *Environmental health perspectives*, 18 (1976) 159.
- [122] K. Maruyama, K. Akita, C. Naitou, M. Yoshida, T. Kitamura, Purification and characterization of an esterase hydrolyzing monoalkyl phthalates from *Micrococcus* sp. YGJ1, *Journal of biochemistry*, 137 (2005) 27-32.
- [123] J.H. Niazi, D.T. Prasad, T. Karegoudar, Initial degradation of dimethylphthalate by esterases from *Bacillus* species, *FEMS Microbiology Letters*, 196 (2001) 201-205.
- [124] T. Nishioka, M. Iwata, T. Imaoka, M. Mutoh, Y. Egashira, T. Nishiyama, T. Shin, T. Fujii, A mono-2-ethylhexyl phthalate hydrolase from a *Gordonia* sp. that is able to dissimilate di-2-ethylhexyl phthalate, *Applied and environmental microbiology*, 72 (2006) 2394-2399.
- [125] R.W. Eaton, Plasmid-encoded phthalate catabolic pathway in *Arthrobacter keyseri* 12B, *Journal of Bacteriology*, 183 (2001) 3689-3703.
- [126] H.-K. Chang, G.J. Zylstra, Characterization of the phthalate permease OphD from *Burkholderia cepacia* ATCC 17616, *Journal of bacteriology*, 181 (1999) 6197-6199.
- [127] C.J. Batie, E. LaHaie, D. Ballou, Purification and characterization of phthalate oxygenase and phthalate oxygenase reductase from *Pseudomonas cepacia*, *Journal of Biological Chemistry*, 262 (1987) 1510-1518.
- [128] C.C. Correll, C.J. Batie, D.P. Ballou, M.L. Ludwig, Phthalate dioxygenase reductase: a modular structure for electron transfer from pyridine nucleotides to [2Fe-2S], *Science*, 258 (1992) 1604-1610.
- [129] G.T. Gassner, D.P. Ballou, Preparation and characterization of a truncated form of phthalate dioxygenase reductase that lacks an iron-sulfur domain, *Biochemistry*, 34 (1995) 13460-13471.
- [130] H. Fujisawa, O. Hayaishi, Protocatechuate 3, 4-dioxygenase I. Crystallization and characterization, *Journal of Biological chemistry*, 243 (1968) 2673-2681.



- [131] A.M. Orville, N. Elango, J.D. Lipscomb, D.H. Ohlendorf, Structures of competitive inhibitor complexes of protocatechuate 3, 4-dioxygenase: multiple exogenous ligand binding orientations within the active site, *Biochemistry*, 36 (1997) 10039-10051.
- [132] K. Sugimoto, T. Senda, H. Aoshima, E. Masai, M. Fukuda, Y. Mitsui, Crystal structure of an aromatic ring opening dioxygenase LigAB, a protocatechuate 4, 5-dioxygenase, under aerobic conditions, *Structure*, 7 (1999) 953-965.
- [133] O.M. Faroon, L. Samuel Keith, C. Smith-Simon, C.T. De Rosa, W.H. Organization, Polychlorinated biphenyls: human health aspects, (2003).
- [134] A. Beyer, M. Biziuk, Environmental fate and global distribution of polychlorinated biphenyls, in: *Reviews of Environmental Contamination and Toxicology Vol 201*, Springer, 2009, pp. 137-158.
- [135] J. Sullivan, Krieger G. Hazardous materials toxicology, in, Baltimore, MD: Williams & Wilkins, 1992.
- [136] B. Ulbrich, R. Stahlmann, Developmental toxicity of polychlorinated biphenyls (PCBs): a systematic review of experimental data, *Archives of toxicology*, 78 (2004) 252-268.
- [137] U.G. Ahlborg, A. Hanberg, K. Kenne, Risk assessment of polychlorinated biphenyls (PCBs), Nordic Council of Ministers, 1992.
- [138] A. Wise, F. Parham, D.A. Axelrad, K.Z. Guyton, C. Portier, L. Zeise, R.T. Zoeller, T.J. Woodruff, Upstream adverse effects in risk assessment: A model of polychlorinated biphenyls, thyroid hormone disruption and neurological outcomes in humans, *Environmental research*, 117 (2012) 90-99.
- [139] M.M. Leijts, G.W. ten Tusscher, K. Olie, T. van Teunenbroek, W.M. van Aalderen, P. de Voogt, T. Vulmsa, A. Bartonova, M.K. von Krauss, C. Mosoiu, Thyroid hormone metabolism and environmental chemical exposure, *Environmental Health*, 11 (2012) S10.
- [140] J.L. Tang-Péronard, H.R. Andersen, T.K. Jensen, B.L. Heitmann, Endocrine-disrupting chemicals and obesity development in humans: A review, *Obesity reviews*, 12 (2011) 622-636.
- [141] A. Brouwer, M.P. Longnecker, L.S. Birnbaum, J. Coglian, P. Kostyniak, J. Moore, S. Schantz, G. Winneke, Characterization of potential endocrine-related health effects at low-dose levels of exposure to PCBs, *Environmental health perspectives*, 107 (1999) 639.
- [142] M.S. McLachlan, Digestive tract absorption of polychlorinated dibenzo-p-dioxins, dibenzofurans, and biphenyls in a nursing infant, *Toxicology and applied pharmacology*, 123 (1993) 68-72.
- [143] B.R. Sonawane, Chemical contaminants in human milk: an overview, *Environmental health perspectives*, 103 (1995) 197.
- [144] W.J. Rogan, B.C. Gladen, J.D. McKinney, N. Carreras, P. Hardy, J. Thullen, J. Tinglestad, M. Tully, Neonatal effects of transplacental exposure to PCBs and DDE, *The Journal of pediatrics*, 109 (1986) 335-341.
- [145] R. Wester, D. Bucks, H. Maibach, J. Anderson, Polychlorinated biphenyls (PCBs): dermal absorption, systemic elimination, and dermal wash efficiency, *Journal of Toxicology and Environmental Health, Part A Current Issues*, 12 (1983) 511-519.
- [146] S.L. Schantz, J.J. Widholm, D.C. Rice, Effects of PCB exposure on neuropsychological function in children, *Environmental health perspectives*, 111 (2003) 357.

- [147] Y. Hirota, S. Tokunaga, K. Kataoka, S. Shinohara, Symptoms and blood PCB level among chronic Yusho patients, twenty-five years after outbreak, *Fukuoka igaku zasshi= Hukuoka acta medica*, 88 (1997) 220-225.
- [148] K. Furukawa, H. Fujihara, Microbial degradation of polychlorinated biphenyls: biochemical and molecular features, *Journal of bioscience and bioengineering*, 105 (2008) 433-449.
- [149] P. Morris, W. Mohn, J.d. Quensen, J. Tiedje, S. Boyd, Establishment of polychlorinated biphenyl-degrading enrichment culture with predominantly meta dechlorination, *Applied and environmental microbiology*, 58 (1992) 3088-3094.
- [150] D.H. Pieper, Aerobic degradation of polychlorinated biphenyls, *Applied microbiology and biotechnology*, 67 (2005) 170-191.
- [151] A.W. Boyle, C.J. Silvin, J.P. Hassett, J.P. Nakas, S. Tanenbaum, Bacterial PCB biodegradation, *Biodegradation*, 3 (1992) 285-298.
- [152] K.N. Timmis, T. McGenity, J.R. Van Der Meer, V. de Lorenzo, *Handbook of hydrocarbon and lipid microbiology*, Springer Berlin, 2010.
- [153] J.F. Quensen, S.A. Boyd, J.M. Tiedje, Dechlorination of four commercial polychlorinated biphenyl mixtures (Aroclors) by anaerobic microorganisms from sediments, *Applied and Environmental Microbiology*, 56 (1990) 2360-2369.
- [154] J.F. Brown, D.L. Bedard, M.J. Brennan, J.C. Carnahan, H. Feng, R.E. Wagner, Polychlorinated biphenyl dechlorination in aquatic sediments, *Science*, 236 (1987) 709-712.
- [155] C. Holliger, G. Wohlfarth, G. Diekert, Reductive dechlorination in the energy metabolism of anaerobic bacteria, *FEMS Microbiology Reviews*, 22 (1998) 383-398.
- [156] W.W. Mohn, J.M. Tiedje, Microbial reductive dehalogenation, *Microbiological reviews*, 56 (1992) 482-507.
- [157] L. Nies, T.M. Vogel, Effects of organic substrates on dechlorination of Aroclor 1242 in anaerobic sediments, *Applied and environmental microbiology*, 56 (1990) 2612-2617.
- [158] J. Wiegel, Q. Wu, Microbial reductive dehalogenation of polychlorinated biphenyls, *FEMS microbiology ecology*, 32 (2000) 1-15.
- [159] J. Moore, Reassessment of liver findings in PCB studies for rats, Washington: Institute for Evaluating Health Risks, (1991).
- [160] K. Furukawa, F. Matsumura, Microbial metabolism of polychlorinated biphenyls. Relative degradability of polychlorinated biphenyl components by *Alkaligenes* species, *Journal of agricultural and food chemistry*, 24 (1976) 251-256.
- [161] J. Borja, D.M. Taleon, J. Auresenia, S. Gallardo, Polychlorinated biphenyls and their biodegradation, *Process biochemistry*, 40 (2005) 1999-2013.
- [162] K. Furukawa, K. Tonomura, A. Kamibayashi, Effect of chlorine substitution on the biodegradability of polychlorinated biphenyls, *Applied and Environmental Microbiology*, 35 (1978) 223-227.
- [163] D.L. Bedard, M.L. Haberl, Influence of chlorine substitution pattern on the degradation of polychlorinated biphenyls by eight bacterial strains, *Microbial ecology*, 20 (1990) 87-102.
- [164] D. Bedard, M. Brennan, R. Unterman, Bacterial degradation of PCBs: evidence of distinct pathways in *Corynebacterium* sp. MB1 and *Alcaligenes eutrophus* H850, in: *Proceedings: 1983 PCB Seminar*. Electrical Power Research Inst., Palo Alto, Calif. p, 1984, pp. 4-101.

- [165] D.L. Bedard, R. Unterman, L.H. Bopp, M.J. Brennan, M.L. Haberl, C. Johnson, Rapid assay for screening and characterizing microorganisms for the ability to degrade polychlorinated biphenyls, *Applied and Environmental Microbiology*, 51 (1986) 761-768.
- [166] S. Allender, M. Rayner, The burden of overweight and obesity-related ill health in the UK, *Obesity reviews*, 8 (2007) 467-473.
- [167] P. Hossain, B. Kavar, M. El Nahas, Obesity and diabetes in the developing world—a growing challenge, *N Engl j med*, 2007 (2007) 213-215.
- [168] K.M. McTigue, Y.F. Chang, C. Eaton, L. Garcia, K.C. Johnson, C.E. Lewis, S. Liu, R.H. Mackey, J. Robinson, M.C. Rosal, Severe obesity, heart disease, and death among white, African American, and Hispanic postmenopausal women, *Obesity*, 22 (2014) 801-810.
- [169] P.F. Baillie-Hamilton, Chemical toxins: a hypothesis to explain the global obesity epidemic, *The Journal of Alternative & Complementary Medicine*, 8 (2002) 185-192.
- [170] K.M. Flegal, M.D. Carroll, R.J. Kuczmarski, C.L. Johnson, Overweight and obesity in the United States: prevalence and trends, 1960–1994, *International journal of obesity*, 22 (1998) 39.
- [171] C.H. Hurst, D.J. Waxman, Activation of PPAR $\alpha$  and PPAR $\gamma$  by environmental phthalate monoesters, *Toxicological Sciences*, 74 (2003) 297-308.
- [172] T. Kanayama, N. Kobayashi, S. Mamiya, T. Nakanishi, J.-i. Nishikawa, Organotin compounds promote adipocyte differentiation as agonists of the peroxisome proliferator-activated receptor  $\gamma$ /retinoid X receptor pathway, *Molecular pharmacology*, 67 (2005) 766-774.
- [173] H.-K. Kim, C. Nelson-Dooley, M.A. Della-Fera, J.-Y. Yang, W. Zhang, J. Duan, D.L. Hartzell, M.W. Hamrick, C.A. Baile, Genistein decreases food intake, body weight, and fat pad weight and causes adipose tissue apoptosis in ovariectomized female mice, *The Journal of nutrition*, 136 (2006) 409-414.
- [174] T. Takeuchi, O. Tsutsumi, Y. Ikezaki, Y. TAKAI, Y. TAKETANI, Positive relationship between androgen and the endocrine disruptor, bisphenol A, in normal women and women with ovarian dysfunction, *Endocrine journal*, 51 (2004) 165-169.
- [175] F.S. Vom Saal, B.T. Akingbemi, S.M. Belcher, L.S. Birnbaum, D.A. Crain, M. Eriksen, F. Farabollini, L.J. Guillette Jr, R. Hauser, J.J. Heindel, Chapel Hill bisphenol A expert panel consensus statement: integration of mechanisms, effects in animals and potential to impact human health at current levels of exposure, *Reproductive toxicology (Elmsford, NY)*, 24 (2007) 131.
- [176] F. Grun, B. Blumberg, Minireview: the case for obesogens, *Molecular Endocrinology*, 23 (2009) 1127-1134.
- [177] F. Grün, B. Blumberg, Perturbed nuclear receptor signaling by environmental obesogens as emerging factors in the obesity crisis, *Reviews in Endocrine and Metabolic Disorders*, 8 (2007) 161-171.
- [178] B.A. Swinburn, G. Sacks, K.D. Hall, K. McPherson, D.T. Finegood, M.L. Moodie, S.L. Gortmaker, The global obesity pandemic: shaped by global drivers and local environments, *The Lancet*, 378 (2011) 804-814.
- [179] D.H. Bessesen, Update on obesity, *The Journal of Clinical Endocrinology & Metabolism*, 93 (2008) 2027-2034.
- [180] F. Cordido, R.V. Garcia-Mayor, A. Larranaga, Obesity, adipose tissue, inflammation and update on obesity management, *Obes Control Ther*, 1 (2014) 1-8.
- [181] R.V. García-Mayor, A.L. Vidal, M.F.D. Caamano, A.L. Giménez, Endocrine disruptors and obesity: obesogens, *Endocrinología y Nutrición (English Edition)*, 59 (2012) 261-267.

- [182] O. Horn, S. Nalli, D. Cooper, J. Nicell, Plasticizer metabolites in the environment, *Water Research*, 38 (2004) 3693-3698.
- [183] M. Wittassek, H.M. Koch, J. Angerer, T. Brüning, Assessing exposure to phthalates—the human biomonitoring approach, *Molecular nutrition & food research*, 55 (2011) 7-31.
- [184] B.O. Clarke, S.R. Smith, Review of ‘emerging’ organic contaminants in biosolids and assessment of international research priorities for the agricultural use of biosolids, *Environment international*, 37 (2011) 226-247.
- [185] B. Chang, C. Liao, S. Yuan, Anaerobic degradation of diethyl phthalate, di-n-butyl phthalate, and di-(2-ethylhexyl) phthalate from river sediment in Taiwan, *Chemosphere*, 58 (2005) 1601-1607.
- [186] X. Meng, G. Niu, W. Yang, X. Cao, Di (2-ethylhexyl) phthalate biodegradation and denitrification by a *Pseudoxanthomonas* sp. strain, *Bioresource technology*, 180 (2015) 356-359.
- [187] H.-M. Zhao, H. Du, J. Lin, X.-B. Chen, Y.-W. Li, H. Li, Q.-Y. Cai, C.-H. Mo, H.-M. Qin, M.-H. Wong, Complete degradation of the endocrine disruptor di-(2-ethylhexyl) phthalate by a novel *Agromyces* sp. MT-O strain and its application to bioremediation of contaminated soil, *Science of The Total Environment*, 562 (2016) 170-178.
- [188] D.B. Peakall, Phthalate esters: occurrence and biological effects, in: *Residue reviews*, Springer, 1975, pp. 1-41.
- [189] J. Borch, M. Axelstad, A.M. Vinggaard, M. Dalgaard, Diisobutyl phthalate has comparable anti-androgenic effects to di-n-butyl phthalate in fetal rat testis, *Toxicology letters*, 163 (2006) 183-190.
- [190] A.-M. Saillenfait, J.-P. Sabaté, F. Gallissot, Diisobutyl phthalate impairs the androgen-dependent reproductive development of the male rat, *Reproductive toxicology*, 26 (2008) 107-115.
- [191] M. Sarath Josh, S. Pradeep, K. Vijayalekshmi Amma, S. Balachandran, U. Abdul Jaleel, M. Doble, F. Spener, S. Benjamin, Phthalates efficiently bind to human peroxisome proliferator activated receptor and retinoid X receptor  $\alpha$ ,  $\beta$ ,  $\gamma$  subtypes: an in silico approach, *Journal of Applied Toxicology*, 34 (2014) 754-765.
- [192] M. Sarath Josh, S. Pradeep, V. Adarsh, K. Vijayalekshmi Amma, R. Sudha Devi, S. Balachandran, M. Sreejith, U. Abdul Jaleel, S. Benjamin, In silico evidences for the binding of phthalates onto human estrogen receptor  $\alpha$ ,  $\beta$  subtypes and human estrogen-related receptor  $\gamma$ , *Molecular Simulation*, 40 (2014) 408-417.
- [193] M. Sarath Josh, S. Pradeep, A.K. Balan, M. Sreejith, S. Benjamin, Accessing the molecular interactions of phthalates and their primary metabolites with the human pregnane X receptor using in silico profiling, *Journal of Applied Toxicology*, 36 (2016) 1599-1604.
- [194] I.A. Sheikh, Stereoselectivity and the potential endocrine disrupting activity of di-(2-ethylhexyl) phthalate (DEHP) against human progesterone receptor: a computational perspective, *Journal of Applied Toxicology*, 36 (2016) 741-747.
- [195] J.G. DeKeyser, M.C. Stagliano, S.S. Auerbach, K.S. Prabhu, A.D. Jones, C.J. Omiecinski, Di (2-ethylhexyl) phthalate is a highly potent agonist for the human constitutive androstane receptor splice variant CAR2, *Molecular pharmacology*, 75 (2009) 1005-1013.
- [196] E.P. Hines, A.M. Calafat, M.J. Silva, P. Mendola, S.E. Fenton, Concentrations of phthalate metabolites in milk, urine, saliva, and serum of lactating North Carolina women, *Environmental health perspectives*, 117 (2009) 86.



- [197] J. Högberg, A. Hanberg, M. Berglund, S. Skerfving, M. Remberger, A.M. Calafat, A.F. Filipsson, B. Jansson, N. Johansson, M. Appelgren, Phthalate diesters and their metabolites in human breast milk, blood or serum, and urine as biomarkers of exposure in vulnerable populations, *Environmental health perspectives*, 116 (2008) 334.
- [198] E.E. Hatch, J.W. Nelson, M.M. Qureshi, J. Weinberg, L.L. Moore, M. Singer, T.F. Webster, Association of urinary phthalate metabolite concentrations with body mass index and waist circumference: a cross-sectional study of NHANES data, 1999–2002, *Environmental Health*, 7 (2008) 27.
- [199] R.W. Stahlhut, E. van Wijngaarden, T.D. Dye, S. Cook, S.H. Swan, Concentrations of urinary phthalate metabolites are associated with increased waist circumference and insulin resistance in adult US males, *Environmental health perspectives*, 115 (2007) 876.
- [200] T. James-Todd, R. Stahlhut, J.D. Meeker, S.-G. Powell, R. Hauser, T. Huang, J. Rich-Edwards, Urinary phthalate metabolite concentrations and diabetes among women in the National Health and Nutrition Examination Survey (NHANES) 2001–2008, *Environmental health perspectives*, 120 (2012) 1307.
- [201] H. Wang, Y. Zhou, C. Tang, Y. He, J. Wu, Y. Chen, Q. Jiang, Urinary phthalate metabolites are associated with body mass index and waist circumference in Chinese school children, *PloS one*, 8 (2013) e56800.
- [202] M.T. Bility, J.T. Thompson, R.H. McKee, R.M. David, J.H. Butala, J.P. Vanden Heuvel, J.M. Peters, Activation of mouse and human peroxisome proliferator-activated receptors (PPARs) by phthalate monoesters, *Toxicological Sciences*, 82 (2004) 170-182.
- [203] J.N. Feige, L. Gelman, D. Rossi, V. Zoete, R. Métivier, C. Tudor, S.I. Anghel, A. Grosdidier, C. Lathion, Y. Engelborghs, The endocrine disruptor monoethyl-hexyl-phthalate is a selective peroxisome proliferator-activated receptor  $\gamma$  modulator that promotes adipogenesis, *Journal of Biological Chemistry*, 282 (2007) 19152-19166.
- [204] H. Hauner, G. Entenmann, M. Wabitsch, D. Gaillard, G. Ailhaud, R. Negrel, E. Pfeiffer, Promoting effect of glucocorticoids on the differentiation of human adipocyte precursor cells cultured in a chemically defined medium, *The Journal of clinical investigation*, 84 (1989) 1663-1670.
- [205] H. Hauner, P. Schmid, E. Pfeiffer, Glucocorticoids and insulin promote the differentiation of human adipocyte precursor cells into fat cells, *The Journal of Clinical Endocrinology & Metabolism*, 64 (1987) 832-835.
- [206] H.M. Reichardt, F. Tronche, S. Berger, C. Kellendonk, G. Schütz, New insights into glucocorticoid and mineralocorticoid signaling: lessons from gene targeting, in: *Advances in pharmacology*, Elsevier, 1999, pp. 1-21.
- [207] G. Laryea, G. Schütz, L.J. Muglia, Disrupting hypothalamic glucocorticoid receptors causes HPA axis hyperactivity and excess adiposity, *Molecular endocrinology*, 27 (2013) 1655-1665.
- [208] R.M. Sargis, D.N. Johnson, R.A. Choudhury, M.J. Brady, Environmental endocrine disruptors promote adipogenesis in the 3t3-11 cell line through glucocorticoid receptor activation, *Obesity*, 18 (2010) 1283-1288.
- [209] K. Edman, A. Hosseini, M.K. Bjursell, A. Aagaard, L. Wissler, A. Gunnarsson, T. Kaminski, C. Köhler, S. Bäckström, T.J. Jensen, Ligand binding mechanism in steroid receptors: From conserved plasticity to differential evolutionary constraints, *Structure*, 23 (2015) 2280-2290.

- [210] C.L. Byrne, Iterative image reconstruction algorithms based on cross-entropy minimization, *IEEE Transactions on image processing*, 2 (1993) 96-103.
- [211] G.M. Morris, R. Huey, W. Lindstrom, M.F. Sanner, R.K. Belew, D.S. Goodsell, A.J. Olson, AutoDock4 and AutoDockTools4: Automated docking with selective receptor flexibility, *Journal of computational chemistry*, 30 (2009) 2785-2791.
- [212] O. Trott, A.J. Olson, AutoDock Vina: improving the speed and accuracy of docking with a new scoring function, efficient optimization, and multithreading, *Journal of computational chemistry*, 31 (2010) 455-461.
- [213] W.L. DeLano, The PyMOL molecular graphics system, <http://pymol.org>, (2002).
- [214] D. Van Der Spoel, E. Lindahl, B. Hess, G. Groenhof, A.E. Mark, H.J. Berendsen, GROMACS: fast, flexible, and free, *Journal of computational chemistry*, 26 (2005) 1701-1718.
- [215] W.F. van Gunsteren, S.R. Billeter, A.A. Eising, P.H. Hünenberger, P. Krüger, A.E. Mark, W.R. Scott, I.G. Tironi, *Biomolecular simulation: the {GROMOS96} manual and user guide*, (1996).
- [216] K.B. Koziara, M. Stroet, A.K. Malde, A.E. Mark, Testing and validation of the Automated Topology Builder (ATB) version 2.0: prediction of hydration free enthalpies, *Journal of computer-aided molecular design*, 28 (2014) 221-233.
- [217] A.K. Malde, L. Zuo, M. Breeze, M. Stroet, D. Poger, P.C. Nair, C. Oostenbrink, A.E. Mark, An automated force field topology builder (ATB) and repository: version 1.0, *Journal of chemical theory and computation*, 7 (2011) 4026-4037.
- [218] R. Kumari, R. Kumar, O.S.D.D. Consortium, A. Lynn, g\_mmpbsa□ A GROMACS tool for high-throughput MM-PBSA calculations, *Journal of chemical information and modeling*, 54 (2014) 1951-1962.
- [219] F.M. Gregoire, C.M. Smas, H.S. Sul, Understanding adipocyte differentiation, *Physiological reviews*, 78 (1998) 783-809.
- [220] A.Y.-L. So, T.U. Bernal, M.L. Pillsbury, K.R. Yamamoto, B.J. Feldman, Glucocorticoid regulation of the circadian clock modulates glucose homeostasis, *Proceedings of the National Academy of Sciences*, 106 (2009) 17582-17587.
- [221] J.P. Girod, D.J. Brotman, Does altered glucocorticoid homeostasis increase cardiovascular risk?, *Cardiovascular research*, 64 (2004) 217-226.
- [222] H. Gronemeyer, J.-Å. Gustafsson, V. Laudet, Principles for modulation of the nuclear receptor superfamily, *Nature reviews Drug discovery*, 3 (2004) 950.
- [223] R.K. Bledsoe, V.G. Montana, T.B. Stanley, C.J. Delves, C.J. Apolito, D.D. McKee, T.G. Consler, D.J. Parks, E.L. Stewart, T.M. Willson, Crystal structure of the glucocorticoid receptor ligand binding domain reveals a novel mode of receptor dimerization and coactivator recognition, *Cell*, 110 (2002) 93-105.
- [224] H. Baran, K. Jellinger, L. Deecke, Kynurenine metabolism in Alzheimer's disease, *Journal of neural transmission*, 106 (1999) 165-181.
- [225] S.-I. Fukuoka, K. Ishiguro, K. Yanagihara, A. Tanabe, Y. Egashira, H. Sanada, K. Shibata, Identification and Expression of a cDNA Encoding Human  $\alpha$ -Amino- $\beta$ -carboxymuconate- $\epsilon$ -semialdehyde Decarboxylase (ACMSD) A KEY ENZYME FOR THE TRYPTOPHAN-NIACINE PATHWAY AND "QUINOLINATE HYPOTHESIS", *Journal of Biological Chemistry*, 277 (2002) 35162-35167.



- [226] R. Schwarcz, P. Guidetti, K.V. Sathyaikumar, P.J. Muchowski, Of mice, rats and men: revisiting the quinolinic acid hypothesis of Huntington's disease, *Progress in neurobiology*, 90 (2010) 230-245.
- [227] A.H. Mehler, K. Yano, E.L. May, Nicotinic acid biosynthesis: control by an enzyme that competes with a spontaneous reaction, *Science*, 145 (1964) 817-819.
- [228] F. Moroni, Tryptophan metabolism and brain function: focus on kynurenine and other indole metabolites, *European journal of pharmacology*, 375 (1999) 87-100.
- [229] L. Pucci, S. Perozzi, F. Cimadamore, G. Orsomando, N. Raffaelli, Tissue expression and biochemical characterization of human 2-amino 3-carboxymuconate 6-semialdehyde decarboxylase, a key enzyme in tryptophan catabolism, *The FEBS journal*, 274 (2007) 827-840.
- [230] T.W. Stone, G.M. Mackay, C.M. Forrest, C.J. Clark, L.G. Darlington, Tryptophan metabolites and brain disorders, *Clinical chemistry and laboratory medicine*, 41 (2003) 852-859.
- [231] L. Huo, F. Liu, H. Iwaki, T. Li, Y. Hasegawa, A. Liu, Human  $\alpha$ -amino- $\beta$ -carboxymuconate- $\epsilon$ -semialdehyde decarboxylase (ACMSD): A structural and mechanistic unveiling, *Proteins: Structure, Function, and Bioinformatics*, 83 (2015) 178-187.
- [232] R. Beninger, A. Colton, J. Ingles, K. Jhamandas, R. Boegman, Picolinic acid blocks the neurotoxic but not the neuroexcitant properties of quinolinic acid in the rat brain: evidence from turning behaviour and tyrosine hydroxylase immunohistochemistry, *Neuroscience*, 61 (1994) 603-612.
- [233] S. Garavaglia, S. Perozzi, L. Galeazzi, N. Raffaelli, M. Rizzi, The crystal structure of human  $\alpha$ -amino- $\beta$ -carboxymuconate- $\epsilon$ -semialdehyde decarboxylase in complex with 1, 3-dihydroxyacetonephosphate suggests a regulatory link between NAD synthesis and glycolysis, *The FEBS journal*, 276 (2009) 6615-6623.
- [234] H. Matsuda, M. Sato, M. Yakushiji, M. Koshiguchi, S. Hirai, Y. Egashira, Regulation of rat hepatic  $\alpha$ -amino- $\beta$ -carboxymuconate- $\epsilon$ -semialdehyde decarboxylase, a key enzyme in the tryptophan-NAD pathway, by dietary cholesterol and sterol regulatory element-binding protein-2.
- [235] Y. Guo, K. Kannan, Challenges encountered in the analysis of phthalate esters in foodstuffs and other biological matrices, *Analytical and bioanalytical chemistry*, 404 (2012) 2539-2554.
- [236] Å. Bergman, J.J. Heindel, S. Jobling, K. Kidd, T.R. Zoeller, W.H. Organization, State of the science of endocrine disrupting chemicals 2012: summary for decision-makers, (2013).
- [237] B. Desvergne, J.N. Feige, C. Casals-Casas, PPAR-mediated activity of phthalates: A link to the obesity epidemic?, *Molecular and cellular endocrinology*, 304 (2009) 43-48.
- [238] E. Diamanti-Kandarakis, J.-P. Bourguignon, L.C. Giudice, R. Hauser, G.S. Prins, A.M. Soto, R.T. Zoeller, A.C. Gore, Endocrine-disrupting chemicals: an Endocrine Society scientific statement, *Endocrine reviews*, 30 (2009) 293-342.
- [239] J.L. Lyche, A.C. Gutleb, Å. Bergman, G.S. Eriksen, A.J. Murk, E. Ropstad, M. Saunders, J.U. Skaare, Reproductive and developmental toxicity of phthalates, *Journal of Toxicology and Environmental Health, Part B*, 12 (2009) 225-249.
- [240] T. Fukuwatari, M. Ohta, E. Sugimoto, R. Sasaki, K. Shibata, Effects of dietary di (2-ethylhexyl) phthalate, a putative endocrine disrupter, on enzyme activities involved in the metabolism of tryptophan to niacin in rats, *Biochimica et Biophysica Acta (BBA)-General Subjects*, 1672 (2004) 67-75.

- [241] K. Shibata, T. Fukuwatari, A. Enomoto, E. Sugimoto, Increased conversion ratio of tryptophan to niacin by dietary di-n-butylphthalate, *Journal of nutritional science and vitaminology*, 47 (2001) 263-266.
- [242] T. Fukuwatari, S. Ohsaki, S.-i. Fukuoka, R. Sasaki, K. Shibata, Phthalate esters enhance quinolinate production by inhibiting  $\alpha$ -amino- $\beta$ -carboxymuconate- $\epsilon$ -semialdehyde decarboxylase (ACMSD), a key enzyme of the tryptophan pathway, *Toxicological Sciences*, 81 (2004) 302-308.
- [243] A.D. MacKerell Jr, D. Bashford, M. Bellott, R.L. Dunbrack Jr, J.D. Evanseck, M.J. Field, S. Fischer, J. Gao, H. Guo, S. Ha, All-atom empirical potential for molecular modeling and dynamics studies of proteins, *The journal of physical chemistry B*, 102 (1998) 3586-3616.
- [244] H.-C. Lee, W.-C. Hsu, A.-L. Liu, C.-J. Hsu, Y.-C. Sun, Using thermodynamic integration MD simulation to compute relative protein–ligand binding free energy of a GSK3 $\beta$  kinase inhibitor and its analogs, *Journal of Molecular Graphics and Modelling*, 51 (2014) 37-49.
- [245] R. Kumari, R. Kumar, A. Lynn, O.S.D.D. Consortium, g\_mmpbsa—A GROMACS tool for high-throughput MM-PBSA calculations, *J. Chem. Inf. Model*, 54 (2014) 1951-1962.
- [246] N. Kambia, A. Farce, K. Belarbi, B. Gressier, M. Luyckx, P. Chavatte, T. Dine, Docking study: PPARs interaction with the selected alternative plasticizers to di (2-ethylhexyl) phthalate, *Journal of enzyme inhibition and medicinal chemistry*, 31 (2016) 448-455.
- [247] S. Ahmad, M.F. Khan, S. Parvez, M. Akhtar, S. Raisuddin, Molecular docking reveals the potential of phthalate esters to inhibit the enzymes of the glucocorticoid biosynthesis pathway, *Journal of Applied Toxicology*, 37 (2017) 265-277.
- [248] Z. Zhang, Y. Hu, L. Zhao, J. Li, H. Bai, D. Zhu, J. Hu, Estrogen agonist/antagonist properties of dibenzyl phthalate (DBzP) based on in vitro and in vivo assays, *Toxicology letters*, 207 (2011) 7-11.
- [249] I.A. Sheikh, M. Abu-Elmagd, R.F. Turki, G.A. Damanhour, M.A. Beg, M. Al-Qahtani, Endocrine disruption: In silico perspectives of interactions of di-(2-ethylhexyl) phthalate and its five major metabolites with progesterone receptor, *BMC structural biology*, 16 (2016) 16.
- [250] K. Lee, H. You, J. Choi, K.T. No, Development of pharmacophore-based classification model for activators of constitutive androstane receptor, *Drug Metabolism and Pharmacokinetics*, (2016).
- [251] B.-L. Yuan, X.-Z. Li, N. Graham, Aqueous oxidation of dimethyl phthalate in a Fe (VI)-TiO<sub>2</sub>-UV reaction system, *Water Research*, 42 (2008) 1413-1420.
- [252] D.-W. Liang, T. Zhang, H.H. Fang, J. He, Phthalates biodegradation in the environment, *Applied microbiology and Biotechnology*, 80 (2008) 183-198.
- [253] B. Chang, C. Yang, C. Cheng, S. Yuan, Biodegradation of phthalate esters by two bacteria strains, *Chemosphere*, 55 (2004) 533-538.
- [254] W. Jianlong, L. Ping, S. Hanchang, Q. Yi, Biodegradation of phthalic acid ester in soil by indigenous and introduced microorganisms, *Chemosphere*, 35 (1997) 1747-1754.
- [255] R.L. Stingley, B. Brezna, A.A. Khan, C.E. Cerniglia, Novel organization of genes in a phthalate degradation operon of *Mycobacterium vanbaalenii* PYR-1, *Microbiology*, 150 (2004) 3749-3761.
- [256] J.-Y. Ahn, Y.-H. Kim, J. Min, J. Lee, Accelerated degradation of dipentyl phthalate by *Fusarium oxysporum* f. sp. *pisii* cutinase and toxicity evaluation of its degradation products using bioluminescent bacteria, *Current microbiology*, 52 (2006) 340-344.
- [257] R.W. Eaton, D.W. Ribbons, Metabolism of dimethylphthalate by *Micrococcus* sp. strain 12B, *Journal of bacteriology*, 151 (1982) 465-467.

- [258] R. Kleerebezem, M. Ivalo, L.W.H. Pol, G. Lettinga, High-Rate Treatment of Terephthalate in Anaerobic Hybrid Reactors, *Biotechnology progress*, 15 (1999) 347-357.
- [259] C.D. Cartwright, S.A. Owen, I.P. Thompson, R.G. Burns, Biodegradation of diethyl phthalate in soil by a novel pathway, *FEMS Microbiology Letters*, 186 (2000) 27-34.
- [260] S.-M. Liu, W.-C. Chi, CO<sub>2</sub>-H<sub>2</sub>-dependent anaerobic biotransformation of phthalic acid isomers in sediment slurries, *Chemosphere*, 52 (2003) 951-958.
- [261] H.-F. Cheng, M. Kumar, J.-G. Lin, Degradation kinetics of di-(2-ethylhexyl) phthalate (DEHP) and organic matter of sewage sludge during composting, *Journal of hazardous materials*, 154 (2008) 55-62.
- [262] M. Iwata, T. Imaoka, T. Nishiyama, T. Fujii, Re-characterization of mono-2-ethylhexyl phthalate hydrolase belonging to the serine hydrolase family, *Journal of bioscience and bioengineering*, 122 (2016) 140-145.
- [263] F. Fasim, N. Ahmed, R. Parsons, G.M. Gadd, Solubilization of zinc salts by a bacterium isolated from the air environment of a tannery, *FEMS microbiology letters*, 213 (2002) 1-6.
- [264] S.F. Altschul, W. Gish, W. Miller, E.W. Myers, D.J. Lipman, Basic local alignment search tool, *Journal of molecular biology*, 215 (1990) 403-410.
- [265] B. Webb, A. Sali, Protein structure modeling with MODELLER, *Protein Structure Prediction*, (2014) 1-15.
- [266] R.A. Laskowski, M.W. MacArthur, D.S. Moss, J.M. Thornton, PROCHECK: a program to check the stereochemical quality of protein structures, *Journal of applied crystallography*, 26 (1993) 283-291.
- [267] A. Fiser, R.K.G. Do, Modeling of loops in protein structures, *Protein science*, 9 (2000) 1753-1773.
- [268] N. Guex, M.C. Peitsch, SWISS-MODEL and the Swiss-Pdb Viewer: an environment for comparative protein modeling, *electrophoresis*, 18 (1997) 2714-2723.
- [269] M. Wiederstein, M.J. Sippl, ProSA-web: interactive web service for the recognition of errors in three-dimensional structures of proteins, *Nucleic acids research*, 35 (2007) W407-W410.
- [270] D. Eisenberg, R. Lüthy, J.U. Bowie, [20] VERIFY3D: Assessment of protein models with three-dimensional profiles, *Methods in enzymology*, 277 (1997) 396-404.
- [271] F. Sievers, A. Wilm, D. Dineen, T.J. Gibson, K. Karplus, W. Li, R. Lopez, H. McWilliam, M. Remmert, J. Söding, Fast, scalable generation of high-quality protein multiple sequence alignments using Clustal Omega, *Molecular systems biology*, 7 (2011) 539.
- [272] P. Gouet, E. Courcelle, D.I. Stuart, F. MV© toz, ESPript: analysis of multiple sequence alignments in PostScript, *Bioinformatics (Oxford, England)*, 15 (1999) 305-308.
- [273] N.M. O'Boyle, M. Banck, C.A. James, C. Morley, T. Vandermeersch, G.R. Hutchison, Open Babel: An open chemical toolbox, *Journal of cheminformatics*, 3 (2011) 33.
- [274] E.E. Bolton, Y. Wang, P.A. Thiessen, S.H. Bryant, PubChem: integrated platform of small molecules and biological activities, *Annual reports in computational chemistry*, 4 (2008) 217-241.
- [275] A. Volkamer, D. Kuhn, F. Rippmann, M. Rarey, DoGSiteScorer: a web server for automatic binding site prediction, analysis and druggability assessment, *Bioinformatics*, 28 (2012) 2074-2075.
- [276] S. Ahn, J. Lee, Y. Hong, M. Kim, Identification of the phthalate-degrading bacteria isolated from phthalate-contaminated soil and characterization of their phthalate substrate specificity, *Bulletin of environmental contamination and toxicology*, 72 (2004) 911-915.

- [277] M. Karishma, V.D. Trivedi, A. Choudhary, A. Mhatre, P. Kambli, J. Desai, P.S. Phale, Analysis of preference for carbon source utilization among three strains of aromatic compounds degrading *Pseudomonas*, *FEMS microbiology letters*, 362 (2015) fnv139.
- [278] D. Ribbons, W. Evans, Oxidative metabolism of phthalic acid by soil pseudomonads, *Biochemical Journal*, 76 (1960) 310.
- [279] H. Vojtková, M. Kosina, I. Sedláček, I. Mašlaňová, M. Harwotová, V. Molinková, Characterization of *Pseudomonas monteilii* CCM 3423 and its physiological potential for biodegradation of selected organic pollutants, *Folia microbiologica*, 60 (2015) 411-416.
- [280] C.C. Correll, C.J. Batie, D.P. Ballou, M.L. Ludwig, Phthalate dioxygenase reductase: a modular structure for electron transfer from pyridine nucleotides to [2Fe-2S], *SCIENCE-NEW YORK THEN WASHINGTON-*, 258 (1992) 1604-1604.
- [281] X.-R. Xu, H.-B. Li, J.-D. Gu, Biodegradation of an endocrine-disrupting chemical di-n-butyl phthalate ester by *Pseudomonas fluorescens* B-1, *International Biodeterioration & Biodegradation*, 55 (2005) 9-15.
- [282] G. Benckiser, J. Ottow, Metabolism of the plasticizer di-n-butylphthalate by *Pseudomonas pseudoalcaligenes* under anaerobic conditions, with nitrate as the only electron acceptor, *Applied and environmental microbiology*, 44 (1982) 576-578.
- [283] Y. Wang, Y. Fan, J.-D. Gu, Microbial degradation of the endocrine-disrupting chemicals phthalic acid and dimethyl phthalate ester under aerobic conditions, *Bulletin of Environmental Contamination and Toxicology*, 71 (2003) 0810-0818.
- [284] C. Vamsee-Krishna, Y. Mohan, P. Phale, Biodegradation of phthalate isomers by *Pseudomonas aeruginosa* PP4, *Pseudomonas* sp. PPD and *Acinetobacter lwoffii* ISP4, *Applied microbiology and biotechnology*, 72 (2006) 1263-1269.
- [285] S. Shailaja, M. Ramakrishna, S.V. Mohan, P. Sarma, Biodegradation of di-n-butyl phthalate (DnBP) in bioaugmented bioslurry phase reactor, *Bioresource technology*, 98 (2007) 1561-1566.
- [286] X.-R. Xu, H.-B. Li, J.-D. Gu, Metabolism and biochemical pathway of n-butyl benzyl phthalate by *Pseudomonas fluorescens* B-1 isolated from a mangrove sediment, *Ecotoxicology and environmental safety*, 68 (2007) 379-385.
- [287] F. Zeng, K. Cui, X. Li, J. Fu, G. Sheng, Biodegradation kinetics of phthalate esters by *Pseudomonas fluorescens* FS1, *Process Biochemistry*, 39 (2004) 1125-1129.
- [288] J.-a. Chen, X. Li, J. Li, J. Cao, Z. Qiu, Q. Zhao, C. Xu, W. Shu, Degradation of environmental endocrine disruptor di-2-ethylhexyl phthalate by a newly discovered bacterium, *Microbacterium* sp. strain CQ0110Y, *Applied microbiology and biotechnology*, 74 (2007) 676-682.
- [289] C. Quan, Q. Liu, W. Tian, J. Kikuchi, S. Fan, Biodegradation of an endocrine-disrupting chemical, di-2-ethylhexyl phthalate, by *Bacillus subtilis* No. 66, *Applied microbiology and biotechnology*, 66 (2005) 702-710.
- [290] J. Ding, C. Wang, Z. Xie, J. Li, Y. Yang, Y. Mu, X. Tang, B. Xu, J. Zhou, Z. Huang, Properties of a newly identified esterase from *Bacillus* sp. K91 and its novel function in diisobutyl phthalate degradation, *PloS one*, 10 (2015) e0119216.
- [291] J. Wu, X. Liao, F. Yu, Z. Wei, L. Yang, Cloning of a dibutyl phthalate hydrolase gene from *Acinetobacter* sp. strain M673 and functional analysis of its expression product in *Escherichia coli*, *Applied microbiology and biotechnology*, 97 (2013) 2483-2491.



- [292] X.-Y. Zhang, X. Fan, Y.-J. Qiu, C.-Y. Li, S. Xing, Y.-T. Zheng, J.-H. Xu, Newly identified thermostable esterase from *Sulfobacillus acidophilus*: properties and performance in phthalate ester degradation, *Applied and environmental microbiology*, 80 (2014) 6870-6878.
- [293] P. Fojan, P.H. Jonson, M.T. Petersen, S.B. Petersen, What distinguishes an esterase from a lipase: a novel structural approach, *Biochimie*, 82 (2000) 1033-1041.
- [294] S. Rajagopalan, C. Wang, K. Yu, A.P. Kuzin, F. Richter, S. Lew, A.E. Miklos, M.L. Matthews, J. Seetharaman, M. Su, Design of activated serine-containing catalytic triads with atomic-level accuracy, *Nature chemical biology*, 10 (2014) 386-391.
- [295] A.J. Smith, R. Müller, M.D. Toscano, P. Kast, H.W. Hellinga, D. Hilvert, K. Houk, Structural reorganization and preorganization in enzyme active sites: comparisons of experimental and theoretically ideal active site geometries in the multistep serine esterase reaction cycle, *Journal of the American Chemical Society*, 130 (2008) 15361-15373.
- [296] V. Daggett, S. Schroeder, P. Kollman, Catalytic pathway of serine proteases: classical and quantum mechanical calculations, *Journal of the American Chemical Society*, 113 (1991) 8926-8935.
- [297] Y. Jiang, K.L. Morley, J.D. Schrag, R.J. Kazlauskas, Different Active-Site Loop Orientation in Serine Hydrolases versus Acyltransferases, *ChemBioChem*, 12 (2011) 768-776.
- [298] H. Habe, K. Morii, S. Fushinobu, J.-W. Nam, Y. Ayabe, T. Yoshida, T. Wakagi, H. Yamane, H. Nojiri, T. Omori, Crystal structure of a histidine-tagged serine hydrolase involved in the carbazole degradation (CarC enzyme), *Biochemical and biophysical research communications*, 303 (2003) 631-639.
- [299] G.P. Horsman, S. Bhowmik, S.Y. Seah, P. Kumar, J.T. Bolin, L.D. Eltis, The Tautomeric Half-reaction of BphD, a CC Bond Hydrolase Kinetic and Structural Evidence Supporting a Key Role for Histidine 265 of the Catalytic triad, *Journal of Biological Chemistry*, 282 (2007) 19894-19904.
- [300] T. Schettler, Human exposure to phthalates via consumer products, *International journal of andrology*, 29 (2006) 134-139.
- [301] H.C. Erythropel, M. Maric, J.A. Nicell, R.L. Leask, V. Yargeau, Leaching of the plasticizer di (2-ethylhexyl) phthalate (DEHP) from plastic containers and the question of human exposure, *Applied microbiology and biotechnology*, 98 (2014) 9967-9981.
- [302] R. Ito, F. Seshimo, Y. Haishima, C. Hasegawa, K. Isama, T. Yagami, K. Nakahashi, H. Yamazaki, K. Inoue, Y. Yoshimura, Reducing the migration of di-2-ethylhexyl phthalate from polyvinyl chloride medical devices, *International journal of pharmaceutics*, 303 (2005) 104-112.
- [303] B.C. Blount, M.J. Silva, S.P. Caudill, L.L. Needham, J.L. Pirkle, E.J. Sampson, G.W. Lucier, R.J. Jackson, J.W. Brock, Levels of seven urinary phthalate metabolites in a human reference population, *Environmental health perspectives*, 108 (2000) 979.
- [304] R. Hauser, A. Calafat, Phthalates and human health, *Occupational and environmental medicine*, 62 (2005) 806-818.
- [305] E. Den Hond, G. Schoeters, Endocrine disrupters and human puberty, *International journal of andrology*, 29 (2006) 264-271.
- [306] J.S. Fisher, Environmental anti-androgens and male reproductive health: focus on phthalates and testicular dysgenesis syndrome, *Reproduction*, 127 (2004) 305-315.

- [307] C.-Y. Lin, P.-C. Chen, C.-J. Hsieh, C.-Y. Chen, A. Hu, F.-C. Sung, H.-L. Lee, T.-C. Su, Positive association between urinary concentration of phthalate metabolites and oxidation of DNA and lipid in adolescents and young adults, *Scientific Reports*, 7 (2017) 44318.
- [308] A.R. Zota, A.M. Calafat, T.J. Woodruff, Temporal trends in phthalate exposures: findings from the National Health and Nutrition Examination Survey, 2001–2010, *Environmental health perspectives*, 122 (2014) 235.
- [309] Z. Feng, C. Kunyan, F. Jiamo, S. Guoying, Y. Huifang, Biodegradability of di (2-ethylhexyl) phthalate by *Pseudomonas fluorescens* FS1, *Water, Air, and Soil Pollution*, 140 (2002) 297-305.
- [310] Y. Lu, F. Tang, Y. Wang, J. Zhao, X. Zeng, Q. Luo, L. Wang, Biodegradation of dimethyl phthalate, diethyl phthalate and di-n-butyl phthalate by *Rhodococcus* sp. L4 isolated from activated sludge, *Journal of hazardous materials*, 168 (2009) 938-943.
- [311] D.R. Peterson, C.A. Staples, Degradation of phthalate esters in the environment, in: *Series Anthropogenic Compounds*, Springer, 2003, pp. 85-124.
- [312] D. Pérez-Pantoja, P. Leiva-Novoa, R.A. Donoso, C. Little, M. Godoy, D.H. Pieper, B. González, Hierarchy of carbon source utilization in soil bacteria: hegemonic preference for benzoate in complex aromatic compound mixtures degraded by *Cupriavidus pinatubonensis* strain JMP134, *Applied and environmental microbiology*, 81 (2015) 3914-3924.
- [313] C. Tibazarwa, S. Wuertz, M. Mergeay, L. Wyns, D. van Der Lelie, Regulation of the *cnr* cobalt and nickel resistance determinant of *Ralstonia eutropha* (*Alcaligenes eutrophus*) CH34, *Journal of bacteriology*, 182 (2000) 1399-1409.
- [314] G. Grass, C. GROBE, D.H. Nies, Regulation of the *cnr* cobalt and nickel resistance determinant from *Ralstonia* sp. strain CH34, *Journal of bacteriology*, 182 (2000) 1390-1398.
- [315] R.W. Eaton, D.W. Ribbons, Metabolism of dibutylphthalate and phthalate by *Micrococcus* sp. strain 12B, *Journal of bacteriology*, 151 (1982) 48-57.
- [316] G. Gassner, L. Wang, C. Batie, D.P. Ballou, Reaction of phthalate dioxygenase reductase with NADH and NAD: kinetic and spectral characterization of intermediates, *Biochemistry*, 33 (1994) 12184-12193.
- [317] M. Tarasev, F. Rhames, D.P. Ballou, Rates of the phthalate dioxygenase reaction with oxygen are dramatically increased by interactions with phthalate and phthalate oxygenase reductase, *Biochemistry*, 43 (2004) 12799-12808.
- [318] G. Van Zundert, J. Rodrigues, M. Trellet, C. Schmitz, P. Kastiris, E. Karaca, A. Melquiond, M. van Dijk, S. De Vries, A. Bonvin, The HADDOCK2. 2 web server: user-friendly integrative modeling of biomolecular complexes, *Journal of molecular biology*, 428 (2016) 720-725.
- [319] L.A. Kelley, S. Mezulis, C.M. Yates, M.N. Wass, M.J. Sternberg, The Phyre2 web portal for protein modeling, prediction and analysis, *Nature protocols*, 10 (2015) 845.
- [320] D. Eisenberg, R. Lüthy, J.U. Bowie, [20] VERIFY3D: Assessment of protein models with three-dimensional profiles, in: *Methods in enzymology*, Elsevier, 1997, pp. 396-404.
- [321] V. Hornak, R. Abel, A. Okur, B. Strockbine, A. Roitberg, C. Simmerling, Comparison of multiple Amber force fields and development of improved protein backbone parameters, *Proteins: Structure, Function, and Bioinformatics*, 65 (2006) 712-725.
- [322] S.J. de Vries, A.D. van Dijk, A.M. Bonvin, WHISCY: what information does surface conservation yield? Application to data-driven docking, *Proteins: Structure, Function, and Bioinformatics*, 63 (2006) 479-489.



- [323] S.J. de Vries, A.M. Bonvin, CPOR: a consensus interface predictor and its performance in prediction-driven docking with HADDOCK, *PloS one*, 6 (2011) e17695.
- [324] H. Ashkenazy, S. Abadi, E. Martz, O. Chay, I. Mayrose, T. Pupko, N. Ben-Tal, ConSurf 2016: an improved methodology to estimate and visualize evolutionary conservation in macromolecules, *Nucleic acids research*, 44 (2016) W344-W350.
- [325] Y. Ashikawa, Z. Fujimoto, H. Noguchi, H. Habe, T. Omori, H. Yamane, H. Nojiri, Electron transfer complex formation between oxygenase and ferredoxin components in Rieske nonheme iron oxygenase system, *Structure*, 14 (2006) 1779-1789.
- [326] K. Ballschmiter, M. Zell, Analysis of polychlorinated biphenyls (PCB) by glass capillary gas chromatography, *Fresenius' Zeitschrift für analytische Chemie*, 302 (1980) 20-31.
- [327] A. Poland, J.C. Knutson, 2, 3, 7, 8-Tetrachlorodibenzo-p-dioxin and related halogenated aromatic hydrocarbons: examination of the mechanism of toxicity, *Annual review of pharmacology and toxicology*, 22 (1982) 517-554.
- [328] M.P. Longnecker, W.J. Rogan, G. Lucier, The human health effects of DDT (dichlorodiphenyltrichloroethane) and PCBs (polychlorinated biphenyls) and an overview of organochlorines in public health, *Annual review of public health*, 18 (1997) 211-244.
- [329] R.D. Kimbrough, A.A. Jensen, Halogenated biphenyls, terphenyls, naphthalenes, dibenzodioxins and related products, Elsevier, 2012.
- [330] L.S. Birnbaum, Endocrine effects of prenatal exposure to PCBs, dioxins, and other xenobiotics: implications for policy and future research, *Environmental Health Perspectives*, 102 (1994) 676.
- [331] B. Hargrave, G. Harding, W. Vass, P. Erickson, B. Fowler, V. Scott, Organochlorine pesticides and polychlorinated biphenyls in the Arctic Ocean food web, *Archives of Environmental Contamination and Toxicology*, 22 (1992) 41-54.
- [332] J. Borlak, T. Thum, Induction of nuclear transcription factors, cytochrome P450 monooxygenases, and glutathione S-transferase alpha gene expression in Aroclor 1254-treated rat hepatocyte cultures<sup>1</sup>, *Biochemical pharmacology*, 61 (2001) 145-153.
- [333] M.E. Hahn, The aryl hydrocarbon receptor: A comparative perspective<sup>1</sup>, *Comparative Biochemistry and Physiology Part C: Pharmacology, Toxicology and Endocrinology*, 121 (1998) 23-53.
- [334] T.P. Twaroski, M.L. O'Brien, L.W. Robertson, Effects of selected polychlorinated biphenyl (PCB) congeners on hepatic glutathione, glutathione-related enzymes, and selenium status: implications for oxidative stress<sup>☆ 1</sup>, *Biochemical pharmacology*, 62 (2001) 273-281.
- [335] E.L. Eliel, S.H. Wilen, Stereochemistry of organic compounds, John Wiley & Sons, 2008.
- [336] D. Catelani, G. Mosselmans, J. Nienhaus, C. Sorlini, V. Treccani, Microbial degradation of aromatic hydrocarbons used as reactor coolants, *Experientia*, 26 (1970) 922-923.
- [337] D. Lunt, W. Evans, The microbial metabolism of biphenyl, *Biochemical Journal*, 118 (1970) 54P.
- [338] D.L. Bedard, M.L. Haberl, R.J. May, M.J. Brennan, Evidence for novel mechanisms of polychlorinated biphenyl metabolism in *Alcaligenes eutrophus* H850, *Applied and environmental microbiology*, 53 (1987) 1103-1112.
- [339] L.H. Bopp, Degradation of highly chlorinated PCBs by *Pseudomonas* strain LB400, *Journal of Industrial Microbiology*, 1 (1986) 23-29.

- [340] M.G. Fain, J.D. Haddock, Phenotypic and phylogenetic characterization of *Burkholderia* (*Pseudomonas*) sp. strain LB400, *Current microbiology*, 42 (2001) 269-275.
- [341] L. Pélouquin, C.W. Greer, Cloning and expression of the polychlorinated biphenyl-degradation gene cluster from *Arthrobacter* M5 and comparison to analogous genes from gram-negative bacteria, *Gene*, 125 (1993) 35-40.
- [342] M. Seto, K. Kimbara, M. Shimura, T. Hatta, M. Fukuda, K. Yano, A novel transformation of polychlorinated biphenyls by *Rhodococcus* sp. strain RHA1, *Applied and Environmental Microbiology*, 61 (1995) 3353-3358.
- [343] X. Yang, Y. Sun, S. Qian, Biodegradation of seven polychlorinated biphenyls by a newly isolated aerobic bacterium (*Rhodococcus* sp. R04), *Journal of Industrial Microbiology and Biotechnology*, 31 (2004) 415-420.
- [344] M. Seeger, K.N. Timmis, B. Hofer, Bacterial pathways for the degradation of polychlorinated biphenyls, *Marine chemistry*, 58 (1997) 327-333.
- [345] D.A. Abramowicz, Aerobic and anaerobic biodegradation of PCBs: a review, *Critical Reviews in Biotechnology*, 10 (1990) 241-251.
- [346] B.D. Erickson, F.J. Mondello, Nucleotide sequencing and transcriptional mapping of the genes encoding biphenyl dioxygenase, a multicomponent polychlorinated-biphenyl-degrading enzyme in *Pseudomonas* strain LB400, *Journal of bacteriology*, 174 (1992) 2903-2912.
- [347] K. Taira, J. Hirose, S. Hayashida, K. Furukawa, Analysis of bph operon from the polychlorinated biphenyl-degrading strain of *Pseudomonas pseudoalcaligenes* KF707, *Journal of Biological Chemistry*, 267 (1992) 4844-4853.
- [348] M.M.-J. Couture, C.L. Colbert, E. Babini, F.I. Rosell, A.G. Mauk, J.T. Bolin, L.D. Eltis, Characterization of BphF, a Rieske-type ferredoxin with a low reduction potential, *Biochemistry*, 40 (2001) 84-92.
- [349] L. Gómez-Gil, P. Kumar, D. Barriault, J.T. Bolin, M. Sylvestre, L.D. Eltis, Characterization of biphenyl dioxygenase of *Pandoraea pnomenusa* B-356 as a potent polychlorinated biphenyl-degrading enzyme, *Journal of bacteriology*, 189 (2007) 5705-5715.
- [350] N.Y.R. Agar, Identification of molecular determinants of substrate specificity and activity for biphenyl dioxygenase from *Comamonas testosteroni* B-356, in, Concordia University, 2002.
- [351] C.M. Arnett, J.V. Parales, J.D. Haddock, Influence of Chlorine Substituents on Rates of Oxidation of Chlorinated Biphenyls by the Biphenyl Dioxygenase of *Burkholderia* sp. Strain LB400, *Applied and environmental microbiology*, 66 (2000) 2928-2933.
- [352] D. Barriault, M. Sylvestre, Evolution of the biphenyl dioxygenase BphA from *Burkholderia xenovorans* LB400 by random mutagenesis of multiple sites in region III, *Journal of Biological Chemistry*, 279 (2004) 47480-47488.
- [353] F.J. Mondello, M.P. Turcich, J.H. Lobos, B.D. Erickson, Identification and modification of biphenyl dioxygenase sequences that determine the specificity of polychlorinated biphenyl degradation, *Applied and environmental microbiology*, 63 (1997) 3096-3103.
- [354] H. Suenaga, T. Watanabe, M. Sato, K. Furukawa, Alteration of regiospecificity in biphenyl dioxygenase by active-site engineering, *Journal of bacteriology*, 184 (2002) 3682-3688.
- [355] N.Y. Imbeault, J.B. Powlowski, C.L. Colbert, J.T. Bolin, L.D. Eltis, Steady-state kinetic characterization and crystallization of a polychlorinated biphenyl-transforming dioxygenase, *Journal of Biological Chemistry*, 275 (2000) 12430-12437.

- [356] D. Barriault, M.-M. Plante, M. Sylvestre, Family shuffling of a targeted bphA region to engineer biphenyl dioxygenase, *Journal of bacteriology*, 184 (2002) 3794-3800.
- [357] C.L. Colbert, N.Y. Agar, P. Kumar, M.N. Chakko, S.C. Sinha, J.B. Powlowski, L.D. Eltis, J.T. Bolin, Structural characterization of *Pandoraea pnomenusa* B-356 biphenyl dioxygenase reveals features of potent polychlorinated biphenyl-degrading enzymes, *PLoS One*, 8 (2013) e52550.
- [358] P. Kumar, M. Mohammadi, J.-F. Viger, D. Barriault, L. Gomez-Gil, L.D. Eltis, J.T. Bolin, M. Sylvestre, Structural insight into the expanded PCB-degrading abilities of a biphenyl dioxygenase obtained by directed evolution, *Journal of molecular biology*, 405 (2011) 531-547.
- [359] T.T.M. Pham, M. Sylvestre, Has the bacterial biphenyl catabolic pathway evolved primarily to degrade biphenyl? The diphenylmethane case, *Journal of bacteriology*, 195 (2013) 3563-3574.
- [360] T.T.M. Pham, Y. Tu, M. Sylvestre, Remarkable ability of *Pandoraea pnomenusa* B356 biphenyl dioxygenase to metabolize simple flavonoids, *Applied and environmental microbiology*, 78 (2012) 3560-3570.
- [361] C. Standfuß-Gabisch, D. Al-Halbouni, B. Hofer, Characterization of biphenyl dioxygenase sequences and activities encoded by the metagenomes of highly polychlorobiphenyl-contaminated soils, *Applied and environmental microbiology*, 78 (2012) 2706-2715.
- [362] S. Salentin, S. Schreiber, V.J. Haupt, M.F. Adasme, M. Schroeder, PLIP: fully automated protein–ligand interaction profiler, *Nucleic acids research*, 43 (2015) W443-W447.
- [363] Z. Otwinowski, W. Minor, [20] Processing of X-ray diffraction data collected in oscillation mode, in: *Methods in enzymology*, Elsevier, 1997, pp. 307-326.
- [364] A. Vagin, A. Teplyakov, MOLREP: an automated program for molecular replacement, *Journal of applied crystallography*, 30 (1997) 1022-1025.
- [365] P.V. Afonine, R.W. Grosse-Kunstleve, N. Echols, J.J. Headd, N.W. Moriarty, M. Mustyakimov, T.C. Terwilliger, A. Urzhumtsev, P.H. Zwart, P.D. Adams, Towards automated crystallographic structure refinement with phenix. refine, *Acta Crystallographica Section D: Biological Crystallography*, 68 (2012) 352-367.
- [366] P. Emsley, K. Cowtan, Coot: model-building tools for molecular graphics, *Acta Crystallographica Section D: Biological Crystallography*, 60 (2004) 2126-2132.
- [367] V.B. Chen, W.B. Arendall, J.J. Headd, D.A. Keedy, R.M. Immormino, G.J. Kapral, L.W. Murray, J.S. Richardson, D.C. Richardson, MolProbity: all-atom structure validation for macromolecular crystallography, *Acta Crystallographica Section D: Biological Crystallography*, 66 (2010) 12-21.
- [368] D. Liebschner, P.V. Afonine, N.W. Moriarty, B.K. Poon, O.V. Sobolev, T.C. Terwilliger, P.D. Adams, Polder maps: improving OMIT maps by excluding bulk solvent, *Acta Crystallographica Section D: Structural Biology*, 73 (2017) 148-157.
- [369] M.D. Winn, C.C. Ballard, K.D. Cowtan, E.J. Dodson, P. Emsley, P.R. Evans, R.M. Keegan, E.B. Krissinel, A.G. Leslie, A. McCoy, Overview of the CCP4 suite and current developments, *Acta Crystallographica Section D: Biological Crystallography*, 67 (2011) 235-242.
- [370] M. Mohammadi, M. Sylvestre, Resolving the profile of metabolites generated during oxidation of dibenzofuran and chlorodibenzofurans by the biphenyl catabolic pathway enzymes, *Chemistry & biology*, 12 (2005) 835-846.

- [371] M. Sondossi, D. Barriault, M. Sylvestre, Metabolism of 2, 2'-and 3, 3'-dihydroxybiphenyl by the biphenyl catabolic pathway of *Comamonas testosteroni* B-356, *Applied and environmental microbiology*, 70 (2004) 174-181.
- [372] S. Burley, G. Petsko, Amino-aromatic interactions in proteins, *FEBS letters*, 203 (1986) 139-143.
- [373] C.A. Hunter, K.R. Lawson, J. Perkins, C.J. Urch, Aromatic interactions, *Journal of the Chemical Society, Perkin Transactions 2*, (2001) 651-669.
- [374] R. Anjana, M.K. Vaishnavi, D. Sherlin, S.P. Kumar, K. Naveen, P.S. Kanth, K. Sekar, Aromatic-aromatic interactions in structures of proteins and protein-DNA complexes: a study based on orientation and distance, *Bioinformation*, 8 (2012) 1220.
- [375] W.L. Jorgensen, D.L. Severance, Aromatic-aromatic interactions: free energy profiles for the benzene dimer in water, chloroform, and liquid benzene, *Journal of the American Chemical Society*, 112 (1990) 4768-4774.





